

ALPHA-DIIMINE NICKEL (II) AND PALLADIUM (II) COMPLEXES IN CROSS-
COUPLING REACTIONS

by

Md Muktadir Talukder

APPROVED BY SUPERVISORY COMMITTEE:

Dr. Mihaela C. Stefan, Chair

Dr. Michael C. Biewer, Co-Chair

Dr. Ronald A. Smaldone

Dr. Gabriele Meloni

Copyright 2020

Md Muktadir Talukder

All Rights Reserved

For my Family

ALPHA-DIIMINE NICKEL (II) AND PALLADIUM (II) COMPLEXES IN CROSS-
COUPLING REACTIONS

by

MD MUKTADIR TALUKDER, BS

DISSERTATION

Presented to the Faculty of

The University of Texas at Dallas

in Partial Fulfillment

of the Requirements

for the Degree of

DOCTOR OF PHILOSOPHY IN

CHEMISTRY

THE UNIVERSITY OF TEXAS AT DALLAS

December 2020

ACKNOWLEDGMENTS

First, I want to express my heartfelt appreciation to my research advisor Dr. Mihaela Stefan. Since joining her research group, she encouraged me to take my own ideas and execute them for expanding my research exposure. From the beginning, she guided me to becoming an independent researcher. Most importantly, without her encouragement, I would not have been able to explore my full potential in graduate school. The next person whom I owe to be an organic chemist is Dr. Michael Biewer. Both of them taught me the basic and advanced level of knowledge in chemistry. Whether it is the group meeting, seminar, or conference, I gained proper instruction for becoming a knowledgeable researcher. Moreover, I would like to acknowledge Dr. Ronald Smaldone and Dr. Gabriele Meloni for their valuable guidance as a doctoral committee member.

Furthermore, I profoundly appreciate all the members of Dr. Stefan and Dr. Biewer's lab. I am fortunate to get the opportunity to work with talented students in these labs. Working with fellow members, I have obtained essential knowledge and expertise in my areas of research interest. Without their kind support, guidance, and motivation, I would not find the full potential as a researcher. After joining Dr. Stefan's lab, I found every member supportive as much as I desired them to be. Special gratitude to Yxin Ren for teaching me essential features of catalysis. Notably, Ruwan Gunawardhana taught me various techniques in synthetic organic chemistry. Those skills helped later in my career to explore the unknown phenomena of chemistry. I greatly admire Lakmal Gamage for being my friend and mentor on this journey. I also greatly acknowledge Justin Todd Miller for helping to enhance my writing skills in every way. My appreciation goes to John Michael and Chinthaka Mahesh for allowing me to obtain skills in their research projects.

Moreover, I greatly thank Erika Calubaquib, Pooneh Soltantabar, Hanghang Wang, Abhi Bhadran, Ziyuan Ma, and Tejas Shah for their helpful and hard-working attitudes.

Moreover, I am fortunate enough to receive financial assistance from the department and my research group through teaching and research assistantship, respectively. I want to share my thankfulness to the faculty and staff of the Chemistry and Biochemistry department.

Finally, I want to acknowledge my parents' tremendous sacrifice by supporting me in higher studies in the USA. Additionally, my most profound appreciation goes to my wife, Samia Rifat, for being the most supportive person in my academic and personal life.

November 2020

ALPHA-DIIMINE NICKEL (II) AND PALLADIUM (II) COMPLEXES IN CROSS- COUPLING REACTIONS

Md Muktadir Talukder, PhD
The University of Texas at Dallas, 2020

Supervising Professor: Mihaela C. Stefan, Chair
Dr. Michael C. Biewer, Co-Chair

Cross-couplings reactions are the most versatile synthetic tools and extensively applied for organic syntheses in the industrial production plants. Traditionally established cross-coupling reactions, including Suzuki–Miyaura, have been investigated over the last two decades because of synthetic applicability for manufacturing valuable functionalized building blocks in organic electronics, natural products, and drug discovery. Apart from Suzuki–Miyaura carbon-carbon cross-coupling, carbon-sulfur cross-coupling has been established as a potential synthetic method for synthesizing biologically and pharmaceutically active compounds. Remarkably, the introduction of heteroaromatics through carbon-sulfur cross-coupling added a new dimension to the pharmaceutical industries. Recently, direct arylation has gained much popularity for making π -conjugated monomers and polymers through carbon-carbon bond formation that is an alternative tool to the Suzuki–Miyaura cross-coupling technique. Nonetheless, these useful synthetic procedures are facing enormous challenges arising from the catalytic systems. A significant portion of the catalysts employed in these cross-coupling reactions are air- and moisture-sensitive. Moreover, thermal instability is another drawback of implementing in elevated temperature.

Notably, ligand design plays a crucial role in catalytic outcomes. The existing ligand design for the cross-coupling reactions lacks essential features, including steric and electronic requirements. Consequently, these shortcomings are subject to the poor catalytic performance that significantly hinders the industrial-scale application. In this dissertation, ligand design based on α -diimine frameworks is investigated in the Suzuki–Miyaura cross-coupling, carbon-sulfur cross-coupling, and direct arylation methods. Both nickel and palladium complexes with α -diimine cores were synthesized and applied to examine their potential scope in the cross-coupling reactions.

Recent advances in the nickel and palladium-based catalytic systems in the cross-coupling reactions are described in chapter 1. In situ and well-defined nickel and palladium catalytic systems are discussed in this chapter. Moreover, existing challenges and possible solutions are also explained.

Chapter 2 is designed to investigate the potential application of α -diimine-based nickel (II) and palladium (II) complexes in the Suzuki–Miyaura cross-coupling reaction. Notably, ligand design is extensively examined for making four different complexes by varying the ligand structure and metal center. Notably, a wide variety of substrates having challenging functional moieties are synthesized through carbon-carbon cross-coupling.

Chapter 3 describes the synthesis and application of α -diimine-based nickel (II) and palladium (II) complexes in the carbon-sulfur cross-coupling. Both mono- and dinuclear complexes are synthesized and practiced for making aryl/alkyl sulfides. Mostly, pharmaceutically relevant heteroaryl moieties both from thiols and aryl halides are coupled.

Chapter 4 is dedicated to examining the α -diimine-based nickel (II) and palladium (II) complexes in making valuable functionalized π -conjugated monomers through the direct arylation method.

Mainly, five-membered heteroaromatics, including thiazole and thiophene derivatives, are applied with a wide variety of aryl halides. Moreover, the findings propose that α -diimine-based complexes can deliver direct arylation as an alternative technique to the carbon-carbon bond formation through Suzuki–Miyaura cross-coupling.

TABLE OF CONTENTS

ACKNOWLEDGMENTS	v
ABSTRACT.....	vii
LIST OF FIGURES	xv
LIST OF TABLES	xviii
LIST OF SCHEMES.....	xix
CHAPTER 1 RECENT ADVANCES IN THE NICKEL AND PALLADIUM CATALYZED CROSS-COUPLING REACTIONS.....	1
1.1 Abstract.....	2
1.2 Suzuki–Miyaura Cross-Coupling (SMC)	2
1.2.1 General Reaction Mechanism of SMC	3
1.2.2 Palladium-Based Catalytic Systems in SMC.....	3
1.2.3 Nickel-Based Catalytic Systems in SMC	6
1.2.4 Existing Challenges in Ni and Pd-Catalyzed SMC.....	8
1.3 Carbon-Sulfur (C-S) Cross-Coupling	9
1.3.1 General Reaction Mechanism of C-S Cross-coupling.....	10
1.3.2 Palladium-Based Catalytic Systems in C-S Cross-Coupling.....	11
1.3.3 Photoredox Catalytic Systems in C-S Cross-Coupling.....	12
1.3.4 Nickel-Based Catalytic Systems in C-S Cross-Coupling	13
1.3.5 Existing Challenges in C-S cross-coupling.....	14
1.3.5 Direct C-H Bond Arylation for C-C Bond Formation.....	15
1.4.1 General Reaction Mechanism of Direct C-H Bond Arylation.....	15
1.4.2 Palladium-Based Catalytic Systems in Direct C-H Bond Arylation	17
1.4.3 Nickel-Based Catalytic Systems in Direct C-H Bond Arylation	18
1.4.4 Existing Challenges in Ni and Pd-Catalyzed Direct C-H Bond Arylation	20
1.5 Conclusion	20
1.6 References.....	20

CHAPTER 2 LIGAND STERIC EFFECTS OF α -DIIMINE NICKEL(II) AND PALLADIUM(II) COMPLEXES IN THE SUZUKI–MIYAJIMA CROSS-COUPLED REACTION	27
2.1 Abstract	28
2.2 Introduction	28
2.3 Results and discussion	31
2.3.1 Synthesis of α -Diimine Nickel (II) and Palladium (II) Complexes	31
2.3.2 X-ray Crystallography	32
2.3.3 Thermal Properties of the Complexes	34
2.3.4 Optimization of Reaction Conditions for Suzuki–Miyajima Cross-coupling (SMC)	35
2.3.5 Substrate Scope	37
2.3.6 Expansion of Substrate Scope	40
2.3.7 Steric Effect vs. Catalytic Performance	44
2.4 Conclusion	46
2.5 Experimental Section	47
2.5.1 General materials and method	47
2.5.2 Single-Crystal XRD Data Acquisition and Characterization	48
2.5.3 Percent Buried Volume and Steric Map	48
2.5.4 Synthesis of Iminopyridine-Based Ligand (1a)	48
2.5.5 Synthesis of Acenaphthene-Based Ligand (1b)	49
2.5.6 Synthesis of Bis-Ligated Nickel(II) Complex (Ni A)	50
2.5.7 Synthesis of Mono-Ligated Nickel(II) Complex (Ni B)	50
2.5.8 Synthesis of Iminopyridine-Based Palladium(II) Complex (Pd A)	51
2.5.9 Synthesis of Acenaphthene-Based Palladium(II) Complex (Pd B)	51
2.5.10 General Procedure for Nickel-Catalyzed Suzuki–Miyajima Cross-Coupling	52
2.5.11 General Procedure for Palladium-Catalyzed Suzuki–Miyajima Cross-Coupling	52
2.6 Characterization of the synthesized biaryl products	53
2.7 Supporting Information	59
2.8 References	79

CHAPTER 3 MONO- AND DINUCLEAR α -DIIMINE NICKEL(II) AND PALLADIUM(II) COMPLEXES IN C-S CROSS-COUPLING	91
3.1 Abstract	92
3.2 Introduction	92
3.3 Results and Discussion	94
3.3.1 Synthesis and Characterization of α -Diimine Nickel (II) and Palladium (II) Complexes.....	94
3.3.2 Reaction conditions optimization in C-S Cross-Coupling.....	96
3.3.3 Evaluation of the Complexes in C-S Cross-Coupling	98
3.3.4 Expansion of Substrate Scope: Aromatics	100
3.3.5 Expansion of Substrate Scope: Heteroaromatics	103
3.4 Conclusion	104
3.5 Experimental Section	105
3.5.1 General Materials and Methods	105
3.5.2 Single-Crystal XRD Data Characterization	105
3.5.3 Steric Map and Percent Buried Volume	106
3.5.4 Synthesis of Iminopyridine Ligand N-(4-butylphenyl)-1-(pyridin-2-yl)methanimine (1a).....	106
3.5.5 Synthesis of Iminopyridine Ligand N-(4-isopropylphenyl)-1-(pyridin-2-yl)methanimine (1b).....	106
3.5.6 Synthesis of Iminopyridine Ligand N-(2-isopropylphenyl)-1-(pyridin-2-yl)methanimine (1d).....	107
3.5.7 Synthesis of the Acenaphthene Ligand N1,N2-bis(4-butylphenyl)acenaphthylene-1,2-diimine (1c).....	107
3.5.8 Synthesis of the Iminopyridine Bis-Ligated Nickel(II) Complex (Ni A-1).....	108
3.5.9 Synthesis of the Iminopyridine Palladium(II) Complex (Pd A-1).....	108
3.5.10 Synthesis of the Acenaphthene Palladium(II) Complex (Pd B-1)	109
3.5.11 Synthesis of the Iminopyridine Monoligated Nickel(II) Complex (Ni B-1)	109
3.5.12 General Procedure for Nickel-Catalyzed C-S Cross-Coupling	110
3.5.13 General Procedure for Palladium-Catalyzed C-S Cross-Coupling.....	110
3.6 Characterization of the Synthesized C-S Coupled Compounds	110
3.7 Supporting Information.....	123
3.8 References.....	173

CHAPTER 4 IMINOPYRIDINE-BASED α -DIIMINE NICKEL(II) AND PALLADIUM(II) COMPLEXES IN DIRECT C-H BOND ARYLATION OF FIVE-MEMBERED HETEROAROMATICS	179
4.1 Abstract	180
4.2 Introduction	180
4.3 Results and Discussion	182
4.3.1 Synthesis and Characterization of α -Diimine Nickel (II) and Palladium (II) Complexes.....	182
4.3.2 Optimization of Reaction Conditions in Direct C-H Bond Arylation	183
4.3.3 Evaluation of catalytic performance	186
4.3.4 Expansion of Substrate Scope: Thiophene Derivatives	187
4.3.5 Extension of Substrate Scope: π -Conjugated Monomers	189
4.4 Conclusion	190
4.5 Experimental	191
4.5.1 General Materials and Methods	191
4.5.2 Single-Crystal XRD Data Characterization	191
4.5.3 Steric Map and Percent Buried Volume	192
4.5.4 Synthesis of Iminopyridine Ligand N-(2-ethylphenyl)-1-(pyridin-2-yl)methanimine (L A-1)	192
4.5.5 Synthesis of Iminopyridine Ligand N-(2,3-dimethylphenyl)-1-(pyridin-2-yl)methanimine (L A-2).....	193
4.5.6 Synthesis of the Iminopyridine Bis-Ligated Nickel(II) Complex (Ni X-1).....	193
4.5.7 Synthesis of the Iminopyridine Bis-Ligated Nickel(II) Complex (Ni X-2).....	194
4.5.8 Synthesis of the Iminopyridine Palladium(II) Complex (Pd X-1).....	194
4.5.9 Synthesis of the Iminopyridine Palladium(II) Complex (Pd X-2).....	194
4.5.10 General Procedure for Nickel-Catalyzed Direct Arylation.....	195
4.5.11 General Procedure for Palladium-Catalyzed Direct Arylation	196
4.6 Characterization of the Synthesized Direct Arylated Compounds	196
4.7 Supporting Information.....	204
4.8 References.....	237

BIOGRAPHICAL SKETCH243

CURRICULUM VITAE

LIST OF FIGURES

Figure 1.1. Pharmaceutically active building blocks through SMC.	3
Figure 1.2. General reaction mechanism of SMC.....	4
Figure 1.3. Examples of palladium-based catalytic systems in SMC.....	5
Figure 1.4. Examples of nickel-based catalytic systems in SMC.....	7
Figure 1.5. Biologically and pharmaceutically active aryl sulfides.....	9
Figure 1.6. General reaction mechanism of C-S cross-coupling.	10
Figure 1.7. Examples of palladium-based catalytic systems in C-S cross-coupling..	11
Figure 1.8. Examples of nickel-based catalytic systems in C-S cross-coupling.....	13
Figure 1.9. General reaction mechanism of direct C-H bond arylation.....	16
Figure 1.10. Examples of palladium-based catalytic systems in direct C-H bond arylation.	18
Figure 1.11. Examples of nickel-based catalytic systems in direct C-H bond arylation..	19
Figure 2.1. Previous examples of α -diimine-based catalysts and summary of current work in SMC.	29
Figure 2.2. ORTEP diagrams of the synthesized α -diimine complexes. Solvents of crystallization in the structural packing have been omitted for clarity (Ni B & Pd B)	33
Figure 2.3. TGA (a–d) and DSC (e–h) curves of the synthesized α -diimine complexes..	34
Figure 2.4. Substrate scope: phenylboronic acid	39
Figure 2.5. Expansion of substrate scope.....	41
Figure 2.6. Percent buried volume (%Vbur) and topographic steric map of the complexes (a-d), including their performance with phenylboronic acid (e).....	44
Figure 2.7. ^1H NMR spectrum of ligand 1a.	60
Figure 2.8. ^1H NMR spectrum of ligand 1b.....	60

Figure 2.9. Twin ORTEP (a) and packing (b) of complex Pd B.	61
Figure 2.10. Unit cell representation of complex Pd B.....	61
Figure 2.11. Unit cell representation of complex Pd A.	62
Figure 2.12. Unit cell representation of complex Ni A.....	62
Figure 2.13. Unit cell representation of complex Ni B.....	63
Figure 2.14–2.38. ¹ H NMR spectrum of 1A1–3A7.....	67–79
Figure 3.1. Overview of transition metal-catalyzed C-S cross-coupling.....	93
Figure 3.2. Evaluation of the Complexes in C-S Cross-Coupling.....	100
Figure 3.3. Expansion of Substrate Scope: Aromatics.	101
Figure 3.4. Expansion of substrate scope: Heteroaromatics.	103
Figure 3.5. ¹ H NMR spectrum of ligand 1a.	123
Figure 3.6. ¹ H NMR spectrum of ligand 1b.....	124
Figure 3.7. ¹ H NMR spectrum of ligand 1c.....	124
Figure 3.8. ¹³ C NMR spectrum of ligand 1c.....	125
Figure 3.9. ¹ H NMR spectrum of ligand 1d.....	125
Figure 3.10. Unit cell representation of complex Ni A-1 (Positional disorder with dashed bonds).	126
Figure 3.11. Unit cell representation of complex Ni A-1 (Positional disorder with solid bonds).	126
Figure 3.12. Unit cell representation of complex Pd A-1.....	127
Figure 3.13. Unit cell representation of complex Pd B-1.	127
Figure 3.14. Unit cell representation of complex Ni B-1..	128
Figure 3.15–3.96. ¹ H and ¹³ C NMR spectrum of CD1–CD41.....	132–172

Figure 4.1. Evaluation of catalytic performance.....	186
Figure 4.2. Expansion of substrate scope: thiophene derivatives..	188
Figure 4.3. Expansion of substrate scope: π -conjugated monomers.....	189
Figure 4.4. ^1H NMR spectrum of ligand L A-1.....	205
Figure 4.5. ^1H NMR spectrum of ligand L A-2.....	205
Figure 4.6. Unit cell representation of complex Ni X-1.....	206
Figure 4.7. Unit cell representation of complex Ni X-2.....	207
Figure 4.8. Unit cell representation of complex Pd X-1.....	208
Figure 4.9. Unit cell representation of complex Pd X-2.....	209
Figure 4.10–4.58. ^1H and ^{13}C NMR spectrum of CD1– CD25.....	213–237

LIST OF TABLES

Table 2.1. Optimization of Solvent and Base ^a	36
Table 2.2. Optimization of Temperature ^a	37
Table 2.3. Concentration optimization of Complex, Boronic Acid, and Base ^a	38
Table 2.4. Crystal data, data collection and refinement for complex Ni A and Ni B	64
Table 2.5. Crystal data, data collection and refinement for complex Pd A and Pd B	65
Table 2.6. Selected bond lengths and angles for complexes Ni A and Ni B	67
Table 2.7. Selected bond lengths and angles for complexes Pd A and Pd B	67
Table 3.1 Optimization of base, solvent, and temperature ^a	97
Table 3.2. Optimization of time, concentration of complex, and halide/base ratio ^a	98
Table 3.3. Crystal data, data collection and refinement for complex Ni A-1 and Pd A-1	129
Table 3.4. Crystal data, data collection and refinement for complex Pd B-1 and Ni B-1	130
Table 3.5. Selected bond lengths and angles for complexes Ni A-1 and Ni B-1	131
Table 3.6. Selected bond lengths and angles for complexes Pd A-1 and Pd B-1	131
Table 4.1. Optimization of base, solvent, and acid ^a	184
Table 4.2. Optimization of time, concentration of complex, and temperature ^a	185
Table 4.3. Crystal data, data collection and refinement for complex Ni X-1 and Ni X-2	210
Table 4.4. Crystal data, data collection and refinement for complex Pd X-1 and Pd X-2	211
Table 4.5. Selected bond lengths and angles for complexes Ni A-1 and Ni B-1	212
Table 4.6. Selected bond lengths and angles for complexes Pd A-1 and Pd B-1	212

LIST OF SCHEMES

Scheme 2.1. Synthesis of α -diimine nickel (II) and palladium (II) complexes	32
Scheme 3.1. Synthesis, ORTEP diagrams, ligand bite angle, percent buried volume, and steric maps of the α -diimine Ni(II) and Pd(II) Complexes.....	95
Scheme 4.1 Synthesis, ORTEP diagrams, percent buried volume, and topographic steric maps of the α -diimine Ni(II) and Pd(II) Complexes	183

CHAPTER 1
**RECENT ADVANCES IN THE NICKEL AND PALLADIUM CTALYZED CROSS-
COUPLING REACTIONS**

Authors: Md Muktadir Talukder, John Michael O. Cue, Justin T. Miller, Michael C. Biewer, and
Mihaela C. Stefan*

The Department of Chemistry and Biochemistry, BE26

The University of Texas at Dallas

800 West Campbell Road

Richardson, Texas 75080-3021

1.1 Abstract

In the last two decades, transition metal-catalyzed cross-coupling reactions have received significant recognition for making functionalized biaryl compounds possessing valuable applications in organic electronics, natural products, and drug discovery. Compared to other cross-coupling reactions, Suzuki–Miyaura, Stille, Sonogashira, and Heck type cross-coupling synthetic tools are widely applied for generating C-C bonds.¹ Furthermore, different synthetic methods have emerged to construct carbon-heteroatom bonds by employing transition metal catalysts. Especially, the C-S bond formation prevails as one of the most relevant chemical transformations for pharmaceutical industries.² Moreover, direct heteroarylation has arisen as an alternative synthetic method for synthesizing biaryl compounds through C-C bond formation because of sustainable choices to the existing cross-coupling reactions.³

1.2 Suzuki–Miyaura Cross-Coupling (SMC)

Suzuki–Miyaura cross-coupling (SMC) reaction is a remarkably powerful synthetic tool for the construction of C-C bonds.⁴ This useful method is widely utilized in the areas of natural product synthesis, supramolecular chemistry, catalysis, and materials science. Notably, fine chemical, pharmaceutical, and agrochemical industries heavily rely on the SMC reaction (Figure 1.1).⁵ Since the discovery in 1979, transition-metal-catalyzed SMC between an organic halide and organoboron compound has become the most suitable approach in C-C bond formation.⁶⁻⁷ In contrast to the existing Stille, Sonogashira, and Heck type reactions, the SMC reaction offers additional advantages. This is associated with mild reaction settings and the broad substrate scope and functional group tolerance. Moreover, organoboron compounds are easy to synthesize and

demonstrate high air- and moisture stabilities. Also, low-toxicity associated with the organoboron compounds and easy separation provide additional advantages in SMC reaction.⁸

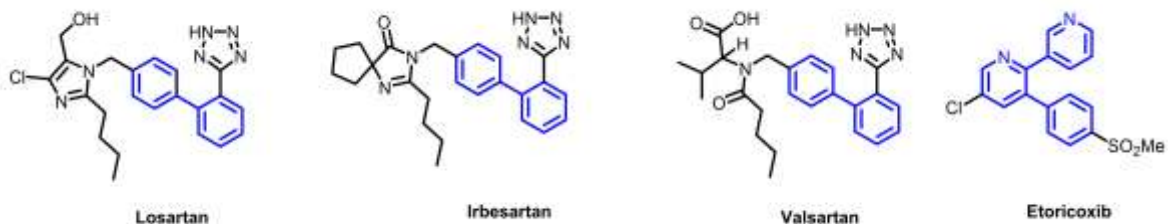


Figure 1.1. Pharmaceutically active building blocks through SMC.

1.2.1 General Reaction Mechanism of SMC

The general reaction mechanism of SMC is shown in Figure 1.2.⁹ This mechanism is explained by the prospect of the palladium catalyst. In the first step, the organopalladium intermediate (3) is produced from the oxidative addition of halide to the palladium. The base reacts with the organopalladium species to form the respected intermediate (4). Afterward, transmetallation happens to form another organopalladium species (8) by reacting intermediate 4 with the boron-ate complex (6). In the final step, the biaryl products (9) are formed from the restoration of the catalyst through reductive elimination.

1.2.2 Palladium-Based Catalytic Systems in SMC

SMC reaction through Pd/C catalytic systems have been exhibited promising performance since the introduction by Marck and coworkers in 1994.¹⁰ This catalyst can be used for coupling various aryl and heteroaryl moieties. Usually, Pd/C has manifested good performance having aqueous solvents with or without the employment of phosphine ligands. Nishida and co-workers

noticed that SMC reactions of haloquinolines and halopyridines necessitate the usage of a

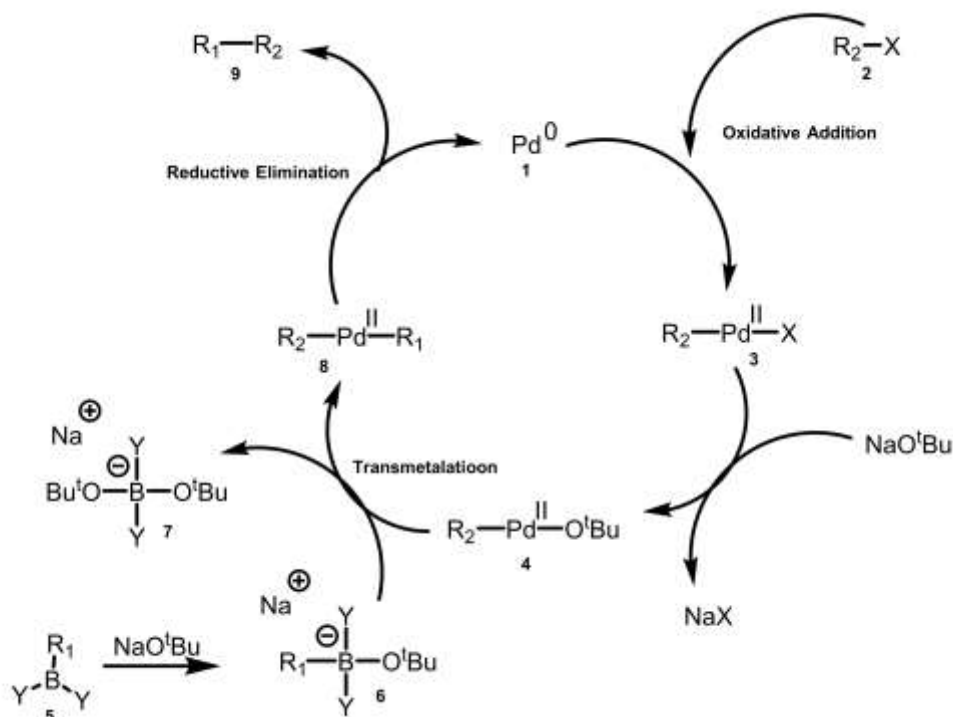


Figure 1.2. General reaction mechanism of SMC.⁹

phosphine ligand for Pd/C systems.¹¹ Homogenous SMC reaction is facilitated by incorporating electron-rich and bulky ligands.¹ Both oxidative addition and reductive elimination are promoted by introducing those ligands. Ligand-free Pd-catalyzed SMC reaction has received noticeable attention because most of the ligand-promoted systems suffer from the air- and moisture sensitivity.⁹ Moreover, Chand et al. has published ligand-free Pd nanoparticles for SMC at ambient temperature. For this purpose, the palladium nanoparticles were generated by applying Pd(OAc)₂ with an equimolar mixture of methanol and acetonitrile.¹² Lately, the supported transition metal catalytic system has gained popularity in SMC. For instance, a magnetic lignosulfonate-supported Pd complex has been applied in SMC as a renewable source of catalyst in the aqueous medium.¹³

Moreover, azine-linked covalent organic polymer-supported ultrafine Pd nanoparticles have been synthesized as a promising catalytic system for SMC.¹⁴

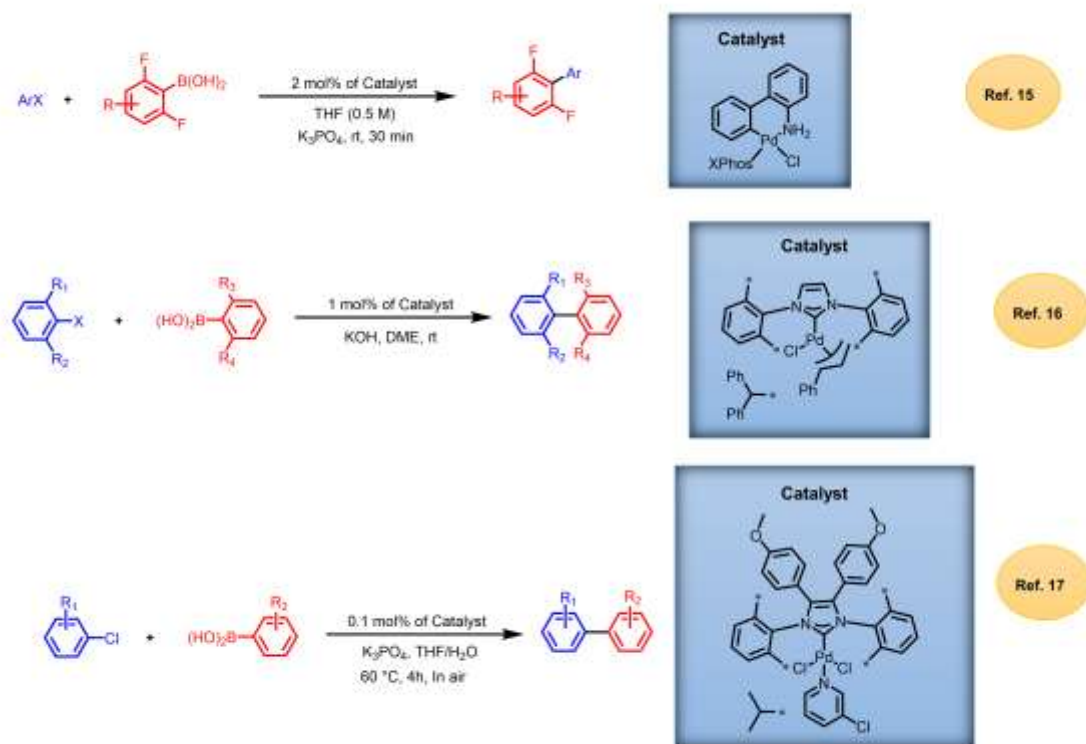


Figure 1.3. Examples of palladium-based catalytic systems in SMC.

Compared to the aforementioned catalytic systems for in situ generations of catalytically active Pd species, a significant shift has been identified towards well-defined Pd catalysts in SMC. Buchwald-type palladacycle,¹⁵ allyl-based precatalysts,¹⁶ and PEPPSI-based precatalyst¹⁷ are among the Pd-based popular systems in SMC. Buchwald and co-workers have applied the XPhos-based palladium complexes at room temperature for coupling fluorinated boronic acid with a wide variety of aryl and heteroaryl halides (Figure 1.3).¹⁵ Particularly, this catalytic system has the capacity to couple five-membered 2-heterocyclic boronic acids having extremely mild reaction settings. Nolan-type allyl-based precatalysts offer significant improvement in SMC regarding the

easy and efficient synthesis of the well-defined palladium catalyst (Figure 1.3).¹⁶ They successfully utilized $[\text{Pd}(\text{IPr}^*)(\text{cin})\text{Cl}]$ for synthesizing tetra-ortho-substituted biaryls (67–99%) with inexpensive base and mild reaction conditions. In 2019, Liu and co-workers have investigated the catalytic performance of N-heterocarbene palladium catalysts containing dianisole backbones (Figure 1.3).¹⁷ For understanding the steric effects of the catalysts in the reaction outcomes, the ligand design was diversified with various alkyl and aryl substituents in the backbone. Notably, more steric bulk of the catalysts promoted to couple challenging heteroaryl boronic acids with a diverse class of aryl halides. These catalytic tools incorporate a wide variety of nucleophiles and electrophiles. Moreover, bulky and heteroaryl organoboron compounds have been successfully attached for making functionalized biaryl or biheteroaryl building blocks. Additionally, they have exhibited good to excellent functional group tolerance.

1.2.3 Nickel-Based Catalytic Systems in SMC

Recently, nickel-catalyzed SMC reaction has gained much popularity compared to the well-established palladium-based synthetic tools. Nickel is comparatively much cheaper and earth-abundant than the palladium metal.⁴ Furthermore, high valent Pd(III) and Pd(IV) species have been studied, whereas nickel displays Ni(0)/Ni(II) as well as Ni(I)/Ni(III) oxidation states. On the other hand, nickel exhibits more nucleophilic character because of higher electron density and smaller size than the palladium.¹⁸ Consequently, a significant shift has been identified in the SMC through nickel-catalyzed cross-coupling reactions.

A crucial aspect of the use of Ni as a catalyst is the design of the ligand. Several ligands of different bulkiness and functionality have been developed to tune the stereoelectronic properties of Ni-based complexes. Analogous of the ligands that have been used for Pd-catalyzed SMC have

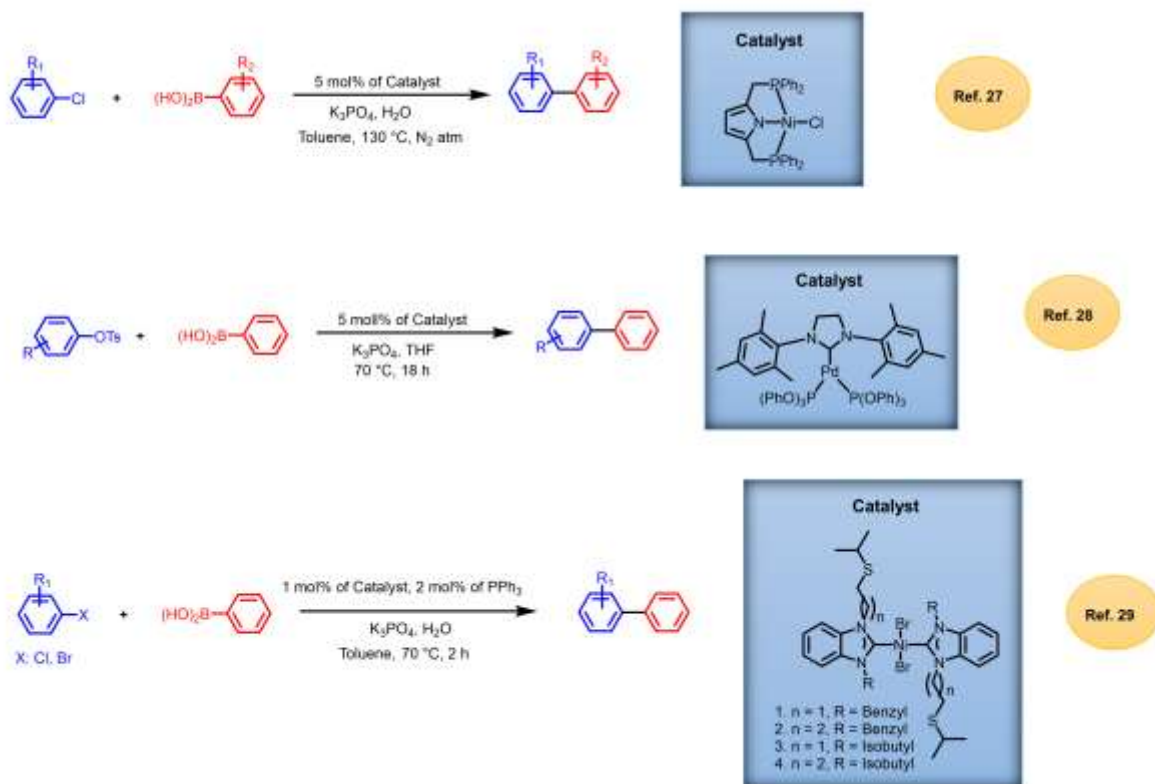


Figure 1.4. Examples of nickel-based catalytic systems in SMC.

been tried for Ni-catalyzed SMC, such as the sterically demanding, electron-rich phosphine¹⁹ and *N*-heterocyclic carbenes (NHC).²⁰ Ni(dppf)Cl₂ (dppf = 1,1'-bis(diphenylphosphino)ferrocene) precatalyst is one of the first to be successfully used for the coupling of aryl chlorides and arylboronic acids.²¹ Other catalysts reported for SMC are Ni(dppe)Cl₂ (dppe = 1,2-bis(diphenylphosphino)ethane),²² and the more bench-stable catalysts are Ni(1-naphthyl)(PCy₃)₂Cl (PCy₃ = tricyclohexylphosphine),²³ and Ni(cinnamyl)(dppf)Cl.²⁴ Several other Ni catalysts of lower oxidation states have also been reported such as Ni(dppf)Cl₂,²⁵ and Ni(COD)₂ (COD = 1,5-cyclooctadiene).²⁵ Ni(COD)₂ is still in use, but it is relatively expensive, thermally unstable, and air sensitive.²⁶ Recently well-defined Ni-based catalysts are gaining popularity for making air- and moisture stable catalytic systems in SMC. The fundamental reason is that the *in-*

situ generations of catalytically active species are air- and moisture-sensitive.²⁶ Accordingly, investigations have been carried out for the construction of more practical well-defined nickel-based catalysts.²⁷⁻²⁹ For instance, Tonzetich and co-workers have investigated the SMC reaction mechanism by introducing a nickel pincer catalyst (Figure 1.4).²⁷ [NiCl(PhPNP)] (PhPNP = anion of 2,5-bis(diphenylphosphinomethyl)pyrrole) exhibited Ni(I)/Ni(III) process in which the boronic acid participated as the source of nucleophile as well as reductant. The first application of low-valent NHC-phosphite nickel complexes has been reported by Duczynski et al., where three-coordinate Ni- (NHC) [P(OAr₃)₂] complexes were synthesized and employed in SMC (Figure 1.4).²⁸ This catalytic system was successfully applied for coupling phenylboronic acid with a library of aryl tosylates. Furthermore, nickel(II) benzimidazolin-2-ylidene complexes including thioether side chains have been utilized in SMC (Figure 1.4).²⁹ This catalytic method afforded good to excellent yields for coupling electron-poor aryl chlorides with boronic acids.

1.2.4 Existing Challenges in Ni and Pd-Catalyzed SMC

Although significant improvement has been made in Ni and Pd-based systems for SMC; however, these catalytic systems need proper alteration for overcoming the existing challenges. For instance, protodeboronation is a common problem in SMC which significantly reduce the catalytic performance.³⁰ Protodeboronation is a chemical phenomenon in which a carbon-hydrogen bond is formed by protonolysis of the organoborane compounds. For this reason, an excess amount of organoborane compounds are required for obtaining the desired yields in SMC. Moreover, the need to activate the precatalysts is another concern in SMC. Also, air- and moisture sensitivity, as well as thermal instability, presents enormous obstacles in SMC through the existing

Ni and Pd systems.²⁶ Furthermore, elevated temperature (100–130 °C), high catalyst loading (2.5–10 mol %), and prolonged reaction time (12–48 h) profoundly affect their success in SMC.^{26-27, 29}

1.3 Carbon-Sulfur (C-S) Cross-Coupling

Carbon-heteroatom bond formation remains one of the most prevalent synthetic tools in organometallic processes. Compared to C-N and C-O cross-coupling, C-S is an underdeveloped synthetic method for synthesizing valuable functionalized biarylsulfides.³¹ Prominently, C-S bond construction continues as one of the most important chemical transformations that possess immense potential in pharmaceutical applications. Moreover, biarylsulfides building blocks

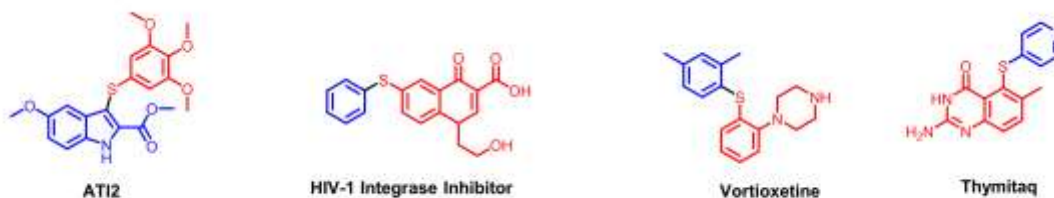


Figure 1.5. Biologically and pharmaceutically active aryl sulfides.

through C-S cross-coupling are found in natural products that exhibit activities against HIV, cancer, Alzheimer's disease, asthma, and inflammation (Figure 1.5).² Synthesizing aryl sulfides without the employment of transition metal-catalyzed systems are usually inefficient, and have severely limited functional group tolerance. Few of these techniques include aromatic substitution reactions, nucleophilic attack on disulfides, and metal-mediated disulfide reductions.³² Accordingly, more practical and effective synthetic tools have arisen within transition metal catalysis for creating aryl sulfides through C-S cross-coupling.

1.3.1 General Reaction Mechanism of C-S Cross-coupling

In 1978, Migita et al. has reported the first palladium-catalyzed thiolation of aryl halides from using $\text{Pd}[\text{PPh}_3]_4$.³³ Although this method is restricted to aryl bromides and needs high temperatures; however, the synthesized biaryl sulfides afford good yields. Generally, bidentate phosphine ligands are utilized in C-S cross-coupling by Migita's technique. Bidentate phosphine ligands exhibit success because of their capacity to stay coordinated with the metal upon the attack

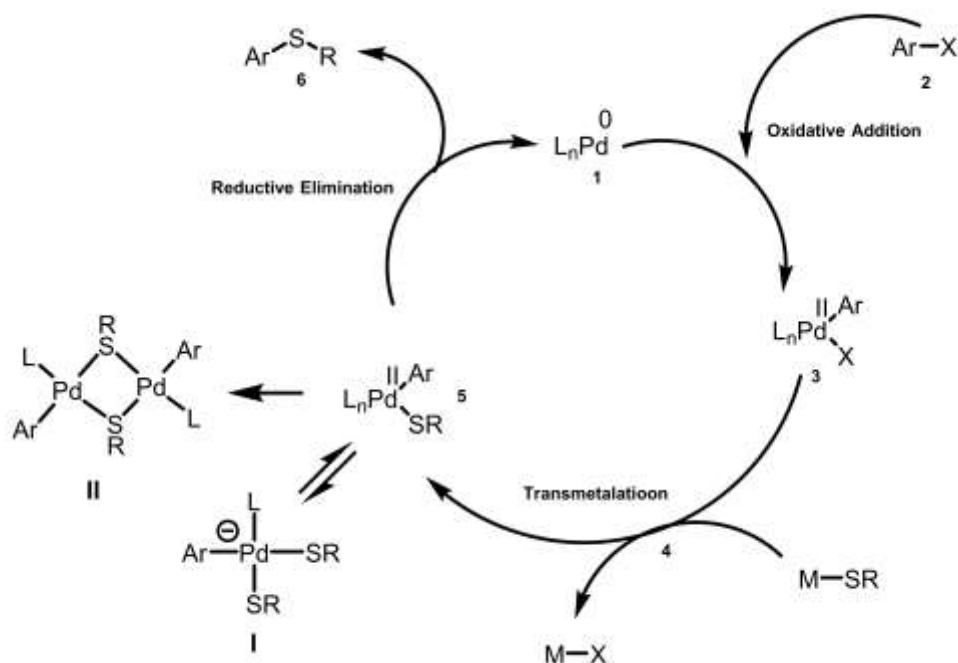


Figure 1.6. General reaction mechanism of C-S cross-coupling.³⁸

of the thiolates.³⁴ The general reaction mechanism of C-S cross-coupling is explained in Figure 1.6. In the first step, oxidative addition occurs between the halide and the palladium complex to form the organopalladium species (3). After that, the organopalladium species go through the transmetalation process with a thiol-containing compound to form organopalladium species (5). Simultaneously, off-cycle by-product bridging (II) or anionic thiolate complexes (I) are formed.

In the final step, reductive elimination takes place to form the sulfide product (6) and restores the original palladium catalyst.

1.3.2 Palladium-Based Catalytic Systems in C-S Cross-Coupling

The first practical synthesis of aryl sulfide from aryl chlorides was disclosed by Buchwald and coworkers.³⁵ This study examined a wide variety of mono- and bidentate phosphine ligands including DiPPF ligand. This catalytic system is highly effective and has good functional group tolerance. Electron-rich aryl chlorides require longer reaction times, a weaker base, and higher temperatures.

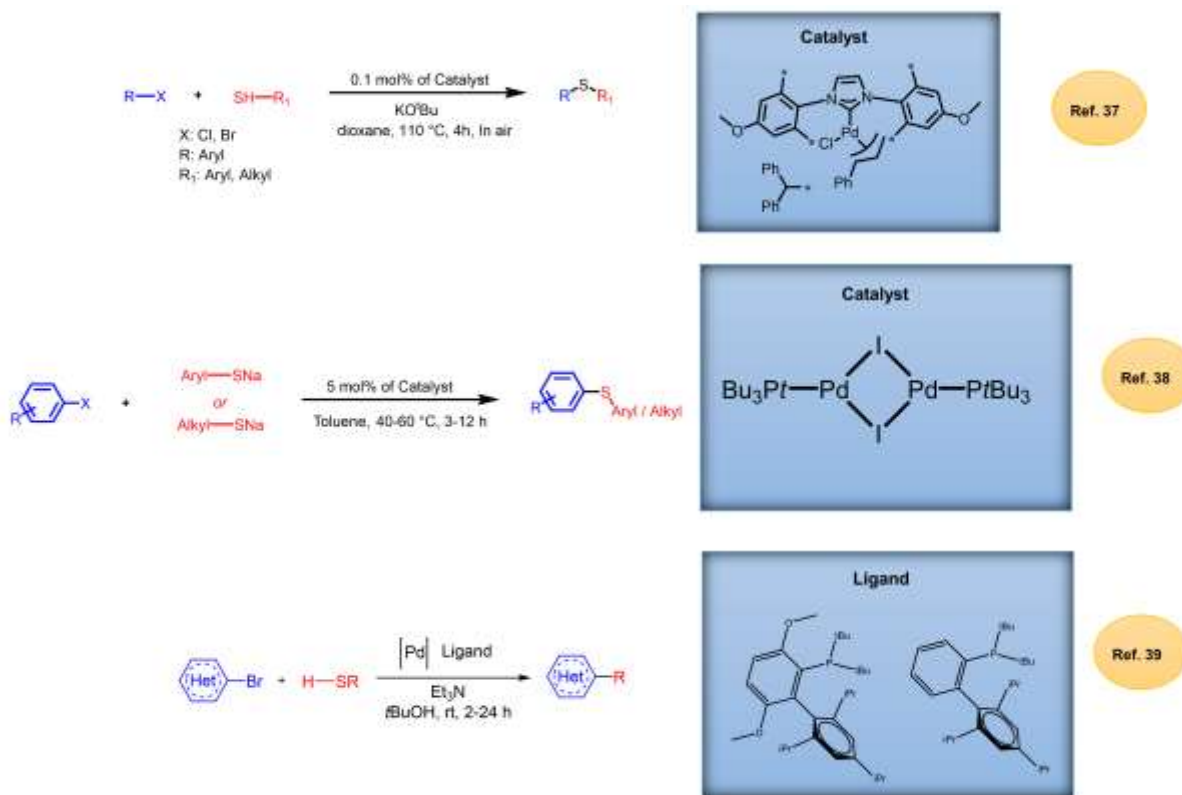


Figure 1.7. Examples of palladium-based catalytic systems in C-S cross-coupling.

Moreover, bulky monodentate phosphine ligands produced unreactive catalysts in the catalytic cycle. This conclusion was reasoned that the inactive palladium species were formed because of

the displacement of the monodentate ligands with highly nucleophilic thiolate anions. Hartwig and co-workers proposed a chiral diphosphine-based ligand that strongly coordinates with the palladium salt for producing profoundly stable and reactive catalytic species.³² The strong coordination ability of the Josiphos ligands offers more efficient catalytic systems for coupling unprotected phenols, anilines, and acids. The first Pd/C catalyzed arylation of thiols was reported by Lin and co-workers.³⁶ Nevertheless, this system only demands activated aryl bromides and iodides. Nolan and co-workers have utilized N-heterocyclic carbene (NHC)-based Pd catalyst for couplings of aryl and alkyl thiols with halides (Figure 1.7).³⁷ They have successfully employed the well-defined N-heterocyclic carbene (NHC) complex for coupling both deactivated and nonactivated aryl halides with a wide variety of alkyl and aryl thiols. Recently, a dinuclear Pd catalyst is successfully utilized as a robust method for synthesizing a wide variety of aryl sulfides through C-S cross-coupling (Figure 1.7).³⁸ This report established that the dinuclear palladium catalyst significantly reduce the off cycle poisonous byproducts. Furthermore, Buchwald and co-workers have investigated the influence of bulkiness of biaryl monophosphine ligands in C-S coupling (Figure 1.7).³⁹ As pharmaceutically relevant heterocycles are challenging to couple in harsh conditions, they have utilized the catalytic system possessing soluble bases at room temperature.

1.3.3 Photoredox Catalytic Systems in C-S Cross-Coupling

Photoredox catalysis has emerged as a powerful synthetic tool for making aryl sulfides under mild reaction settings and wider substrate scope. Oderinde et al. has reported dual photoredox/Ni-catalyzed system having an Ir-photoredox catalyst for cross-couplings of benzyl, alkyl, and aryl thiols with heteroaryl iodides.⁴⁰ Moreover, photoinduced, copper-catalyzed method

was reported for C-S cross-couplings of thiols and halides.⁴¹ More recently, Fu and co-workers reported [fac-Ir(ppy)₃] as an efficient photoredox catalyst without the dual-action having Ni catalyst for coupling aryl halides and thiols.³¹

1.3.4 Nickel-Based Catalytic Systems in C-S Cross-Coupling

In 1995, Percec et al. has reported a nickel-catalyzed system in C-S cross-coupling having 10 mol % diphenylphosphinoferrocenyl nickel(II) chloride for coupling aryl mesylates.⁴² Ying and co-workers have developed first *N*-heterocyclic carbene-based nickel catalyst in C-S cross-coupling including good to excellent yields.⁴³ Furthermore, a series of well-defined Ni(II) PNP

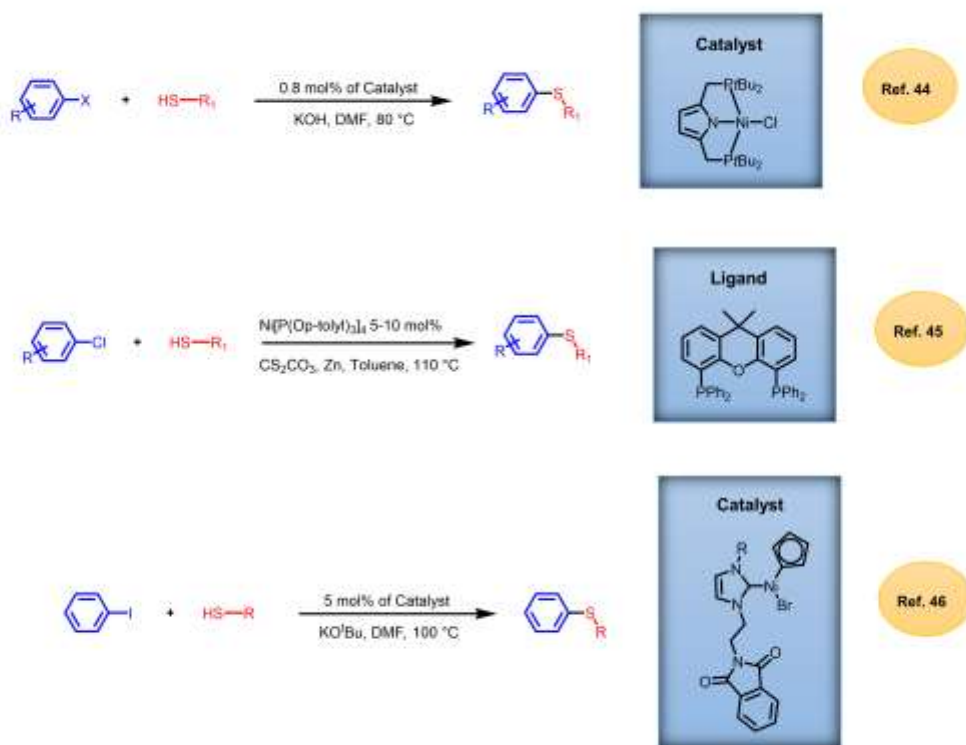


Figure 1.8. Examples of nickel-based catalytic systems in C-S cross-coupling.

pincer complexes having anion of 2,5- bis[(dialkyl/aryl-phosphino)methyl]pyrrole was reported in C-S coupling in good to excellent yields (Figure 1.8).⁴⁴ This catalytic system provided good yields

with alkyl and aryl thiols; however, limited to aryl iodides. Stewart and co-workers have developed a Ni(0) catalytic system by employing Ni[P(OPh)₃]₄ with xantphos ligands (Figure 1.8).⁴⁵ This air- and moisture stable catalytic system demonstrated wide substrate scope in the presence of Cs₂CO₂. Also, NHC-Ni(II) complexes having a phthalimide fragment and a cyclopentadienyl (Cp) ligand is published for C-S cross-coupling of iodobenzene and a wide range of thiols (Figure 1.8).⁴⁶ It was concluded that sterically demanding alkyl substrates afford excellent yields having electron-withdrawing groups.

1.3.5 Existing Challenges in C-S cross-coupling

Off-cycle thiolate complexes significantly reduce the inherent performance of Ni and Pd catalytic systems in C-S cross-coupling reactions. The poisonous off-cycle byproducts produce unreactive catalytic species.³⁸ Moreover, both of the systems require an inert atmosphere which greatly interferes with their potential application in pharmaceutical industries regarding large scale production. Moreover, glovebox reaction settings, higher temperature (100–150 °C), additives, high catalyst loading (5–50 mol%), and longer reaction times (12–72 h) significantly reduce their catalytic performance.² Furthermore, most ligand designs are expensive and require time-consuming synthetic procedures. Heterocycles are essential structural motif and used as building blocks in pharmaceutical industries. Harsh reaction conditions profoundly hinder the cross-coupling of heteroaryl moieties from both thiols and halides.³⁹ Moreover, poor catalytic performance has been identified with the alkyl thiols for alkylthiolation of aryl and heteroaryl halides.⁴⁷ Moreover, Photoredox catalysis has brought recognition as a possible solution, but generally applied iridium and ruthenium-based photosensitizers are expensive and possess inadequate substrate scope.⁴⁸

1.4 Direct C-H Bond Arylation for C-C Bond Formation

Biologically active and pharmaceutically relevant compounds heavily depend on the functionalized biaryl structural motif. Traditionally, Suzuki, Stille, or Negishi cross-coupling reactions are widely used for making those functional materials through the C-C bond formation.⁴⁹ Usually, these reactions require the coupling of an organometallic reagent and aryl halide. Particularly, the installation of activating groups in the organometallic compounds requires time-consuming additional steps and often they are very toxic. Accordingly, these processes are economically inefficient for industrial designs. Nonetheless, direct C-H bond arylation provides a viable alternative for making functionalized biaryls through C-C bond formation.³ Moreover, this synthetic tool is more facile and atom-economical. Particularly, functionalized biheteroaryl building blocks through direct C-H bond arylation has received significant recognition in the field of organic electronics, natural products, and drug discovery.⁵⁰ In this prospect, transition metal-catalyzed direct C-H bond arylation of five-membered heteroaromatics is a thriving field for producing valuable functional materials.

1.4.1 General Reaction Mechanism of Direct C-H Bond Arylation

The reaction mechanism for C-H bond activation has been investigated experimentally and computationally. The feasible pathways include heck-type coupling, electrophilic aromatic substitution, and concerted metalation-deprotonation (CMD).⁵¹ Heterocycles, for instance, thiophenes and indoles are considered to follow the CMD pathway from applying a base. For explaining the reaction mechanism, CMD coupling of thiophene and bromobenzene using cesium carbonate as a base source and palladium/phosphine catalytic system is illustrated in Figure 1.9. This catalytic system is a carboxylate-mediated process. The carbon-halogen bond is formed by

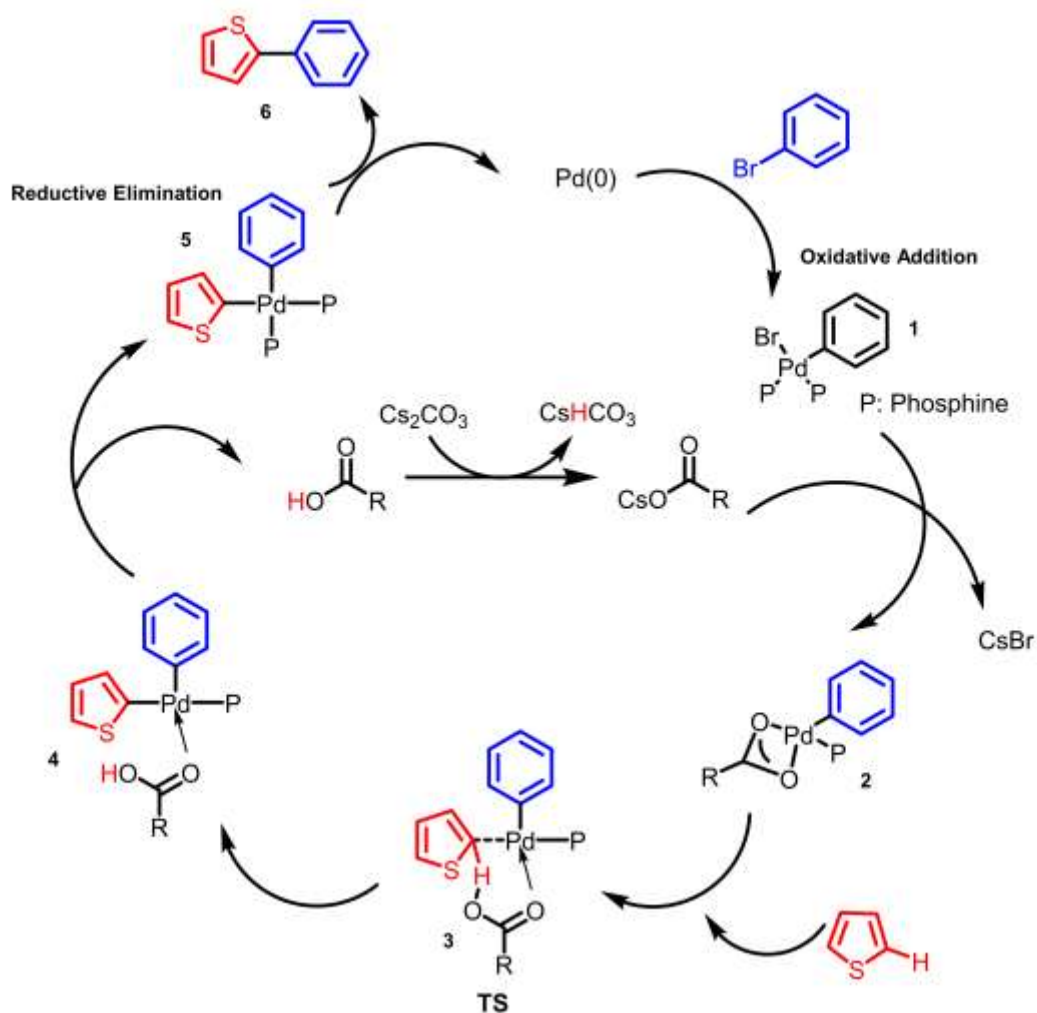


Figure 1.9. General reaction mechanism of direct C-H bond arylation.⁵¹

the oxidative addition. After that, complex 2 is formed from the exchange of the halogen ligand with carboxylate anion. Carboxylate ligand assists to deprotonate the thiophene substrate and simultaneously help to form a metal-carbon bond and proceed to the transition state TS (3). Finally, the biaryl product (6) is formed from the reductive elimination of the organopalladium species (5) and generates the original palladium catalyst.

1.4.2 Palladium-Based Catalytic Systems in Direct C-H Bond Arylation

Among other transition metals, Pd is a commonly used catalyst in the direct C-H bond arylation. For instance, Liu et al. has applied palladium pivalate for direct arylation of thiazole derivatives under ligand-free conditions. This synthetic strategy allows direct arylation of the thiazole units at the 5- position.⁵² Moreover, Greaney and co-workers reported [1,1'-bis(diphenylphosphino)ferrocene]dichloropalladium(II), complex with dichloromethane as an efficient catalyst for direct arylation of thiazoles in the aqueous medium. But this catalytic system requires longer reaction times (24-72h) (Figure 1.10).⁵³ Furthermore, Liu and co-workers have reported versatile α -diimine palladium complexes for direct arylation of five-membered heteroaromatics with good to excellent yields (Figure 1.10).⁵⁴ This catalytic system has demonstrated promising performance for synthesizing conjugated poly(hetero)arenes under aerobic conditions. Direct arylation of pyrroles has been reported with a triethanolamine-mediated palladium-catalyzed system.⁵⁵ C3 and C4 positions of heteroaromatics are challenging for direct arylation through Pd-based systems. In this possibility, palladium acetate and sterically relieved ferrocenyl diphosphane ligand are used for direct arylation of C3 or C4 of oxazoles, pyrazole, and benzofuran using a variety of electron-deficient aryl halides.⁵⁶ Recently, a catalytic system comprising of palladium acetate, tetrafluoroboric acid solution, and lithium *tert*-butoxide has been employed for attaching valuable aryl and heteroaryl moieties to 2-phenylindole.⁵⁷ Wu and co-workers have implemented bis(alkoxo)palladium(II) for direct C-H bond arylation of thiophene units including different electron-donating and electron-withdrawing groups.⁵⁸ Lately, Pd-PEPPSI-type NHC complexes have been synthesized and applied for direct arylation of heteroaromatics with (hetero)aryl bromides.⁵⁹⁻⁶⁰ For instance, a series of Pd-PEPPSI-type NHC

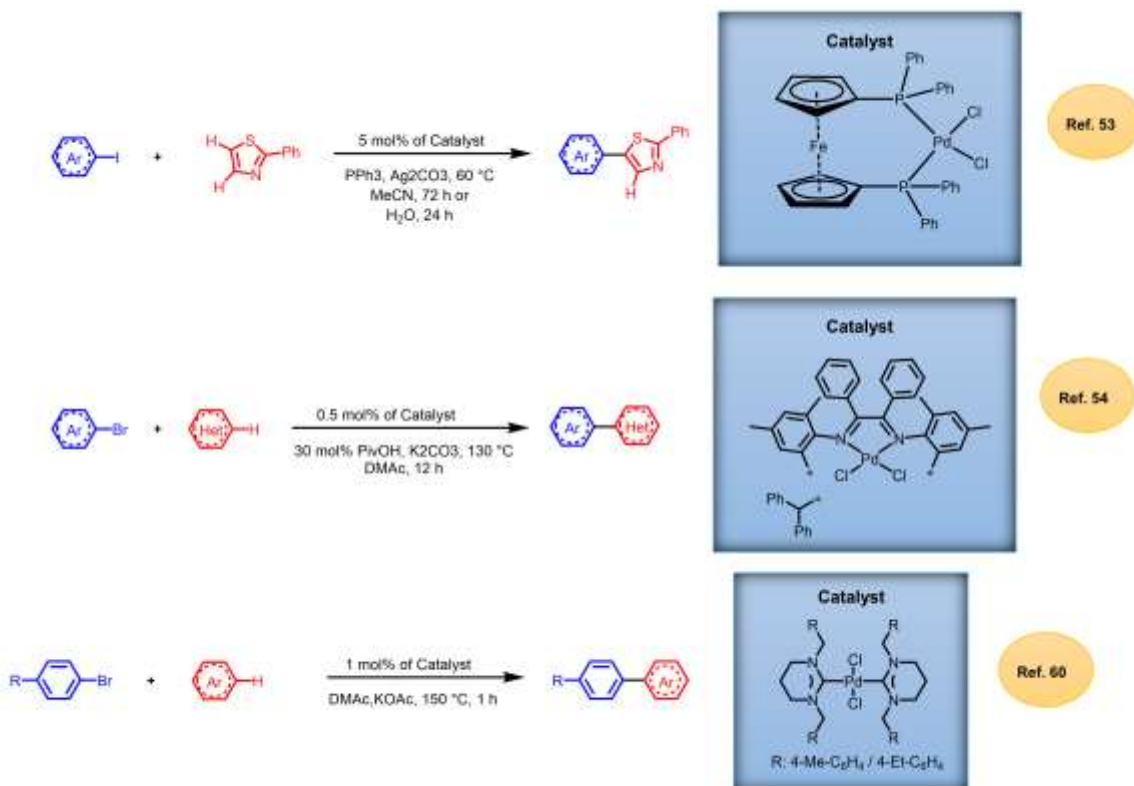


Figure 1.10. Examples of palladium-based catalytic systems in direct C-H bond arylation.

complexes containing tetrahydropyrimidin-2-ylidene ligands have been successfully applied in the direct arylation of thiophene, furan, and thiazole derivatives (Figure 1.10).⁶⁰

1.4.3 Nickel-Based Catalytic Systems in Direct C-H Bond Arylation

Compared to widely utilized Pd-catalyzed systems, Ni counterparts are less investigated in direct arylation, especially in five-membered heteroareamics. Itami and co-workers have successfully used palladium acetate and 1,1'-bis(diphenylphosphino)ferrocene (dppf) ligand for direct arylation of thiazole, oxazole, benzothiazole, and benzoxazole as heteroarene coupling partners (Figure 1.11).⁶¹ Miura and coworkers developed a nickel-catalyzed system by employing commercially accessible nickel bromide with 1,10-phenanthroline as a ligand source.⁶² This

catalytic tool afforded useful biaryl compounds from oxazoles and thiazoles. In 2010, Hachiya et al. has reported

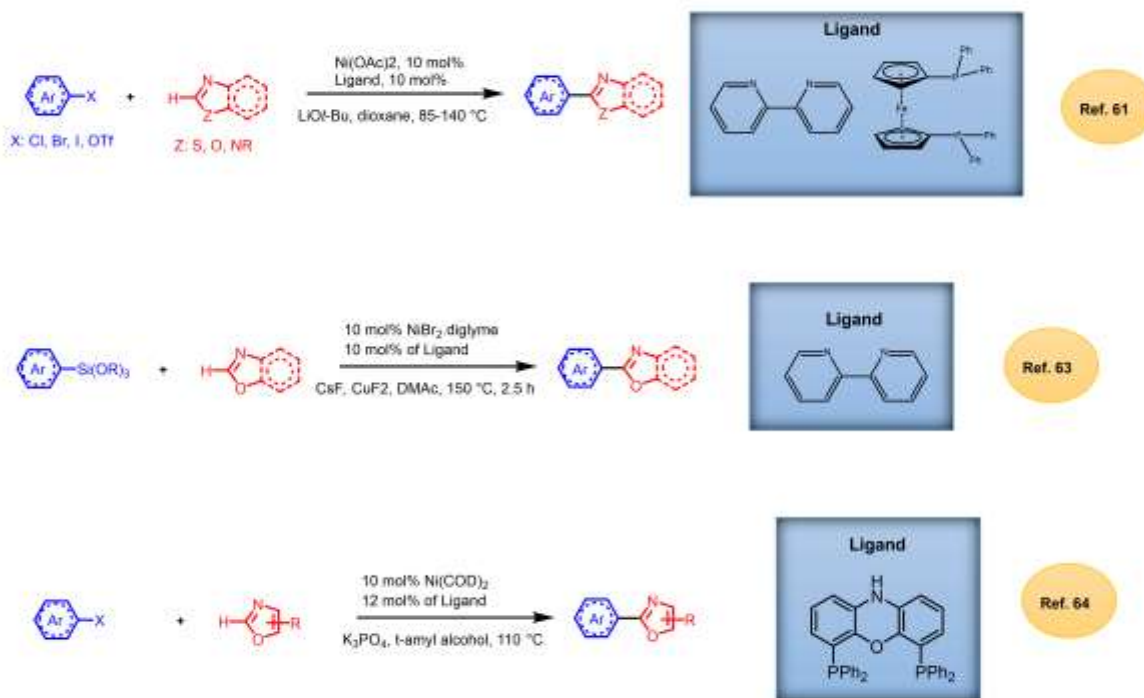


Figure 1.11. Examples of nickel-based catalytic systems in direct C-H bond arylation.

nickel(II) bromide 2-methoxyethyl ether complex as an efficient catalyst for applying in direct arylation of heteroaromatics with organosilicon reagents (Figure 1.11).⁶³ This catalytic system has demonstrated the potential C-H functionalization of organosilicon compounds for synthesizing biheteroaromatic monomers. More recently, commercially available bis(1,5-cyclooctadiene)nickel(0) has been implemented for direct arylation of oxazole and benzoxazole (Figure 1.11).⁶⁴ Notably, both aryl chlorides and bromides were successfully coupled with the electrophiles containing free OH and NH groups.

1.4.4 Existing Challenges in Ni and Pd-Catalyzed Direct C-H Bond Arylation

Both Ni and Pd systems are facing inherent challenges from the air- and moisture sensitivities. These synthetic tools often require the usage of an inert atmosphere.⁶² Also, well-defined catalysts are very limited compared to the in situ generations from expensive metal precursors. Moreover, they greatly suffer from high catalyst loading (5 – 10 mol%), high temperature (100 – 150 °C), and longer reaction time (12 – 36 h).^{54, 65} Consequently, a robust catalytic system having good to excellent substrate scope and functional group tolerance is yet to be recognized in the direct C-H bond arylation of five-membered heteroaromatics.

1.5 Conclusion

Various nickel and palladium-catalyzed systems were discussed for Suzuki–Miyaura cross-coupling, carbon-sulfur cross-coupling, and direct arylation. Both in situ and well-defined catalytic tools were compared for analyzing the catalytic performance. Especially, the ligand design in the catalytic system has profound effects regarding the substrate scope and functional group tolerance. All the cross-coupling tools have existing challenges including air- and moisture sensitivities. Moreover, metal precursors for in situ generations of catalytic species are expensive, whereas, for the well-defined catalysts, the ligand design needs multi-step time-consuming procedures. Consequently, these setbacks significantly hinder the potential applicability of the existing nickel and palladium-based systems in cross-coupling chemistry.

1.6 References

- (1) Yin; Liebscher, J. Carbon–Carbon Coupling Reactions Catalyzed by Heterogeneous Palladium Catalysts. *Chem. Rev.* **2007**, *107*, 133-173.
- (2) Lee, C.-F.; Liu, Y.-C.; Badsara, S. S. Transition-Metal-Catalyzed C–S Bond Coupling Reaction. *Chem. - Asian J.* **2014**, *9*, 706-722.

- (3) Mainville, M.; Leclerc, M. Direct (Hetero)arylation: A Tool for Low-Cost and Eco-Friendly Organic Photovoltaics. *ACS Appl. Polym. Mater.* **2020**.
- (4) Han, F.-S. Transition-metal-catalyzed Suzuki–Miyaura cross-coupling reactions: a remarkable advance from palladium to nickel catalysts. *Chem. Soc. Rev.* **2013**, *42*, 5270-5298.
- (5) Torborg, C.; Beller, M. Recent Applications of Palladium-Catalyzed Coupling Reactions in the Pharmaceutical, Agrochemical, and Fine Chemical Industries. *Adv. Synth. Catal.* **2009**, *351*, 3027-3043.
- (6) Miyaura, N.; Suzuki, A. Stereoselective synthesis of arylated (E)-alkenes by the reaction of alk-1-enylboranes with aryl halides in the presence of palladium catalyst. *J. Chem. Soc., Chem. Commun.* **1979**, 866-867.
- (7) Miyaura, N.; Yamada, K.; Suzuki, A. A new stereospecific cross-coupling by the palladium-catalyzed reaction of 1-alkenylboranes with 1-alkenyl or 1-alkynyl halides. *Tetrahedron Lett.* **1979**, *20*, 3437-3440.
- (8) Miyaura, N.; Suzuki, A. Palladium-Catalyzed Cross-Coupling Reactions of Organoboron Compounds. *Chem. Rev.* **1995**, *95*, 2457-2483.
- (9) Hussain, I.; Capricho, J.; Yawer, M. A. Synthesis of Biaryls via Ligand-Free Suzuki–Miyaura Cross-Coupling Reactions: A Review of Homogeneous and Heterogeneous Catalytic Developments. *Adv. Synth. Catal.* **2016**, *358*, 3320-3349.
- (10) Marck, G.; Villiger, A.; Buchecker, R. Aryl couplings with heterogeneous palladium catalysts. *Tetrahedron Lett.* **1994**, *35*, 3277-3280.
- (11) Tagata, T.; Nishida, M. Palladium Charcoal-Catalyzed Suzuki–Miyaura Coupling To Obtain Arylpyridines and Arylquinolines. *J. Org. Chem.* **2003**, *68*, 9412-9415.
- (12) Mandali, P. K.; Chand, D. K. Palladium nanoparticles catalyzed Suzuki cross-coupling reactions in ambient conditions. *Catal. Commun.* **2013**, *31*, 16-20.
- (13) Nasrollahzadeh, M.; Issaabadi, Z.; Varma, R. S. Magnetic Lignosulfonate-Supported Pd Complex: Renewable Resource-Derived Catalyst for Aqueous Suzuki–Miyaura Reaction. *ACS Omega* **2019**, *4*, 14234-14241.
- (14) Fan, M.; Wang, W. D.; Wang, X.; Zhu, Y.; Dong, Z. Ultrafine Pd Nanoparticles Modified on Azine-Linked Covalent Organic Polymers for Efficient Catalytic Suzuki–Miyaura Coupling Reaction. *Ind. Eng. Chem. Res.* **2020**, *59*, 12677-12685.
- (15) Kinzel, T.; Zhang, Y.; Buchwald, S. L. A New Palladium Precatalyst Allows for the Fast Suzuki–Miyaura Coupling Reactions of Unstable Polyfluorophenyl and 2-Heteroaryl Boronic Acids. *J. Am. Chem. Soc.* **2010**, *132*, 14073-14075.

- (16) Chartoire, A.; Lesieur, M.; Falivene, L.; Slawin, A. M. Z.; Cavallo, L.; Cazin, C. S. J.; Nolan, S. P. [Pd(IPr*)(cinnamyl)Cl]: An Efficient Pre-catalyst for the Preparation of Tetra-ortho-substituted Biaryls by Suzuki–Miyaura Cross-Coupling. *Chem. - Eur. J.* **2012**, *18*, 4517-4521.
- (17) Li, D.-H.; He, X.-X.; Xu, C.; Huang, F.-D.; Liu, N.; Shen, D.-S.; Liu, F.-S. N-Heterocarbene Palladium Complexes with Dianisole Backbones: Synthesis, Structure, and Catalysis. *Organometallics* **2019**, *38*, 2539-2552.
- (18) Rosen, B. M.; Quasdorf, K. W.; Wilson, D. A.; Zhang, N.; Resmerita, A.-M.; Garg, N. K.; Percec, V. Nickel-Catalyzed Cross-Couplings Involving Carbon–Oxygen Bonds. *Chem. Rev.* **2011**, *111*, 1346-1416.
- (19) Inada, K.; Miyaura, N. Synthesis of Biaryls via Cross-Coupling Reaction of Arylboronic Acids with Aryl Chlorides Catalyzed by NiCl₂/Triphenylphosphine Complexes. *Tetrahedron* **2000**, *56*, 8657-8660.
- (20) Zhang, K.; Conda-Sheridan, M.; R. Cooke, S.; Louie, J. N-Heterocyclic Carbene Bound Nickel(I) Complexes and Their Roles in Catalysis. *Organometallics* **2011**, *30*, 2546-2552.
- (21) Indolese, A. F. Suzuki-type coupling of chloroarenes with arylboronic acids catalysed by nickel complexes. *Tetrahedron Lett.* **1997**, *38*, 3513-3516.
- (22) Zhao, Y.-L.; Li, Y.; Li, S.-M.; Zhou, Y.-G.; Sun, F.-Y.; Gao, L.-X.; Han, F.-S. A Highly Practical and Reliable Nickel Catalyst for Suzuki–Miyaura Coupling of Aryl Halides. *Adv. Synth. Catal.* **2011**, *353*, 1543-1550.
- (23) Leowanawat, P.; Zhang, N.; Safi, M.; Hoffman, D. J.; Fryberger, M. C.; George, A.; Percec, V. trans-Chloro(1-Naphthyl)bis(triphenylphosphine)nickel(II)/PCy₃ Catalyzed Cross-Coupling of Aryl and Heteroaryl Neopentylglycolboronates with Aryl and Heteroaryl Mesylates and Sulfamates at Room Temperature. *J. Org. Chem.* **2012**, *77*, 2885-2892.
- (24) Ge, S.; Hartwig, J. F. Highly Reactive, Single-Component Nickel Catalyst Precursor for Suzuki–Miyuara Cross-Coupling of Heteroaryl Boronic Acids with Heteroaryl Halides. *Angew. Chem., Int. Ed.* **2012**, *51*, 12837-12841.
- (25) Anderson, T. J.; Jones, G. D.; Vicic, D. A. Evidence for a Ni⁰ Active Species in the Catalytic Cross-Coupling of Alkyl Electrophiles. *J. Am. Chem. Soc.* **2004**, *126*, 8100-8101.
- (26) Talukder, M. M.; Cue, J. M. O.; Miller, J. T.; Gamage, P. L.; Aslam, A.; McCandless, G. T.; Biewer, M. C.; Stefan, M. C. Ligand Steric Effects of α -Diimine Nickel(II) and Palladium(II) Complexes in the Suzuki–Miyaura Cross-Coupling Reaction. *ACS Omega* **2020**, *5*, 24018-24032.

- (27) Madera, J.; Slattery, M.; Arman, H. D.; Tonzetich, Z. J. Suzuki-Miyaura coupling catalyzed by a Ni(II) PNP pincer complex: Scope and mechanistic insights. *Inorg. Chim. Acta* **2020**, *504*, 119457.
- (28) Duczynski, J.; Sobolev, A. N.; Moggach, S. A.; Dorta, R.; Stewart, S. G. The Synthesis and Catalytic Activity of New Mixed NHC-Phosphite Nickel(0) Complexes. *Organometallics* **2020**, *39*, 105-115.
- (29) Bernhammer, J. C.; Huynh, H. V. Nickel(II) Benzimidazolin-2-ylidene Complexes with Thioether-Functionalized Side Chains as Catalysts for Suzuki–Miyaura Cross-Coupling. *Organometallics* **2014**, *33*, 5845-5851.
- (30) Molander, G. A.; Canturk, B.; Kennedy, L. E. Scope of the Suzuki–Miyaura Cross-Coupling Reactions of Potassium Heteroaryltrifluoroborates. *J. Org. Chem.* **2009**, *74*, 973-980.
- (31) Jiang, M.; Li, H.; Yang, H.; Fu, H. Room-Temperature Arylation of Thiols: Breakthrough with Aryl Chlorides. *Angew. Chem., Int. Ed.* **2017**, *56*, 874-879.
- (32) Fernández-Rodríguez, M. A.; Shen, Q.; Hartwig, J. F. A General and Long-Lived Catalyst for the Palladium-Catalyzed Coupling of Aryl Halides with Thiols. *J. Am. Chem. Soc.* **2006**, *128*, 2180-2181.
- (33) Migita, T.; Shimizu, T.; Asami, Y.; Shiobara, J.-i.; Kato, Y.; Kosugi, M. The Palladium Catalyzed Nucleophilic Substitution of Aryl Halides by Thiolate Anions. *Bull. Chem. Soc. Jpn.* **1980**, *53*, 1385-1389.
- (34) Eichman, C. C.; Stambuli, J. P. Transition Metal Catalyzed Synthesis of Aryl Sulfides. *Molecules* **2011**, *16*, 590-608.
- (35) Murata, M.; Buchwald, S. L. A general and efficient method for the palladium-catalyzed cross-coupling of thiols and secondary phosphines. *Tetrahedron* **2004**, *60*, 7397-7403.
- (36) Jiang, Z.; She, J.; Lin, X. Palladium on Charcoal as a Recyclable Catalyst for C–S Cross-Coupling of Thiols with Aryl Halides under Ligand-Free Conditions. *Adv. Synth. Catal.* **2009**, *351*, 2558-2562.
- (37) Bastug, G.; Nolan, S. P. Carbon–Sulfur Bond Formation Catalyzed by [Pd(IPr*OMe)(cin)Cl] (cin = cinnamyl). *J. Org. Chem.* **2013**, *78*, 9303-9308.
- (38) Scattolin, T.; Senol, E.; Yin, G.; Guo, Q.; Schoenebeck, F. Site-Selective C–S Bond Formation at C–Br over C–OTf and C–Cl Enabled by an Air-Stable, Easily Recoverable, and Recyclable Palladium(I) Catalyst. *Angew. Chem., Int. Ed.* **2018**, *57*, 12425-12429.

- (39) Xu, J.; Liu, R. Y.; Yeung, C. S.; Buchwald, S. L. Monophosphine Ligands Promote Pd-Catalyzed C–S Cross-Coupling Reactions at Room Temperature with Soluble Bases. *ACS Catal.* **2019**, *9*, 6461-6466.
- (40) Oderinde, M. S.; Frenette, M.; Robbins, D. W.; Aquila, B.; Johannes, J. W. Photoredox Mediated Nickel Catalyzed Cross-Coupling of Thiols With Aryl and Heteroaryl Iodides via Thiyl Radicals. *J. Am. Chem. Soc.* **2016**, *138*, 1760-1763.
- (41) Uyeda, C.; Tan, Y.; Fu, G. C.; Peters, J. C. A New Family of Nucleophiles for Photoinduced, Copper-Catalyzed Cross-Couplings via Single-Electron Transfer: Reactions of Thiols with Aryl Halides Under Mild Conditions (0 °C). *J. Am. Chem. Soc.* **2013**, *135*, 9548-9552.
- (42) Percec, V.; Bae, J.-Y.; Hill, D. H. Aryl Mesylates in Metal Catalyzed Homo- and Cross-Coupling Reactions. 4. Scope and Limitations of Aryl Mesylates in Nickel Catalyzed Cross-Coupling Reactions. *J. Org. Chem.* **1995**, *60*, 6895-6903.
- (43) Zhang, Y.; Ngeow, K. C.; Ying, J. Y. The First N-Heterocyclic Carbene-Based Nickel Catalyst for C–S Coupling. *Org. Lett.* **2007**, *9*, 3495-3498.
- (44) Venkanna, G. T.; Arman, H. D.; Tonzetich, Z. J. Catalytic C–S Cross-Coupling Reactions Employing Ni Complexes of Pyrrole-Based Pincer Ligands. *ACS Catal.* **2014**, *4*, 2941-2950.
- (45) Jones, K. D.; Power, D. J.; Bierer, D.; Gericke, K. M.; Stewart, S. G. Nickel Phosphite/Phosphine-Catalyzed C–S Cross-Coupling of Aryl Chlorides and Thiols. *Org. Lett.* **2018**, *20*, 208-211.
- (46) Rodríguez-Cruz, M. A.; Hernández-Ortega, S.; Valdés, H.; Rufino-Felipe, E.; Morales-Morales, D. CS cross-coupling catalyzed by a series of easily accessible, well defined Ni(II) complexes of the type [(NHC)Ni(Cp)(Br)]. *J. Catal.* **2020**, *383*, 193-198.
- (47) Gehrtz, P. H.; Geiger, V.; Schmidt, T.; Sršan, L.; Fleischer, I. Cross-Coupling of Chloro(hetero)arenes with Thiolates Employing a Ni(0)-Precatalyst. *Org. Lett.* **2019**, *21*, 50-55.
- (48) Sikari, R.; Sinha, S.; Das, S.; Saha, A.; Chakraborty, G.; Mondal, R.; Paul, N. D. Achieving Nickel Catalyzed C–S Cross-Coupling under Mild Conditions Using Metal–Ligand Cooperativity. *J. Org. Chem.* **2019**, *84*, 4072-4085.
- (49) Mercier, L. G.; Leclerc, M. Direct (Hetero)Arylation: A New Tool for Polymer Chemists. *Acc. Chem. Res.* **2013**, *46*, 1597-1605.
- (50) Zhang, L.; Colella, N. S.; Cherniawski, B. P.; Mannsfeld, S. C. B.; Briseno, A. L. Oligothiophene Semiconductors: Synthesis, Characterization, and Applications for Organic Devices. *ACS Appl. Mater. Interfaces* **2014**, *6*, 5327-5343.

- (51) Alberico, D.; Scott, M. E.; Lautens, M. Aryl–Aryl Bond Formation by Transition-Metal-Catalyzed Direct Arylation. *Chem. Rev.* **2007**, *107*, 174-238.
- (52) Liu, X.-W.; Shi, J.-L.; Yan, J.-X.; Wei, J.-B.; Peng, K.; Dai, L.; Li, C.-G.; Wang, B.-Q.; Shi, Z.-J. Regioselective Arylation of Thiazole Derivatives at 5-Position via Pd Catalysis under Ligand-Free Conditions. *Org. Lett.* **2013**, *15*, 5774-5777.
- (53) Turner, G. L.; Morris, J. A.; Greaney, M. F. Direct Arylation of Thiazoles on Water. *Angew. Chem., Int. Ed.* **2007**, *46*, 7996-8000.
- (54) Ouyang, J.-S.; Li, Y.-F.; Shen, D.-S.; Ke, Z.; Liu, F.-S. Bulky α -diimine palladium complexes: highly efficient for direct C–H bond arylation of heteroarenes under aerobic conditions. *Dalton Trans.* **2016**, *45*, 14919-14927.
- (55) Jafarpour, F.; Rahiminejadan, S.; Hazrati, H. Triethanolamine-Mediated Palladium-Catalyzed Regioselective C-2 Direct Arylation of Free NH-Pyrroles. *J. Org. Chem.* **2010**, *75*, 3109-3112.
- (56) Roy, D.; Mom, S.; Royer, S.; Lucas, D.; Hierso, J.-C.; Doucet, H. Palladium-Catalyzed Direct Arylation of Heteroaromatics with Activated Aryl Chlorides Using a Sterically Relieved Ferrocenyl-Diphosphane. *ACS Catal.* **2012**, *2*, 1033-1041.
- (57) Yamaguchi, M.; Hagiwara, R.; Gayama, K.; Suzuki, K.; Sato, Y.; Konishi, H.; Manabe, K. Direct C3-Selective Arylation of N-Unsubstituted Indoles with Aryl Chlorides, Triflates, and Nonaflates Using a Palladium–Dihydroxyterphenylphosphine Catalyst. *J. Org. Chem.* **2020**, *85*, 10902-10912.
- (58) Li, Y.; Wang, J.; Huang, M.; Wang, Z.; Wu, Y.; Wu, Y. Direct C–H Arylation of Thiophenes at Low Catalyst Loading of a Phosphine-Free Bis(alkoxo)palladium Complex. *J. Org. Chem.* **2014**, *79*, 2890-2897.
- (59) Zhao, Q.; Meng, G.; Nolan, S. P.; Szostak, M. N-Heterocyclic Carbene Complexes in C–H Activation Reactions. *Chem. Rev.* **2020**, *120*, 1981-2048.
- (60) Karaca, E. Ö.; Gürbüz, N.; Özdemir, İ.; Doucet, H.; Şahin, O.; Büyükgüngör, O.; Çetinkaya, B. Palladium Complexes with Tetrahydropyrimidin-2-ylidene Ligands: Catalytic Activity for the Direct Arylation of Furan, Thiophene, and Thiazole Derivatives. *Organometallics* **2015**, *34*, 2487-2493.
- (61) Canivet, J.; Yamaguchi, J.; Ban, I.; Itami, K. Nickel-Catalyzed Biaryl Coupling of Heteroarenes and Aryl Halides/Triflates. *Org. Lett.* **2009**, *11*, 1733-1736.
- (62) Hachiya, H.; Hirano, K.; Satoh, T.; Miura, M. Nickel-Catalyzed Direct Arylation of Azoles with Aryl Bromides. *Org. Lett.* **2009**, *11*, 1737-1740.

(63) Hachiya, H.; Hirano, K.; Satoh, T.; Miura, M. Nickel-Catalyzed Direct C–H Arylation and Alkenylation of Heteroarenes with Organosilicon Reagents. *Angew. Chem., Int. Ed.* **2010**, *49*, 2202-2205.

(64) Larson, H.; Schultz, D.; Kalyani, D. Ni-Catalyzed C–H Arylation of Oxazoles and Benzoxazoles Using Pharmaceutically Relevant Aryl Chlorides and Bromides. *J. Org. Chem.* **2019**, *84*, 13092-13103.

(65) Song, A. X.; Zeng, X.-X.; Ma, B.-B.; Xu, C.; Liu, F.-S. Direct (Hetero)arylation of Heteroarenes Catalyzed by Unsymmetrical Pd-PEPPSI-NHC Complexes under Mild Conditions. *Organometallics* **2020**, *39*, 3524-3534.

CHAPTER 2

LIGAND STERIC EFFECTS OF α -DIIMINE NICKEL(II) AND PALLADIUM(II) COMPLEXES IN THE SUZUKI–MIYAJIURA CROSS-COUPPLING REACTION

Authors: Md MuktaDir Talukder, John Michael O. Cue, Justin T. Miller, Prabhath L. Gamage,
Amina Aslam, Gregory T. McCandless, Michael C. Biewer, and Mihaela C. Stefan*

The Department of Chemistry and Biochemistry, BE26

The University of Texas at Dallas

800 West Campbell Road

Richardson, Texas 75080-3021

Reprinted (Adapted) with permission from Talukder, M. M.; Cue, J. M. O.; Miller, J. T.; Gamage, P. L.; Aslam, A.; McCandless, G. T.; Biewer, M. C.; Stefan, M. C. Ligand Steric Effects of α -Diimine Nickel(II) and Palladium(II) Complexes in the Suzuki–Miyajura Cross-Coupling Reaction. *ACS Omega* **2020**, *5*, 24018-24032. Copyright (2020) American Chemical Society.

2.1 Abstract

Nickel catalysts represent a low cost and environmentally friendly alternative to palladium-based catalytic systems in Suzuki–Miyaura cross-coupling (SMC) reactions. However, nickel catalysts have suffered from poor air, moisture, and thermal stabilities, especially at high catalyst loading, requiring controlled reaction conditions. In this report, we examine a family of mono and dinuclear Ni(II) and Pd(II) complexes with a diverse and versatile α -diimine ligand environment for SMC reactions. To evaluate the ligand steric effects, including the bite angle in the reaction outcomes, the structural variation of the complexes was achieved by incorporating iminopyridine and acenaphthene-based ligands. Moreover, the impact of substrate bulkiness was investigated by reacting various aryl bromides with phenylboronic acid, 2-naphthylboronic acid, and 9-phenanthracenylboronic acid. Yields were best with the dinuclear complex, being nearly quantitative (93–99%), followed by the mononuclear complexes, giving yields of 78–98%. Consequently, α -diimine-based ligands have the potential to deliver Ni-based systems as sustainable catalysts in SMC.

2.2 Introduction

The Suzuki-Miyaura cross-coupling (SMC) reaction is one of the most prevalent methods of synthesizing biaryl compounds through the C-C bond constructions in the pharmaceutical industry.^{1–5} Compared to other transition metals, palladium-based catalytic systems such as Buchwald-type palladacycles,⁶ Nolan-type allyl-based pre-catalysts,^{7–9} Organ-type PEPPSI-based pre-catalysts,^{10–12} and others,^{13–18} have promising substrate versatility. However, the auxiliary ligands for these catalysts are expensive and often require time-consuming and complex synthesis

procedures.^{19,20} Due to the cost and toxicity of palladium, nickel-based catalysts have received considerable recognition for their use in SMC in recent years.^{20–25}

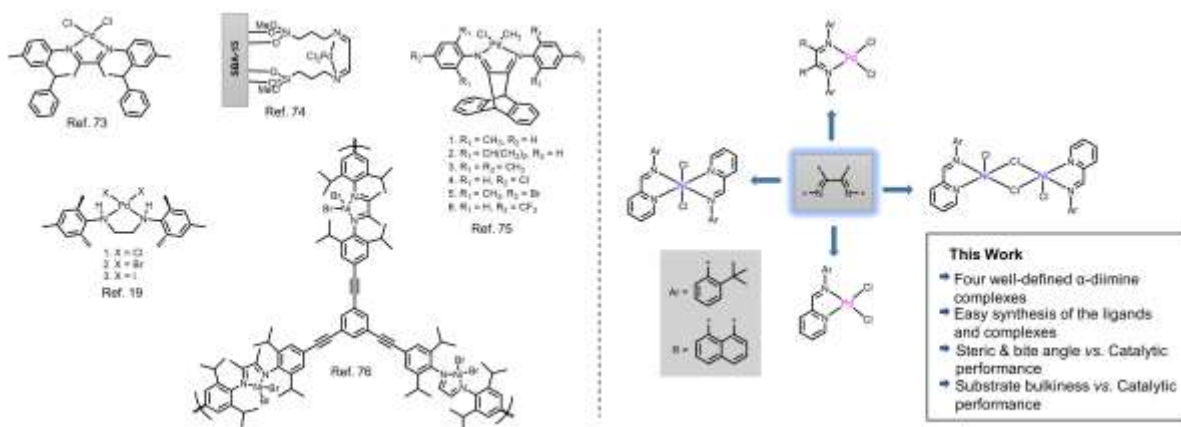


Figure 2.1. Previous examples of α -diimine-based catalysts and summary of current work in SMC.

The smaller size of Ni(0) relative Pd(0) results in higher nucleophilicity and facilitates the oxidative addition of non-traditional substrates.^{20,24,25–29} In the early stages of nickel catalyst development, Ni(COD)₂ (COD = 1,5-cyclooctadiene) was used as a Ni(0) precursor along with a free ligand for producing catalytically active species.^{23,25,30,31} Ni(COD)₂ is relatively expensive, thermally unstable, and air-sensitive.^{20,32,33} As opposed to nickel-based systems in SMC, various well-defined palladium catalysts have been reported.^{20,34–36} Consequently, studies have been conducted for the development of more practicable well-defined nickel-based catalysts.^{32,33,37–46} Nonetheless, the greater expansion of nickel-based catalytic systems in SMC is facing inherent challenges from the activation of pre-catalysts,^{41,43,44} and air- and moisture sensitivity.^{20,25,37,43,46} Moreover, high catalyst loading (2.5–10 mol%),^{25,41,43,44,46,47} elevated temperature (100–130 °C),^{25,44,47–50} and prolonged reaction time (12–48 h)^{25,41,44,46,48,50,51} significantly affect their prospects in SMC compared to the Pd counterparts. Also, there is a need for a large excess of the

boronic acid (2.5–5 equivalent)^{25,41,43,44,48} for generating the desired yield due to competitive protodeboronation.⁵²

Sterically hindered ligands are perceived to be advantageous in SMC reactions because they facilitate the oxidative addition and reductive elimination for incorporating a wide variety of substrates.^{17,53–59} Due to these factors, α -diimine-based catalysts represent an outstanding candidate for SMC. After the introduction of Brookhart-type α -diimine-based transition metal catalysts, notable progress has been made in olefin polymerization owing to its structural versatility, facile synthesis, and air, moisture, and thermal stabilities.^{60–67} Moreover, steric and electronic properties are highly adjustable through the insertion of the various functional groups in the ligand environment.^{65,68–70} In SMC, the bulky α -diimine ligand containing electron-donating groups in the *N*-aryl moieties enhances the catalytic performance from generating the catalytic species *in situ* with the metal precursor.^{71,72} Although well-defined α -diimine complexes are less explored in SMC, and their outcomes are promising (Figure 2.1). For instance, in milder reaction settings, moderate activity (Yields = 60–95%) of an α -diimine Pd(II) complex was observed possessing chiral *sec*-phenethyl groups in the ligand environment.⁷³ Moreover, Pd-diimine with functionalized mesoporous silica SBA-15 is reported as a highly efficient catalyst for coupling various aryl halides, including chlorinated aromatics.⁷⁴ Furthermore, a series of α -diimine methyl palladium chloride complexes bearing bulky 9,10-dihydro-9,10-ethanoanthracene-11,12-diimine moieties have been applied in SMC with a low concentration of 0.01 mol%.⁷⁵ This study also established that electron-donating and bulky substituents in the *N*-aryl rings are responsible for superior catalytic performance. Liu et al.¹⁹ developed Pd(II) complexes containing *N,N'*-bis(2,4,6-trimethylphenyl)ethane-1,2-diamine), analogous to an α -diimine ligand for SMC of aryl chlorides

having 0.01 mol % of catalyst loading with excellent yields (90-95%). In pursuit of a sustainable alternative to the Pd catalysts, a porous organic polymer-based Ni(II)- α -diimine was successfully synthesized and used in SMC of various aryl halides and boronic acids.⁷⁶

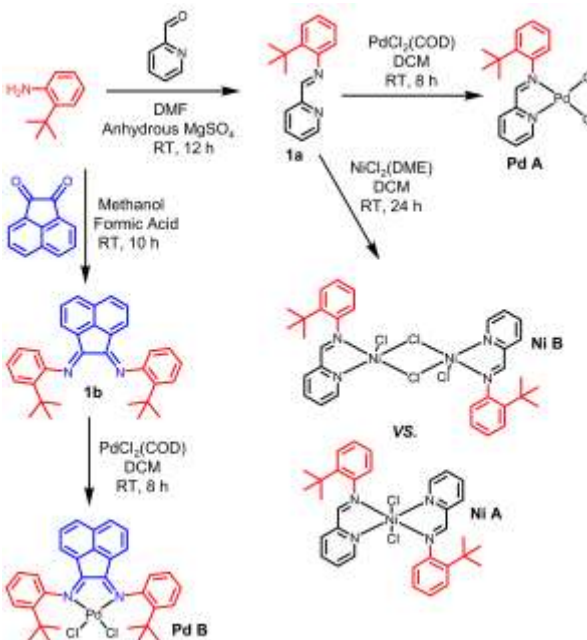
In this report, to explore the promising features of the α -diimine system in SMC, four nickel (II) and palladium (II) complexes were synthesized from iminopyridine and acenaphthene-based ligands. Reaction outcomes were analyzed and correlated with the steric attributes and coordination nature of the synthesized mono- and dinuclear complexes. Also, the influence of the sterics of the substrates was examined by reacting various aryl bromides with phenylboronic acid, 2-naphthylboronic acid, and 9-phenanthracenylboronic acid.

2.3 Results and discussion

2.3.1 Synthesis of α -Diimine Nickel (II) and Palladium (II) Complexes.

The ligands were obtained through condensation reactions shown in Scheme 2.1. The iminopyridine-based ligand (**1a**) was synthesized from the condensation reaction of 2-pyridinecarboxaldehyde and 2-*tert*-butylaniline in dimethylformamide. The acenaphthene-based ligand (**1b**) was prepared from the condensation reaction of acenaphthoquinone and 2-*tert*-butylaniline in methanol containing a small amount of formic acid.⁷⁷ The reaction of NiCl₂(DME) (DME = ethylene glycol dimethyl ether) with one equivalent of the ligand 1a in dichloromethane produced the mono-ligated Ni B, whereas two equivalents afforded the bis-ligated Ni A complex.⁷⁸ For the synthesis of the Pd(II) Complexes, Pd A and Pd B, PdCl₂(COD) (COD = 1,5-cyclooctadiene) was reacted in dichloromethane with one equivalent of the iminopyridine and acenaphthene-based ligands, respectively.⁷⁷ These complexes were obtained as light-yellow, dark-

yellow, or orange powder in 68–85% yields. To characterize the synthesized complexes, elemental analysis and X-ray crystallography were performed.



Scheme 2.1. Synthesis of α -diimine nickel (II) and palladium (II) complexes.

2.3.2 X-ray Crystallography

ORTEP diagrams of the synthesized complexes are displayed in Figure 2.2. X-ray diffraction analysis of the Ni(II) complexes was conducted after obtaining suitable single crystals by slow diffusion of diethyl ether into a saturated methanol solution at room temperature. The bis-ligated complex, **Ni A**, exhibited a distorted octahedral geometry. Four nitrogen atoms originating from iminopyridine ligands are coordinated directly to the nickel center along with two terminal chlorine atoms. The monoligated complex, **Ni B**, formed a distorted octahedral geometry as a centrosymmetric dimer at the two-nickel center. Each nickel atom is coordinated with two nitrogen atoms from an iminopyridine ligand, two bridging chlorine atoms, one terminal chlorine, and one additional oxygen from the methanol solvent. Additionally, ether solvent molecules are filling the

structural voids in the structural packing of **Ni B**. Moreover, N-aryl rings having tert-butyl group both in **Ni A** and **Ni B** are approximately perpendicular to the coordination plane and opposite to each other. The free chlorine atom attached to the nickel center is roughly perpendicular to the coordination plane.

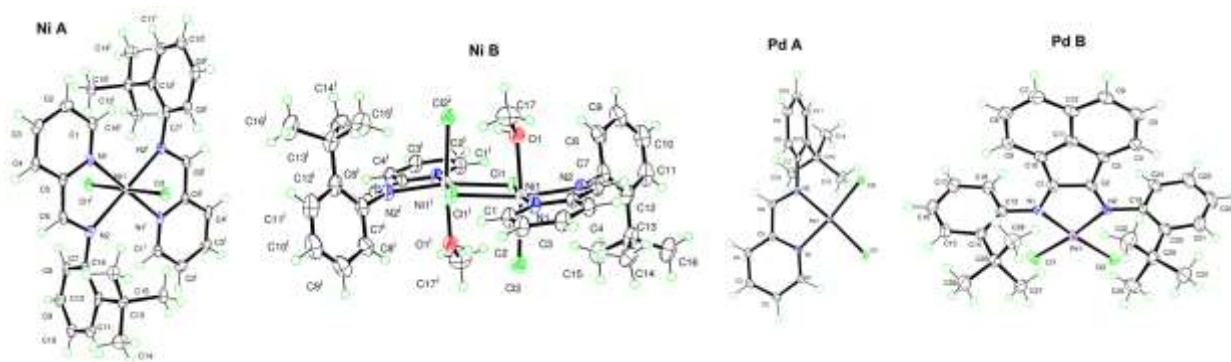


Figure 2.2. ORTEP diagrams of the synthesized α -diimine complexes. Solvents of crystallization in the structural packing have been omitted for clarity (**Ni B** & **Pd B**).

For XRD analysis of the remaining two Pd(II) complexes, suitable single crystals were obtained by slow evaporation of saturated dimethylsulfoxide (DMSO) solution at room temperature. Both **Pd A** and **Pd B** exhibited a distorted square planar geometry. In the **Pd B** crystal structure, there are two crystallographically unique complexes and two crystallographically unique DMSO solvent molecules (Figure S3). The main difference in the Pd complexes is the orientation of tert-butyl substituents, where the DMSO solvent molecules are filling the structural voids between the complexes. Unit cell representations of the synthesized complexes are illustrated in Figure S4–S7. Information regarding the crystal data collection, refinement, selected bond distances along with bond angles is compiled in Table S1–S4.

2.3.3 Thermal Properties of the Complexes.

Thermal properties of the synthesized complexes were studied with thermal gravimetric analysis (TGA) and differential scanning calorimetry (DSC). The corresponding TGA curves and DSC thermograms are presented in Figure 2.3. All the complexes except **Ni B** were thermally stable, having decomposition temperature (T_d at 95% weight) more than 200 °C.

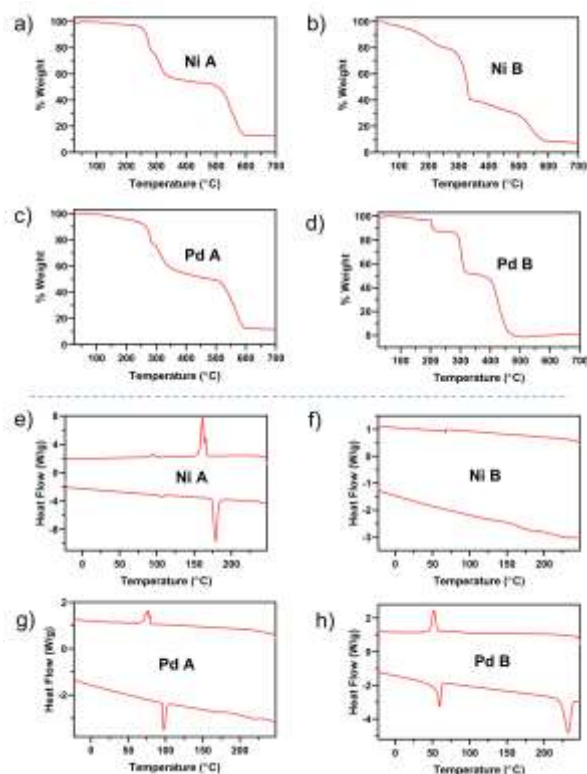


Figure 2.3. TGA (a–d) and DSC (e–h) curves of the synthesized α -diimine complexes.

The corresponding decomposition temperatures of **Ni A**, **Ni B**, **Pd A**, and **Pd B** are 252, 120, 204, and 201 °C, respectively. A bridge-like structure in the mono-ligated (**Ni B**) complex is responsible for the lower thermal stability compared to the bis-ligated complex (**Ni A**).⁷⁸ The results were consistent

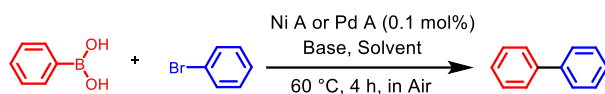
with the DSC data of the complexes. The thermally less stable **Ni B** did not reveal any prominent melting or cold crystallization peak, while the remaining complexes exhibited both melting and crystallization. **Ni A** displayed a sharp melting peak in the heating cycle at 177.4 °C and cold crystallization peak in the cooling cycle at 161.2 °C, respectively, while **Pd A** showed the corresponding peaks at 99.4 and 78.5 °C. However, **Pd B** revealed an additional peak in the heating trace at 53.4 °C apart from its crystallization and melting temperatures at 50.2 and 217.0 °C. Some trace peaks are recognized in the DSC of **Ni A** as well.

2.3.4 Optimization of Reaction Conditions for Suzuki–Miyaura Cross-coupling (SMC)

To explore the catalytic performance of the synthesized α -diimine complexes in Suzuki–Miyaura cross-coupling (SMC), both nickel and palladium-catalyzed systems were established. For this purpose, the reaction between phenylboronic acid and bromobenzene was chosen for optimizing the conditions for **Ni A** and **Pd A**, respectively. As the base^{79,80} and solvent⁸¹ have a vital role in SMC, these parameters were analyzed with 0.1 mol% of the complexes at 60 °C for 4 h (Table 2.1). Previously nickel-based systems found success in SMC from using 1,4-dioxane and K₃PO₄.^{25,45,50} Consequently, this combination contributed the best yield for **Ni A** (entry 4, Table 2.1). Moreover, the catalytic system containing DMF and K₂CO₃ worked well for **Pd A** (entry 5, Table 2.1). To find the optimum reaction temperature, another set of reactions was conducted from 40–100 °C (Table 2.2). **Ni A** exhibited an increase in yield by raising the temperature to 80 °C; however, a decrease is observed at 100 °C (entry 3 & 4, Table 2). Conversely, the yield for **Pd A** did not improve by raising the temperature above 60 °C.

Subsequently, the most critical variations were examined regarding the concentration of the complexes, base, and boronic acid (Table 2.3). As the transmetalation process in the catalytic

Table 2.1. Optimization of Solvent and Base^a



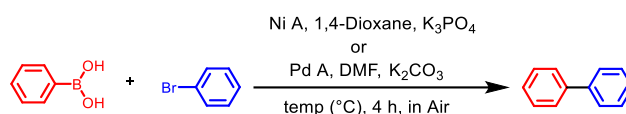
entry	solvent	base	yield (%) ^b	
			(Ni A)	(Pd A)
1	H ₂ O	K ₂ CO ₃	34	61
2	H ₂ O	K ₃ PO ₄	29	59
3	1,4-Dioxane	K ₂ CO ₃	61	63
4	1,4-Dioxane	K ₃ PO ₄	68	57
5	DMF	K ₂ CO ₃	53	85
6	DMF	K ₃ PO ₄	51	73

^aReaction conditions: bromobenzene (1 mmol), phenylboronic acid (1.1 mmol), base (1 mmol), 0.1 mol% of **Ni A** or **Pd A**, solvent (6 mL).

^bIsolated yields from flash column chromatography (*n*-hexane as eluent).

cycle starts with the reaction of the organoboronic acid and base, it is crucial to determine the best ratio.⁷⁹ Four experiments were conducted by adjusting the base concentration while keeping the complex as 0.1 mol% and 1.1 equivalent of boronic acid. Both for **Ni A** and **Pd A**, the yields improved from increasing the base concentration; however, further adding decreased the yields (entry 1–4, Table 2.3). The base activates the boronic acid and assists in engaging in the catalytic cycle.^{82,83} Nonetheless, the excess use of base might have some detrimental effects. The decrease in yields in the presence of excess base has been previously observed in both Ni and Pd catalytic systems.^{50,84} The next seven experiments are dedicated to **Ni A** regarding the variation in the

Table 2.2. Optimization of Temperature^a



entry	temp (°C)	yield (%) ^b	
		(Ni A)	(Pd A)
1	40	–	53
2	60	68	85
3	80	79	77
4	100	71	–

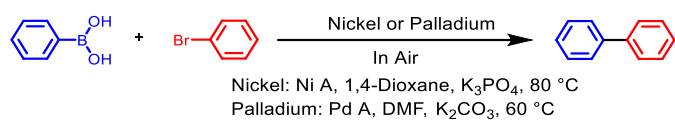
^aReaction conditions: bromobenzene (1 mmol), phenylboronic acid (1.1 mmol), base (1 mmol), 0.1 mol% of **Ni A** or **Pd A**, solvent (6 mL). Entry 1 for only **Pd A**, whereas 4 for **Ni A**. ^bIsolated yields from flash column chromatography (*n*-hexane as eluent).

concentration of boronic acid and complex along with the influence of reaction time. Although the increased ratio of boronic acid did not increase the yield, an increased amount of **Ni A** having 0.3 mol% afforded a higher yield (entry 8, Table 2.3). Increasing the reaction time to six hours mostly generated quantitative yields (98%) using **Ni A** with the optimized conditions (entry 10, Table 2.3). Likewise, similar variations were performed for **Pd A**. The highest yield was achieved by running the reaction for four hours with 0.2 mol% of **Pd A**, 1.1 equivalent of boronic acid, and 1.5 equivalent of base (entry 13, Table 2.3).

2.3.5 Substrate Scope

For exploring the substrate scope in SMC, all the complexes were reacted with phenylboronic acid and a variety of aryl bromides (Figure 2.4). A total of eleven compounds were

Table 2.3. Concentration optimization of Complex, Boronic Acid, and Base^a



entry	time (h)	complex	boronic acid	base	yield (%) ^b	yield (%) ^b
		(mol%)	(equivalent)	(equivalent)	(Ni A)	(Pd A)
1	4	0.1	1.1	1	79	85
2	4	0.1	1.1	1.5	83	91
3	4	0.1	1.1	2	87	83
4	4	0.1	1.1	2.5	80	–
5	4	0.1	1.3	2	81	–
6	4	0.1	1.5	2	77	–
7	4	0.2	1.1	2	92	–
8	4	0.3	1.1	2	96	–
9	4	0.4	1.1	2	90	–
10	6	0.3	1.1	2	98	–
11	8	0.3	1.1	2	88	–
12	4	0.1	1.3	1.5	–	87
13	4	0.2	1.1	1.5	–	96
14	4	0.3	1.1	1.5	–	84
15	6	0.2	1.1	1.5	–	89
16	3	0.2	1.1	1.5	–	78

^aReaction conditions: bromobenzene (1 mmol), phenylboronic acid, base, solvent (6 mL), **Ni A** or **Pd A**. Entry 4–11 only for **Ni A**,

whereas entry 12–16 only for **Pd A**. ^bIsolated yields from flash column chromatography (*n*-hexane as eluent).

synthesized using four catalysts. Generally, **Ni B** exhibited the highest yields followed by **Pd B**, **Pd A**, and **Ni A**. Variation in the type and position of the functional groups is well tolerated, with **Ni B** having quantitative yields (94–99%), and **Pd B** suffering only a very minor decrease,

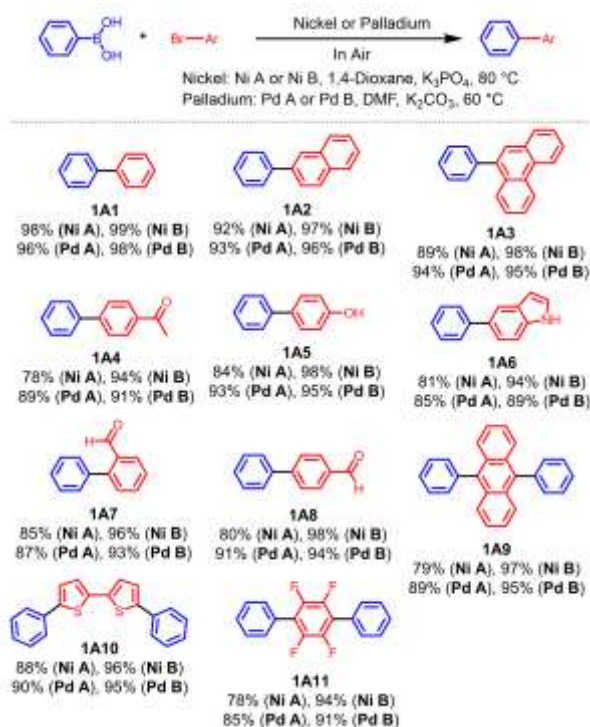


Figure 2.4. Substrate scope: phenylboronic acid.

retaining excellent yields (89–98%). **Pd A** afforded satisfactory yields (85–96%), whereas **Ni A** gave lower yields (78–98%). For instance, *ortho* and *para* aldehyde functionality in **1A7** and **1A8** did not significantly affect the catalytic performance of **Ni B** and **Pd B**. All the complexes provided modest to quantitative yields (84–99%) for **1A1** and **1A5**. In contrast, Pd nanoparticles having amine-functionalized graphene oxide produced 96% of **1A1** through aryl iodide, whereas aryl bromide manifested only 50% in **1A5**.¹⁴ Recently, a cobalt(II) phthalocyanine complex assembled to a nickel oxide semiconductor was applied in SMC for generating **1A5**; still, the recorded yield is low as 39%.⁸⁵ Furthermore, compounds **1A6** and **1A8** presented comparable yields with **Ni B** and **Pd B** compared to a reported study containing higher concentration (2–4 mol%) of 1,1'-bis(diphenylphosphino)ferrocene-based commercially accessible catalysts.⁴⁵ PdCu bimetallic

nanoparticles supported with diamines yielded only 78% of **1A6**, whereas all the applied complexes afforded 81–94% yields.⁸⁶

Moreover, **Ni B**, **Pd B**, and **Pd A** manifested higher yields (91–98%) in **1A8** compared to the catalytic system (90%) composed of magnetic lignosulfonate-supported Pd complex.¹⁵ Furthermore, a nickel catalyst comprised of a metal-organic framework afforded only 79% of **1A8**.⁵¹ Bithiophene, an active unit in organic semiconductors that demands particular ligands associated with poisonous tin reagents for engaging in the coupling reactions.⁸⁷ Besides, the highest recorded yield (90%) for **1A10** through SMC containing commercially available palladium(II) acetate is lower than we have obtained within **Ni B** (96%) and **Pd B** (95%).⁸⁸ Moreover, nickel(II) benzimidazolin-2-ylidene complex was unsuccessful in SMC for combining phenylboronic acid with 2-bromothiophene.³⁷ Likewise, 1,4-dibromo-2,3,5,6-tetrafluorobenzene, an essential unit in the polyfluorinated organic compounds was successfully attached through **Ni B** and **Pd B** catalytic systems, including yields over 90%.

2.3.6 Expansion of Substrate Scope

As **Ni B** and **Pd B** manifested excellent yields with phenylboronic acid, the ability to couple more sterically demanding aromatic cores was analyzed by reacting 2-naphthylboronic acid and 9-phenanthracenylboronic acid with aryl bromides (Figure 2.5). Introducing 2-naphthylboronic acid with comparable aryl bromides applied in the first series, **Ni B** and **Pd B** produced quantitative (95–99%) and modest (89–95%) yields, respectively. For instance, compounds **2A1–2A3** and **1A1–1A3** exhibited similar yields with **Ni B** and **Pd B** (Figure 2.4 & 2.5). Notably, **Ni B** and **Pd B** afforded more than 90% yields for unsubstituted biaryl compounds **1A2** and **2A1** synthesized from phenylboronic acid and 2-naphthylboronic acid, respectively, whereas, a catalytic system

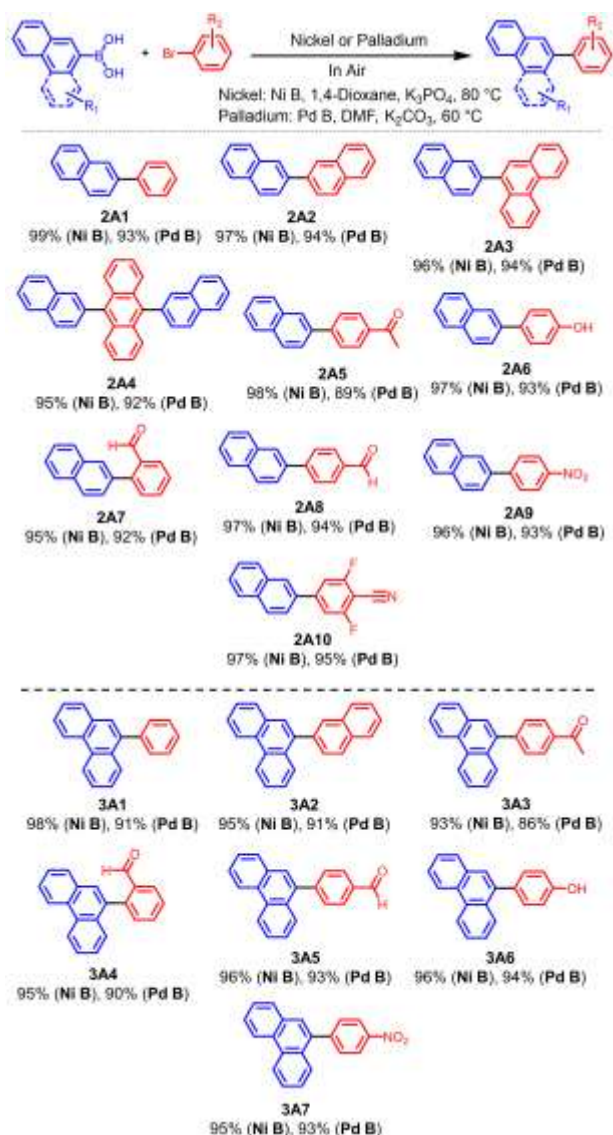


Figure 2.5. Expansion of substrate scope.

comprising hexylbiguanide as a free ligand and commercially available palladium(II) acetate presented only 22% yield.¹³ In OLED application, anthracene is an essential structural motif that contributes strong blue electroluminescence associated with a low electronic bandgap.⁸⁹ In this interest, both sterically hindered 9,10-dibromoanthracene and 2-naphthylboronic acid were successfully coupled for generating **2A4**, maintaining a comparable yield to **1A9** (Figure 2.4 &

2.5) regardless of the steric difference. Moreover, catalytic systems comprised of **Ni B** and **Pd B** provided much higher yields (95 & 92% respectively) of **2A4** than the highest reported yield (70%) in SMC through commercially available palladium(II) acetate.⁹⁰ **2A6** afforded more desirable yields (97 & 93%) compared to the catalytic system (87%), possessing an aminophosphine palladium pincer complex.⁹¹ Moreover, variation in the relative position of the aldehyde group did not affect much in the yields of **2A7** & **2A8**. Biphenyl compounds occupying nitrile functionality have applications in medicinal chemistry.⁹² For instance, 2-cyano-4'-methyl biphenyl is an essential intermediate that arises through SMC and is frequently employed in the sartan class of drugs.³ Here, **2A10** having a 2,6-difluorobenzonitrile moiety, is successfully synthesized with excellent yields (95 & 97%).

Using 9-phenanthracenylboronic acid as a coupling partner with some of the aryl bromides used before, the catalytic performance did not alter appreciably (Figure 2.5). For example, comparable yields are noted among the unsubstituted biaryl compounds **2A1**, **2A2**, **3A1**, and **3A2** synthesizing from 2-naphthylboronic acid and 9-phenanthracenylboronic acid. Additionally, the *para*-substituted phenyl moieties possessing acetyl, hydroxyl, and nitro functionality in the biaryl compounds **2A5**, **2A6**, **2A9**, **3A3**, **3A6**, and **3A7** have similar yields. *Ortho* or *para*-substitution with an aldehyde functionality manifested analogous yields in the biaryl compounds, for instance, **2A7**, **2A8**, **3A4**, and **3A5**. Also, **3A4** provided higher yields through **Ni B** (95%) and **Pd B** (90%) than the catalytic system possessing 5 mol% of commercially available bis(triphenylphosphine)palladium(II) dichloride.⁹³ The highest reported yield of **3A6** is achieved through SMC of 4-methoxyphenylboronic acid and 9-bromophenanthrene followed by the demethylation process.⁹⁴ Also, the yield is much lower (80%) than our catalytic systems

comprising **Ni B** (96%) and **Pd B** (94%). Compound **3A7** exhibited better yields with **Ni B** (95%) and **Pd B** (93%) than the reported yield (54%) with commercially available Pd(PPh₃)₄, including lithium *N*-phenylsydnone-4-carboxylate as an additive.⁹⁵ Moreover, the catalytic system containing palladium carbodicarbene complex afforded 84% of **3A7** by running the reaction for 20 h at 120 °C.⁹⁶

Steric hindrance of the bulky aryl boronic acid has previously been found to reduce the yield by inhibiting the transmetalation process.^{12,56} However, the catalytic systems using **Ni B** and **Pd B** demonstrated excellent yields, while using sterically challenging 2-naphthylboronic and 9-phenanthracenylboronic acid. Analogous to **Ni B**, NHC-based palladium dimer complexes with bridging structure have been applied successfully in SMC for generating tetra-*ortho*-substituted biphenyl from sterically hindered substrates.^{34,55,97} To reduce the protodeboronation, a significant excess of boronic acid is usually applied not only to manage unwanted side reactions but also to generate desired yields.⁵² A considerable portion of the reported studies of Ni-catalyzed SMC employed approximately 2.5 equivalent or more of boronic acid.^{25,41,43,44,48} However, within our optimized conditions, **Ni B** provided quantitative yields from applying a small excess of boronic acid (1.1 equivalent).

The thermal stability of a catalyst is crucial to preserve the inherent catalytic performance over prolonged reaction times, particularly for industrial applications. Supported transition metal catalytic system usually demonstrates thermal stability for SMC application.^{15,49} Nonetheless, a major portion of the catalytic systems in SMC are lacking thermal properties as they demand high catalyst loading and temperature along with extended reaction time.^{41,43,44,46,47,50,96} In contrast, our complexes' high thermal stability is evident from the data presented earlier (Figure 2.3). Although

Ni B is comparatively less stable due to its bridge-like structure, the optimized temperature (80 °C) used in SMC reactions is much lower than the decomposition temperature ($T_d = 120$ °C at 95% weight).

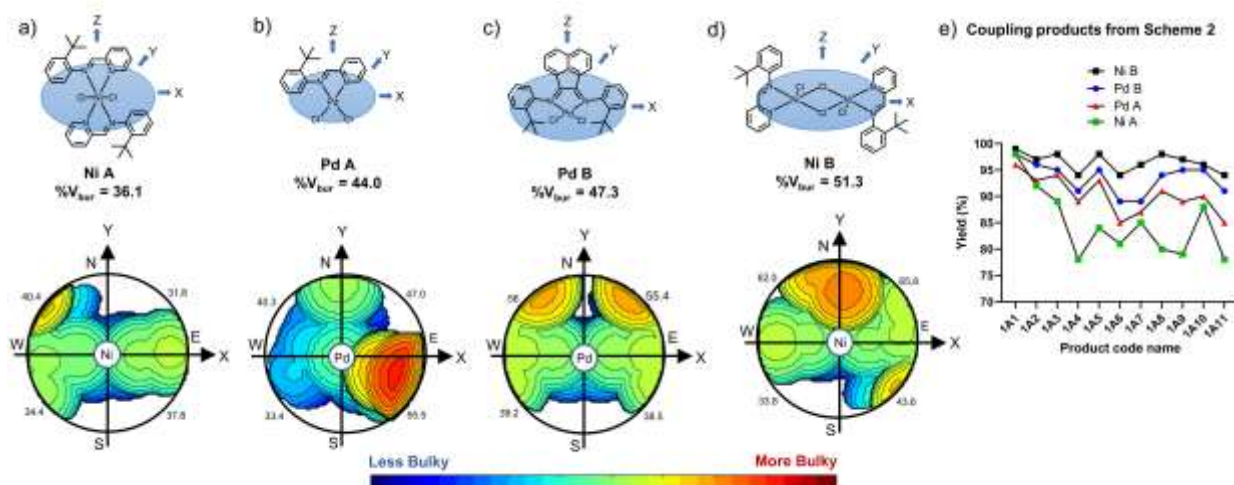


Figure 2.6. Percent buried volume ($\%V_{bur}$) and topographic steric map of the complexes (a-d), including their performance with phenylboronic acid (e).

2.3.7 Steric Effect vs. Catalytic Performance

To quantify the steric attributes of the synthesized complexes and correlate the outcomes in SMC, the percent buried volume ($\%V_{bur}$) was applied as a molecular descriptor. $\%V_{bur}$ calculation has received much popularity for evaluating the catalytic performance of *N*-heterocyclic carbene (NHC) and other ligand-based complexes.^{12,98–103} Moreover, steric topography around the metal center represents vital information regarding the catalytic performance in SMC.¹⁰ We have used SambVca 2.1, a free web tool developed by Falivene et al.,¹⁰⁴ for generating topographic steric maps associated with the $\%V_{bur}$. The topographic steric map illustrates the steric profile via colored contours surrounding the metal center by splitting the

entire %Vbur into four quadrants. These features of the synthesized complexes are displayed in Figure 2.6a–d.

Ni A exhibits a %Vbur of 36.1, whereas **Pd A** displays a more prominent %Vbur of 44. Moreover, **Pd B** shows even a higher %Vbur (47.3) and provides a symmetrical steric map. The higher steric hindrance arises from the bulky acenaphthene ligand environment containing the *tert*-butyl group in the *ortho* position of *N*-aryl rings. Interestingly, **Ni B** having a bridge-like structure, provides the highest %Vbur (51.3). Higher steric bulk and higher bite angle are correlated with the higher catalytic performance of **Pd A** (%Vbur & bite angle = 44 & 80.72(6)) compared to **Ni A** (%Vbur & bite angle = 36.1 & 78.4(2)) in the first series with phenylboronic acid (Figure 2.6e). Higher steric hindrance facilitates the SMC,^{53–55} and consequently, **Pd A** is providing better yields than **Ni A**. The bite angle of bidentate ligands plays an essential role in the metal-catalyzed reactions regarding the stabilization or destabilization of critical intermediates of the reaction mechanism.¹⁰⁵ For example, bulkiness, combined with the wider bite angle, facilitates the reductive elimination in palladium catalysis through orbital overlapping.^{106,107} Accordingly, a wider bite angle associated with **Pd A** is responsible for better yields than **Ni A**. Similar understandings are applicable for evaluating the improved performance of **Pd B** (%Vbur & bite angle = 47.3 & 81.32 (13)) over **Pd A** with regards to phenylboronic acid (Figure 2.6e). The electron-donating *tert*-butyl group in the *ortho* position of the *N*-aryl rings has a noticeable impact on the metal center in **Pd B**. The combination of sterics, and the electronic effects of the ligand environment facilitate the oxidative addition and reductive elimination in the SMC mechanism.^{55–59} These effects were recognized in SMC by Huo et al.⁷⁵ when using an α -diimine Pd complex comprising electron-donating and withdrawing groups on the *N*-aryl rings of the ligand

environment. The increase of both electron-donating ability and steric hindrance manifested excellent yields through the enhanced rate of oxidative addition and, ultimately, stabilization of the metal center. In contrast, the electron-withdrawing groups resulted in low yields. Therefore, the *tert*-butyl group in the *N*-aryl rings of **Pd B** enhances the electron-density near the metal center. Consequently, an electron-rich environment associated with the higher sterics and bite angle is subject to **Pd B** for becoming a more competent catalyst than **Pd A**.

Although **Ni B** has a lower bite angle (79.16 (8)), this monoligated dinuclear nickel complex has the highest steric hindrance (%Vbur = 51.3) compared to the remaining mononuclear complexes. Accordingly, **Ni B** presented the highest yields with phenylboronic acid, 2-naphthylboronic acid, and 9-phenanthracenylboronic acid. Apart from the metal identity and electron density, the coordination number of the metal complex offers additional advantages in reductive elimination.^{108,109} Moreover, the dinuclear complex has more offerings than mononuclear counterparts in cross-coupling chemistry.^{110,111} Consequently, **Ni B**, a dinuclear five-coordinate complex (except the coordinated solvent molecules) have surpassed other four- or six-coordinate mononuclear complexes regarding the catalytic performance.

2.4 Conclusion

The unique advantages of α -diimine transition metal complexes in Suzuki–Miyaura cross-coupling (SMC) was demonstrated through the synthesis of four nickel (II) and palladium (II) complexes. The effect of sterics on the reaction outcomes was shown by synthesizing iminopyridine and acenaphthene-based α -diimine ligand frameworks. Percent buried volume (%Vbur) and topographic steric maps illustrated the variation in the steric profile of the complexes and ultimately was correlated with catalytic performance. Accordingly, **Ni B**, a dinuclear bridge-

like five-coordinate nickel complex with the highest steric hindrance afforded quantitative yields compared to the four- or six-coordinate mononuclear complexes (**Pd B**, **Pd A**, and **Ni A**). Moreover, the robust catalytic system containing **Ni B** did not compromise its performance upon sterically demanding 2-naphthylboronic acid and 9-phenanthracenylboronic acid. Furthermore, structural versatility, facile synthesis, air- and moisture, and thermal stability of the α -diimine complexes provide outstanding advantages in SMC. Therefore, recognizing sustainable choices to Pd, Ni-based systems with α -diimine ligands have the potential to be at the forefront in SMC.

2.5 Experimental section

2.5.1 General materials and method

The required chemicals were obtained from Sigma-Aldrich or Fisher Scientific and employed without additional refinement otherwise specified. For reporting ^1NMR spectra, a 500 MHz Bruker AVANCE IIIITM spectrometer was operated, maintaining chloroform as the reference solvent. To obtain TGA and DSC spectra of the synthesized complexes, the Mettler Toledo TGA/DSC-1 system was utilized. For this purpose, an inert atmosphere containing nitrogen, including a heating rate of 10 $^{\circ}\text{C}/\text{min}$ and subsequently a cooling rate of -10 $^{\circ}\text{C}/\text{min}$ were considered. Thermo FLASH 2000 CHN elemental analyzer was operated to characterize the α -diimine transition metal complexes. ESI-MS were collected by operating a Waters ACQUITY UPLC M-Class, including BEH C4 column for separation, whereas Water Synapt G2- Si Q-TOF was used for detection. Furthermore, SambVca 2.1, a web tool, was applied for acquiring the percent buried volumes (%Vbur) and topographic steric maps of the α -diimine transition metal complexes.

2.5.2 Single-Crystal XRD Data Acquisition and Characterization

Bruker Kappa D8 Quest CPAD diffractometer possessing an Incoatec microfocus Mo K α radiation source ($\lambda = 0.71073 \text{ \AA}$) was employed for receiving the single-crystal X-ray diffraction data sets. A Photon 100 CMOS detector was applied for the measurements possessing an Oxford Cryosystems cooler. In the Bruker APEX3 graphical interface, cell refinement and data reduction were performed with Bruker SAINT. Eventually, Bruker SADABS and XPREP were involved for scaling with multi-scan absorption correction and evaluating space groups, sequentially. Moreover, for solving the structure, SHELXTL (intrinsic phasing method)¹¹² was exercised before using SHELXL2017¹¹³ for refining the structure. Finally, ORTEP-3 for Windows was utilized for molecular graphics, including publCIF software for preparing the Crystallographic Information File (CIF).

2.5.3 Percent Buried Volume and Steric Map

The percent buried volumes (%V_{Bur}), and steric maps were obtained with SambVca 2.1, developed by Falivene et al.¹⁰⁴ CIF or converted XYZ files of the synthesized complexes were uploaded in that freely available web tool. For all the calculations, similar parameters were maintained, including 3.5 \AA as the radius of the sphere surrounding the metal center. A mesh of 0.1 \AA and the bond radii scaled by 1.17 were exercised. The accessed web address is <https://www.molnac.unisa.it/OMtools/sambvca2.1/index.html>.

2.5.4 Synthesis of Iminopyridine-Based Ligand (1a)

N-(2-(*tert*-butyl)phenyl)-1-(pyridin-2-yl)methanimine (1a) was synthesized by combining 2-pyridinecarboxaldehyde (3 mL, 0.032 mol), and 2-*tert*-butylaniline (4.78 g, 0.032 mol) in a one-neck 100 mL flask having DMF (40 mL) as the reaction medium with anhydrous MgSO₄ (120 mg,

1 mmol). The reaction mixture was stirred for 12 hours at room temperature. After that three extractions were performed with ethyl acetate (30 mL) and distilled water (30 mL). The crude product was obtained after drying the ethyl acetate layer with anhydrous MgSO_4 followed by rotary evaporation. Flash column chromatography having *n*-hexane as an eluent was used to isolate the pure product as a light-yellow oil (Yield = 6.24 g, 81.65 %). ESI-MS m/z $[\text{M}+\text{H}]^+ = 239.0013$ (calculated for $\text{C}_{16}\text{H}_{18}\text{N}_2 = 239.0024$). ^1H NMR (500 MHz, CDCl_3 , 300 K), δ (ppm): 8.70 (d, $J = 4.7$ Hz, 1H), 8.49 (s, 1H), 8.24 (d, $J = 7.9$ Hz, 1H), 7.80 (t, $J = 7.80$ Hz, 1H), 7.42 (d, $J = 7.75$ Hz, 1H), 7.34 (t, $J = 5.0$ Hz, 1H), 7.19 – 7.26 (m, 2H), 6.94 (d, $J = 7.50$ Hz, 1H), 1.48 (s, 9H). ^1H NMR data is consistent with the reported literature.¹¹⁴

2.5.5 Synthesis of Acenaphthene-Based Ligand (1b)

N^1, N^2 -Bis(2-(*tert*-butyl)phenyl)acenaphthylene-1,2-diimine (1b) was synthesized from an adapted procedure.⁷⁷ In a 100.0 mL one-neck round bottom flask, 2-*tert*-butylaniline (2.87 g, 19.2 mmol) and acenaphthoquinone (1.71 g, 9.39 mmol) were mixed in methanol (50 mL) containing formic acid (1 mL). The reaction mixture was stirred for 10 hours at room temperature. After that, it was filtered and washed with cold methanol (40.0 mL). The solid product was dissolved in dichloromethane and after filtration through celite, it was evaporated at room temperature. The pure product was isolated as an orange solid (Yield = 3.28 g, 78.63 %). ESI-MS m/z $[\text{M}+\text{H}]^+ = 445.0064$ (calculated for $\text{C}_{32}\text{H}_{32}\text{N}_2 = 445.0079$). ^1H NMR (500 MHz, CDCl_3 , 300 K), δ (ppm): 7.87 (d, $J = 8.25$ Hz, 2H), 7.54 (dd, $J = 7.10, 5.50$ Hz, 2H), 7.37 (t, $J = 7.95$ Hz, 2H), 7.20 – 7.25 (m, 4H), 6.94 (d, $J = 6.95$ Hz, 2H), 6.84 (d, $J = 7.20$ Hz, 2H), 1.40 (s, 18H). ^1H NMR data is consistent with the reported literature.⁷⁷

2.5.6 Synthesis of Bis-Ligated Nickel(II) Complex (Ni A)

Complex **Ni A** was synthesized from an adapted procedure.⁷⁸ In a dry one-neck (50.0 mL) round bottom flask, dichloro(dimethoxyethane)nickel(II) $\text{NiCl}_2(\text{DME})$ (219.72 mg, 1 mmol) and ligand 1a (525 mg, 2 mmol) were added, and it was purged with nitrogen gas. Then, dichloromethane (15 mL) was transferred to the flask, and the reaction mixture was stirred under the nitrogen atmosphere at room temperature. After stirring for 24 hours, precipitated solid from the reaction mixture was filtered and washed with dichloromethane (30 mL) and diethyl ether (30 mL). The pure product was isolated as a dark-yellow solid after drying in the vacuum for 24 hours (Yield = 474.21 mg, 78.22 %). Elemental analysis: calculated for $\text{C}_{32}\text{H}_{36}\text{Cl}_2\text{N}_4\text{Ni}$: C = 63.40, H = 5.99, N = 9.24 ; found: C = 63.32, H = 6.08, N = 9.28. For single-crystal XRD analysis, a suitable single crystal was grown by vapor diffusion of diethyl ether into a saturated methanol solution of the complex at room temperature. Crystal color: yellow; crystal shape: plate; crystal size: $0.30 \times 0.22 \times 0.01 \text{ mm}^3$.

2.5.7 Synthesis of Mono-Ligated Nickel(II) Complex (Ni B)

Complex **Ni B** was synthesized from an adapted procedure.⁷⁸ In a dry one-neck (50 mL) round bottom flask, $\text{NiCl}_2(\text{DME})$ (219.72 mg, 1 mmol), and ligand 1a (238.33 mg, 1 mmol) were added, and it was purged with nitrogen gas. Then, dichloromethane (15 mL) was transferred to the flask, and the reaction mixture was stirred under the nitrogen atmosphere at room temperature. After stirring for 24 hours, precipitated solid from the reaction mixture was filtered and washed with dichloromethane (30 mL) and diethyl ether (30 mL). The pure product was isolated as a light-yellow solid after drying in the vacuum for 24 hours (Yield = 502.29 mg, 68.26 %). Elemental analysis: calculated for $\text{C}_{32}\text{H}_{36}\text{Cl}_4\text{N}_4\text{Ni}_2$: C = 52.23, H = 4.93, N = 7.61; found: C = 52.31, H =

4.88, N = 7.53. For single-crystal XRD analysis, a suitable single crystal was grown by vapor diffusion of diethyl ether into a saturated methanol solution of the complex at room temperature. Crystal color: yellow; crystal shape: fragment; crystal size: $0.36 \times 0.24 \times 0.12 \text{ mm}^3$.

2.5.8 Synthesis of Iminopyridine-Based Palladium(II) Complex (Pd A)

Complex **Pd A** was synthesized from an adapted procedure.⁷⁷ In a dry one-neck (25 mL) round bottom flask, dichloro(1,5-cyclooctadiene)palladium(II) known as PdCl₂(cod) (200 mg, 0.7 mmol) and ligand 1a (166.83 mg, 0.70 mmol) were added and it was purged with nitrogen gas. Then, dichloromethane (10 mL) was transferred to the flask, and the reaction mixture was stirred under the nitrogen atmosphere at room temperature. After stirring for 8 hours, precipitated solid from the reaction mixture was filtered and washed with dichloromethane (30 mL) and hexane (30 mL). The pure product was isolated as a dark-yellow solid after drying in the vacuum for 24 hours (Yield = 244.75 mg, 84.12 %). Elemental analysis: calculated for C₁₆H₁₈Cl₂N₂Pd: C = 46.23, H = 4.37, N = 6.74 ; found: C = 46.17, H = 4.40, N = 6.79. For single-crystal XRD analysis, a suitable single crystal was grown from slow evaporation of saturated dimethylsulfoxide solution of the complex at room temperature. Crystal color: yellow; crystal shape: tablet; crystal size: $0.34 \times 0.16 \times 0.04 \text{ mm}^3$.

2.5.9 Synthesis of Acenaphthene-Based Palladium(II) Complex (Pd B)

Complex **Pd B** was synthesized from implementing the above procedure from PdCl₂(cod) (200 mg, 0.7 mmol) and ligand 1b (311.23 mg, 0.70 mmol). The pure product was isolated as an orange solid (Yield = 337.43 mg, 77.51 %). Elemental analysis: calculated for C₃₂H₃₂Cl₂N₂Pd: C = 61.80, H = 5.19, N = 4.50; found: C = 61.91, H = 5.23, N = 4.46. For single-crystal XRD analysis, a suitable single crystal was grown from slow evaporation of saturated dimethylsulfoxide solution

of the complex at room temperature. Crystal color: orange; crystal shape: fragment; crystal size: $0.20 \times 0.15 \times 0.07 \text{ mm}^3$.

2.5.10 General Procedure for Nickel-Catalyzed Suzuki–Miyaura Cross-Coupling

25 mL two-neck round-bottom flask equipped with a condenser was used for the reaction setup, where aryl bromide (1 mmol), boronic acid (1.1 mmol), K_3PO_4 (2 mmol), 0.3 mol% of complex Ni A or Ni B, and 1,4-dioxane (6 mL) were combined. The reaction mixture was stirred in the air atmosphere for 6 h at 80 °C. After cooling the mixture at room temperature, subsequently, three extractions were performed with ethyl acetate (10 mL) and distilled water (10 mL). The crude product was obtained after drying the ethyl acetate layer with anhydrous MgSO_4 followed by rotary evaporation. Column chromatography having *n*-hexane or a mixture of *n*-hexane-ethyl acetate as the eluent was used to isolate the pure product.

2.5.11 General Procedure for Palladium-Catalyzed Suzuki–Miyaura Cross-Coupling

25 mL two-neck round-bottom flask equipped with a condenser was used for the reaction setup, where aryl bromide (1 mmol), boronic acid (1.1 mmol), K_2CO_3 (1.5 mmol), 0.2 mol% of complex Pd A or Pd B, and DMF (6 mL) were combined. The reaction mixture was stirred in the air atmosphere for 4 h at 60 °C. After cooling the mixture at room temperature, subsequently, three extractions were performed with ethyl acetate (10 mL) and distilled water (10 mL). The crude product was obtained after drying the ethyl acetate layer with anhydrous MgSO_4 followed by rotary evaporation. Column chromatography having *n*-hexane or a mixture of *n*-hexane-ethyl acetate as the eluent was used to isolate the pure product.

2.6 Characterization of the synthesized biaryl products

Biphenyl (1A1). Eluent: *n*-hexane. White solid. Yield: 151.2 mg, 98% (Ni A); 152.6 mg, 99% (Ni B); 148.2 mg, 96% (Pd A); 152.2 mg, 98% (Pd B). ESI-MS m/z $[M+H]^+ = 155.0712$ (calculated for $C_{12}H_{10} = 155.0732$). 1H NMR (500 MHz, $CDCl_3$, 300 K), δ (ppm): 7.60 (d, $J = 7.7$ Hz, 4H), 7.45 (t, $J = 7.5$ Hz, 4H), 7.36 (t, $J = 7.4$ Hz, 2H). 1H NMR data is consistent with the reported literature.^{91,115,116}

2-Phenylnaphthalene (1A2 & 2A1). Eluent: *n*-hexane. White solid. Yield for 1A2: 187.8 mg, 92% (Ni A); 198.2 mg, 97% (Ni B); 190 mg, 93% (Pd A); 196.2 mg, 96% (Pd B). Yield for 2A1: 202.2 mg, 99% (Ni B); 189.8 mg, 93% (Pd B). ESI-MS m/z $[M+H]^+ = 205.0813$ (calculated for $C_{16}H_{12} = 205.0867$). 1H NMR (500 MHz, $CDCl_3$, 300 K), δ (ppm): 8.05 (s, 1H), 7.92 (t, $J = 8.6$ Hz, 2H), 7.87 (d, $J = 7.5$ Hz, 1H), 7.77–7.73 (m, 3H), 7.53–7.48 (m, 4H), 7.39 (t, $J = 7.3$ Hz, 1H). 1H NMR data is consistent with the reported literature.^{115,117}

9-Phenylphenanthrene (1A3 & 3A1). Eluent: *n*-hexane. Light brown solid. Yield for 1A3: 226.4 mg, 89% (Ni A); 249.2 mg, 98% (Ni B); 239 mg, 94% (Pd A); 241.6 mg, 95% (Pd B). Yield for 3A1: 249.2 mg, 98% (Ni B); 231.2 mg, 91% (Pd B). ESI-MS m/z $[M+H]^+ = 255.0631$ (calculated for $C_{20}H_{14} = 255.0539$). 1H NMR (500 MHz, $CDCl_3$, 300 K), δ (ppm): 8.80 (d, $J = 8.3$ Hz, 1H), 8.74 (d, $J = 8.2$ Hz, 1H), 7.92 (dd, $J = 14.0, 5.5$ Hz, 2H), 7.68 (t, $J = 9.6$, 3H), 7.63 (t, $J = 7.6$ Hz, 1H), 7.58–7.52 (m, 5H), 7.47 (t, $J = 6.6$ Hz, 1H). 1H NMR data is consistent with the reported literature.¹¹⁸

4-Acetylbiphenyl (1A4). Eluent: *n*-hexane and ethyl acetate 20:1 (V/V). White solid. Yield: 153 mg, 78% (Ni A); 184.4 mg, 94% (Ni B); 174.6 mg, 89% (Pd A); 178.6 mg, 91% (Pd B). ESI-MS m/z $[M+H]^+ = 197.0512$ (calculated for $C_{14}H_{12}O = 197.0593$). 1H NMR (500 MHz,

CDCl₃, 300 K), δ (ppm): 8.04 (d, $J = 8.4$ Hz, 2H), 7.69 (d, $J = 8.4$ Hz, 2H), 7.63 (d, $J = 7.2$ Hz, 2H), 7.48 (t, $J = 7.3$ Hz, 2H), 7.41 (t, $J = 7.3$ Hz, 1H), 2.64 (s, 3H). ¹H NMR data is consistent with the reported literature.^{96,115,116,119,120}

4-Phenylphenol (1A5). Eluent: *n*-hexane and ethyl acetate 15:1 (V/V). White solid. Yield: 142.8 mg, 84% (Ni A); 166.6 mg, 98% (Ni B); 158.2 mg, 93% (Pd A); 161.4 mg, 95% (Pd B). ESI-MS m/z [M+H]⁺ = 171.0798 (calculated for C₁₂H₁₀O = 171.0755). ¹H NMR (500 MHz, CDCl₃, 300 K), δ (ppm): 7.55–7.53 (m, 2H), 7.48 (d, $J = 8.6$, 2H), 7.42 (t, $J = 7.5$ Hz, 2H), 7.31 (t, $J = 7.3$ Hz, 1H), 6.91 (d, $J = 8.6$ Hz, 2H), 4.72 (s, 1H). ¹H NMR data is consistent with the reported literature.^{115,119}

5-Phenyl-1H-indole (1A6). Eluent: *n*-hexane and ethyl acetate 20:1 (V/V). Light brown solid. Yield: 156.6 mg, 81% (Ni A); 181.6 mg, 94% (Ni B); 164.2 mg, 85% (Pd A); 171.8 mg, 89% (Pd B). ESI-MS m/z [M+H]⁺ = 194.0898 (calculated for C₁₄H₁₁N = 194.0951). ¹H NMR (500 MHz, CDCl₃, 300 K), δ (ppm): 8.17 (s, 1H), 7.87 (s, 1H), 7.66 (d, $J = 7.9$ Hz, 2H), 7.45 (t, $J = 10.4$ Hz, 4H), 7.31 (t, $J = 7.4$ Hz, 1H), 7.24 (d, $J = 2.7$ Hz, 1H), 6.61 (d, $J = 2.0$ Hz, 1H). ¹H NMR data is consistent with the reported literature.¹²¹

Biphenyl-2-carboxaldehyde (1A7). Eluent: *n*-hexane and ethyl acetate 20:1 (V/V). Light brown solid. Yield: 154.8 mg, 85% (Ni A); 175 mg, 96% (Ni B); 158.6 mg, 87% (Pd A); 169.4 mg, 93% (Pd B). ESI-MS m/z [M+H]⁺ = 183.0098 (calculated for C₁₃H₁₀O = 183.0075). ¹H NMR (500 MHz, CDCl₃, 300 K), δ (ppm): 9.99 (s, 1H), 8.04 (d, $J = 7.8$ Hz, 1H), 7.66–7.63 (m, 1H), 7.52–7.45 (m, 5H), 7.40–7.38 (m, 2H). ¹H NMR data is consistent with the reported literature.¹¹⁹

Biphenyl-4-carboxaldehyde (1A8). Eluent: *n*-hexane and ethyl acetate 20:1 (V/V). White solid. Yield: 145.6 mg, 80% (Ni A); 178.6 mg, 98% (Ni B); 165.8 mg, 91% (Pd A); 171.2 mg,

94% (Pd B). ESI-MS m/z $[M+H]^+ = 183.0011$ (calculated for $C_{13}H_{10}O = 183.0035$). 1H NMR (500 MHz, $CDCl_3$, 300 K), δ (ppm): 10.06 (s, 1H), 7.96 (d, $J = 8.0$ Hz, 2H), 7.76 (d, $J = 8.2$ Hz, 2H), 7.64 (d, $J = 7.4$ Hz, 2H), 7.49 (t, $J = 7.2$ Hz, 2H), 7.42 (t, $J = 7.5$ Hz, 1H). 1H NMR data is consistent with the reported literature.^{115,116}

9,10-Diphenylanthracene (1A9). Eluent: *n*-hexane and ethyl acetate 30:1 (V/V). White solid. Yield: 261 mg, 79% (Ni A); 320.6 mg, 97% (Ni B); 294.2 mg, 89% (Pd A); 313.8 mg, 95% (Pd B). ESI-MS m/z $[M+H]^+ = 331.0914$ (calculated for $C_{26}H_{18} = 331.0869$). 1H NMR (500 MHz, $CDCl_3$, 300 K), δ (ppm): 7.70 (dd, $J = 6.8, 3.6$ Hz, 4H), 7.61 (t, $J = 7.2$ Hz, 4H), 7.55 (t, $J = 7.2$ Hz, 2H), 7.49 (d, $J = 7.0$ Hz, 4H), 7.33 (dd, $J = 6.8, 3.7$ Hz, 4H). 1H NMR data is consistent with the reported literature.^{90,122}

5,5'-Diphenyl-2,2'-bithiophene (1A10). Eluent: *n*-hexane and ethyl acetate 30:1 (V/V). Light grey solid. Yield: 280.2 mg, 88% (Ni A); 305.6 mg, 96% (Ni B); 286.6 mg, 90% (Pd A); 302.4 mg, 95% (Pd B). ESI-MS m/z $[M+H]^+ = 319.0531$ (calculated for $C_{20}H_{14}S_2 = 319.0491$). 1H NMR (500 MHz, $CDCl_3$, 300 K), δ (ppm): 7.61 (d, $J = 7.7$ Hz, 4H), 7.39 (t, $J = 7.5$ Hz, 4H), 7.29 (d, $J = 7.5$ Hz, 2H), 7.24 (d, $J = 3.8$ Hz, 2H), 7.17 (d, $J = 3.7$ Hz, 2H). 1H NMR data is consistent with the reported literature.⁸⁸

1, 4 -Diphenyltetrafluorobenzene (1A11). Eluent: *n*-hexane. Light green solid. Yield: 235.6 mg, 78% (Ni A); 284.2 mg, 94% (Ni B); 256.8 mg, 85% (Pd A); 275 mg, 91% (Pd B). ESI-MS m/z $[M+H]^+ = 303.039$ (calculated for $C_{18}H_{10}F_4 = 303.0183$). 1H NMR (500 MHz, $CDCl_3$, 300 K), δ (ppm): 7.53–7.47 (m, 10H). 1H NMR data is consistent with the reported literature.¹²³

2,2'-Binaphthalene (2A2). Eluent: *n*-hexane. White solid. Yield: 246.4 mg, 97% (Ni B); 238.8 mg, 94% (Pd B). ESI-MS m/z $[M+H]^+ = 255.0099$ (calculated for $C_{20}H_{14} = 255.0044$). 1H

NMR (500 MHz, CDCl₃, 300 K), δ (ppm): 8.18 (s, 2 H), 7.96 (dd, $J = 8.0, 5.0$ Hz, 4 H), 7.89 (d, $J = 7.1$ Hz, 4 H), 7.55–7.49 (m, 4 H). ¹H NMR data is consistent with the reported literature.^{124,125}

9-(naphthalen-2-yl)phenanthrene (2A3 & 3A2). Eluent: *n*-hexane. White solid. Yield for 2A3 for : 292.2 mg, 96% (Ni B); 286.2 mg, 94% (Pd B). Yield for 3A2: 289 mg, 95% (Ni B); 277 mg, 91% (Pd B). ESI-MS m/z [M+H]⁺ = 305.0861 (calculated for C₂₄H₁₆ = 305.0364). ¹H NMR (500 MHz, CDCl₃, 300 K), δ (ppm): 8.81 (d, $J = 8.3$ Hz, 1H), 8.76 (d, $J = 8.2$ Hz, 1H), 8.04 (s, 1H), 8.0–7.92 (m, 5H), 7.79 (s, 1H), 7.71–7.63 (m, 4H), 7.58–7.55 (m, 3H). ¹H NMR data is consistent with the reported literature.¹¹⁸

9,10-Di(naphthalen-2-yl)anthracene (2A4). Eluent: *n*-hexane. White solid. Yield: 409 mg, 95% (Ni B); 396.2 mg, 92% (Pd B). ESI-MS m/z [M+H]⁺ = 431.0217 (calculated for C₃₄H₂₂ = 431.0129). ¹H NMR (500 MHz, CDCl₃, 300 K), δ (ppm): 8.09 (d, $J = 8.3$ Hz, 2H), 8.04 (d, $J = 6.6$ Hz, 2H), 8.01 (s, 2H), 7.94 (d, $J = 7.4$ Hz, 2H), 7.74 (dd, $J = 6.8, 3.5$ Hz, 4H), 7.65 (br, 1H), 7.63–7.60 (m, 5H), 7.32 (dd, $J = 6.9, 3.7$ Hz, 4H). ¹H NMR data is consistent with the reported literature.⁹⁰

1-(4-(naphthalen-2-yl)phenyl)ethan-1-one (2A5). Eluent: *n*-hexane and ethyl acetate 30:1 (V/V). White solid. Yield: 241.4 mg, 98% (Ni B); 219.2 mg, 89% (Pd B). ESI-MS m/z [M+H]⁺ = 247.0098 (calculated for C₁₈H₁₄O = 247.0064). ¹H NMR (500 MHz, CDCl₃, 300 K), δ (ppm): 8.09 (d, $J = 4.4$ Hz, 2H), 8.07 (s, 1H), 7.96–7.91 (m, 2H), 7.88 (d, $J = 8.2$ Hz, 1H), 7.82 (d, $J = 7.5$ Hz, 2H), 7.76 (d, $J = 8.5$ Hz, 1H), 7.55–7.50 (m, 2H), 2.66 (s, 3H). ¹H NMR data is consistent with the reported literature.¹²⁵

4-(naphthalen-2-yl)phenol (2A6). Eluent: *n*-hexane and ethyl acetate 20:1 (V/V). White solid. Yield: 213.6 mg, 97% (Ni B); 204.8 mg, 93% (Pd B). ESI-MS m/z [M+H]⁺ = 221.0349

(calculated for $C_{16}H_{12}O = 221.0467$). 1H NMR (500 MHz, $CDCl_3$, 300 K), δ (ppm): 7.98 (s, 1H), 7.90–7.80 (m, 3H), 7.70 (dd, $J = 8.5, 6.7$ Hz, 1H), 7.62 (d, $J = 8.5$ Hz, 2H), 7.51–7.45 (m, 2H), 6.95 (d, $J = 8.5$ Hz, 2H), 4.81 (s, 1H). As opposed to the obtained 1H NMR data, it is quite unlikely to have a singlet peak at 9.65 ppm in the reported literature.^{91,126}

2-(naphthalen-2-yl)benzaldehyde (2A7). Eluent: *n*-hexane and ethyl acetate 20:1 (V/V). White solid. Yield: 220.4 mg, 95% (Ni B); 213.4 mg, 92% (Pd B). ESI-MS m/z $[M+H]^+ = 233.0088$ (calculated for $C_{17}H_{12}O = 233.0104$). 1H NMR (500 MHz, $CDCl_3$, 300 K), δ (ppm): 10.03 (s, 1H), 8.06 (d, $J = 7.8$ Hz, 1H), 7.94 (d, $J = 8.3$ Hz, 1H), 7.92–7.88 (m, 2H), 7.82 (br, 1H), 7.68 (t, $J = 7.4$ Hz, 1H), 7.56–7.52 (m, 5H). 1H NMR data is consistent with the reported literature.⁹³

4-(naphthalen-2-yl)benzaldehyde (2A8). Eluent: *n*-hexane and ethyl acetate 20:1 (V/V). White solid. Yield: 225.2 mg, 97% (Ni B); 218.8 mg, 94% (Pd B). ESI-MS m/z $[M+H]^+ = 233.0122$ (calculated for $C_{17}H_{12}O = 233.0104$). 1H NMR (500 MHz, $CDCl_3$, 300 K), δ (ppm): 10.09 (s, 1H), 8.11 (s, 1H), 8.04–7.89 (m, 7H), 7.79 (dd, $J = 17, 8.2$ Hz, 1H), 7.57–7.53 (m, 2H). 1H NMR data is consistent with the reported literature.¹¹⁶

2-(4-nitrophenyl)naphthalene (2A9). Eluent: *n*-hexane and ethyl acetate 20:1 (V/V). Light grey solid. Yield: 239.2 mg, 96% (Ni B); 231.8 mg, 93% (Pd B). ESI-MS m/z $[M+H]^+ = 250.0178$ (calculated for $C_{16}H_{11}NO_2 = 250.0116$). 1H NMR (500 MHz, $CDCl_3$, 300 K), δ (ppm): 8.35 (d, $J = 8.6$ Hz, 2H), 8.10 (s, 1H), 7.97 (d, $J = 8.5$ Hz, 1H), 7.95–7.93 (m, 1H), 7.91–7.87 (m, 3H), 7.75 (d, $J = 8.4$ Hz, 1H), 7.56–7.55 (t, $J = 4.4$ Hz, 2H). 1H NMR data is consistent with the reported literature.¹²⁷

2,6-Difluoro-4-(naphthalen-2-yl)benzotrile (2A10). Eluent: *n*-hexane and ethyl acetate 20:1 (V/V). Light yellow solid. Yield: 257.2 mg, 97% (Ni B); 251.8 mg, 95% (Pd B). ESI-MS m/z $[M+H]^+ = 266.0635$ (calculated for $C_{17}H_9F_2N = 266.0710$). 1H NMR (500 MHz, $CDCl_3$, 300 K), δ (ppm): 8.05 (s, 1H), 7.97 (d, $J = 8.5$ Hz, 1H), 7.94–7.89 (m, 2H), 7.65 (dd, $J = 8.6, 6.8$ Hz, 1H), 7.57 (dd, $J = 6.2, 3.0$ Hz, 2H), 7.40 (d, $J = 8.8$ Hz, 2H).

1-(4-(phenanthren-9-yl)phenyl)ethan-1-one (3A3). Eluent: *n*-hexane and ethyl acetate 20:1 (V/V). Light grey solid. Yield: 275.6 mg, 93% (Ni B); 254.8 mg, 86% (Pd B). ESI-MS m/z $[M+H]^+ = 297.0813$ (calculated for $C_{22}H_{16}O = 297.0936$). 1H NMR (500 MHz, $CDCl_3$, 300 K), δ (ppm): 8.80 (d, $J = 8.3$ Hz, 1H), 8.75 (d, $J = 8.2$ Hz, 1H), 8.13 (d, $J = 8.05$ Hz, 2H), 7.91 (d, $J = 7.8$ Hz, 1H), 7.85 (d, $J = 8.2$ Hz, 1H), 7.71–7.62 (m, 6H), 7.55 (t, $J = 2.9$ Hz, 1H), 2.71 (s, 3H). 1H NMR data is consistent with the reported literature.¹²⁰

2-(phenanthren-9-yl)benzaldehyde (3A4). Eluent: *n*-hexane and ethyl acetate 20:1 (V/V). White solid. Yield: 268.2 mg, 95% (Ni B); 254 mg, 90% (Pd B). ESI-MS m/z $[M+H]^+ = 283.0204$ (calculated for $C_{21}H_{14}O = 283.0127$). 1H NMR (500 MHz, $CDCl_3$, 300 K), δ (ppm): 9.74 (s, 1H), 8.80 (d, $J = 8.25$ Hz, 1H), 8.76 (d, $J = 8.35$ Hz, 1H), 8.16 (d, $J = 7.8$ Hz, 1H), 7.90 (d, $J = 7.8$ Hz, 1H), 7.75–7.70 (m, 4H), 7.68–7.66 (m, 1H), 7.64–7.60 (m, 1H), 7.54–7.51 (m, 3H). 1H NMR data is consistent with the reported.⁹³

4-(phenanthren-9-yl)benzaldehyde (3A5). Eluent: *n*-hexane and ethyl acetate 20:1 (V/V). White solid. Yield: 271 mg, 96% (Ni B); 262.4 mg, 93% (Pd B). ESI-MS m/z $[M+H]^+ = 283.0087$ (calculated for $C_{21}H_{14}O = 283.0127$). 1H NMR (500 MHz, $CDCl_3$, 300 K), δ (ppm): 10.15 (s, 1H), 8.80 (d, $J = 8.3$ Hz, 1H), 8.74 (d, $J = 8.3$ Hz, 1H), 8.05 (d, $J = 7.9$ Hz, 2H), 7.92 (d,

$J = 7.8$ Hz, 1H), 7.84 (d, $J = 8.25$ Hz, 1H), 7.75–7.69 (m, 5H), 7.65 (t, $J = 7.6$ Hz, 1H), 7.56 (t, $J = 7.85$ Hz, 1H). ^1H NMR data is consistent with the reported literature.¹²⁸

4-(phenanthren-9-yl)phenol (3A6). Eluent: *n*-hexane and ethyl acetate 20:1 (V/V). White solid. Yield: 259.4 mg, 96% (Ni B); 254 mg, 94% (Pd B). ESI-MS m/z $[\text{M}+\text{H}]^+ = 271.0483$ (calculated for $\text{C}_{20}\text{H}_{14}\text{O} = 271.0456$). ^1H NMR (500 MHz, CDCl_3 , 300 K), δ (ppm): 8.78 (d, $J = 8.25$ Hz, 1H), 8.73 (d, $J = 8.2$ Hz, 1H), 7.95 (d, $J = 8.25$ Hz, 1H), 7.89 (d, $J = 7.9$ Hz, 1H), 7.69–7.65 (m, 3H), 7.62 (t, $J = 6.8$ Hz, 1H), 7.55 (d, $J = 7.1$ Hz, 1H), 7.43 (d, $J = 8.5$ Hz, 2H), 6.99 (d, $J = 8.55$ Hz, 2H), 4.90 (s, 1H). ^1H NMR data is consistent with the reported literature.⁹⁴

9-(4-nitrophenyl)phenanthrene (3A7). Eluent: *n*-hexane and ethyl acetate 20:1 (V/V). White solid. Yield: 284.2 mg, 95% (Ni B); 278.4 mg, 93% (Pd B). ESI-MS m/z $[\text{M}+\text{H}]^+ = 300.0297$ (calculated for $\text{C}_{20}\text{H}_{13}\text{NO}_2 = 300.0641$). ^1H NMR (500 MHz, CDCl_3 , 300 K), δ (ppm): 8.81 (d, $J = 8.3$ Hz, 1H), 8.75 (d, $J = 8.3$ Hz, 1H), 8.39 (d, $J = 8.7$ Hz, 2H), 7.92 (d, $J = 7.9$ Hz, 1H), 7.79 (d, $J = 8.25$ Hz, 1H), 7.74–7.69 (m, 5H), 7.66 (t, $J = 6.9$ Hz, 1H), 7.57 (t, $J = 7.0$ Hz, 1H). ^1H NMR data is consistent with the reported literature.⁹⁶

2.7 Supporting Information

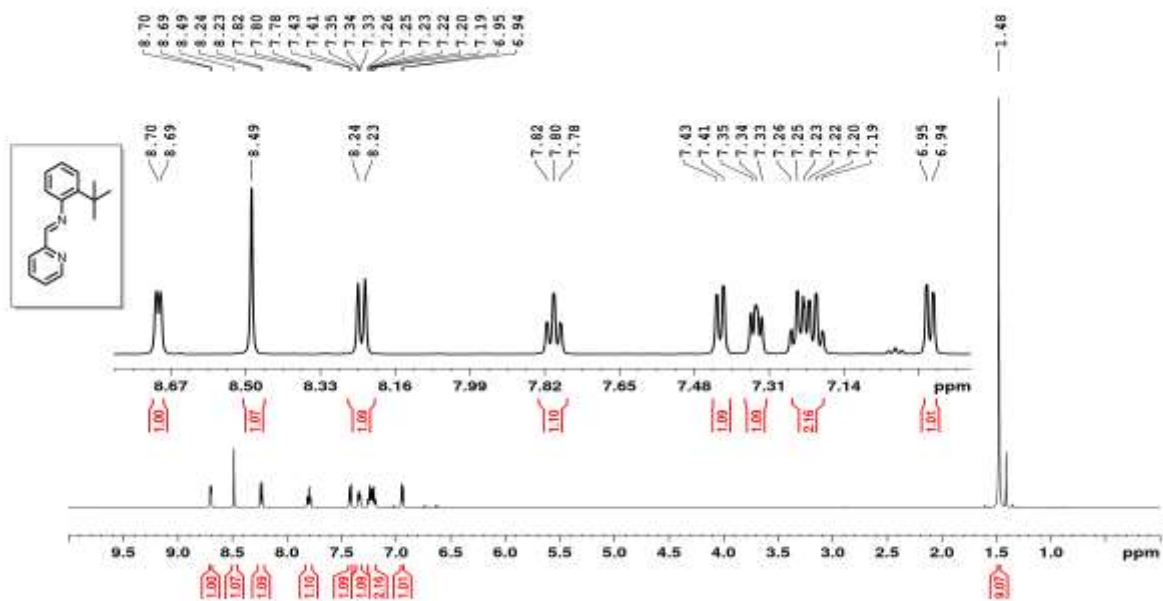


Figure 2.7. ^1H NMR spectrum of ligand **1a**.

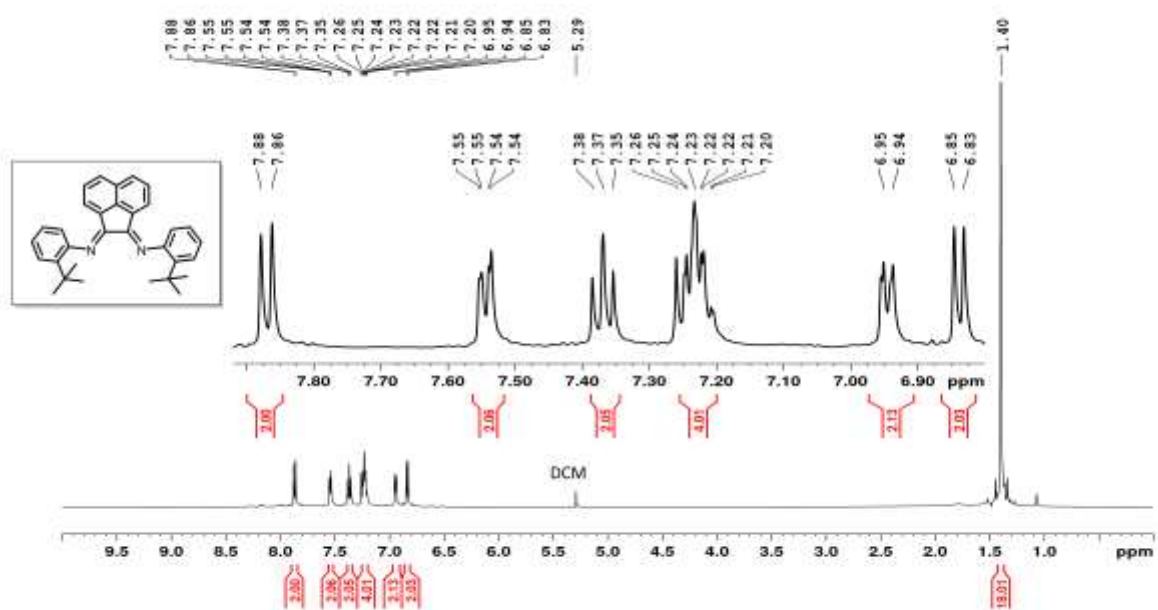


Figure 2.8. ^1H NMR spectrum of ligand **1b**.

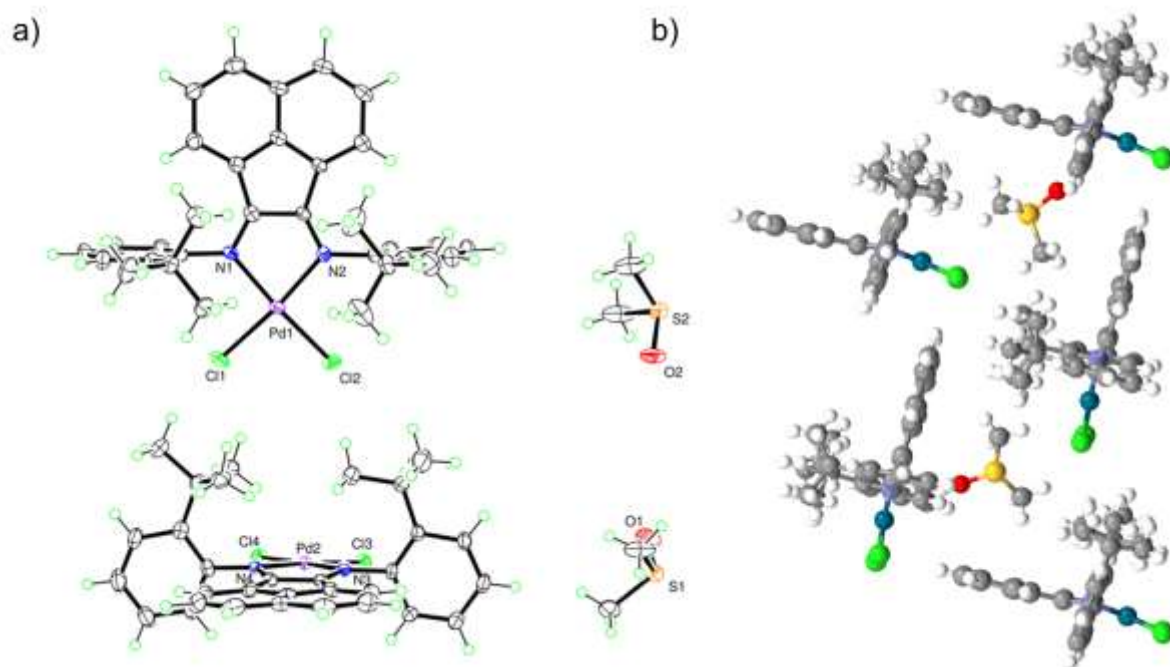


Figure 2.9. Twin ORTEP (a) and packing (b) of complex **Pd B**.

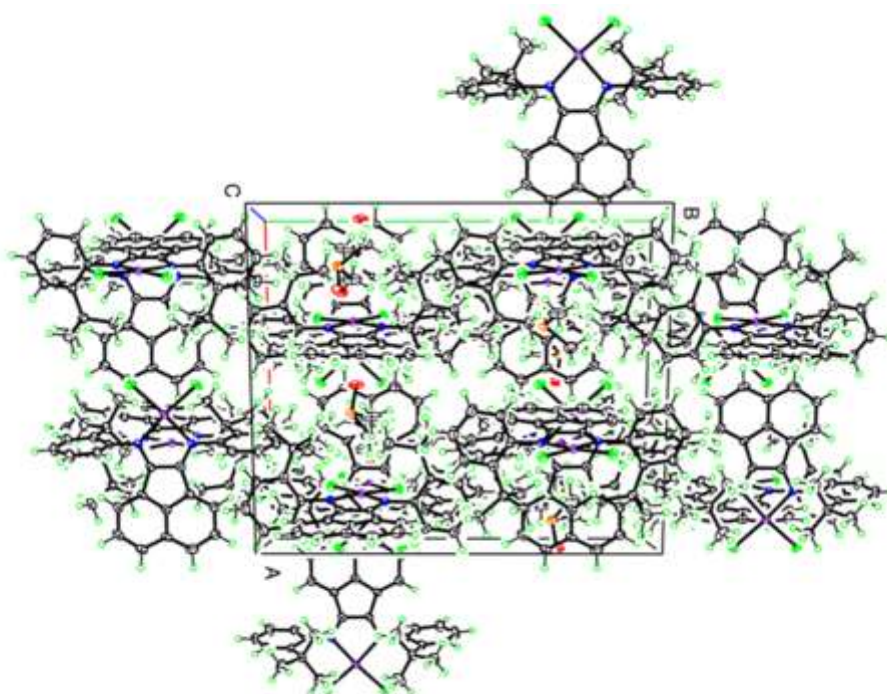


Figure 2.10. Unit cell representation of complex **Pd B**.

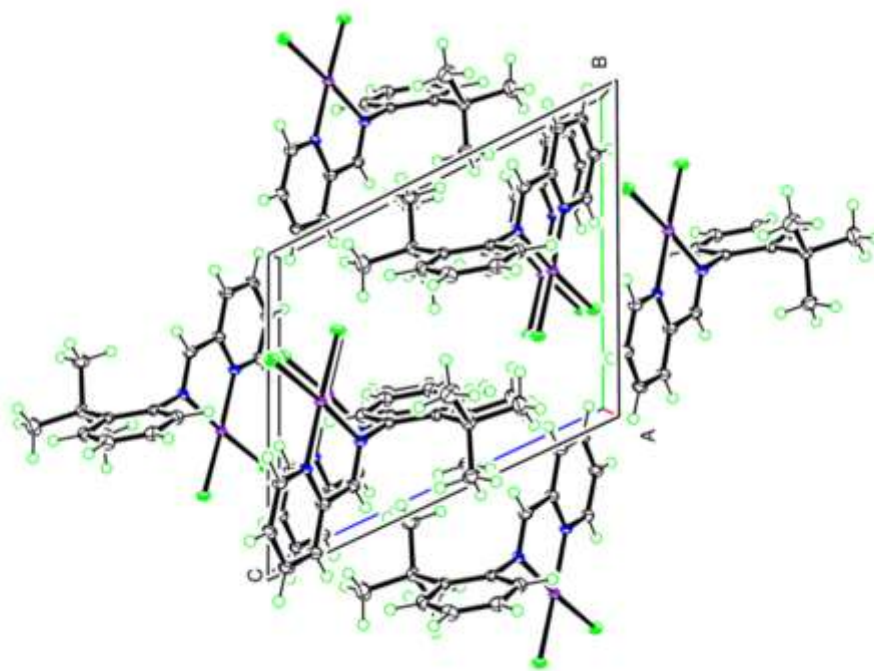


Figure 2.11. Unit cell representation of complex **Pd A**.

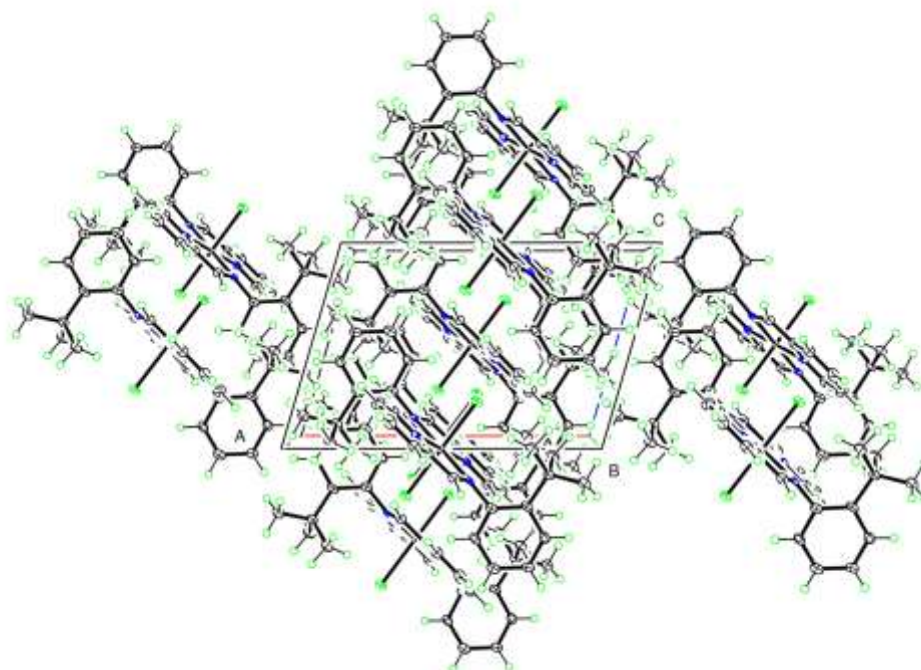


Figure 2.12. Unit cell representation of complex **Ni A**.

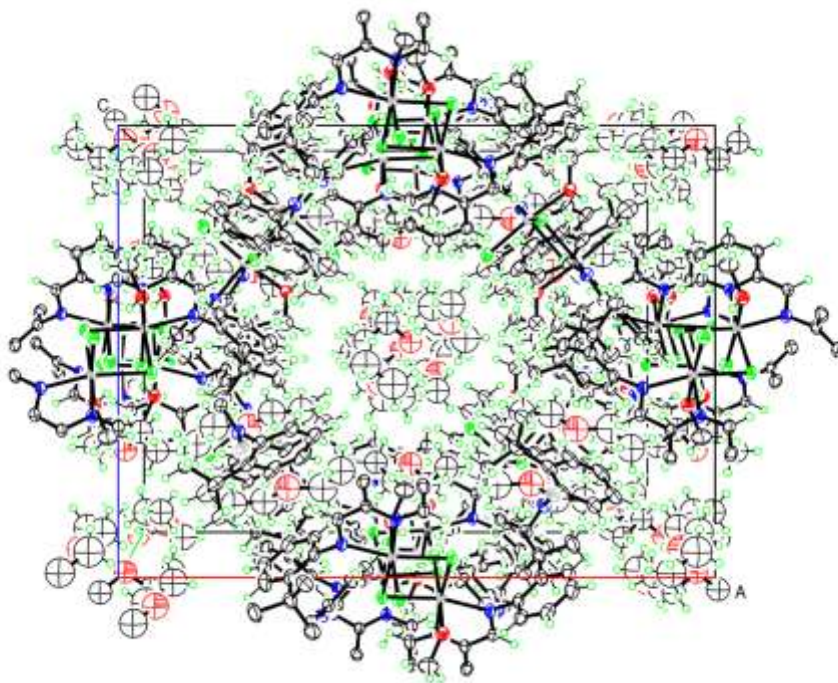


Figure 2.13. Unit cell representation of complex **Ni B**.

Table 2.4. Crystal data, data collection and refinement for complex **Ni A** and **Ni B**.

CCDC	2004629	2004628
Complexes	Ni A	Ni B
Crystallized from	Et ₂ O/CH ₃ OH	Et ₂ O/CH ₃ OH
Chemical formula	C ₃₂ H ₃₆ Cl ₂ N ₄ Ni	C ₃₄ H ₄₄ Cl ₄ N ₄ Ni ₂ O ₂ ·1.429(C ₄ H ₁₀ O)
Formula weight [g mol⁻¹]	606.26	905.88
Crystal color, habit	Yellow, Plate	Yellow, Fragment
Crystal size (mm³)	0.30 × 0.22 × 0.01	0.36 × 0.24 × 0.12
T (K)	100	100
Crystal system	Monoclinic	Tetragonal
Space group	<i>P</i> 2 ₁ / <i>c</i>	<i>I</i> 4 ₁ / <i>a</i>
a, b, c (Å)	12.730 (4), 14.003 (4), 8.513 (2)	a = 24.275 (5), c = 18.364 (6)
α, β, γ (°)	β = 106.232 (10)	
V (Å³)	1456.9 (7)	10822 (6)
Z	2	8
D_x (Mg m⁻³)	1.382	1.112
μ (Mo-Kα) (mm⁻¹)	0.88	0.93
F (000), θ range (°)	636, 2.2–27.5	3808, 2.5–30.4
No. of measured, independent and observed [I > 2σ(I)] reflections	34420, 34420, 22811	199886, 8273, 6515
R_{int}	0.123	0.057
Δρ_{max}, Δρ_{min} (e Å⁻³)	1.65, -1.48	0.79, -0.81
No. of parameters	183	250
Refinement R[F² > 2σ(F²)], wR(F²), S	0.103, 0.261, 1.06	0.053, 0.175, 1.27

Table 2.5. Crystal data, data collection and refinement for complex **Pd A** and **Pd B**.

CCDC	2004630	2004631
Complexes	Pd A	Pd B
Crystallized from	DMSO	DMSO
Chemical formula	C ₁₆ H ₁₈ Cl ₂ N ₂ Pd	C ₃₂ H ₃₂ Cl ₂ N ₂ Pd·C ₂ H ₆ OS
Formula weight [g mol ⁻¹]	415.62	700.02
Crystal color, habit	Yellow, Tablet	Orange, Fragment
Crystal size (mm ³)	0.34 × 0.16 × 0.04	0.20 × 0.15 × 0.07
T (K)	100	100
Crystal system	Triclinic	Monoclinic
Space group	$\bar{P}1$	$P2_1/n$
a, b, c (Å)	8.623 (3), 9.493 (3), 11.552 (4)	19.383 (4), 20.236 (4), 19.392 (4)
α, β, γ (°)	112.209 (10), 107.067 (9), 96.813 (10)	β = 119.84 (1)
V (Å ³)	808.2 (4)	6598 (3)
Z	2	8
D _x (Mg m ⁻³)	1.708	1.409
μ (Mo-Kα) (mm ⁻¹)	1.47	0.82
F (000), θ range (°)	416, 2.4–30.5	2880, 2.3–26.9
No. of measured, independent and observed [I > 2σ(I)] reflections	25531, 4950, 4558	110929, 15135, 13225
R _{int}	0.034	0.069
Δρ _{max} , Δρ _{min} (e Å ⁻³)	0.81, -0.99	1.53, -1.02
No. of parameters	194	756
Refinement R[F ² > 2σ(F ²)], wR(F ²), S	0.022, 0.054, 1.12	0.040, 0.095, 1.07

Table 2.6. Selected bond lengths and angles for complexes **Ni A** and **Ni B**

Complex	Selected bond distances (Å)	Selected bond angles [°]
Ni A	Ni1—N1 ⁱ 2.099 (6), Ni1—N1 2.099 (6), Ni1—N2 2.188 (6), Ni1—N2 ⁱ 2.188 (6), Ni1—Cl1 ⁱ 2.373 (2), Ni1—Cl1 2.373 (2)	N1 ⁱ —Ni1—N1 180.0, N1 ⁱ —Ni1—N2 101.6 (2), N1—Ni1—N2 78.4 (2), N1 ⁱ —Ni1—N2 ⁱ 78.4 (2), N1—Ni1—N2 ⁱ 101.6 (2), N2—Ni1—N2 ⁱ 180.0 (3), N1 ⁱ —Ni1—Cl1 ⁱ 87.47 (18), N1—Ni1—Cl1 ⁱ 92.53 (18), N2—Ni1—Cl1 ⁱ 87.14 (17), N2 ⁱ —Ni1—Cl1 ⁱ 92.86 (17), N1 ⁱ —Ni1—Cl1 92.53 (18), N1—Ni1—Cl1 87.47 (18), N2—Ni1—Cl1 92.86 (17), N2 ⁱ —Ni1—Cl1 87.14 (17), Cl1 ⁱ —Ni1—Cl1 180.0
Ni B	Ni1—N1 2.060 (2), Ni1—N2 2.111 (2), Ni1—Cl1 2.3765 (8), Ni1—Cl2 2.3850 (9), Ni1—Cl1 ⁱ 2.4344 (8), Cl1—Ni1 ⁱ 2.4343 (8)	N1—Ni1—N2 79.16 (8), N1—Ni1—Cl1 174.14 (6), N2—Ni1—Cl1 95.05 (6), N1—Ni1—Cl2 90.46 (7), N2—Ni1—Cl2 100.09 (7), Cl1—Ni1—Cl2 91.40 (3), N1—Ni1—Cl1 ⁱ 94.46 (6), N2—Ni1—Cl1 ⁱ 167.34 (7), Cl1—Ni1—Cl1 ⁱ 91.06 (2), Cl2—Ni1—Cl1 ⁱ 90.81 (2), Ni1—Cl1—Ni1 ⁱ 88.94 (2)

Table 2.7. Selected bond lengths and angles for complexes **Pd A** and **Pd B**.

Complex	Selected bond distances (Å): Pd1—N1, Pd1—N2, Pd1—Cl2, Pd1—Cl1	Selected bond angles [°]: N1—Pd1—N2, N1—Pd1—Cl2, N2—Pd1—Cl2, N1—Pd1—Cl1, N2—Pd1—Cl1, Cl2—Pd1—Cl1
Pd A	2.0383 (15), 2.0392 (15), 2.2694 (7), 2.2929 (8)	80.72 (6), 173.55 (4), 93.50 (5), 95.22 (5), 175.92 (4), 90.54 (3)
Pd B	2.062 (3), 2.054 (3), 2.2830 (11), 2.2769 (11)	81.32 (13), 175.42 (9), 94.42 (10), 92.92 (9), 173.44 (10), 91.24 (4)

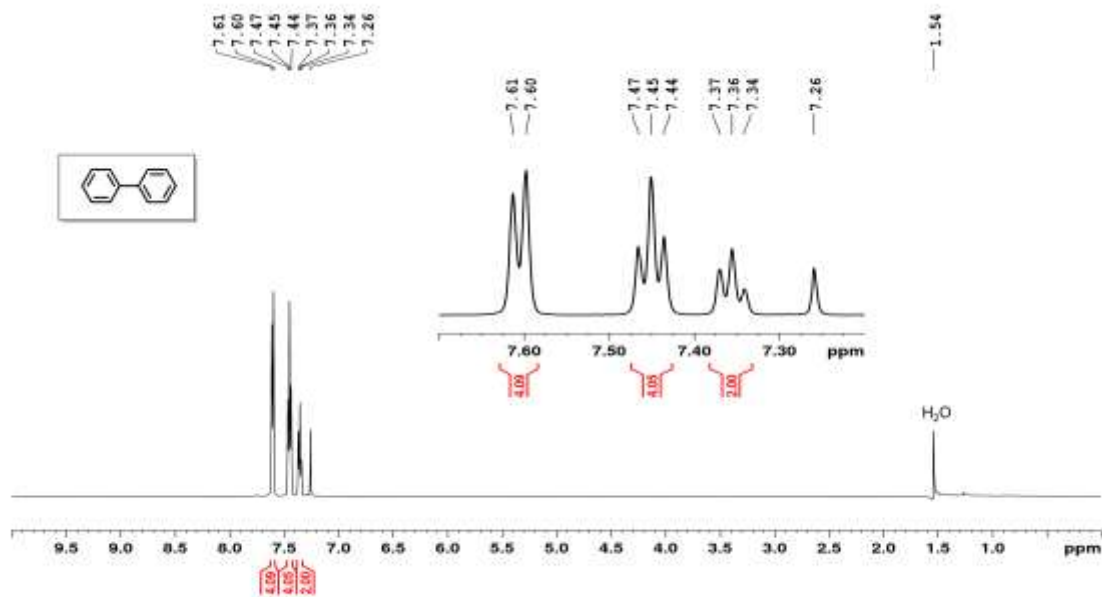


Figure 2.14. ^1H NMR spectrum of **1A1**.

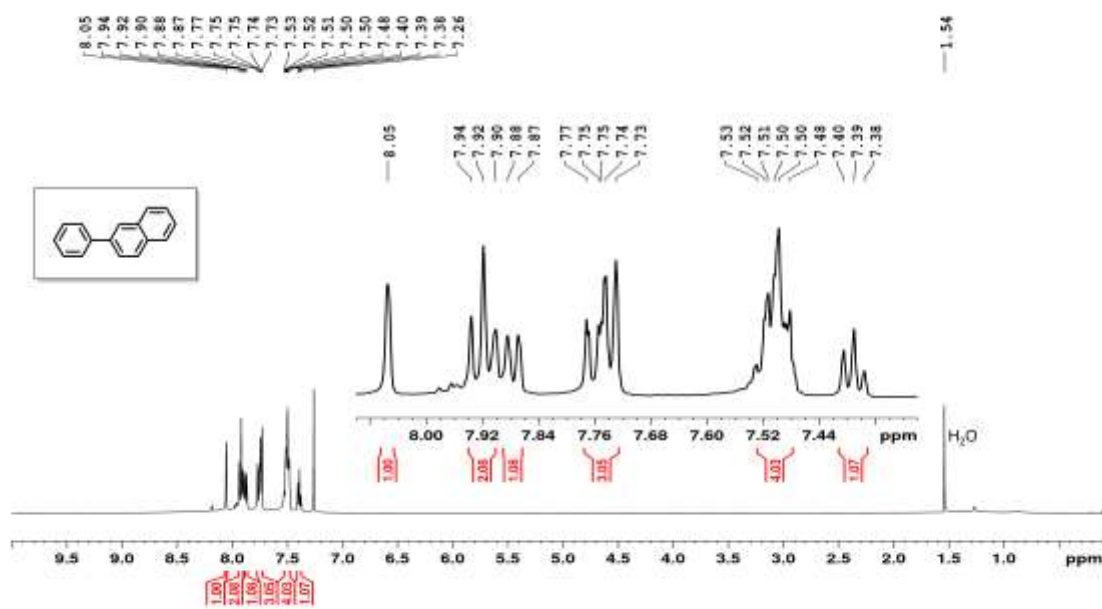


Figure 2.15. ^1H NMR spectrum of **1A2 & 2A1**.

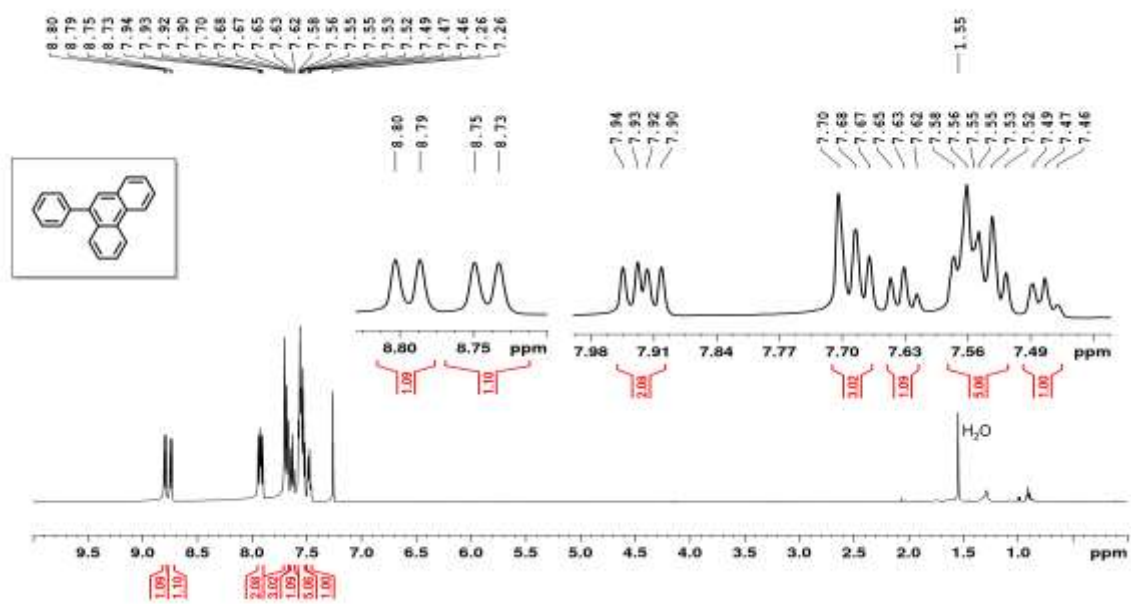


Figure 2.16. ^1H NMR spectrum of **1A3** & **3A1**

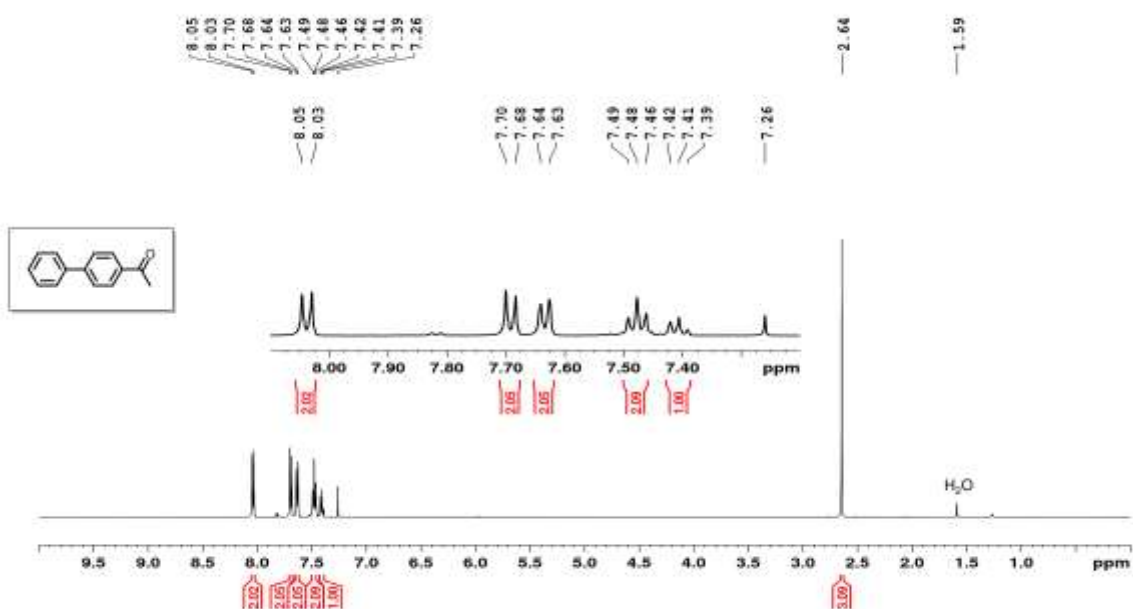


Figure 2.17. ^1H NMR spectrum of **1A4**.

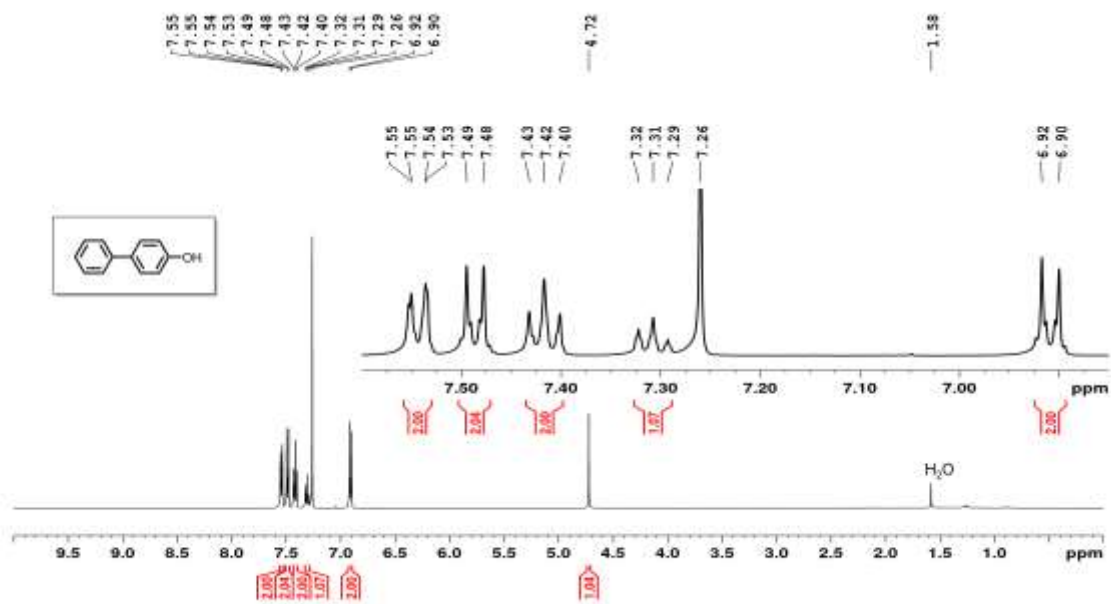


Figure 2.18. ^1H NMR spectrum of **1A5**.

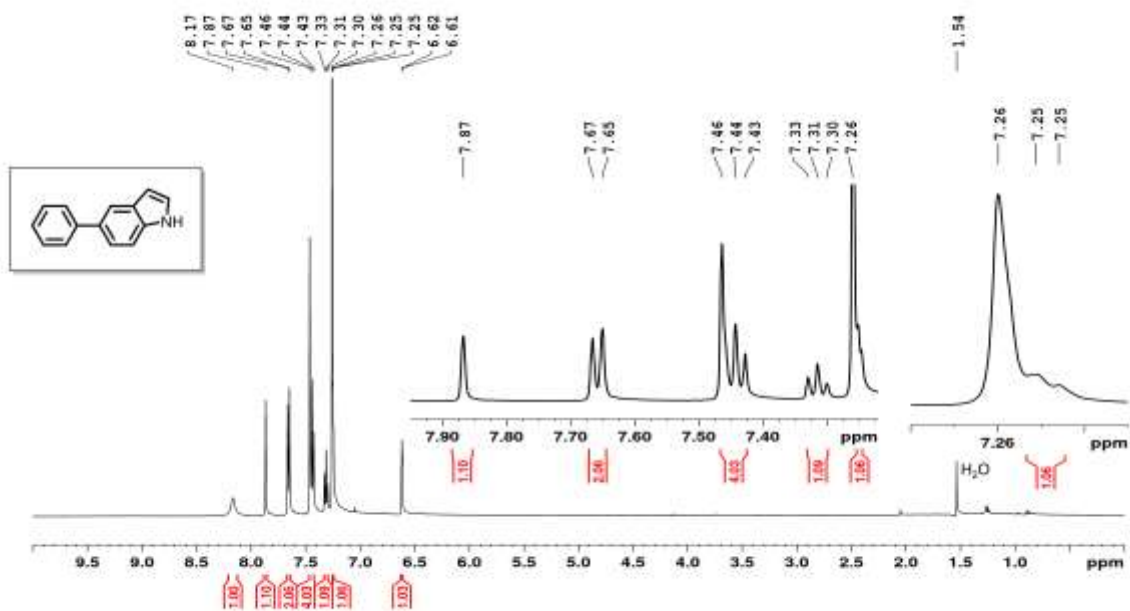


Figure 2.19. ^1H NMR spectrum of **1A6**.

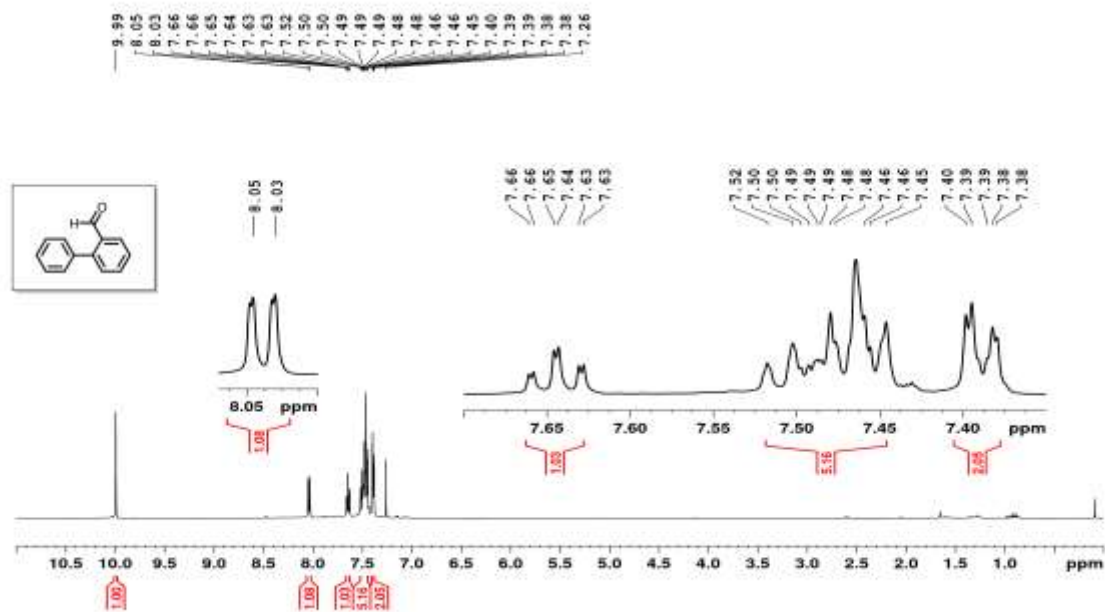


Figure 2.20. ¹H NMR spectrum of **1A7**.

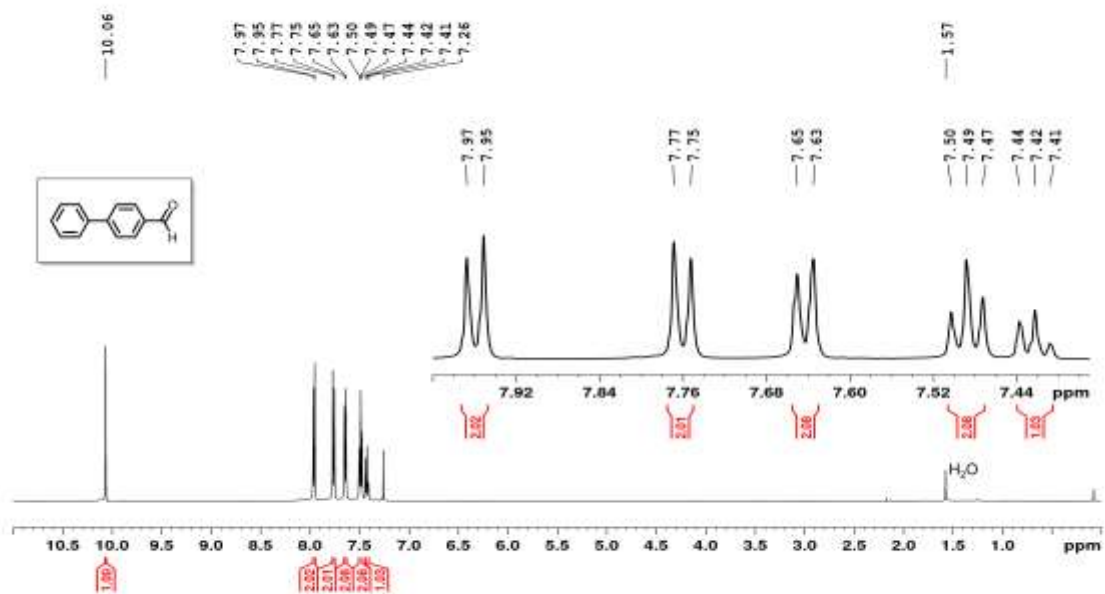


Figure 2.21. ¹H NMR spectrum of **1A8**.

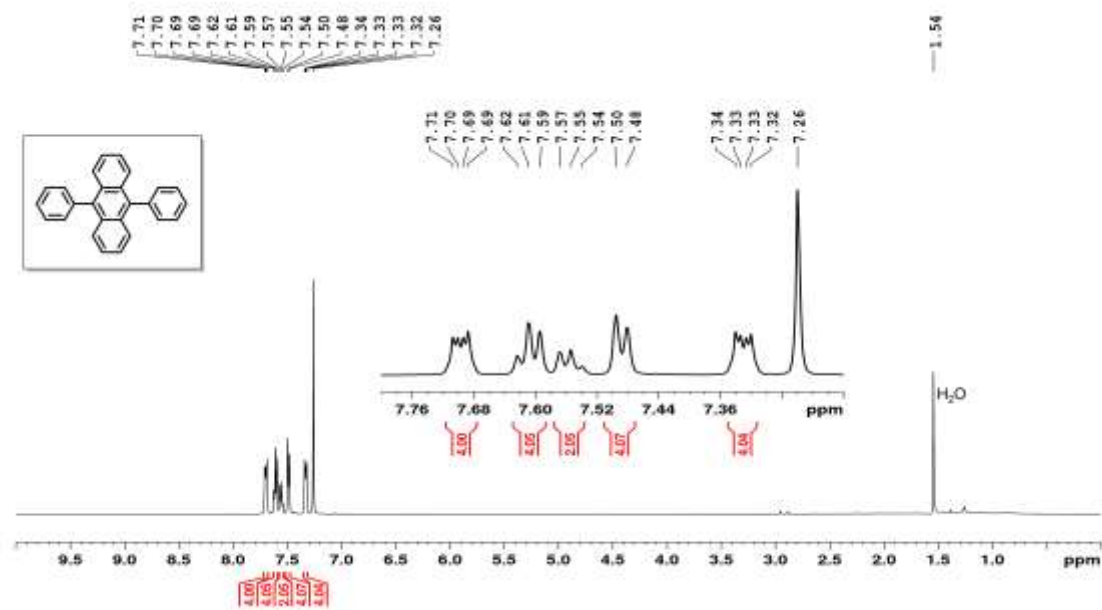


Figure 2.22. ¹H NMR spectrum of **1A9**.

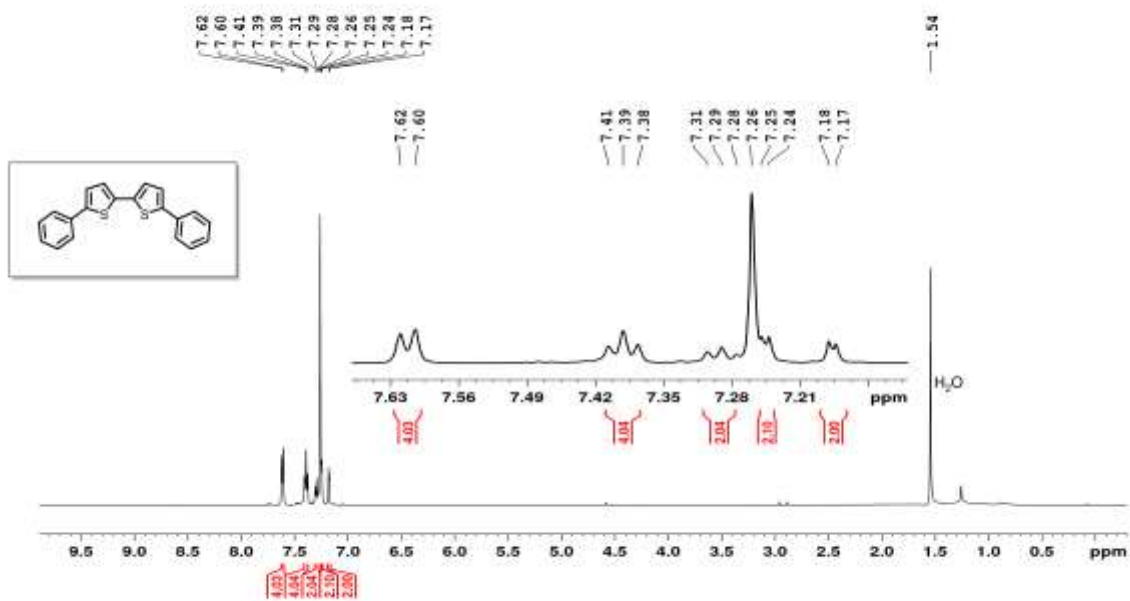


Figure 2.23. ¹H NMR spectrum of **1A10**.

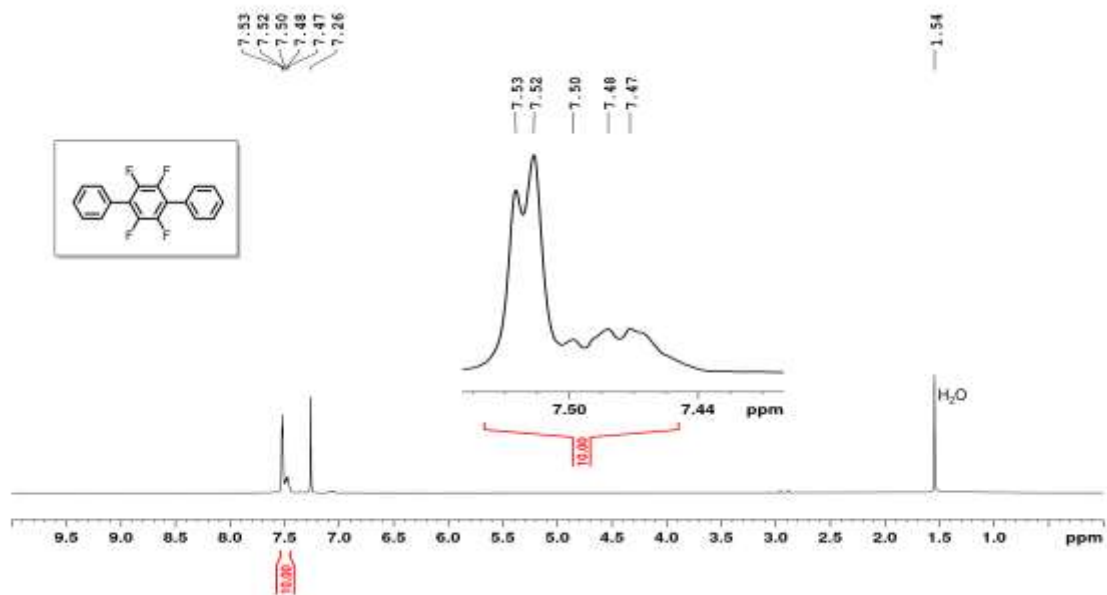


Figure 2.24. ¹H NMR spectrum of **1A11**.

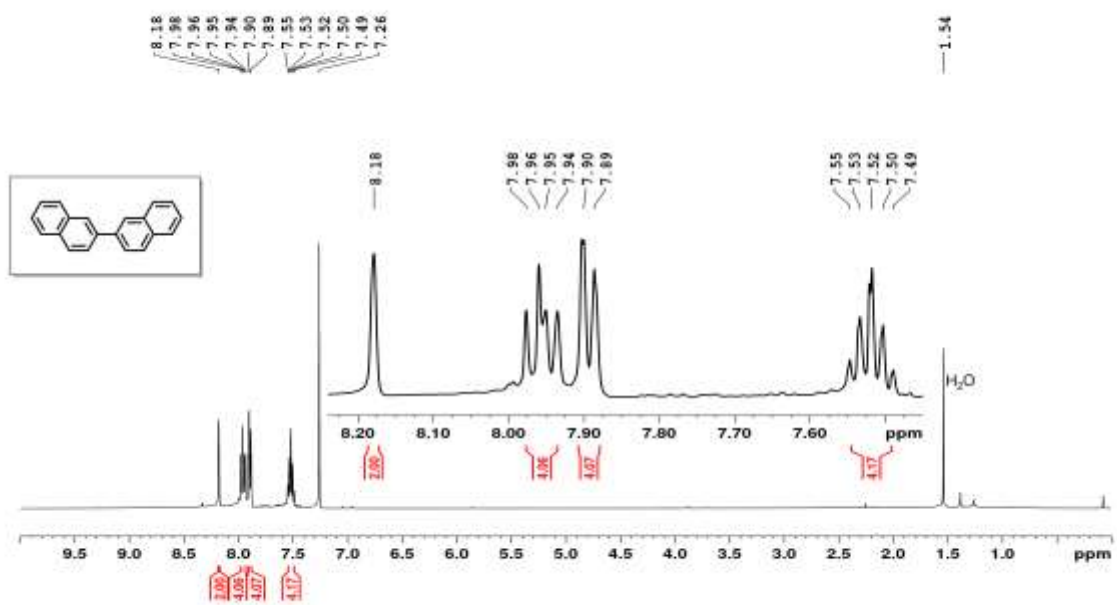


Figure 2.25. ¹H NMR spectrum of **2A2**.

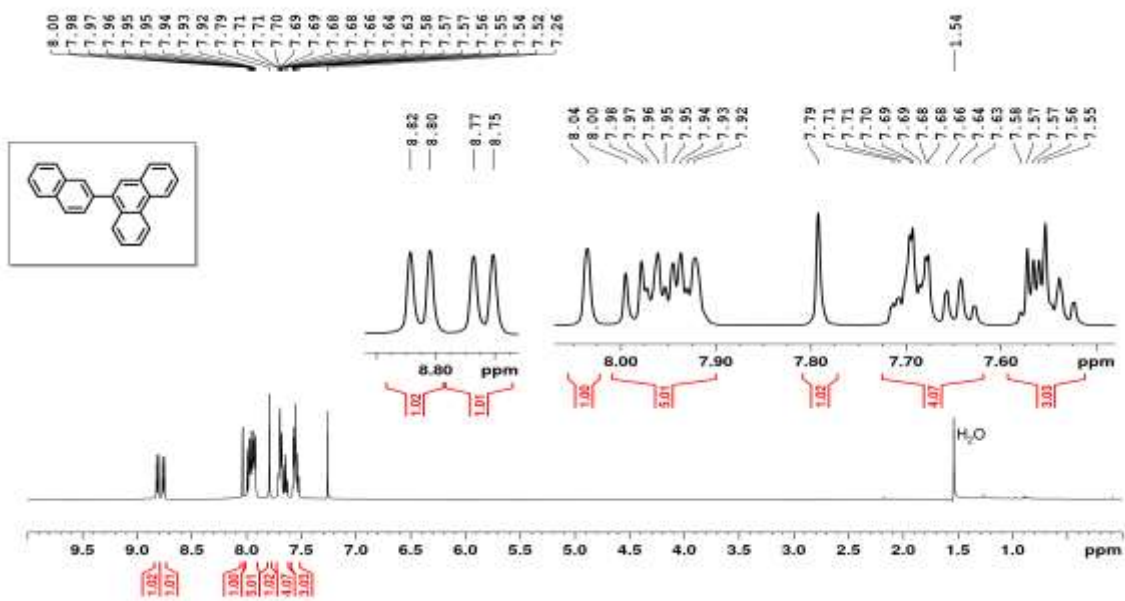


Figure 2.26. ¹H NMR spectrum of 2A3 & 3A2.

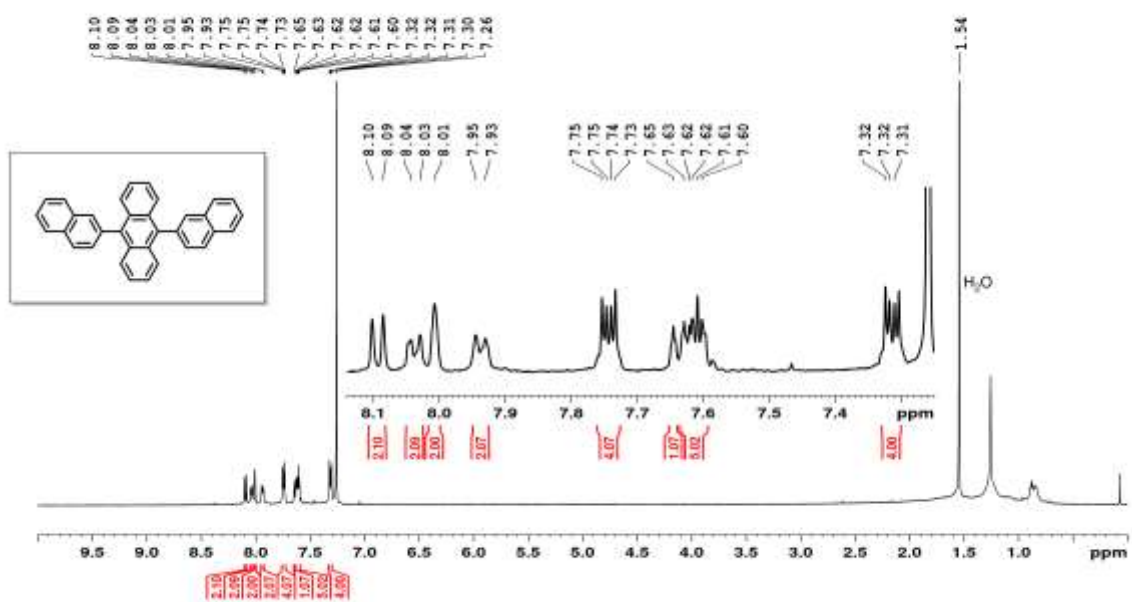


Figure 2.27. ¹H NMR spectrum of 2A4.

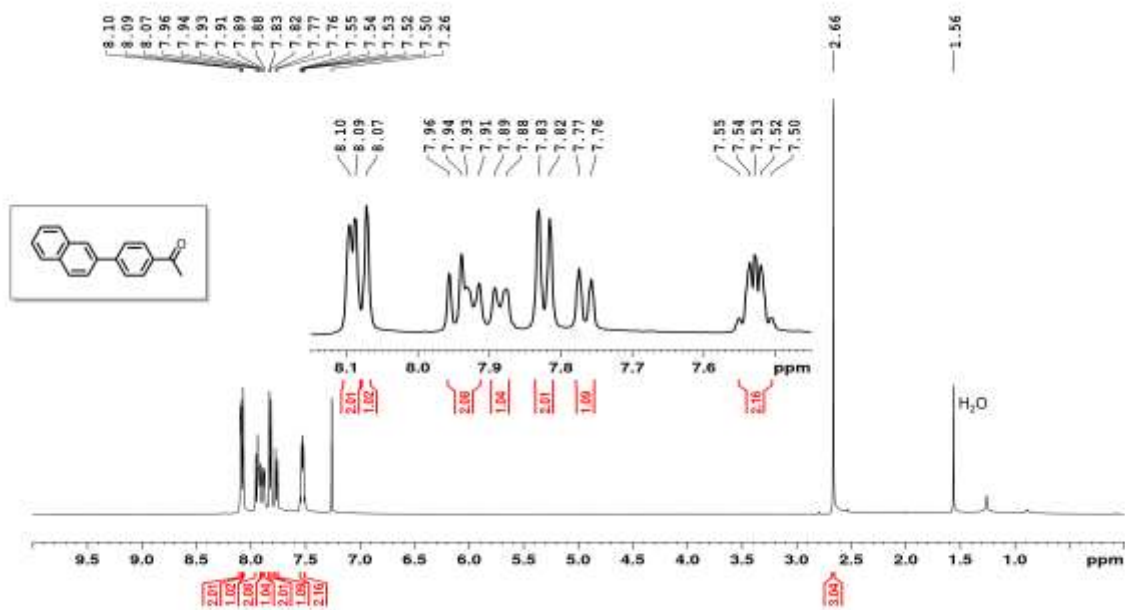


Figure 2.28. ^1H NMR spectrum of **2A5**.

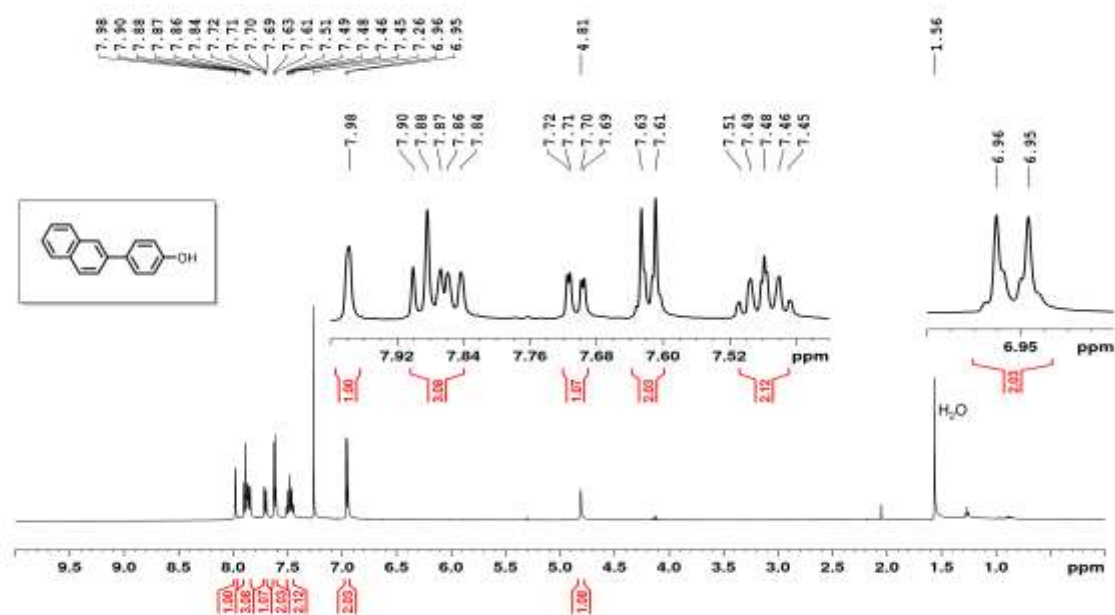


Figure 2.29. ^1H NMR spectrum of **2A6**.

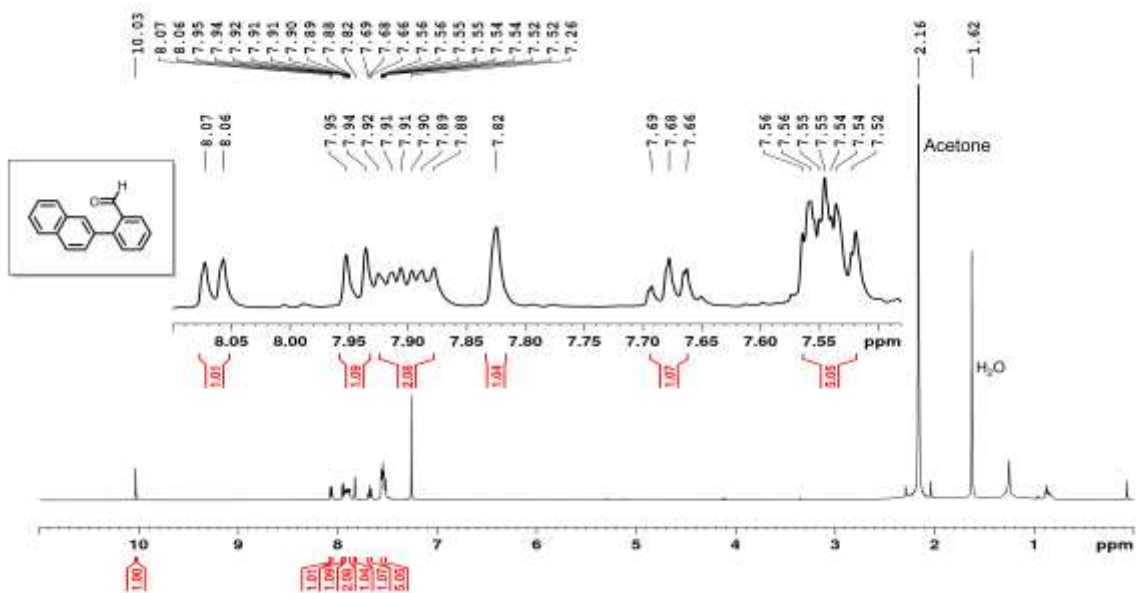


Figure 2.30. ^1H NMR spectrum of **2A7**.

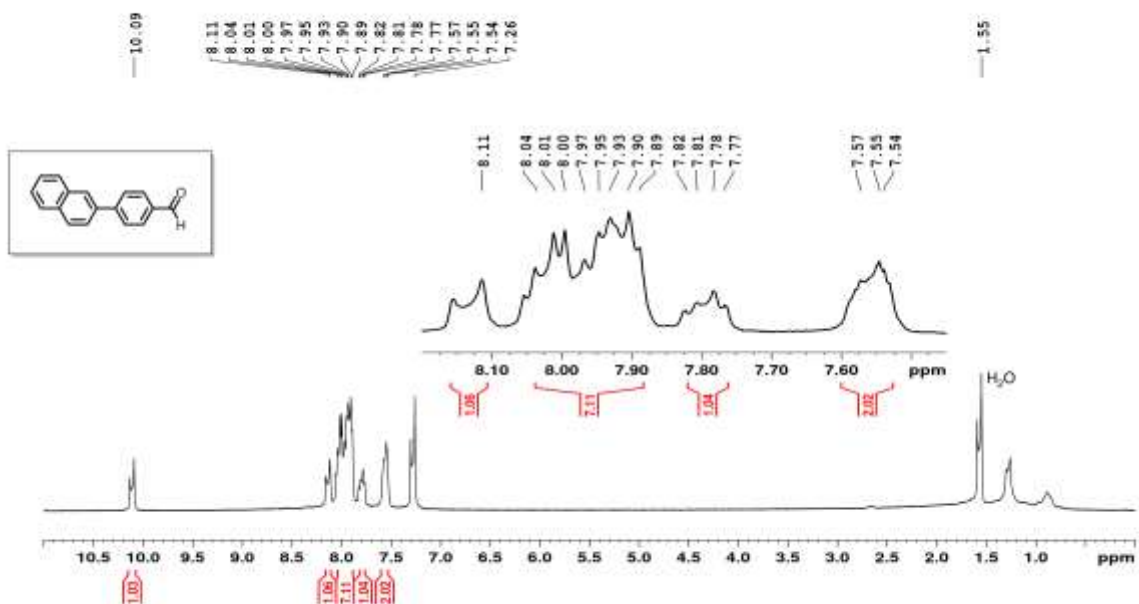


Figure 2.31. ^1H NMR spectrum of **2A8**.

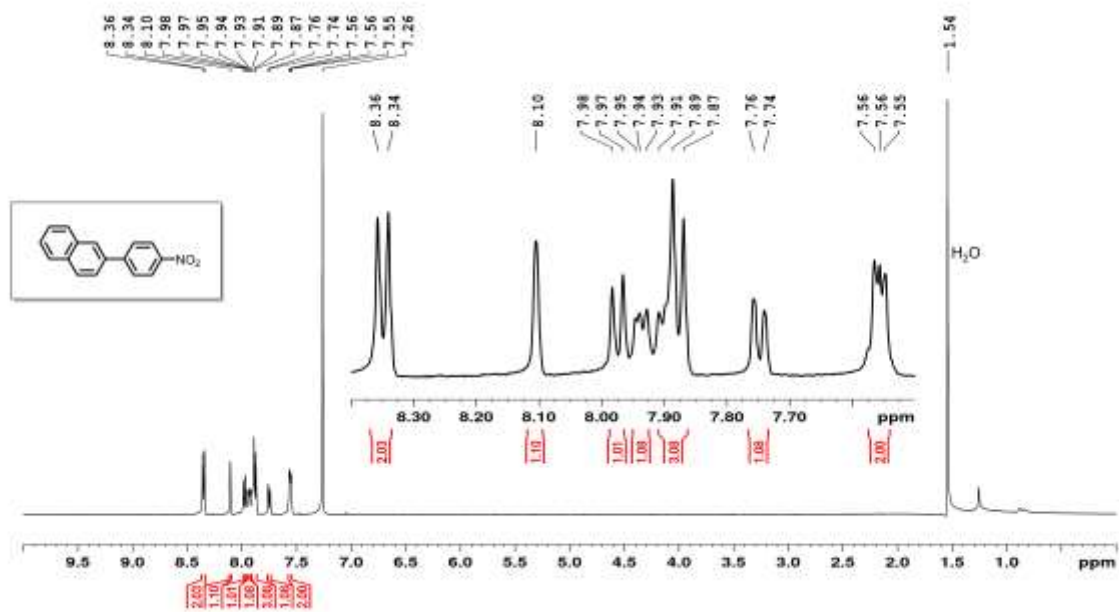


Figure 2.32. ¹H NMR spectrum of **2A9**.

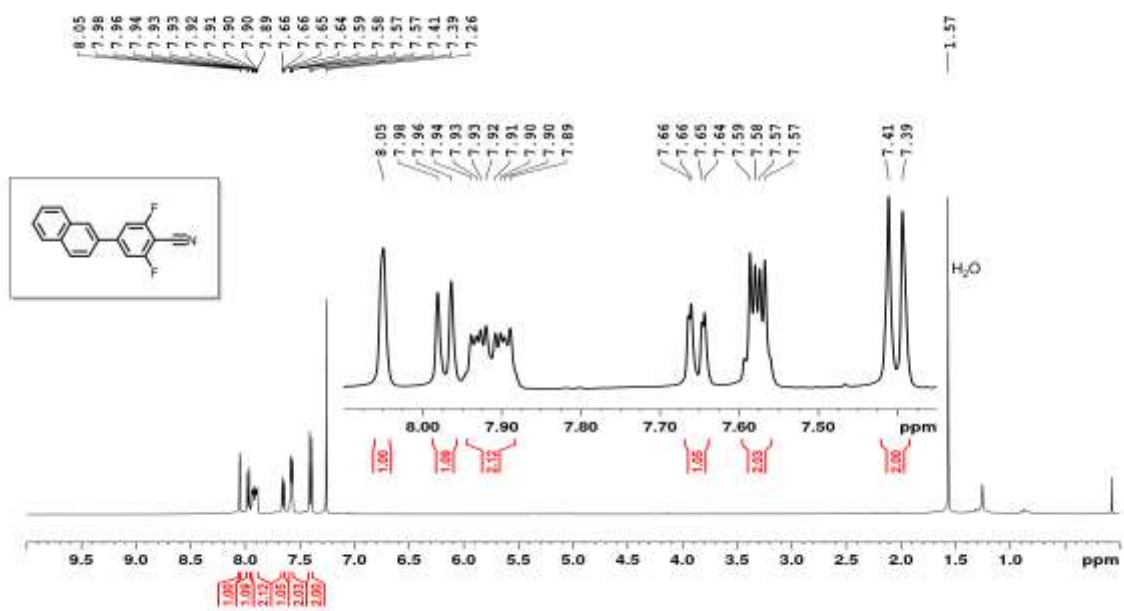


Figure 2.33. ¹H NMR spectrum of **2A10**.

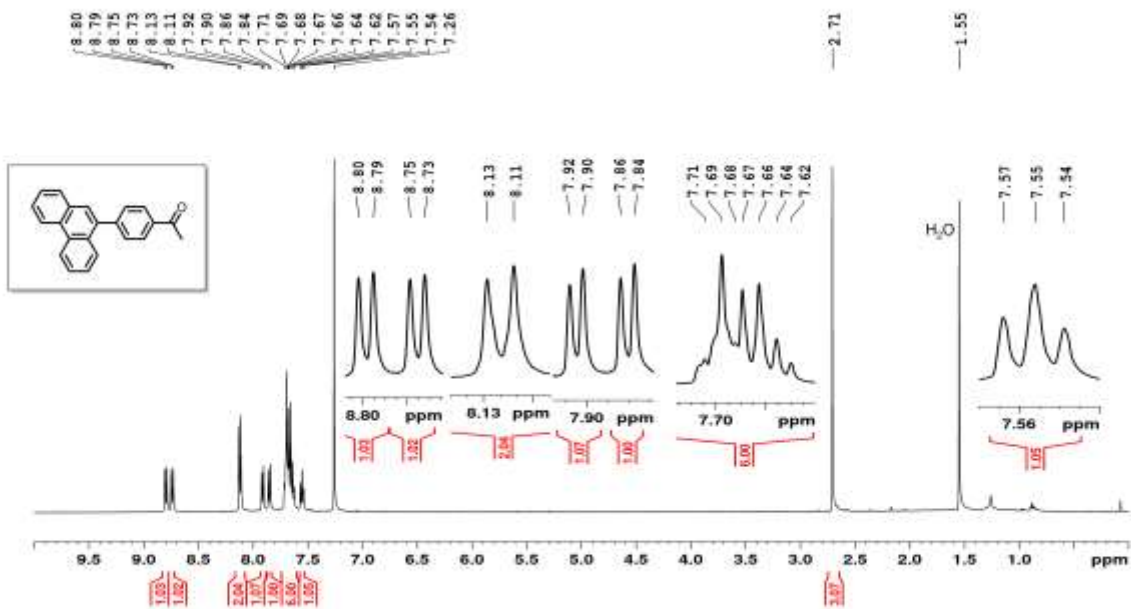


Figure 2.34. ¹H NMR spectrum of 3A3.

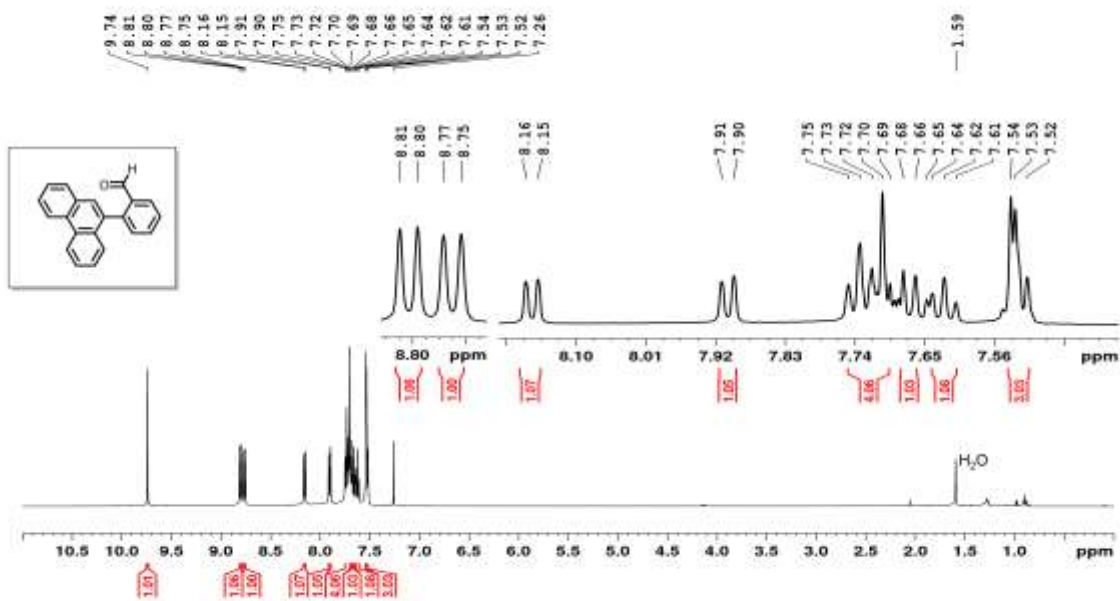


Figure 2.35. ¹H NMR spectrum of 3A4.

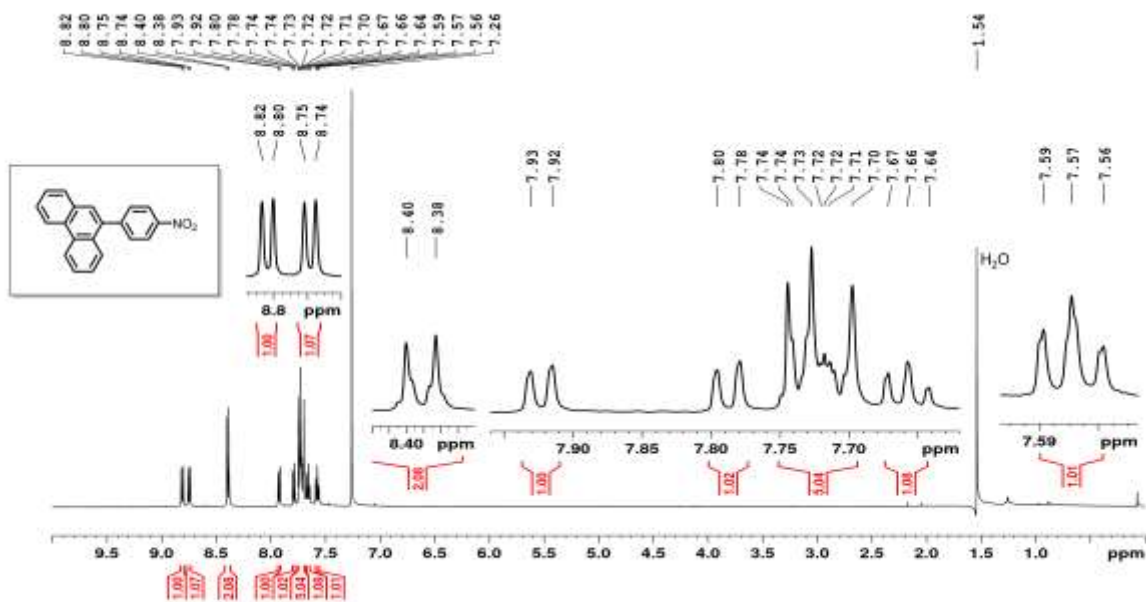


Figure 2.38. ¹H NMR spectrum of **3A7**.

2.8 References

- (1) Miyaura, N.; Suzuki, A. Stereoselective synthesis of arylated (E)-alkenes by the reaction of alk-1-enylboranes with aryl halides in the presence of palladium catalyst. *J. Chem. Soc., Chem. Commun.* **1979**, 866–867.
- (2) Miyaura, N.; Suzuki, A. Palladium-catalyzed cross-coupling reactions of organoboron compounds. *Chem. Rev.* **1995**, *95*, 2457–2483.
- (3) Torborg, C.; Beller, M. Recent applications of palladium-catalyzed coupling reactions in the pharmaceutical, agrochemical, and fine chemical industries. *Adv. Synth. Catal.* **2009**, *351*, 3027–3043.
- (4) Magano, J.; Dunetz, J. R. Large-scale applications of transition metal-catalyzed couplings for the synthesis of pharmaceuticals. *Chem. Rev.* **2011**, *111*, 2177–2250.
- (5) Campeau, L.-C.; Hazari, N. Cross-coupling and related reactions: connecting past success to the development of new reactions for the future. *Organometallics* **2019**, *38*, 3–35.

- (6) Kinzel, T.; Zhang, Y.; Buchwald, S. L. A new palladium precatalyst allows for the fast Suzuki–Miyaura coupling reactions of unstable polyfluorophenyl and 2-heteroaryl boronic acids. *J. Am. Chem. Soc.* **2010**, *132*, 14073–14075.
- (7) Chartoire, A.; Lesieur, M.; Falivene, L.; Slawin, A. M. Z.; Cavallo, L.; Cazin, C. S. J.; Nolan, S. P. [Pd(IPr*) (cinnamyl)Cl]: an efficient pre-catalyst for the preparation of tetra-ortho-substituted biaryls by Suzuki–Miyaura cross-coupling. *Chem. - Eur. J.* **2012**, *18*, 4517–4521.
- (8) Marion, N.; Navarro, O.; Mei, J.; Stevens, E. D.; Scott, N. M.; Nolan, S. P. Modified (NHC)Pd(allyl)Cl (NHC = N-heterocyclic carbene) complexes for room-temperature Suzuki–Miyaura and Buchwald–Hartwig reactions. *J. Am. Chem. Soc.* **2006**, *128*, 4101–4111.
- (9) Shi, S.; Nolan, S. P.; Szostak, M. Well-defined palladium(II)–NHC precatalysts for cross-coupling reactions of amides and esters by selective N–C/O–C cleavage. *Acc. Chem. Res.* **2018**, *51*, 2589–2599.
- (10) Valente, C.; Calimsiz, S.; Hoi, K. H.; Mallik, D.; Sayah, M.; Organ, M. G. The development of bulky palladium NHC complexes for the most-challenging cross-coupling reactions. *Angew. Chem., Int. Ed.* **2012**, *51*, 3314–3332.
- (11) Organ, M. G.; Çalimsiz, S.; Sayah, M.; Hoi, K. H.; Lough, A. J. Pd-PEPPSI-IPent: an active, sterically demanding cross-coupling catalyst and its application in the synthesis of tetra-ortho-substituted biaryls. *Angew. Chem., Int. Ed.* **2009**, *48*, 2383–2387.
- (12) Li, D.-H.; He, X.-X.; Xu, C.; Huang, F.-D.; Liu, N.; Shen, D.-S.; Liu, F.-S. N heterocarbene palladium complexes with dianisole backbones: synthesis, structure, and catalysis. *Organometallics* **2019**, *38*, 2539–2552.
- (13) Fortun, S.; Schmitzer, A. R. Synthesis and characterization of biguanide and biguanidium surfactants for efficient and recyclable application in the Suzuki–Miyaura reaction. *ACS Omega* **2018**, *3*, 1889–1896.
- (14) Saptal, V. B.; Saptal, M. V.; Mane, R. S.; Sasaki, T.; Bhanage, B. M. Amine-functionalized graphene oxide-stabilized Pd nanoparticles (Pd@APGO): a novel and efficient catalyst for the Suzuki and carbonylative Suzuki–Miyaura coupling reactions. *ACS Omega* **2019**, *4*, 643–649.
- (15) Nasrollahzadeh, M.; Issaabadi, Z.; Verma, R. S. Magnetic lignosulfonate-supported Pd complex: renewable resource-derived catalyst for aqueous Suzuki–Miyaura reaction. *ACS Omega* **2019**, *4*, 14234–14241.
- (16) Hamdi, J.; Blanco, A. A.; Diehl, B.; Wiley, J. B.; Trudell, M. L. Room-temperature aqueous Suzuki–Miyaura cross-coupling reactions catalyzed via a recyclable palladium@halloysite nanocomposite. *Org. Lett.* **2019**, *21*, 3471–3475.

- (17) Shen, D.; Xu, Y.; Shi, S.-L. A bulky chiral N heterocyclic carbene palladium catalyst enables highly enantioselective Suzuki–Miyaura cross-coupling reactions for the synthesis of biaryl atropisomers. *J. Am. Chem. Soc.* **2019**, *141*, 14938–14945.
- (18) Takahashi, R.; Kubota, K.; Ito, H. Air- and moisture-stable xantphos-ligated palladium dialkyl complex as a precatalyst for cross-coupling reactions. *Chem. Commun.* **2020**, *56*, 407–410.
- (19) Liu, G.; Han, F.; Liu, C.; Wu, H.; Zeng, Y.; Zhu, R.; Yu, X.; Rao, S.; Huang, G.; Wang, J. A highly active catalyst system for Suzuki–Miyaura coupling of aryl chlorides. *Organometallics* **2019**, *38*, 1459–1467.
- (20) Hazari, N.; Melvin, P. R.; Beromi, M. M. Well-defined nickel and palladium precatalysts for cross-coupling. *Nat. Rev. Chem.* **2017**, *1*, 0025.
- (21) Tobisu, M.; Chatani, N. Cross-couplings using aryl ethers via C–O bond activation enabled by nickel catalysts. *Acc. Chem. Res.* **2015**, *48*, 1717–1726.
- (22) Zultanski, S. L.; Fu, G. C. Nickel-catalyzed carbon-carbon bond-forming reactions of unactivated tertiary alkyl halides: Suzuki arylations. *J. Am. Chem. Soc.* **2013**, *135*, 624–627.
- (23) Tasker, S. Z.; Standley, E. A.; Jamison, T. F. Recent advances in homogeneous nickel catalysis. *Nature* **2014**, *509*, 299–309.
- (24) Ge, S.; Hartwig, J. F. Highly reactive, single-component nickel catalyst precursor for Suzuki–Miyaura cross-coupling of heteroaryl boronic acids with heteroaryl halides. *Angew. Chem., Int. Ed.* **2012**, *51*, 12837–12841.
- (25) Han, F.-S. Transition-metal-catalyzed Suzuki–Miyaura cross-coupling reactions: a remarkable advance from palladium to nickel catalysts. *Chem. Soc. Rev.* **2013**, *42*, 5270–5298.
- (26) Yu, D.-G.; Yu, M.; Guan, B.-T.; Li, B.-J.; Zheng, Y.; Wu, Z.-H.; Shi, Z.-J. Carbon-carbon formation via Ni-catalyzed Suzuki–Miyaura coupling through C–CN bond cleavage of aryl nitrile. *Org. Lett.* **2009**, *11*, 3374–3377.
- (27) Tobisu, M.; Xu, T.; Shimasaki, T.; Chatani, N. Nickel-catalyzed Suzuki–Miyaura reaction of aryl fluorides. *J. Am. Chem. Soc.* **2011**, *133*, 19505–19511.
- (28) Muto, K.; Yamaguchi, J.; Musaev, D.; Itami, K. Decarbonylative organoboron cross-coupling of esters by nickel catalysis. *Nat. Commun.* **2015**, *6*, 7508.
- (29) Takise, R.; Muto, K.; Yamaguchi, J. Cross-coupling of aromatic esters and amides. *Chem. Soc. Rev.* **2017**, *46*, 5864–5888.

- (30) Rosen, B. M.; Quasdorf, K. W.; Wilson, D. A.; Zhang, N.; Resmerita, A.-M.; Garg, N. K.; Percec, V. Nickel-catalyzed cross-couplings involving carbon-oxygen bonds. *Chem. Rev.* **2011**, *111*, 1346–1416.
- (31) Kuwano, R.; Shimizu, R. An improvement of nickel catalyst for cross-coupling reaction of arylboronic acids with aryl carbonates by using a ferrocenyl bisphosphine ligand. *Chem. Lett.* **2011**, *40*, 913–915.
- (32) Shields, J. D.; Gray, E. E.; Doyle, A. G. A modular, air-stable nickel precatalyst. *Org. Lett.* **2015**, *17*, 2166–2169.
- (33) Magano, J.; Monfette, S. Development of an air-stable, broadly applicable nickel source for nickel-catalyzed cross-coupling. *ACS Catal.* **2015**, *5*, 3120–3123.
- (34) Marion, N.; Nolan, S. P. Well-defined N-heterocyclic carbenes-palladium(II) precatalysts for cross-coupling reactions. *Acc. Chem. Res.* **2008**, *41*, 1440–1449.
- (35) Bruno, N. C.; Tudge, M. T.; Buchwald, S. L. Design and preparation of new palladium precatalysts for C-C and C-N cross-coupling reactions. *Chem. Sci.* **2013**, *4*, 916–920.
- (36) Froese, R. D. J.; Lombardi, C.; Pompeo, M.; Rucker, R.; Organ, M. G. Designing Pd-N-heterocyclic carbene complexes for high reactivity and selectivity for cross-coupling applications. *Acc. Chem. Res.* **2017**, *50*, 2244–2253.
- (37) Bernhammer, J. C.; Huynh, H. V. Nickel(II) benzimidazolin-2-ylidene complexes with thioether-functionalized side chains as catalysts for Suzuki–Miyaura cross-coupling. *Organometallics* **2014**, *33*, 5845–5851.
- (38) Standley, E. A.; Smith, S. J.; Muller, P.; Jamison, T. F. A broadly applicable strategy for entry into homogeneous nickel(0) catalysts from air-stable nickel(II) complexes. *Organometallics* **2014**, *33*, 2012–2018.
- (39) Guard, L. M.; Beromi, M. M.; Brudvig, G. W.; Hazari, N.; Vinyard, D. J. Comparison of dppf-supported nickel precatalysts for the Suzuki–Miyaura reaction: the observation and activity of nickel(I). *Angew. Chem., Int. Ed.* **2015**, *54*, 13352–13356.
- (40) Malineni, J.; Jezorek, R. L.; Zhang, N.; Percec, V. An indefinitely air-stable σ -Ni^{II} precatalyst for quantitative cross-coupling of unreactive aryl halides and mesylates with aryl neopentylglycolboronates. *Synthesis* **2016**, *48*, 2795–2807.
- (41) Beromi, M. M.; Nova, A.; Balcells, D.; Brasacchio, A. M.; Brudvig, G. W.; Guard, L. M.; Hazari, N.; Vinyard, D. J. Mechanistic study of an improved Ni precatalyst for Suzuki–Miyaura reactions of aryl sulfamates: understanding the role of Ni(I) species. *J. Am. Chem. Soc.* **2017**, *139*, 922–936.

- (42) Nirmala, M.; Prakash, G.; Ramahandran, R.; Viswanathamurthi, P.; Malecki, J. G.; Linert, W. Nickel(II) complex incorporating methylene bridged tetradentate dicarbene ligands as an efficient catalyst toward C-C and C-N bond formation reactions. *J. Mol. Catal. A. Chem.* **2015**, *397*, 56–67.
- (43) Beromi, M. M.; Banerjee, G.; Brudvig, G. W.; Charboneau, D. J.; Hazari, N.; Lant, H. M. C.; Mercado, B. Q. Modifications to the aryl group of dppf-ligated Ni σ aryl precatalysts: impact on speciation and catalytic activity in Suzuki–Miyaura coupling reactions. *Organometallics* **2018**, *37*, 3943–3955.
- (44) Barth, E. L.; Davis, R. M.; Beromi, M. M.; Walden, A. G.; Balcells, D.; Brudvig, G. W.; Dardir, A. H.; Hazari, N.; Lant, H. M. C.; Mercado, B. Q.; Peczak, I. L. Bis(dialkylphosphino)ferrocene-ligated nickel(II) precatalysts for Suzuki–Miyaura reactions of aryl carbonates. *Organometallics* **2019**, *38*, 3377–3387.
- (45) West, M. J.; Watson, A. J. B. Ni vs. Pd in Suzuki–Miyaura sp^2 – sp^2 cross-coupling: a head-to-head study in a comparable precatalyst/ligand system. *Org. Biomol. Chem.* **2019**, *17*, 5055–5059.
- (46) Duczynski, J.; Sobolev, A. N.; Moggach, S. A.; Dorta, R.; Stewart, S. G. The synthesis and catalytic activity of new mixed NHC-phosphite nickel(0) complexes. *Organometallics* **2020**, *39*, 105–115.
- (47) Madera, J.; Slattery, M.; Arman, H. D.; Tonzetich, Z. J. Suzuki–Miyaura coupling catalyzed by a Ni(II) PNP pincer complex: scope and mechanistic insights. *Inorg. Chim. Acta* **2020**, *504*, 119457.
- (48) Ramgren, S. D.; Hie, L.; Ye, Y.; Garg, N. K. Nickel-catalyzed Suzuki–Miyaura couplings in green solvents. *Org. Lett.* **2013**, *15*, 3950–3953.
- (49) Inaloo, I. D.; Majnooni, S.; Eslahi, H.; Esmailpour, M. Nickel(II) nanoparticles immobilized on EDTA-modified Fe₃O₄@SiO₂ nanospheres as efficient and recyclable catalysts for ligand-free Suzuki–Miyaura coupling of aryl carbamates and sulfamates. *ACS Omega* **2020**, *5*, 7406–7417.
- (50) Key, R. J.; Tengco, J. M. M.; Smith, M. D.; Vannucci, A. K. A molecular/heterogeneous nickel catalyst for Suzuki–Miyaura coupling. *Organometallics* **2019**, *38*, 2007–2014.
- (51) Elumalai, P.; Mamlouk, H.; Yiming, W.; Feng, L.; Yuan, S.; Zhou, H.-C.; Madrahimov, S. T. Recyclable and reusable heteroleptic nickel catalyst immobilized on metal–organic framework for Suzuki–Miyaura coupling. *ACS Appl. Mater. Interfaces* **2018**, *10*, 41431–41438.
- (52) Molander, G. A.; Canturk, B.; Kennedy, L. E. Scope of the Suzuki–Miyaura cross-coupling reactions of potassium heteroaryltrifluoroborates, *J. Org. Chem.* **2009**, *74*, 973–980.

- (53) Christmann, U.; Vilar, R. Monoligated palladium species as catalysts in cross-coupling reactions. *Angew. Chem., Int. Ed.* **2005**, *44*, 366–374.
- (54) Schnyder, A.; Indolese, A. F.; Studer, M.; Blaser, H.-U. A new generation of air stable, highly active Pd complexes for C-C and C-N coupling reactions with aryl chlorides. *Angew. Chem., Int. Ed.* **2002**, *41*, 3668–3671.
- (55) Altenhoff, G.; Goddard, R.; Lehmann, C. W.; Glorius, F. Sterically demanding, bioxazoline-derived N-heterocyclic carbene ligands with restricted flexibility for catalysis. *J. Am. Chem. Soc.* **2004**, *126*, 15195–15201.
- (56) Wurtz, S.; Glorius, F. Surveying sterically demanding N-heterocyclic carbene ligands with restricted flexibility for palladium-catalyzed cross-coupling reactions. *Acc. Chem. Res.* **2008**, *41*, 1523–1533.
- (57) Szilvasi, T.; Veszpremi, T. Internal catalytic effect of bulky NHC ligands in Suzuki–Miyaura cross-coupling reaction. *ACS Catal.* **2013**, *3*, 1984–1991.
- (58) Wolfe, J. P.; Tomori, H.; Sadighi, J. P.; Yin, J.; Buchwald, S. L. Simple, efficient catalyst system for the palladium-catalyzed amination of aryl chlorides, bromides, and triflates. *J. Org. Chem.* **2000**, *65*, 1158–1174.
- (59) Altenhoff, G.; Goddard, R.; Lehmann, C. W.; Glorius, F. An N-heterocyclic carbene ligand with flexible steric bulk allows Suzuki cross-coupling of sterically hindered aryl chlorides at room temperature. *Angew. Chem., Int. Ed.* **2003**, *42*, 3690–3693.
- (60) Gates, D. P.; Svejda, S. A.; Onate, E.; Killian, C. M.; Johnson, L. K.; White, P. S.; Brookhart, M. Synthesis of branched polyethylene using (α -diimine)nickel(II) catalysts: influence of temperature, ethylene pressure, and ligand structure on polymer properties. *Macromolecules* **2000**, *33*, 2320–2334.
- (61) Killian, C. M.; Johnson, L. K.; Brookhart, M. Preparation of linear α -olefins using cationic nickel(II) α -diimine catalysts. *Organometallics* **1997**, *16*, 2005–2007.
- (62) Gottfried, A. C.; Brookhart, M. Living and block copolymerization of ethylene and α -olefins using palladium(II)- α -diimine catalysts. *Macromolecules* **2003**, *36*, 3085–3100.
- (63) Zhang, D.; Nadres, E. T.; Brookhart, M.; Daugulis, O. Synthesis of highly branched polyethylene using “sandwich” (8 p tolyl naphthyl α diimine)nickel(II) catalysts. *Organometallics* **2013**, *32*, 5136–5143.
- (64) Rhinehart, J. L.; Brown, L. A.; Long, B. K. A robust Ni(II) α diimine catalyst for high temperature ethylene polymerization. *J. Am. Chem. Soc.* **2013**, *135*, 16316–16319.

- (65) Zhong, L.; Li, G.; Liang, G.; Gao, H.; Wu, Q. Enhancing thermal stability and living fashion in α diimine-nickel-catalyzed (co)polymerization of ethylene and polar monomer by increasing the steric bulk of ligand backbone. *Macromolecules* **2017**, *50*, 2675–2682.
- (66) Johnson, L. K.; Killian, C. M.; Brookhart, M. New Pd (II)- and Ni (II)-based catalysts for polymerization of ethylene and α -olefins. *J. Am. Chem. Soc.* **1995**, *117*, 6414–6415.
- (67) Tempel, D. J.; Johnson, L. K.; Huff, L.; White, P. S.; Brookhart, M. Mechanistic studies of Pd(II)- α -diimine-catalyzed olefin polymerizations¹. *J. Am. Chem. Soc.* **2000**, *122*, 6686–6700.
- (68) Dai, S.; Sui, X.; Chen, C. Highly robust palladium(II) α -diimine catalysts for slow-chain-walking polymerization of ethylene and copolymerization with methyl acrylate. *Angew. Chem., Int. Ed.* **2015**, *54*, 9948–9953.
- (69) Popeney, C. S.; Guan, Z. Ligand electronic effects on late transition metal polymerization catalysts. *Organometallics* **2005**, *24*, 1145–1155.
- (70) Popeney, C. S.; Guan, Z. Effect of ligand electronics on the stability and chain transfer rates of substituted Pd(II) α -diimine catalysts¹. *Macromolecules* **2010**, *43*, 4091–4097.
- (71) Grasa, G. A.; Hillier, A. C.; Nolan, S. P. Convenient and efficient Suzuki–Miyaura cross-coupling catalyzed by a palladium/diazabutadiene system. *Org. Lett.* **2001**, *3*, 1077–1080.
- (72) Zhou, J.; Guo, X.; Tu, C.; Li, X.; Sun, H. Aqueous Suzuki coupling reaction catalyzed by water-soluble diimine/Pd(II) systems. *J. Organomet. Chem.* **2009**, *694*, 697–702.
- (73) Wanga, F.; Tanakaa, R.; Caib, Z.; Nakayamaa, Y.; Shiono, T. Room-temperature Suzuki–Miyaura cross-coupling reaction with α -diimine Pd(II) catalysts. *Appl. Organometal. Chem.* **2015**, *29*, 771–776.
- (74) Yu, J.; Shen, A.; Cao, Y.; Lu, G. Preparation of Pd-diimine@SBA-15 and its catalytic performance for the Suzuki coupling reaction. *Catalysts* **2016**, *6*, 181.
- (75) Huo, P.; Li, J.; Liu, W.; Mei, G. Highly efficient bulky α -diimine palladium complexes for Suzuki–Miyaura cross-coupling reaction. *Chin. J. Chem.* **2017**, *35*, 363–367.
- (76) Dong, Y.; Jv, J.-J.; Li, Y.; Li, W.-H.; Chen, Y.-Q.; Sun, Q.; Ma, J.-P.; Dong, Y.-B. Nickel-metalated porous organic polymer for Suzuki–Miyaura cross-coupling reaction. *RSC Adv.* **2019**, *9*, 20266–20272.
- (77) Leone, A. K.; Souther, K. D.; Vitek, A. K.; Lapointe, A. M.; Coates, G. W.; Zimmerman, P. M.; Mcneil, A. J. Mechanistic insight into thiophene catalyst-transfer polymerization mediated by nickel diimine catalysts. *Macromolecules* **2017**, *50*, 9121–9127.

- (78) Song, G.; Guo, L.; Du, Q.; Kong, W.; Li, W.; Liu, Z. Highly active mono and bis-ligated iminopyridyl nickel catalysts for 1-hexene reactions. *J. Organomet. Chem.* **2018**, *858*, 1–7.
- (79) Braga, A. A. C.; Morgon, N. H.; Ujaque, G.; Maseras, F. Computational characterization of the role of the base in the Suzuki–Miyaura cross-coupling reaction. *J. Am. Chem. Soc.* **2005**, *127*, 9298–9307.
- (80) Zhang, H.; Kwong, F. Y.; Tian, Y.; Chan, K. S. Base and cation effects on the Suzuki cross-coupling of bulky arylboronic acid with halopyridines: synthesis of pyridylphenols. *J. Org. Chem.* **1998**, *63*, 6886–6890.
- (81) Proutiere, F.; Schoenebeck, F. Solvent effect on palladium-catalyzed cross-coupling reactions and implications on the active catalytic species. *Angew. Chem., Int. Ed.* **2011**, *50*, 8192–8195.
- (82) Lima, C. F. R. A. C.; Rodrigues, A. S. M. C.; Silva, V. L. M.; Silva, A. M. S.; Santos, L. M. N. B. F. Role of the base and control of selectivity in the Suzuki–Miyaura cross-coupling reaction. *ChemCatChem* **2014**, *6*, 1291–1302.
- (83) Lennox, A. J. J.; Lloyd-Jones, G. C. Selection of boron reagents for Suzuki–Miyaura coupling. *Chem. Soc. Rev.* **2014**, *43*, 412–443.
- (84) Schroeter, F.; Soellner, J.; Strassner, T. Cyclometalated palladium NHC complexes bearing PEG chains for Suzuki–Miyaura cross-coupling in water. *Organometallics* **2018**, *37*, 4267–4275.
- (85) Prajapati, P. K.; Saini, S.; Jain, S. L. Nickel mediated palladium free photocatalytic Suzuki-coupling reaction under visible light irradiation. *J. Mater. Chem. A* **2020**, *8*, 5246–5254.
- (86) Jamwal, B.; Kaur, M.; Sharma, H.; Khajuria, C.; Paul, S.; Clark, J. H. Diamines as interparticle linkers for silica-titania supported PdCu bimetallic nanoparticles in Chan-Lam and Suzuki cross-coupling reactions. *New J. Chem.* **2019**, *43*, 4919–4928
- (87) Reddy, V. P.; Qiu, R.; Iwasaki, T.; Kambe, N. Rhodium-catalyzed intermolecular oxidative cross-coupling of (hetero)arenes with chalcogenophenes. *Org. Lett.* **2013**, *15*, 1290–1293.
- (88) Song, J.; Wei, F.; Sun, W.; Cao, X.; Liu, C.; Xie, L.; Huang, W. Highly efficient C-C cross-coupling for installing thiophene rings into π -conjugated systems. *Org. Chem. Front.* **2014**, *1*, 817–820.
- (89) Sarsah, S. R. S.; Lutz, M. R.; Zeller, M.; Crumrine, D.; Becker, D. P. Rearrangement of cyclotrimeratrylene (CTV) diketone: 9,10- diarylanthracenes with OLED applications. *J. Org. Chem.* **2013**, *78*, 2051–2058.

- (90) Zende, V. M.; Schulzke, C.; Kapdi, A. R. Pincer CNC bis-N-heterocyclic carbenes: robust ligands for palladium-catalysed Suzuki–Miyaura arylation of bromoanthracene and related substrates. *Org. Chem. Front.* **2015**, *2*, 1397–1410.
- (91) Bolliger, J. L.; Frecha, C. M. The 1,3-diaminobenzene-derived aminophosphine palladium pincer complex $\{C_6H_3[NHP(piperidiny)]_2\}Pd(Cl)$ – a highly active Suzuki–Miyaura catalyst with excellent functional group tolerance. *Adv. Synth. Catal.* **2010**, *352*, 1075–1080.
- (92) Fleming, F. F.; Yao, L.; Ravikumar, P. C.; Funk, L.; Shook, B. C. Nitrile-containing pharmaceuticals: efficacious roles of the nitrile pharmacophore. *J. Med. Chem.* **2010**, *53*, 7902–7917.
- (93) Discolo, C. A.; Touney, E. E.; Pronin, S. V. Catalytic asymmetric radical-polar crossover hydroalkoxylation. *J. Am. Chem. Soc.* **2019**, *141*, 17527–17532.
- (94) Kamal, A.; Sreekanth, K.; Kumar, P. P.; Shankaraiah, N.; Balaishan, G.; Ramaiah, M. J.; Pushpavalli, S. N. C. V. L.; Ray, P.; Bhadra, M. P. Synthesis and potential cytotoxic activity of new phenanthrylphenol-pyrrolobenzodiazepines. *Eur. J. Med. Chem.* **2010**, *45*, 2173–2181
- (95) Pruschinski, L.; Lucke, A.-L.; Freese, T.; Kahnert, S.-R.; Mummel, S.; Schmidt, A. Suzuki–Miyaura cross-couplings under acidic conditions. *Synthesis* **2020**, *52*, 882–892.
- (96) Hsu, Y.-C.; Wang, V. C.-C.; Au-Yeung, K.-C.; Tsai, C.-Y.; Chang, C.-C.; Lin, B.-C.; Chan, Y.-T.; Hsu, C.-P.; Yap, G. P. A.; Jurca, T.; Ong, T.-G. One-pot tandem photoredox and cross-coupling catalysis with a single Pd-carbodicarbene complex. *Angew. Chem., Int. Ed.* **2018**, *57*, 4622–4626.
- (97) Shi, M.; Qian, H.-X. A stable dimeric mono-coordinated NHC-Pd(II) complex: synthesis, characterization, and reactivity in Suzuki–Miyaura cross-coupling reaction. *Appl. Organometal. Chem.* **2005**, *19*, 1083–1089.
- (98) Poater, A.; Ragone, F.; Guidice, S.; Costabile, C.; Dorta, R.; Nolan, S. P.; Cavallo, L. Thermodynamics of N-heterocyclic carbene dimerization: the balance of sterics and electronics. *Organometallics* **2008**, *27*, 2679–2681.
- (99) Ragone, F.; Poater, A.; Cavallo, L. Flexibility of N-heterocyclic carbene ligands in ruthenium complexes relevant to olefin metathesis and their impact in the first coordination sphere of the metal. *J. Am. Chem. Soc.* **2010**, *132*, 4249–4258.
- (100) Poater, A.; Ragone, F.; Mariz, R.; Dorta, R.; Cavallo, L. Comparing the enantioselective power of steric and electrostatic effects in transition-metal-catalyzed asymmetric synthesis. *Chem. - Eur. J.* **2010**, *16*, 14348–14353.

- (101) Falivene, L.; Cavallo, L.; Talarico, G. Buried volume analysis for propene polymerization catalysis promoted by group 4 metals: a tool for molecular mass prediction. *ACS Catal.* **2015**, *5*, 6815–6822.
- (102) Zhao, Y.; Nguyen, H. V.; Male, L.; Craven, P.; Buckley, B. R.; Fossey, J. S. Phosphino-triazole ligands for palladium-catalyzed cross-coupling. *Organometallics* **2018**, *37*, 4224–4241.
- (103) Falivene, L.; Credendino, R.; Poater, A.; Petta, A.; Serra, L.; Oliva, R.; Scarano, V.; Cavallo, L. SambVca 2. a web tool for analyzing catalytic pockets with topographic steric maps. *Organometallics* **2016**, *35*, 2286–2293.
- (104) Falivene, L.; Cao, Z.; Petta, A.; Serra, L.; Poater, A.; Oliva, R.; Scarano, V.; Cavallo, L. Towards the online computer-aided design of catalytic pockets. *Nat. Chem.* **2019**, *11*, 872–879.
- (105) Leeuwen, P. W. N. M. V.; Kamer, P. C. J.; Reek, J. N. H.; Dierkes, P. Ligand bite angle effects in metal-catalyzed C-C bond formation. *Chem. Rev.* **2000**, *100*, 2741–2769.
- (106) Marcone, J. F.; Moloy, K. G. Kinetic study of reductive elimination from the complexes (diphosphine)Pd(R)(CN). *J. Am. Chem. Soc.* **1998**, *120*, 8527–8528.
- (107) Birkholz, M.-N.; Freixab, Z.; Leeuwen, P. W. N. M. V. Bite angle effects of diphosphines in C-C and C-X bond forming cross coupling reactions. *Chem. Soc. Rev.* **2009**, *38*, 1099–1118.
- (108) Giovannini, R.; Studemann, T.; Dussin, G.; Knochel, P. An efficient nickel-catalyzed cross-coupling between sp³ carbon centers. *Angew. Chem., Int. Ed.* **1998**, *37*, 2387–2390.
- (109) Crumpton-Bregel, D. M.; Goldberg, K. I. Mechanisms of C-C and C-H alkane reductive eliminations from octahedral Pt(IV): reaction via five-coordinate intermediates or direct elimination? *J. Am. Chem. Soc.* **2003**, *125*, 9442–9456.
- (110) Lin, S.; Agapie, T. Cross-coupling chemistry at mononuclear and dinuclear nickel complexes. *Synlett* **2011**, *1*, 1–5.
- (111) Velian, A.; Lin, S.; Miller, A. J. M.; Day, M. W.; Agapie, T. Synthesis and C-C coupling reactivity of a dinuclear Ni^I-Ni^I complex supported by a terphenyl diphosphine. *J. Am. Chem. Soc.* **2010**, *132*, 6296–6297.
- (112) Sheldrick, G. M. SHELXT-integrated space-group and crystal-structure determination. *Acta Crystallogr. Sect. A-Found. Adv.* **2015**, *71*, 3–8.
- (113) Sheldrick, G. M. Crystal structure refinement with SHELXL. *Acta Crystallogr. Sect. C-Struct. Chem.* **2015**, *71*, 3–8.

- (114) Shejwalkar, P.; Rath, N. P.; Bauer, E. B. New iron(II) α -iminopyridine complexes and their catalytic activity in the oxidation of activated methylene groups and secondary alcohols to ketones. *Dalton Trans.* **2011**, *40*, 7617–7631.
- (115) Bai, L.; Wang, J.-X. Reusable, polymer-supported, palladium-catalyzed, atom-efficient coupling reaction of aryl halides with sodium tetraphenylborate in water by focused microwave irradiation. *Adv. Synth. Catal.* **2008**, *350*, 315–320.
- (116) Zhao, C.-W.; Ma, J.-P.; Liu, Q.-K.; Yu, Y.; Wang, P.; Li, Y.-A.; Wang, K.; Dong, Y.-B. A self-assembled Pd₆L₈ nanoball for Suzuki–Miyaura coupling reactions in both homogeneous and heterogeneous formats. *Green Chem.* **2013**, *15*, 3150–3154.
- (117) Guo, L.; Srimontree, W.; Zhu, C.; Maity, B.; Liu, X.; Cavallo, L.; Rueping, M. Nickel-catalyzed Suzuki–Miyaura cross-couplings of aldehydes. *Nat. Commun.* **2019**, *10*, 1957.
- (118) Serrano, J. L.; Perez, J.; Garcia, L.; Sanchez, G.; Garcia, J.; Lozano, P.; Zende, V.; Kapdi, A. N-heterocyclic-carbene complexes readily prepared from di- μ -hydroxopalladacycles catalyze the Suzuki arylation of 9-bromophenanthrene. *Organometallics* **2015**, *34*, 522–533.
- (119) Keyhaniyan, M.; Shiri, A.; Eshghi, H.; Khojastehnezhad, A. Synthesis, characterization and first application of covalently immobilized nickel-porphyrin on graphene oxide for Suzuki cross-coupling reaction. *New J. Chem.* **2018**, *42*, 19433–19441.
- (120) Shih, W.-C.; Chiang, Y.-T.; Wang, Q.; Wu, M.-C.; Yap, G. P. A.; Zhao, L.; Ong, T.-G. Invisible chelating effect exhibited between carbodicarbene and phosphine through π - π interaction and the implication in cross coupling reaction. *Organometallics* **2017**, *36*, 4287–4297.
- (121) Ando, S.; Matsunaga, H.; Ishizuka, T. An N-heterocyclic carbene-nickel half-sandwich complex as a precatalyst for Suzuki–Miyaura coupling of aryl/heteroaryl halides with aryl/heteroarylboronic acids. *J. Org. Chem.* **2017**, *82*, 1266–1272.
- (122) Abdellah, I.; Kasongo, P.; Labattut, A.; Guillot, R.; Schulz, E.; Martini, C.; Huca, V. Benzyloxycalix[8]arene : new valuable support for NHC palladium complexes in C-C Suzuki–Miyaura couplings. *Dalton Trans.* **2018**, *47*, 13843–13848.
- (123) Mandali, P. K.; Chand, D. K. Palladium nanoparticles catalyzed Suzuki cross-coupling reactions in ambient conditions. *Catal. Commun.* **2013**, *31*, 16–20.
- (124) Takahashi, F.; Nogi, K.; Yorimitsu, H. Intramolecular desulfurative coupling: nickel-catalyzed transformation of diaryl sulfones into biaryls via extrusion of SO₂. *Org. Lett.* **2018**, *20*, 6601–6605.
- (125) Chen, D.-L.; Sun, Y.; Chen, M.; Li, X.; Zhang, L.; Huang, X.; Bai, Y.; Luo, F.; Peng, B. Desulfurization of diaryl(heteroaryl) sulfoxides with benzyne. *Org. Lett.* **2019**, *21*, 3986–3989.

(126) Mewshaw, R. E.; Edsall, R. J.; Yang, C.; Manas, E. S.; Xu, Z. B.; Henderson, R. A.; Keith, J. C.; Harris, H. A. ER β Ligands. 3. Exploiting two binding orientations of the 2-phenylnaphthalene scaffold to achieve ER β selectivity. *J. Med. Chem.* **2005**, *48*, 3953–3979.

(127) Gooben, L. J.; Rodriguez, N.; Lange, P. P.; Linder, C. Decarboxylative cross-coupling of aryl tosylates with aromatic carboxylate salts. *Angew. Chem., Int. Ed.* **2010**, *49*, 1111–1114.

(128) Lei, X.; Obregon, K. A.; Alla, J. Suzuki–Miyaura coupling reactions of aryl chlorides catalyzed by a new nickel(II) σ -Aryl Complex. *Appl. Organometal. Chem.* **2013**, *27*, 419–424.

CHAPTER 3

MONO- AND DINUCLEAR α -DIIMINE NICKEL(II) AND PALLADIUM(II)

COMPLEXES IN C–S CROSS-COUPLING

Authors: Md Muktadir Talukder, Justin T. Miller, John Michael O. Cue, Chinthaka M Udamulle, Abhi Bhadran, Michael C. Biewer, and Mihaela C. Stefan*

The Department of Chemistry and Biochemistry, BE26

The University of Texas at Dallas

800 West Campbell Road

Richardson, Texas 75080-3021

Manuscript titled “Mono- and Dinuclear α -Diimine Nickel (II) and Palladium (II) Complexes in C–S Cross-Coupling” submitted to Organometallics.

3.1 Abstract

The usefulness of transition metal catalytic systems in C-S cross-coupling reactions is significantly reduced by air- and moisture sensitivity, as well as harsh reaction conditions. Herein, we report four highly air- and moisture-stable well-defined mononuclear and bridged dinuclear α -diimine Ni (II) and Pd (II) complexes for C-S cross-coupling. Various ligand frameworks, including acenaphthene- and iminopyridine-based ligands, were employed, and the resulting steric properties of the catalysts were evaluated and correlated with reaction outcomes. Under aerobic conditions and low temperatures, both Ni and Pd systems exhibited broader substrate scope and functional group tolerance than previously reported catalysts. Over 40 compounds were synthesized from thiols containing alkyl, benzyl, and heteroaryl groups. Also, pharmaceutically active heteroaryl moieties are incorporated from thiol and halide sources. Notably, the bridged dinuclear five-coordinate Ni complex has outperformed the remaining three mono four- or six-coordinate complexes by giving almost quantitative yields across a broad scope of substrates.

3.2 Introduction

Numerous innovative synthetic methods have arisen from the desire to form carbon-heteroatom bonds through transition metal catalysts.¹⁻² C-S bond formation remains one of the most valuable chemical transformations for pharmaceutical applications.³⁻⁴ The first transition metal-catalyzed C-S cross-coupling reaction between thiols and aryl halides was reported by Migita et al. using Pd(PPh₃)₄.⁵⁻⁶ Subsequently, extensive studies have been performed using Pd⁷⁻¹⁶ and other transition metals, including Co,¹⁷ Ni,¹⁸⁻²⁵ Cu,²⁶⁻²⁸ Rh,²⁹ and In.³⁰

Many Pd-catalyzed systems are air- and moisture sensitive. Besides, systems for *in situ* catalyst generation suffer from expensive precursors.⁸ Moreover, deactivation of Pd catalysts

through off-cycle thiolate complexes significantly reduces their efficacy.^{8, 13} Recently, Ni-based systems have gained popularity for their environmental friendliness, cost-effectiveness, and decreased tendency to deposit metallic nanoparticles.³¹ Still, Pd and Ni-catalytic systems demand high catalyst loading (5–50 mol%),^{8, 18, 22–25, 31} high temperature (100–150 °C),^{7, 9, 11–12, 15–16, 23, 31} glovebox settings,^{13, 15, 19, 23} expensively designed ligands,^{3, 17} additives,^{20, 23–24} and longer reaction times (12–72 h).^{7–9, 11–13, 15, 18, 23, 25, 29, 31} Consequently, harsh reaction conditions significantly hinder the C-S coupling of alkyl-substituted thiols^{20, 32} and pharmaceutically important heterocycles.^{14, 33} Photoredox catalysis has attracted attention as a possible solution, but widely used iridium and ruthenium-based photosensitizers are expensive and have inadequate substrate scope.²²

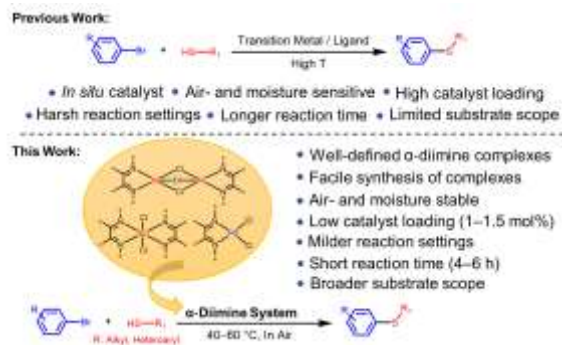


Figure 3.1. Overview of transition metal-catalyzed C-S cross-coupling.

To overcome the existing challenges in transition metal-catalyzed C-S coupling, the influence of steric topography around the metal center and the ligand bite angle has been studied. For instance, promoting oxidative addition and reductive elimination through higher steric bulk and ligand bite angle significantly reduces the off-cycle thiolate complexes.^{9–13} Moreover, Scattolin et al. has reported a bridged dinuclear Pd catalyst in C-S cross-coupling that displayed promising performance by preventing off-cycle thiolate complexes.⁸ In light of these factors, α -diimine-based transition metal catalysts represent an excellent candidate for C-S cross-coupling

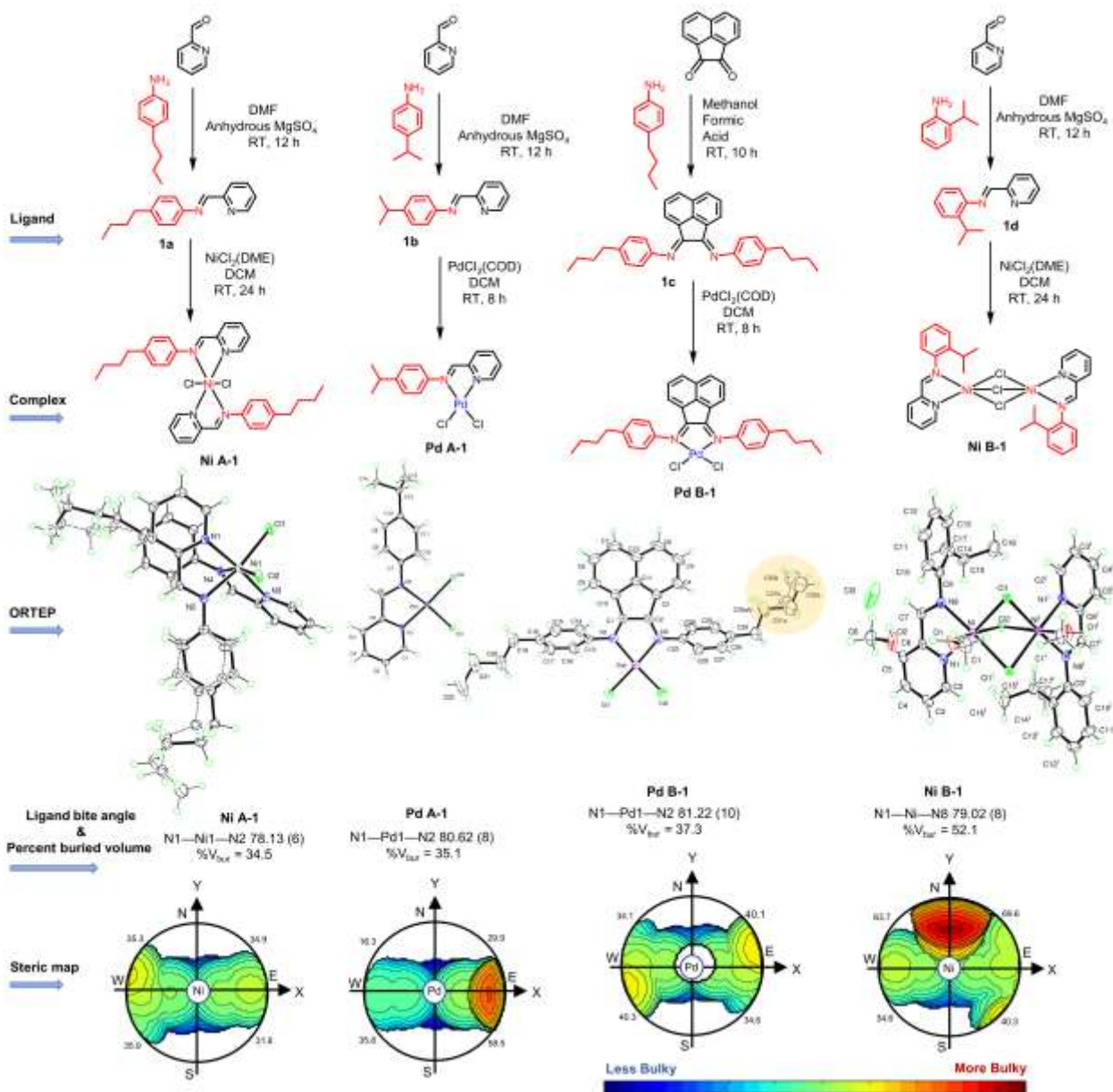
due to tunable sterics and bite angles. Olefin polymerization was revolutionized through the introduction of Brookhart-type α -diimine transition metal catalysts, bringing facile synthesis, structural versatility, high thermal stability as well as air and moisture stabilities.³⁴⁻³⁶ In addition, electronic and steric features, including the ligand bite angle, are adjustable by incorporating various functional moieties in the ligand structure.^{34, 37-38}

In a recent publication, we have demonstrated a series of α -diimine Ni(II) and Pd(II) complexes for C-C bond formation through the Suzuki–Miyaura cross-coupling reaction. The catalytic performance exhibited a correlation with the steric bulk and ligand bite angle of the complexes.³⁴ Here, we have investigated the promising features of α -diimine transition metal complexes in C-S cross-coupling (Figure 1). We report the first application of mono- and dinuclear Ni (II) and Pd (II) complexes in C-S cross-coupling. Acenaphthene and iminopyridine-based ligands were applied to synthesize the Ni (II) and Pd (II) complexes. Variation in the steric features was analyzed and correlated to the reaction outcomes. Notably, significant consideration was given to examine the substrate scope through the coupling of thiols containing heteroaryl or alkyl moieties with various aryl halides.

3.3 Results and Discussion

3.3.1 Synthesis and Characterization of α -Diimine Nickel (II) and Palladium (II) Complexes

Synthesis and structural characterization of the complexes are displayed in Scheme 3.1. The ligands and complexes were synthesized by adopting a reported procedure.³⁴ Iminopyridine (**1a**, **1b** & **1d**) and acenaphthene-based (**1c**) ligands were prepared through condensation reactions of primary aryl amines with 2-pyridinecarboxaldehyde and acenaphthoquinone, respectively. Two



Scheme 3.1. Synthesis, ORTEP diagrams, ligand bite angle, percent buried volume, and steric maps of the α -diimine Ni(II) and Pd(II) Complexes.

equivalents of the ligand **1a** with NiCl₂(DME) afforded the mononuclear bis-ligated complex, **Ni A-1**, whereas one equivalent of ligand **1d** generated the dinuclear monoligated complex, **Ni B-1**.

The remaining two mononuclear Pd (II) complexes, **Pd A-1** and **Pd B-1** are synthesized by reacting the ligands **1b** and **1c** with one equivalent of PdCl₂(COD), respectively.

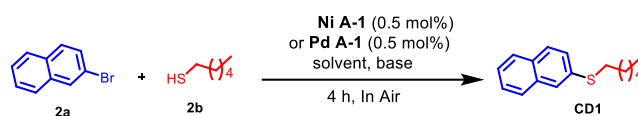
Scheme 3.1 shows the ORTEP diagrams of the synthesized complexes. Distorted octahedral geometry is observed in both **Ni A-1** and **Ni B-1**. For **Ni A-1**, the nickel atom is coordinated by two free chlorine atoms and four nitrogen atoms of the iminopyridine ligands. It has some positional disorder resulting from the phenyl ring bearing the butyl substituent, however, this does not significantly alter the packing of the complex in the solid-state. **Ni B-1** is a centrosymmetric dimer with an octahedral geometry about each of the two nickel centers. Two nitrogen atoms arising from the ligand are directly coordinated with each of the nickel centers as well as three bridging chlorine atoms. A methanol molecule from the solvent used in crystal growth is coordinated to each Ni center. In addition, one free methanol and a chloride anion are present in the structural packing of **Ni B-1**. Meanwhile, **Pd A-1** and **Pd B-1** exhibit a distorted square planar geometry with two nitrogen atoms from the ligand that are directly coordinated with the Pd center along with two free chlorine atoms. **Pd B-1** has some positional disorder from one of the butyl chains. Unit cell representations, crystal data collection, selected bond angles, and distances are provided in the supporting information.

3.3.2 Reaction conditions optimization in C-S Cross-Coupling

Both Ni- and Pd-based catalytic systems are established through **Ni A-1** and **Pd A-1**, respectively. For this purpose, 0.5 mol% of these complexes are employed with 2-bromonaphthalene (**2a**), and 1-hexanethiol (**2b**). The base, solvent, and temperature were screened by running the reaction with a molar ratio of **2a** and **2b** as 1:1.5 (Table 3.1). At 40 °C, nine experiments (Table 3.1, entry 1-9) were executed for finding the best solvent and base combination

for both **Ni A-1** and **Pd A-1** catalytic systems. Water and NaOH provided the best yield for **Pd A-1**, whereas 1,4-dioxane and KOH for **Ni A-1** (Table 3.1, entry 5 & 7). Another five experiments are performed from 30-80 °C for finding the optimum temperature (Table 3.1, entry 10-14). Comparing to the previously obtained highest yield for **Ni A-1** (Table 1, entry 7), altering the temperature did not improve the performance (Table 3.1, entry 10-14). On the other hand, **Pd A-1** generated the best yield by increasing the temperature to 60 °C (Table 3.1, entry 10). Another set of experiments was performed to identify the optimum concentration of complexes. In addition,

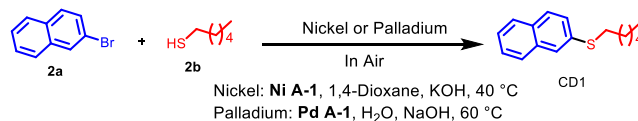
Table 3.1. Optimization of base, solvent, and temperature^a



entry	temp	solvent	base	yield (%) ^b (Ni A-1 / Pd A-1)
1	40	DMF	KOH	22 / 33
2	40	DMF	NaOH	22 / 65
3	40	DMF	K ₂ CO ₃	43 / 57
4	40	H ₂ O	KOH	34 / 49
5	40	H ₂ O	NaOH	40 / 66
6	40	H ₂ O	K ₂ CO ₃	47 / 51
7	40	1,4-dioxane	KOH	58 / 51
8	40	1,4-dioxane	NaOH	42 / 58
9	40	1,4-dioxane	K ₂ CO ₃	19 / 50
10	30	H ₂ O	NaOH	36 / 61
11	60	H ₂ O	NaOH	33 / 71
12	80	H ₂ O	NaOH	27 / 63
13	30	1,4-dioxane	KOH	41 / 47
14	60	1,4-dioxane	KOH	36 / 49

^aReaction conditions: 2-bromonaphthalene (**2a**) (1 mmol), 1-hexanethiol (**2b**) (1.5 mmol), base (1.2 mmol), 0.5 mol% of **Ni A-1** or **Pd A-1**, and solvent (5 mL). ^bIsolated yields after silica gel column chromatography.

Table 3.2. Optimization of time, concentration of complex, and halide/base ratio^a



entry	time	com (mol%)	halide / base	yield (%) ^b (Ni
				A-1 / Pd A-1)
1	4	0.5	1 / 1.5	65 / 83
2	4	0.5	1 / 1.8	56 / 77
3	4	1	1 / 1.5	81 / 89
4	4	1.5	1 / 1.5	73 / 94
5	4	2	1 / 1.5	- / 91
6	6	1	1 / 1.5	89 / 87
7	8	1	1 / 1.5	78 / -
8	6	1.5	1 / 1.5	69 / 88
9	3	1.5	1 / 1.5	65 / 79

^aReaction conditions: 2-bromonaphthalene (**2a**) (1 mmol), 1-hexanethiol (**2b**) (1.5 mmol), base, **Ni A1** or **Pd A1**, and solvent (5 mL). ^bIsolated yields after silica gel column chromatography. Entry 5 for only **Pd A-1**; entry 7 for **Ni A-1** only.

the ratio of **2a**, and the base at different times was analyzed for finding the optimum conditions (Table 3.2). At 0.5 mol% of complexes, both **Ni A-1** and **Pd A-1** experienced an increase in yields by changing the ratio of **2a** and the base from 1:1.2 to 1:1.5; however, a decrease is observed when applying 1:1.8 (Table 3.2, entry 1 & 2). With the optimized conditions, **Pd A-1** provided the highest yield (94%) from using 1.5 mol% of the complex for four hours, whereas 1 mol% of the complex for six hours afforded the best yield (89%) for **Ni A-1** (Table 3.2, entry 4 & 6).

3.3.3 Evaluation of the Complexes in C-S Cross-Coupling

Percent buried volume (%*V*_{bur}) is used as a molecular descriptor for estimating the complexes' catalytic performance in C-S cross-coupling. %*V*_{bur} has been used for quantifying the steric attributes of catalysts.^{34, 39-40} Here, we have applied SambVca 2.1, a free web application

designed by Falivene et al., to produce the topographic steric maps and calculate the %*V*_{bur} of the complexes (Scheme 3.1).⁴⁰ **Ni A-1** exhibits the lowest buried volume (%*V*_{bur} = 34.5) and ligand bite angle (N1—Ni1—N2 = 78.13 (6)). **Pd A-1** has a higher buried volume (%*V*_{bur} = 35.1) and ligand bite angle (N1—Pd1—N2 = 80.62 (8)) than **Ni A1**. **Pd B-1**, having an acenaphthene-based symmetrical ligand structure, shows a notable increase in the buried volume (%*V*_{bur} = 37.3) and ligand bite angle (N1—Pd1—N2 = 81.22 (10)). The bridged dinuclear **Ni B-1** complex has a lower bite angle (N1—Ni—N8 = 79.02 (8)); however, it has the highest buried volume (%*V*_{bur} = 52.1) of the synthesized complexes.

%*V*_{bur} and ligand bite angles of the complexes are examined for correlation with the reaction outcomes (Scheme 3.1). For this purpose, nine compounds were synthesized by applying each of the four complexes (Figure 3.2). Thiols containing alkyl, benzyl, and heteroaryl moieties were reacted with aryl or heteroaryl bromides. Generally, the bridged dinuclear **Ni B-1** complex provided the highest yields. **Pd B-1** was superior to the **Pd A-1** and **Ni A-1**, whereas **Ni A-1** exhibited the lowest yields. The difference in the catalytic performance is more significant in the compounds containing heteroaryl moieties (Scheme 2, CD6-CD9). Greater steric bulk and ligand bite angle facilitates the reductive elimination and oxidative addition.⁹⁻¹³ Moreover, reductive elimination is promoted by greater orbital overlap due to a wider bite angle.^{34, 41} Accordingly, **Pd A-1**, possessing a higher %*V*_{bur} and ligand bite angle, affords better yields than **Ni A-1**. For understanding the improved performance of **Pd B-1**, similar observations are relevant. Noticeably, the bridged dinuclear **Ni B-1**, with an overwhelming amount of steric bulk, has outperformed the remaining three mononuclear complexes.

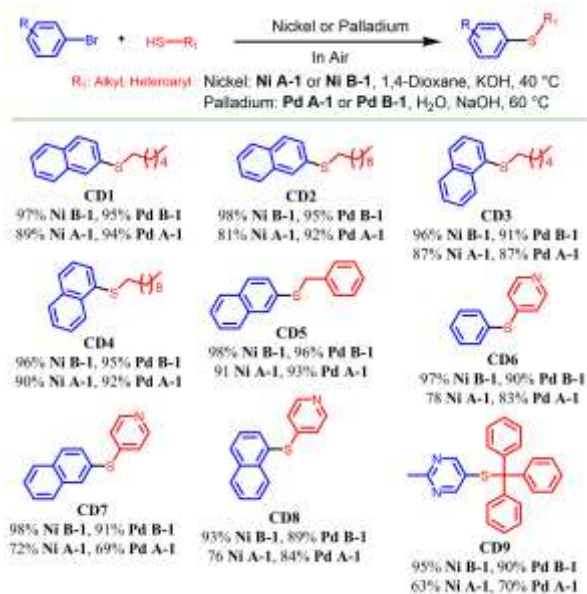


Figure 3.2. Evaluation of the Complexes in C-S Cross-Coupling

Off-cycle thiolate complexes are responsible for diminishing the catalytic performance of transition metal complexes in C-S cross-coupling.^{8, 13} A dinuclear Pd complex overcomes this shortcoming by preventing the formation of off-cycle complexes.⁸ Higher nucleophilicity emerging from the smaller size of Ni(0) compared to Pd(0) promotes oxidative addition.³⁴ Moreover, in reductive elimination, the six-coordinate complex generates a five-coordinate intermediate through ligand loss rather than the direct coupling compared to a five-coordinate complex.⁴² Accordingly, without the coordinated solvent methanol, the bridged dinuclear five-coordinate **Ni B-1** complex has outperformed the remaining three mononuclear four- or six-coordinate complexes in the reaction performance.

3.3.4 Expansion of Substrate Scope: Aromatics

Two promising complexes, **Ni B-1** and **Pd B-1** were selected for expansion of substrate scope in C-S cross-coupling (Figure 3.3). Different primary and tertiary alkyl thiols as well as

benzyl thiols were reacted with aryl bromides for synthesizing sixteen compounds carrying hydroxyl, acetyl, nitro, and nitrile functionality. **Ni B-1** outperformed **Pd B-1** with nearly quantitative yields, whereas **Pd B-1** afforded lesser, but still excellent yields.

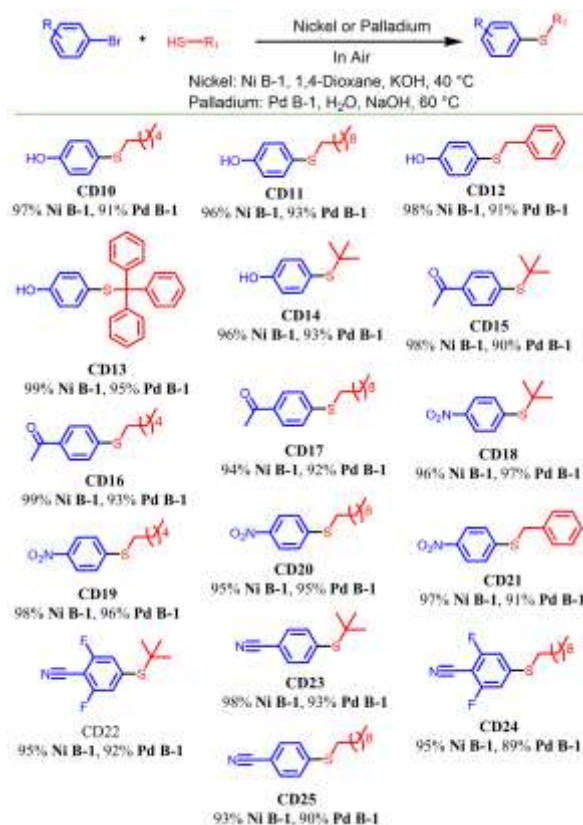


Figure 3.3. Expansion of Substrate Scope: Aromatics

Aryl halides containing free hydroxyl groups are challenging to couple with thiols because they often need to be protected with a silyl group.¹⁶ However, in our attempts, without protecting the free hydroxyl group, high yields are recorded from 4-bromophenol and different alkyl thiols. For instance, thiols containing *tert*-butyl or bulkier triphenylmethyl moieties gave comparable yields. Aryl halides containing reactive acetyl functionality are another class of compounds which often result in poor yields in C-S cross-coupling with alkyl thiols.³² Nonetheless, introducing acetyl

functionality through 4-bromoacetophenone and alkyl thiols did not significantly adversely impact **Ni B-1** and **Pd B-1** catalytic systems, which continued to deliver excellent to quantitative yields.

Nitroaromatic compounds are very useful building blocks for nucleophilic aromatic substitution. Alkylation of nitroaromatic compounds through C-C cross-coupling is achieved by utilizing pyrophoric organometallic reagents such as butyllithium.⁴³ C-S cross-coupling allows a more desirable way to produce the alkylthiolated nitroaromatic compounds. We have employed alkyl and benzyl thiols for alkylthiolation of 1-bromo-4-nitrobenzene obtaining yields of 91-98%. Aryl nitriles are biologically active organic compounds found in pharmaceuticals and natural products. Nitrile functionality has the capacity to install other useful functionality including amines, aldehydes, and acid derivatives.⁴⁴ Here, we have synthesized four alkylthiolated benzonitriles through **Ni B-1** and **Pd B-1** systems with excellent yields. Both 4-bromobenzonitrile and 4-Bromo-2,6-difluorobenzonitrile are coupled with *tert*-butylthiol with similar yields.

3.3.5. Expansion of Substrate Scope: Heteroaromatics

The field of organic electronics heavily depends on the five-membered heteroaryl compounds. Alkylated thiophene and thiazole moieties in particular are essential building blocks for designing photovoltaic materials.⁴⁵⁻⁴⁶ Alkylthiol side chains have been shown to improve the photovoltaic properties of the polymer.⁴⁷ We have synthesized eleven compounds containing different alkylthiol side chains on the thiophene and thiazole units (Figure 3.4, CD26-CD36). These useful compounds have the potential to be utilized as building blocks for organic semiconducting materials. Through **Ni B-1** and **Pd B-1**, we have obtained good to quantitative

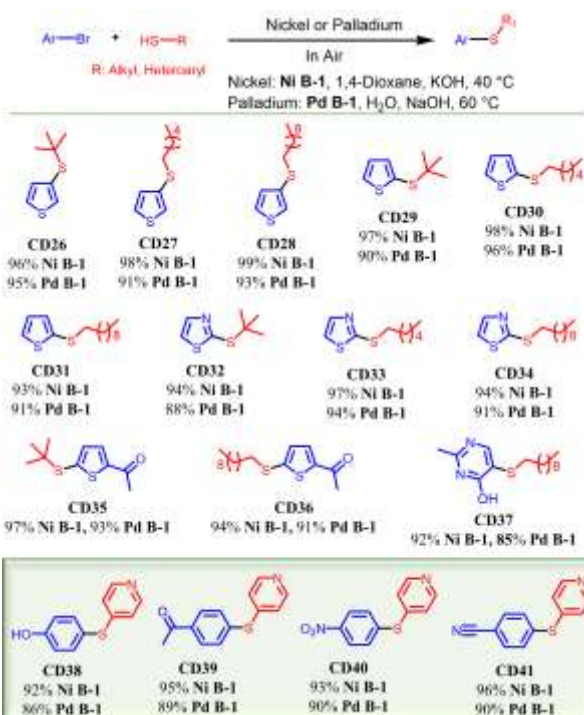


Figure 3.4. Expansion of substrate scope: Heteroaromatics.

yields (88–99%) for alkylation of 2-bromothiophene, 3-bromothiophene, and 2-bromothiazole with various alkyl thiols. Nitrogen as an additional heteroatom in the thiazole unit did not significantly decrease the yields compared to the one heteroatom in thiophene units. Moreover, alkylation of 2-acetyl-5-bromothiophene with primary and tertiary thiols gave comparable yields (Figure 3.4, CD35 & CD36) to the products from unsubstituted bromothiophenes and bromothiazole (Figure 3.4, CD26-CD34). Moreover, a heteroaryl ring possessing an *ortho*-substituted hydroxyl group is successfully coupled with 1-decanethiol (Figure 3.4, CD37).

Having demonstrated C-S coupling from alkyl thiols, we now extend the scope of these catalysts by introducing 4-pyridinethiol for attaching heteroaryl ring with *para*-substituted aryl bromide containing hydroxy, acetyl, nitro, and nitrile functionality (Figure 3.4, CD38-CD41).

Introducing a heteroaryl moiety in the presence of these reactive groups, **Ni B-1** and **Pd B-1** maintained good to excellent yields. Wang et al. has reported an electrochemical system for synthesizing CD41 (Figure 3.4) by *in situ* production of the catalyst in glovebox settings.¹⁸ In contrast, well-defined **Ni B-1** and **Pd B-1** catalytic systems have afforded excellent yields in aerobic reaction settings. Moreover, the need for harsh reaction conditions profoundly limits the C-S coupling of alkyl and heteroaryl thiols for generating medicinally important heteroaryl compounds.^{14, 20, 32-33} However, **Ni B-1** and **Pd B-1** manifested promising performance in milder reaction settings.

3.4 Conclusion

We have demonstrated highly air- and moisture-stable well-defined α -diimine Ni (II) and Pd (II) complexes in C-S cross-coupling. Versatile features of the α -diimine environment are examined by synthesizing four mono- and bridged dinuclear complexes from iminopyridine and acenaphthene-based ligand cores. Further, topographic steric maps and percent buried volume of the complexes are generated for understanding the shift in the steric characteristics. Steric attributes affiliated with the coordination nature are analyzed and correlated with the catalytic performance in Ni and Pd-based systems. Prominently, the highest steric bulk associated with the bridged dinuclear **Ni B-1** afforded nearly quantitative yields in the cross-coupling of alkyl, heteroaryl thiols with aryl and heteroaryl bromides. Accordingly, Ni-based systems within α -diimine frameworks have the capacity to be more sustainable and economical substitutes for Pd analogs for fabricating pharmaceutically active building blocks in C-S cross-coupling.

3.5. Experimental Section

3.5.1 General Materials and Methods

All the chemicals were purchased from Fisher Scientific or Sigma-Aldrich and applied without further purification unless described. The ^1H NMR and ^{13}C NMR spectra were obtained by operating a 500 MHz Bruker AVANCE III spectrometer, using chloroform as the reference solvent. Elemental analysis of the synthesized α -diimine complexes was achieved through Thermo FLASH 2000 CHN elemental analyzer. A Waters ACQUITY UPLC M-Class was applied for collecting the ESI-MS data. SambVca 2.1, a free web tool, was employed to generate the topographic steric maps and percent buried volume ($\%V_{\text{bur}}$) of the α -diimine complexes. All the reactions except for the synthesis of the α -diimine complexes were performed in air. As the thiols have an offensive smell, proper work practices were followed.

3.5.2 Single-Crystal XRD Data Characterization

For collecting the single-crystal X-ray diffraction data, an Incoatec microfocus Mo K α radiation source ($\lambda = 0.71073 \text{ \AA}$) was applied within a Bruker Kappa D8 Quest CPAD diffractometer. For the measurements, a Photon 100 CMOS detector was used, including an Oxford Cryosystems cooler. Data reduction and cell refinement were achieved through Bruker SAINT and Bruker APEX3 graphical interface. The space groups' estimation and multi-scan absorption correction were implemented using Bruker XPREP and SADABS, respectively. SHELXTL (intrinsic phasing method)⁴⁸ and SHELXL2017⁴⁹ were used for solving and refining the structure, sequentially. Ultimately, ORTEP-3 was used for molecular graphics and publCIF software for obtaining the crystallographic Information File (CIF).

3.5.3 Steric Map and Percent Buried Volume

For generating the steric maps and the percent buried volumes (%V_{Bur}), SambVca 2.1⁴⁰ was applied through <https://www.molnac.unisa.it/OMtools/sambvca2.1/index.html>. In this purpose, CIF or converted XYZ files of the complexes were applied including the radius of the sphere as 3.5 Å, bond radii scaled by 1.17, and a mesh of 0.1 Å.

3.5.4 Synthesis of Iminopyridine Ligand *N*-(4-butylphenyl)-1-(pyridin-2-yl)methanimine (**1a**).

The iminopyridine ligand **1a** was synthesized by following a reported procedure.³⁴ A one-neck 100 mL flask was charged with 2-pyridinecarboxaldehyde (3 mL, 0.032 mol), 4-butylaniline (5.05 mL, 0.032 mol), DMF (40 mL), and anhydrous MgSO₄ (120 mg, 1 mmol). After stirring the reaction mixture for 12 hours at room temperature, three extractions were performed with ethyl acetate (40 mL) and distilled water (40 mL). The ethyl acetate layer was dried with anhydrous MgSO₄. The crude product from the rotary evaporation was purified by employing *n*-hexane as an eluent through silica gel column chromatography. The pure product was isolated as a yellow oil (Yield = 5.98 g, 78.65 %). ESI-MS *m/z* [M+H]⁺ = 239.0083 (calculated for C₁₆H₁₈N₂ = 239.0054). ¹H NMR (500 MHz, CDCl₃, 300 K), δ (ppm): 8.69 (d, *J* = 4.70 Hz, 1H), 8.64 (s, 1H), 8.19 (d, *J* = 7.90 Hz, 1H), 7.76 (t, *J* = 7.80 Hz, 1H), 7.31 (q, *J* = 5.65 Hz, 1H), 7.23 (q, *J* = 8.05 Hz, 4H), 2.63 (t, *J* = 7.70 Hz, 2H), 1.62 (q, *J* = 7.55 Hz, 2H), 1.33 – 1.41 (m, 2H), 0.94 (t, *J* = 7.4 Hz, 3H).

3.5.5 Synthesis of Iminopyridine Ligand *N*-(4-isopropylphenyl)-1-(pyridin-2-yl)methanimine (**1b**).⁵⁰

The iminopyridine ligand **1b** was synthesized by employing the above procedure using 2-pyridinecarboxaldehyde (3 mL, 0.032 mol), and 4-isopropylaniline (4.4 mL, 0.032 mol). The pure

product was isolated as a light-yellow oil (Yield = Yield = 5.66 g, 78.81 %). ESI-MS m/z $[M+H]^+$ = 225.0013 (calculated for $C_{15}H_{16}N_2$ = 225.0097). 1H NMR (500 MHz, $CDCl_3$, 300 K), δ (ppm): 8.70 (d, J = 4.65 Hz, 1H), 8.62 (s, 1H), 8.20 (d, J = 7.90 Hz, 1H), 7.79 (t, J = 7.65 Hz, 1H), 7.34 (t, J = 5.65 Hz, 1H), 7.25 (br, 4H), 2.94 (br, 1H), 1.27 (br, 6H).

3.5.6 Synthesis of Iminopyridine Ligand N-(2-isopropylphenyl)-1-(pyridin-2-yl)methanimine (1d).⁵¹

The iminopyridine ligand **1d** was synthesized by employing the above procedure using 2-pyridinecarboxaldehyde (3 mL, 0.032 mol), and 2-isopropylaniline (4.5 mL, 0.032 mol). The pure product was isolated as a light orange oil (Yield = 6.29 g, 87.67 %). ESI-MS m/z $[M+H]^+$ = 225.0057 (calculated for $C_{15}H_{16}N_2$ = 225.0074). 1H NMR (500 MHz, $CDCl_3$, 300 K), δ (ppm): 8.71 (d, J = 4.60 Hz, 1H), 8.53 (s, 1H), 8.26 (d, J = 7.90 Hz, 1H), 7.82 (t, J = 7.65 Hz, 1H), 7.33 – 7.38 (m, 2H), 7.21 – 7.25 (m, 2H), 7.00 (d, J = 6.95 Hz, 1H), 3.52 – 3.60 (m, 1H), 1.26 (d, J = 6.95 Hz, 6H).

3.5.7 Synthesis of the Acenaphthene Ligand N^1,N^2 -bis(4-butylphenyl)acenaphthylene-1,2-diimine (1c).

The acenaphthene ligand **1c** was synthesized by following a reported procedure.³⁴ A one-neck 100 mL flask was charged with acenaphthoquinone (1.71 g, 9.39 mmol), 4-butylaniline (2.87 g, 19.2 mmol), methanol (50 mL), and formic acid (1 mL). The reaction mixture was filtered after stirring for 10 h at room temperature. The isolated solid was washed with cold methanol (50 mL) followed by dissolving in dichloromethane. After filtering the solution through celite, the pure product was obtained as an orange solid from slow evaporation (Yield = 2.98 g, 71.55 %). ESI-MS m/z $[M+H]^+$ = 445.0069 (calculated for $C_{32}H_{32}N_2$ = 445.0014). 1H NMR (500 MHz, $CDCl_3$,

300 K), δ (ppm): 7.87 (d, J = 8.2 Hz, 2H), 7.36 (t, J = 7.60 Hz, 2H), 7.27 (d, J = 7.90 Hz, 4H), 7.04 (d, J = 8.20 Hz, 4H), 6.87 (d, J = 7.25 Hz, 2H), 2.71 (t, J = 7.7 Hz, 4H), 1.70 (q, J = 7.40 Hz, 4H), 1.40 – 1.47 (m, 4H), 0.99 (t, J = 7.35 Hz, 6H). ^{13}C NMR (500 MHz, CDCl_3 , 300 K), δ (ppm): 161.41, 149.53, 141.73, 139.06, 132.69, 131.25, 128.84, 128.76, 127.62, 123.89, 118.23, 35.30, 33.81, 22.49, 14.12.

3.5.8 Synthesis of the Iminopyridine Bis-Ligated Nickel(II) Complex (Ni A-1)

Complex **Ni A-1** was synthesized by following a reported procedure.³⁴ A one-neck 50 mL flask was charged with dichloro- (dimethoxyethane)nickel(II) $\text{NiCl}_2(\text{DME})$ (219.72 mg, 1 mmol) with a magnetic stirrer. The flask was purged with nitrogen gas before adding the ligand **1a** (525 mg, 2 mmol) dissolved in dichloromethane (15 mL). The reaction mixture was filtered after stirring for 24 h at room temperature under a nitrogen atmosphere. The precipitated solid was washed with hexane (40 mL) and diethyl ether (40 mL). After drying for 24 h in vacuum, the pure product was isolated as a green solid (Yield = 474.21 mg, 78.22%). Elemental analysis: calculated for $\text{C}_{32}\text{H}_{36}\text{Cl}_2\text{N}_4\text{Ni}$: C, 63.40; H, 5.99; N, 9.24. Found: C, 63.30; H, 6.06; N, 9.17. Methanol solvent was used to make a saturated solution of the complex. After slow evaporation at room temperature, a suitable single crystal was obtained for single-crystal XRD analysis. Crystal size: $0.50 \times 0.25 \times 0.07 \text{ mm}^3$; crystal color: yellow; crystal shape: tablet.

3.5.9 Synthesis of the Iminopyridine Palladium(II) Complex (Pd A-1)

Complex **Pd A-1** was synthesized by following a reported procedure.³⁴ A one-neck 50 mL flask was charged with ligand **1b** (166.83 mg, 0.70 mmol), dichloro(1,5-cyclooctadiene)palladium(II) known as $\text{PdCl}_2(\text{cod})$ (200 mg, 0.7 mmol) and a magnetic stirrer. The flask was purged with nitrogen gas before adding dichloromethane (15 mL). The reaction mixture

was filtered after stirring for 8 h at room temperature under a nitrogen atmosphere. The precipitated solid was washed with hexane (40 mL) and diethyl ether (40 mL). After drying for 24 h in vacuum, the pure product was isolated as a dark orange solid (Yield = 174.21 mg, 83.56%). Elemental analysis: calculated for $C_{15}H_{16}Cl_2N_2Pd$: C, 44.86; H, 4.02; N, 6.98. Found: C, 44.79; H, 4.09; N, 6.88. Dimethylsulfoxide solvent was used to make a saturated solution of the complex. After slow evaporation at room temperature, a suitable single crystal was obtained for single-crystal XRD analysis. Crystal size: $0.70 \times 0.64 \times 0.08 \text{ mm}^3$; crystal color: orange; crystal shape: plate.

3.5.10 Synthesis of the Acenaphthene Palladium(II) Complex (Pd B-1)

Complex **Pd B-1** was synthesized utilizing the aforementioned procedure from $PdCl_2(cod)$ (200 mg, 0.7 mmol) and ligand **1c** (311.23 mg, 0.70 mmol). The pure product was isolated as a dark orange solid (Yield = 421.21 mg, 87.28%). Elemental analysis: calculated for $C_{32}H_{32}Cl_2N_2Pd$: C, 61.80; H, 5.19; N, 4.50. Found: C, 61.71; H, 5.09; N, 4.63. Dimethylsulfoxide solvent was used to make a saturated solution of the complex. After slow evaporation at room temperature, a suitable single crystal was obtained for single-crystal XRD analysis. Crystal size: $0.36 \times 0.34 \times 0.12 \text{ mm}^3$; crystal color: orange; crystal shape: tablet.

3.5.11 Synthesis of the Iminopyridine Monoligated Nickel(II) Complex (Ni B-1)

Complex **Ni B-1** was synthesized utilizing the procedure for **Ni A-1** possessing ligand **1d** (525 mg, 1 mmol) and dichloro- (dimethoxyethane)nickel(II) $NiCl_2(DME)$ (219.72 mg, 1 mmol). The pure product was isolated as a dark green solid (Yield = 595.27 mg, 89.45%). Elemental analysis: calculated for $C_{30}H_{32}Cl_4N_4Ni_2$: C, 50.91; H, 4.56; N, 7.92. Found: C, 50.78; H, 4.41; N, 7.84. Methanol solvent was used to make a saturated solution of the complex. After slow

evaporation at room temperature, a suitable single crystal was obtained for single-crystal XRD analysis. Crystal size: $0.54 \times 0.34 \times 0.16 \text{ mm}^3$; crystal color: green; crystal shape: fragment.

3.5.12 General Procedure for Nickel-Catalyzed C-S Cross-Coupling

A one-neck 25 mL flask was charged with thiol (1.5 mmol), aryl halide (1 mmol), KOH (1.5 mmol), 1,4-dioxane (5 mL), 1 mol% of complex **Ni A-1** or **Ni B-1**, and a magnetic stirrer. After capping with a rubber septum, the reaction mixture was stirred for 6 h at 40 °C in air. Three extractions were carried out with water (20 mL) and ethyl acetate (20 mL). The crude product was collected after subsequent drying and concentrating the ethyl acetate layer. The pure product was isolated after silica gel (200–300 mesh) column chromatography purification.

3.5.13 General Procedure for Palladium-Catalyzed C-S Cross-Coupling

A two-neck 25 mL flask carrying a condenser was charged with thiol (1.5 mmol), aryl halide (1 mmol), NaOH (1.5 mmol), H₂O (5 mL), 1.5 of complex **Pd A-1** or **Pd B-1**, and a magnetic stirrer. After capping with rubber septa, the reaction mixture was stirred for 4 h at 60 °C in air. Three extractions were carried out with water (20 mL) and ethyl acetate (20 mL). The crude product was collected after subsequent drying and concentrating the ethyl acetate layer. The pure product was isolated after silica gel (200–300 mesh) column chromatography purification.

3.6 Characterization of the Synthesized C-S Coupled Compounds

Hexyl(naphthalen-2-yl)sulfane (CD1).³⁰ Silica gel column chromatography having eluent as *n*-hexane. Colorless oil. Yield: 217.5 mg, 89% (**Ni A-1**); 237.1 mg, 97% (**Ni B-1**); 229.7 mg, 94% (**Pd A-1**); 232.1 mg, 95% (**Pd B-1**). ESI-MS m/z $[M + H]^+ = 245.0029$ (calculated for C₁₆H₂₀S, 245.0047). ¹H NMR (500 MHz, CDCl₃, 300 K): δ (ppm): 7.81 – 7.75 (m, 4H), 7.50 – 7.42 (m, 3H), 3.04 (t, $J = 7.39$ Hz, 2H), 1.75 – 1.69 (m, 2H), 1.52 – 1.46 (m, 2H), 1.20 (s, 4H),

0.89 (t, $J = 6.65$ Hz, 3H). ^{13}C NMR (500 MHz, CDCl_3 , 300 K), δ (ppm): 134.80, 133.94, 131.74, 128.36, 127.81, 127.34, 127.09, 126.55, 126.42, 125.55, 33.63, 31.49, 29.20, 28.69, 22.66, 14.12.

Decyl(naphthalen-2-yl)sulfane (CD2). Silica gel column chromatography having eluent as *n*-hexane. Colorless oil. Yield: 243.4 mg, 81 % (**Ni A-1**); 294.4 mg, 98% (**Ni B-1**); 276.4 mg, 92% (**Pd A-1**); 285.4 mg, 95% (**Pd B-1**). ESI-MS m/z $[\text{M} + \text{H}]^+ = 301.0075$ (calculated for $\text{C}_{20}\text{H}_{28}\text{S}$, 301.0147). ^1H NMR (500 MHz, CDCl_3 , 300 K): δ (ppm): 7.773–7.832 (m, 4H), 7.448 – 7.525 (m, 3H), 3.058–3.087 (t, $J = 7.47$ Hz, 2H), 1.733 – 1.793 (m, 2H), 1.499–1.527 (m, 2H), 1.34 (12H), 0.97 (t, $J = 6.56$ Hz, 3H). ^{13}C NMR (500 MHz, CDCl_3 , 300 K), δ (ppm): 134.83, 133.93, 131.70, 128.32, 127.77, 127.27, 127.04, 126.52, 126.32, 125.47, 33.54, 32.01, 29.66, 29.63, 29.43, 29.29, 29.20, 28.99, 22.79, 14.23.

Hexyl(naphthalen-1-yl)sulfane (CD3).³⁰ Silica gel column chromatography having eluent as *n*-hexane. Colorless oil. Yield: 212.6 mg, 87% (**Ni A-1**); 234.6 mg, 96% (**Ni B-1**); 212.6 mg, 87% (**Pd A-1**); 222.4 mg, 91% (**Pd B-1**). ESI-MS m/z $[\text{M} + \text{H}]^+ = 245.0021$ (calculated for $\text{C}_{16}\text{H}_{20}\text{S}$, 245.00847). ^1H NMR (500 MHz, CDCl_3 , 300 K): δ (ppm): 8.50 (d, $J = 8.36$ Hz, 1H), 7.89 (d, $J = 8.02$ Hz, 1H), 7.76 (d, $J = 8.18$ Hz, 1H), 7.63 – 7.60 (m, 2H), 7.55 (t, $J = 7.80$ Hz, 1H), 7.46 (t, $J = 7.70$ Hz, 1H), 3.04 (t, $J = 7.35$ Hz, 2H), 1.75 – 1.72 (m, 2H), 1.52 – 1.49 (m, 2H), 1.36 (s, 4H), 0.96 (t, $J = 6.67$ Hz, 3H). ^{13}C NMR (500 MHz, CDCl_3 , 300 K), δ (ppm): 134.39, 133.97, 132.95, 128.57, 127.40, 126.83, 126.26, 126.18, 125.59, 125.10, 34.26, 31.47, 29.20, 28.65, 22.62, 14.09.

Decyl(naphthalen-1-yl)sulfane (CD4).³⁰ Silica gel column chromatography having eluent as *n*-hexane. Colorless oil. Yield: 270.4 mg, 90% (**Ni A-1**); 288.4 mg, 96% (**Ni B-1**); 276.4 mg, 92% (**Pd A-1**); 285.4 mg, 95% (**Pd B-1**). ESI-MS m/z $[\text{M} + \text{H}]^+ = 301.0103$ (calculated for

C₂₀H₂₈S, 301.0089). ¹H NMR (500 MHz, CDCl₃, 300 K): δ (ppm): 8.49 (d, *J* = 8.41 Hz, 1H) 7.88 (d, *J* = 7.95 Hz, 1H), 7.75 (d, *J* = 8.2 Hz, 1H), 7.71 – 7.57 (m, 2H), 7.56 (t, *J* = 6.72 Hz, 1H), 7.45 (t, *J* = 7.75 Hz, 1H), 3.03 (t, *J* = 7.38 Hz, 2H), 1.76 – 1.70 (m, 2H), 1.55 – 1.49 (m, 2H), 1.32 (s, 12H), 0.97 (t, *J* = 6.99 Hz, 3H). ¹³C NMR (500 MHz, CDCl₃, 300 K), δ (ppm): 134.43, 134.01, 132.99, 128.61, 127.45, 126.86, 126.29, 126.22, 125.63, 125.14, 34.29, 32.02, 29.66, 29.63, 29.43, 29.32, 29.27, 29.02, 22.81, 14.23.

Benzyl(naphthalen-2-yl)sulfane(CD5).⁵² Silica gel column chromatography having eluent as *n*-hexane. Yellow oil. Yield: 227.8 mg, 91% (**Ni A-1**); 245.3 mg, 98% (**Ni B-1**); 232.8 mg, 93% (**Pd A-1**); 240.3 mg, 96% (**Pd B-1**). ESI-MS *m/z* [M + H]⁺ = 251.0119 (calculated for C₁₇H₁₄S, 251.0128). ¹H NMR (500 MHz, CDCl₃, 300 K): δ (ppm): 7.88 (s, 1H), 7.83 – 7.77 (m, 2H), 7.72 (s, 1H), 7.70 (s, 1H), 7.48 – 7.40 (m, 4H), 7.34 – 7.22 (m, 3H), 4.22 (s, 2H). ¹³C NMR (500 MHz, CDCl₃, 300 K), δ (ppm): 137.51, 134.1, 132.47, 132.05, 128.99, 128.67, 127.85, 127.57, 127.36, 127.29, 126.76, 126.60, 126.35, 125.87, 39.09.

4-(phenylthio)pyridine (CD6).⁵³ Silica gel column chromatography having eluent as *n*-hexane and ethyl acetate of 10:1 (v/v). Yellow solid. Yield: 146.0 mg, 78% (**Ni A-1**); 181.6 mg, 97% (**Ni B-1**); 155.4 mg, 83% (**Pd A-1**); 168.5 mg, 90% (**Pd B-1**). ESI-MS *m/z* [M + H]⁺ = 188.0013 (calculated for C₁₁H₉NS, 188.026). ¹H NMR (500 MHz, CDCl₃, 300 K): δ (ppm): 8.362 (2H), 7.448-7.547 (m, 5H), 6.941 (2H). ¹³C NMR (500 MHz, CDCl₃, 300 K), δ (ppm): 150.43, 149.48, 135.26, 130.01, 129.76, 129.54, 120.99.

4-(naphthalen-2-ylthio)pyridine (CD7).⁵⁴ Silica gel column chromatography having eluent as *n*-hexane and ethyl acetate of 10:1 (v/v). Yellow solid. Yield: 170.8 mg, 72% (**Ni A-1**); 232.5 mg, 98% (**Ni B-1**); 163.7 mg, 69% (**Pd A-1**); 215.9 mg, 91% (**Pd B-1**). ESI-MS *m/z* [M +

$[H]^+ = 238.0128$ (calculated for $C_{15}H_{11}NS$, 238.0113). 1H NMR (500 MHz, $CDCl_3$, 300 K): δ (ppm): 8.339 (s, 2H), 8.106 (s, 1H), 7.835-7.907 (m, 3H), 7.520-7.589 (m, 3H), 6.979 (s, 2H). ^{13}C NMR (500 MHz, $CDCl_3$, 300 K), δ (ppm): 150.46, 149.49, 135.21, 134.03, 133.53, 131.25, 129.86, 128.02, 128.00, 127.59, 127.12, 126.78, 121.17.

4-(naphthalen-1-ylthio)pyridine (CD8). Silica gel column chromatography having eluent as *n*-hexane and ethyl acetate of 10:1 (v/v). Dark yellow solid. Yield: 180.3 mg, 76% (**Ni A-1**); 220.7 mg, 93% (**Ni B-1**); 199.3 mg, 84% (**Pd A-1**); 211.2 mg, 89% (**Pd B-1**). ESI-MS m/z $[M + H]^+ = 238.0102$ (calculated for $C_{15}H_{11}NS$, 238.0113). 1H NMR (500 MHz, $CDCl_3$, 300 K): δ (ppm): 8.25(m, 3H), 7.98(d, $J = 8.25$ Hz, 1H), 7.90(d, $J = 7.45$ Hz, 1H), 7.76(d, $J = 6.92$ Hz, 1H) 7.52 (m, 3H), 6.80 (d, $J = 6.25$ Hz, 2H). ^{13}C NMR (500 MHz, $CDCl_3$, 300 K), δ (ppm): 150.14, 149.33, 135.92, 134.46, 134.34, 131.41, 128.85, 127.72, 126.85, 126.08, 125.99, 125.62, 120.48.

2-methyl-5-(tritylthio)pyrimidine (CD9). Silica gel column chromatography having eluent as *n*-hexane and ethyl acetate of 10:1 (v/v). Dark yellow solid. Yield: 232.1 mg, 63% (**Ni A-1**); 350.0 mg, 95% (**Ni B-1**); 257.9 mg, 70% (**Pd A-1**); 331.6 mg, 90% (**Pd B-1**). ESI-MS m/z $[M + H]^+ = 369.0183$ (calculated for $C_{24}H_{20}N_2S$, 369.0155). 1H NMR (500 MHz, $CDCl_3$, 300 K): δ (ppm): 8.35 (s, 2H), 7.00-7.10 (m, 9H), 6.88 (d, $J = 6.0$ Hz, 6H), 2.50 (s, 3H). ^{13}C NMR (500 MHz, $CDCl_3$, 300 K), δ (ppm): 158.47, 144.58, 143.34, 131.75, 130.88, 129.47, 128.59, 126.70, 56.54.

4-(hexylthio)phenol (CD10). Silica gel column chromatography having eluent as *n*-hexane and ethyl acetate of 10:1 (v/v). White solid. Yield: 204.0 mg, 97% (**Ni B-1**); 191.4 mg, 91% (**Pd B-1**). ESI-MS m/z $[M + H]^+ = 211.0015$ (calculated for $C_{12}H_{18}OS$, 211.0034). 1H NMR (500 MHz, $CDCl_3$, 300 K): δ (ppm): 7.28 (d, $J = 8.50$ Hz, 2H), 6.77 (d, $J = 8.50$ Hz, 2H), 5.28 (s,

1H), 2.80 (t, $J = 7.39$ Hz, 2H), 1.60 – 1.54 (m, 2H), 1.41 – 1.36 (m, 2H), 1.29 – 1.25 (m, 4H), 0.89 (t, $J = 6.90$ Hz, 3H). ^{13}C NMR (500 MHz, CDCl_3 , 300 K), δ (ppm): 153.93, 133.26, 127.17, 116.13, 36.01, 31.51, 29.43, 28.51, 22.66, 14.13.

4-(decylthio)phenol (CD11). Silica gel column chromatography having eluent as *n*-hexane and ethyl acetate of 10:1 (v/v). White solid. Yield: 255.7 mg, 96% (**Ni B-1**); 247.7 mg, 93% (**Pd B-1**). ESI-MS m/z $[\text{M} + \text{H}]^+ = 267.0126$ (calculated for $\text{C}_{16}\text{H}_{26}\text{OS}$, 267.0076). ^1H NMR (500 MHz, CDCl_3 , 300 K): δ (ppm): 7.28 (d, $J = 8.27$ Hz, 2H), 6.77 (d, $J = 8.28$ Hz, 2H), 5.38 (s, 1H), 2.80 (t, $J = 7.32$ Hz, 2H), 1.58 – 1.54 (m, 2H), 1.37 (br, 2H), 1.25 (br, 12H), 0.87 (t, $J = 6.45$ Hz, 3H). ^{13}C NMR (500 MHz, CDCl_3 , 300 K), δ (ppm): 154.99, 133.27, 127.15, 116.12, 36.02, 32.02, 29.67, 29.65, 29.48, 29.43, 29.31, 28.85, 22.81, 14.23.

4-(benzylthio)phenol (CD12).⁵⁵ Silica gel column chromatography having eluent as *n*-hexane and ethyl acetate of 20:1 (v/v). White solid. Yield: 211.9 mg, 98% (**Ni B-1**); 196.8 mg, 91% (**Pd B-1**). ESI-MS m/z $[\text{M} + \text{H}]^+ = 217.0103$ (calculated for $\text{C}_{13}\text{H}_{12}\text{OS}$, 217.0018). ^1H NMR (500 MHz, CDCl_3 , 300 K): δ (ppm): 7.07 – 7.17 (m, 7H), 6.61 – 6.63 (m, 2H), 4.90 (br, 1H), 3.89 (s, 2H). ^{13}C NMR (500 MHz, CDCl_3 , 300 K), δ (ppm): 155.44, 138.17, 134.48, 129.01, 128.48, 127.11, 126.18, 116.06, 41.37.

4-(tritylthio)phenol (CD13). Silica gel column chromatography having eluent as *n*-hexane and ethyl acetate of 30:1 (v/v). White solid. Yield: 364.8 mg, 99% (**Ni B-1**); 350.0 mg, 95% (**Pd B-1**). ESI-MS m/z $[\text{M} + \text{H}]^+ = 369.0063$ (calculated for $\text{C}_{25}\text{H}_{20}\text{OS}$, 369.0071). ^1H NMR (500 MHz, CDCl_3 , 300 K): δ (ppm): 7.80 – 7.82 (m, 4H), 7.59 (t, $J = 7.4$ Hz, 2H), 7.49 (t, $J = 7.8$ Hz, 4H), 7.28 (t, $J = 7.2$ Hz, 4H), 7.21 (m, 3H), 7.11 – 7.13 (m, 3H). ^{13}C NMR (500 MHz, CDCl_3 , 300 K), δ (ppm): 144.05, 137.78, 132.55, 131.33, 130.20, 129.60, 128.42, 127.53, 126.44.

4-(*tert*-butylthio)phenol (CD14).¹² Silica gel column chromatography having eluent as *n*-hexane and ethyl acetate of 10:1 (v/v). White solid. Yield: 174.9 mg, 96% (**Ni B-1**); 169.5 mg, 93% (**Pd B-1**). ESI-MS m/z $[M + H]^+$ = 183.0169 (calculated for C₁₀H₁₄OS, 183.0146). ¹H NMR (500 MHz, CDCl₃, 300 K): δ (ppm): 7.39 (d, J = 8.58 Hz, 2H), 6.80 (d, J = 8.59 Hz, 2H), 5.762 (br, 1H), 1.26 (s, 9H). ¹³C NMR (500 MHz, CDCl₃, 300 K), δ (ppm): 156.52, 139.18, 123.58, 115.72, 45.83, 30.81.

1-(4-(*tert*-butylthio)phenyl)ethan-1-one (CD15).²⁶ Silica gel column chromatography having eluent as *n*-hexane and ethyl acetate of 20:1 (v/v). Brown solid. Yield: 204.1 mg, 98% (**Ni B-1**); 187.4 mg, 90% (**Pd B-1**). ESI-MS m/z $[M + H]^+$ = 209.0254 (calculated for C₁₂H₁₆OS, 209.0187). ¹H NMR (500 MHz, CDCl₃, 300 K): δ (ppm): 7.89 (d, J = 8.24 Hz, 2H), 7.60 (d, J = 8.23 Hz, 2H), 2.60 (s, 3H), 1.32 (s, 9H). ¹³C NMR (500 MHz, CDCl₃, 300 K), δ (ppm): 197.82, 139.56, 137.00, 136.92, 128.31, 47.01, 31.24, 26.78.

1-(4-(hexylthio)phenyl)ethan-1-one (CD16).³² Silica gel column chromatography having eluent as *n*-hexane and ethyl acetate of 10:1 (v/v). Brown solid. Yield: 289.5 mg, 99% (**Ni B-1**); 272.0 mg, 93% (**Pd B-1**). ESI-MS m/z $[M + H]^+$ = 237.0033 (calculated for C₁₄H₂₀OS, 237.0067). ¹H NMR (500 MHz, CDCl₃, 300 K): δ (ppm): 7.85 (d, J = 8.44 Hz, 2H), 7.29 (d, J = 8.48 Hz, 2H), 3.00 (t, J = 7.40 Hz, 2H), 2.57 (s, 3H), 1.73 – 1.67 (m, 2H), 1.49 – 1.43 (m, 2H), 1.32 (br, 4H), 0.90 (t, J = 6.73 Hz, 3H). ¹³C NMR (500 MHz, CDCl₃, 300 K), δ (ppm): 197.03, 145.04, 133.71, 128.72, 126.23, 31.97, 31.33, 28.72, 28.57, 26.36, 22.52, 14.00.

1-(4-(decylthio)phenyl)ethan-1-one (CD17). Silica gel column chromatography having eluent as *n*-hexane and ethyl acetate of 10:1 (v/v). White solid. Yield: 274.9 mg, 94% (**Ni B-1**); 269.0 mg, 92% (**Pd B-1**). ESI-MS m/z $[M + H]^+$ = 293.0167 (calculated for C₁₈H₂₈OS, 293.0172).

¹H NMR (500 MHz, CDCl₃, 300 K): δ (ppm): 7.84 (d, J = 8.46 Hz, 2H), 7.29 (d, J = 8.47 Hz, 2H), 2.98 (t, J = 7.41 Hz, 2H), 2.56 (s, 3H), 1.72 – 1.66 (m, 2H), 1.47 – 1.41 (m, 2H), 1.26 (s, 12H), 0.88 (t, J = 6.83 Hz, 3H). ¹³C NMR (500 MHz, CDCl₃, 300 K), δ (ppm): 197.30, 145.16, 133.86, 128.87, 126.40, 32.12, 32.01, 29.65, 29.61, 29.42, 29.27, 29.03, 28.88, 26.54, 22.80, 14.23.

tert-butyl(4-nitrophenyl)sulfane (CD18).⁵⁶ Silica gel column chromatography having eluent as *n*-hexane and ethyl acetate of 20:1 (v/v). White solid. Yield: 202.8 mg, 96% (**Ni B-1**); 204.9 mg, 97% (**Pd B-1**). ESI-MS m/z [M + H]⁺ = 212.0102 (calculated for C₁₀H₁₃NO₂S, 212.0197). ¹H NMR (500 MHz, CDCl₃, 300 K): δ (ppm): 7.21 (d, J = 8.49 Hz, 2H), 6.53 (d, J = 8.50 Hz, 2H), 1.17 (s, 9H). ¹³C NMR (500 MHz, CDCl₃, 300 K), δ (ppm): 147.23, 138.87, 120.69, 114.99, 45.40, 30.80.

Hexyl(4-nitrophenyl)sulfane (CD19).⁵⁷ Silica gel column chromatography having eluent as *n*-hexane and ethyl acetate of 10:1 (v/v). White solid. Yield: 234.5 mg, 98% (**Ni B-1**); 229.7 mg, 96% (**Pd B-1**). ESI-MS m/z [M + H]⁺ = 240.0063 (calculated for C₁₂H₁₇NO₂S, 240.0017). ¹H NMR (500 MHz, CDCl₃, 300 K): δ (ppm): 7.51 (d, J = 8.34 Hz, 2H), 6.85 (d, J = 8.29 Hz, 2H), 3.05 (t, J = 7.41 Hz, 2H), 1.87 – 1.82 (m, 2H), 1.68 – 1.65 (m, 2H), 1.58 – 1.54 (m, 4H), 1.16 (t, J = 6.96 Hz, 3H). ¹³C NMR (500 MHz, CDCl₃, 300 K), δ (ppm): 145.64, 133.66, 124.03, 115.73, 36.50, 31.47, 29.45, 28.45, 22.61, 14.09.

Decyl(4-nitrophenyl)sulfane (CD20). Silica gel column chromatography having eluent as *n*-hexane and ethyl acetate of 10:1 (v/v). White solid. Yield: 280.6 mg, 95% (**Ni B-1**); 280.6 mg, 95% (**Pd B-1**). ESI-MS m/z [M + H]⁺ = 296.0028 (calculated for C₁₆H₂₅NO₂S, 296.0046). ¹H NMR (500 MHz, CDCl₃, 300 K): δ (ppm): 7.27 (d, J = 7.16 Hz, 2H), 6.66 (d, J = 7.09 Hz, 2H), 2.80 (t, J = 6.84 Hz, 2H), 1.60 – 1.58 (m, 2H), 1.41 (br, 2H), 1.29 (br, 12H), 0.92 (t, J = 6.68 Hz,

3H). ^{13}C NMR (500 MHz, CDCl_3 , 300 K), δ (ppm): 145.47, 133.80, 129.32, 115.70, 36.54, 32.02, 29.67, 29.54, 29.43, 29.32, 28.85, 22.80, 14.24.

Benzyl(4-nitrophenyl)sulfane (CD21).⁵⁸ Silica gel column chromatography having eluent as *n*-hexane and ethyl acetate of 20:1 (v/v). White solid. Yield: 237.9 mg, 97% (**Ni B-1**); 223.2 mg, 91% (**Pd B-1**). ESI-MS m/z $[\text{M} + \text{H}]^+ = 246.0215$ (calculated for $\text{C}_{13}\text{H}_{11}\text{NO}_2\text{S}$, 246.00138). ^1H NMR (500 MHz, CDCl_3 , 300 K): δ (ppm): 7.29 – 7.15 (m, 7H), 6.58 (d, $J = 7.56$ Hz, 2H), 3.97 (s, 2H). ^{13}C NMR (500 MHz, CDCl_3 , 300 K), δ (ppm): 146.22, 138.57, 134.80, 129.05, 126.94, 123.22, 115.64, 41.92.

4-(tert-butylthio)-2,6-difluorobenzonitrile (CD22). Silica gel column chromatography having eluent as *n*-hexane and ethyl acetate of 10:1 (v/v). White solid. Yield: 215.9mg, 95% (**Ni B-1**); 209.1 mg, 92% (**Pd B-1**). ESI-MS m/z $[\text{M} + \text{H}]^+ = 228.0192$ (calculated for $\text{C}_{11}\text{H}_{11}\text{F}_2\text{NS}$, 228.0075). ^1H NMR (500 MHz, CDCl_3 , 300 K): δ (ppm): 7.78 (s, 2H), 1.32 (s, 9H). ^{13}C NMR (500 MHz, CDCl_3 , 300 K), δ (ppm): 146.39, 138.21, 138.12, 129.09, 117.20, 49.74, 31.19.

4-(tert-butylthio)benzonitrile (CD23).⁵⁹ Silica gel column chromatography having eluent as *n*-hexane and ethyl acetate of 30:1 (v/v). White solid. Yield: 187.4 mg, 98% (**Ni B-1**); 177.8 mg, 93% (**Pd B-1**). ESI-MS m/z $[\text{M} + \text{H}]^+ = 192.0351$ (calculated for $\text{C}_{11}\text{H}_{13}\text{NS}$, 192.0187). ^1H NMR (500 MHz, CDCl_3 , 300 K): δ (ppm): 7.57-7.61 (m, 4H), 1.30 (s, 9H). ^{13}C NMR (500 MHz, CDCl_3 , 300 K), δ (ppm): 139.87, 137.18, 131.94, 118.57, 112.18, 47.35, 31.13.

4-(decylthio)-2,6-difluorobenzonitrile (CD24). Silica gel column chromatography having eluent as *n*-hexane and ethyl acetate of 30:1 (v/v). White solid. Yield: 295.8 mg, 95% (**Ni B-1**); 277.1 mg, 89% (**Pd B-1**). ESI-MS m/z $[\text{M} + \text{H}]^+ = 312.0217$ (calculated for $\text{C}_{17}\text{H}_{23}\text{F}_2\text{NS}$, 312.0146). ^1H NMR (500 MHz, CDCl_3 , 300 K): δ (ppm): 7.30 (s, 1H), 7.23 (s, 1H), 3.03, (t, $J =$

7.01 Hz, 2H), 1.76 – 1.73 (m, 2H), 1.32 (s, 14H), 0.92 (t, $J = 6.43$ Hz, 3H). ^{13}C NMR (500 MHz, CDCl_3 , 300 K), δ (ppm): 146.29, 127.73, 126.30, 114.78, 110.37, 33.31, 32.02, 29.65, 29.57, 29.42, 29.21, 28.89, 28.55, 22.81, 14.24.

4-(decylthio)benzotrile (CD25). Silica gel column chromatography having eluent as *n*-hexane and ethyl acetate of 10:1 (v/v). White solid. Yield: 256.1 mg, 93% (**Ni B-1**); 247.9 mg, 90% (**Pd B-1**). ESI-MS m/z $[\text{M} + \text{H}]^+ = 276.0078$ (calculated for $\text{C}_{17}\text{H}_{25}\text{NS}$, 276.0043). ^1H NMR (500 MHz, CDCl_3 , 300 K): δ (ppm): 7.51 (d, $J = 8.41$ Hz, 2H), 7.28 (d, $J = 8.41$ Hz, 2H), 2.96 (t, $J = 7.40$ Hz, 2H), 1.66-1.72 (m, 2H), 1.41-1.47 (m, 2H), 1.261 (b, 12H), 0.88 (t, $J = 6.91$ Hz, 3H). ^{13}C NMR (500 MHz, CDCl_3 , 300 K), δ (ppm): 145.48, 132.32, 126.82, 119.09, 108.06, 32.07, 32.01, 29.64, 29.59, 29.41, 29.24, 29.00, 28.71, 22.80, 14.23.

3-(tert-butylthio)thiophene (CD26). Silica gel column chromatography having eluent as *n*-hexane and ethyl acetate of 30:1 (v/v). Colorless oil. Yield: 165.4 mg, 96% (**Ni B-1**); 163.6 mg, 95% (**Pd B-1**). ESI-MS m/z $[\text{M} + \text{H}]^+ = 173.0032$ (calculated for $\text{C}_8\text{H}_{12}\text{S}_2$, 173.0077). ^1H NMR (500 MHz, CDCl_3 , 300 K): δ (ppm): 7.43(d, 1H), 7.31 (m, 1H), 7.10 (d, 1H), 1.31 (s, 9H). ^{13}C NMR (500 MHz, CDCl_3 , 300 K), δ (ppm): 134.51, 131.98, 129.22, 125.30, 45.96, 31.05.

3-(hexylthio)thiophene (CD27).⁶⁰ Silica gel column chromatography having eluent as *n*-hexane and ethyl acetate of 30:1 (v/v). Colorless oil. Yield: 196.3 mg, 98% (**Ni B-1**); 182.3 mg, 91% (**Pd B-1**). ESI-MS m/z $[\text{M} + \text{H}]^+ = 201.0032$ (calculated for $\text{C}_{10}\text{H}_{16}\text{S}_2$, 201.0077). ^1H NMR (500 MHz, CDCl_3 , 300 K): δ (ppm): 7.30 (dd, $J = 7.96$ Hz, $J = 4.96$ Hz, 1H), 7.10 (d, $J = 7.95$ Hz, 1H), 7.01 (d, $J = 4.95$ Hz, 1H), 2.84 (t, $J = 7.62$ Hz, 2H), 1.57-1.61 (m, 2H), 1.37-1.40 (m, 2H), 1.26-1.31 (m, 4H), 0.87-0.90 (m, 3H). ^{13}C NMR (500 MHz, CDCl_3 , 300 K), δ (ppm): 132.49, 129.78, 126.09, 122.99, 35.47, 31.49, 29.50, 28.51, 22.69, 14.12

3-(decylthio)thiophene (CD28).⁶¹ Silica gel column chromatography having eluent as *n*-hexane and ethyl acetate of 30:1 (v/v). Colorless oil. Yield: 253.9 mg, 99% (**Ni B-1**); 238.5 mg, 93% (**Pd B-1**). ESI-MS m/z $[M + H]^+ = 257.0068$ (calculated for $C_{14}H_{24}S_2$, 257.0057). 1H NMR (500 MHz, $CDCl_3$, 300 K): δ (ppm): 7.31 (d, $J = 2.89$ Hz, 1H), 7.12 (d, $J = 2.69$ Hz, 1H), 7.02 (d, $J = 4.92$ Hz, 1H), 2.85 (t, $J = 7.28$ Hz, 2H), 1.64 – 1.61 (m, 2H), 1.29 (s, 14H), 0.90 (t, $J = 6.82$ Hz, 3H). ^{13}C NMR (500 MHz, $CDCl_3$, 300 K), δ (ppm): 132.51, 129.73, 126.03, 122.90, 35.43, 32.00, 29.65, 29.62, 29.51, 29.41, 29.28, 28.82, 22.79, 14.21.

2-(tert-butylthio)thiophene (CD29). Silica gel column chromatography having eluent as *n*-hexane and ethyl acetate of 30:1 (v/v). Colorless oil. Yield: 167.1 mg, 97% (**Ni B-1**); 155.0 mg, 90% (**Pd B-1**). ESI-MS m/z $[M + H]^+ = 173.0029$ (calculated for $C_8H_{12}S_2$, 173.0077). 1H NMR (500 MHz, $CDCl_3$, 300 K): δ (ppm): 7.41 (d, $J = 5.37$ Hz, 1H), 7.14 (d, $J = 3.50$ Hz, 1H), 7.02-7.04 (dd, $J = 5.36$ Hz, $J =$ Hz, 3.49, 1H), 1.31 (s, 9H). ^{13}C NMR (500 MHz, $CDCl_3$, 300 K), δ (ppm): 137.02, 132.02, 130.83, 127.60, 46.84, 30.67.

2-(hexylthio)thiophene (CD30).⁶⁰ Silica gel column chromatography having eluent as *n*-hexane and ethyl acetate of 30:1 (v/v). Colorless oil. Yield: 196.3 mg, 98% (**Ni B-1**); 192.3 mg, 96% (**Pd B-1**). ESI-MS m/z $[M + H]^+ = 201.0051$ (calculated for $C_{10}H_{16}S_2$, 201.0077). 1H NMR (500 MHz, $CDCl_3$, 300 K): δ (ppm): 7.30 (dd, $J = 5.35$, 1.10 Hz, 1H), 7.11 (dd, $J = 3.55$, 1.10 Hz, 1H), 6.97 (dd, $J = 5.25$, 3.62 Hz, 1H), 2.80 (t, $J = 7.07$ Hz, 2H), 1.65 – 1.56 (m, 2H), 1.44 – 1.38 (m, 2H) 1.33 – 1.28 (m, 4H), 0.91 (t, $J = 6.99$ Hz, 3H). ^{13}C NMR (500 MHz, $CDCl_3$, 300 K), δ (ppm): 135.16, 133.21, 128.87, 127.47, 39.05, 31.44, 29.45, 28.19, 22.62, 14.10.

2-(decylthio)thiophene (CD31).⁶² Silica gel column chromatography having eluent as *n*-hexane and ethyl acetate of 30:1 (v/v). Colorless oil. Yield: 238.5 mg, 93% (**Ni B-1**); 233.3 mg,

91% (**Pd B-1**). ESI-MS m/z $[M + H]^+ = 257.0093$ (calculated for $C_{14}H_{24}S_2$, 257.0057). 1H NMR (500 MHz, $CDCl_3$, 300 K): δ (ppm): 7.32 (dd, $J = 5.33, 0.86$ Hz, 1H), 7.11 (dd, $J = 3.45, 0.91$ Hz, 1H), 6.96 (dd, $J = 5.30, 3.55$ Hz, 1H), 2.80 (t, $J = 7.37$ Hz, 2H), 1.65 – 1.59 (m, 2H), 1.42 – 1.39 (m, 2H) 1.28, (s, 12H), 0.90 (t, $J = 6.89$ Hz, 3H). ^{13}C NMR (500 MHz, $CDCl_3$, 300 K), δ (ppm): 135.21, 133.20, 128.86, 127.46, 39.07, 32.01, 29.65, 29.62, 29.51, 29.42, 29.26, 28.54, 22.79, 14.21.

2-(tert-butylthio)thiazole (CD32). Silica gel column chromatography having eluent as *n*-hexane and ethyl acetate of 10:1 (v/v). Colorless oil. Yield: 162.8 mg, 94% (**Ni B-1**); 152.4 mg, 88% (**Pd B-1**). ESI-MS m/z $[M + H]^+ = 174.0193$ (calculated for $C_7H_{11}NS_2$, 174.0094). 1H NMR (500 MHz, $CDCl_3$, 300 K): δ (ppm): 7.78 (d, $J = 3.40$ Hz, 1H), 7.31 (d, $J = 3.43$ Hz, 1H), 1.38(s, 9H). ^{13}C NMR (500 MHz, $CDCl_3$, 300 K), δ (ppm): 160.39, 143.99, 122.72, 49.42, 30.94.

2-(hexylthio)thiazole (CD33). Silica gel column chromatography having eluent as *n*-hexane and ethyl acetate of 10:1 (v/v). Colorless oil. Yield: 195.3 mg, 97% (**Ni B-1**); 189.2 mg, 94% (**Pd B-1**). ESI-MS m/z $[M + H]^+ = 202.0241$ (calculated for $C_9H_{15}NS_2$, 202.0176). 1H NMR (500 MHz, $CDCl_3$, 300 K): δ (ppm): 7.63 (d, $J = 3.36$ Hz, 1H), 7.18 (d, $J = 3.38$ Hz, 1H), 3.19 (t, $J = 7.30$ Hz, 2H), 1.72-1.75 (m, 2H), 1.41-1.44 (m, 2H), 1.29 (b, 4H), 0.87 (t, $J = 6.84$ Hz, 3H). ^{13}C NMR (500 MHz, $CDCl_3$, 300 K), δ (ppm): 165.51, 142.79, 118.65, 34.72, 31.36, 29.29, 28.51, 22.59, 14.07.

2-(decylthio)thiazole (CD34). Silica gel column chromatography having eluent as *n*-hexane and ethyl acetate of 10:1 (v/v). Colorless oil. Yield: 242.0 mg, 94% (**Ni B-1**); 234.2 mg, 91% (**Pd B-1**). ESI-MS m/z $[M + H]^+ = 258.0075$ (calculated for $C_{13}H_{23}NS_2$, 258.0034). 1H NMR (500 MHz, $CDCl_3$, 300 K): δ (ppm): 7.63 (d, $J = 3.35$ Hz, 1H), 7.17 (d, $J = 3.37$ Hz, 1H), 3.18 (t,

$J = 7.37$ Hz, 2H), 1.76 – 1.70 (m, 2H), 1.43 – 1.39 (m, 2H), 1.24 (s, 12H), 0.86 (t, $J = 6.87$ Hz, 3H). ^{13}C NMR (500 MHz, CDCl_3 , 300 K), δ (ppm): 165.49, 142.77, 118.61, 34.69, 31.96, 29.59, 29.54, 29.37, 29.31, 29.17, 28.82, 22.75, 14.17.

1-(5-(tert-butylthio)thiophen-2-yl)ethan-1-one (CD35). Silica gel column chromatography having eluent as *n*-hexane and ethyl acetate of 10:1 (v/v). Light brown solid. Yield: 207.9 mg, 97% (**Ni B-1**); 199.3 mg, 93% (**Pd B-1**). ESI-MS m/z $[\text{M} + \text{H}]^+ = 215.0066$ (calculated for $\text{C}_{10}\text{H}_{14}\text{OS}_2$, 215.0079). ^1H NMR (500 MHz, CDCl_3 , 300 K): δ (ppm): 7.59 (d, $J = 3.77$ Hz, 1H), 7.13 (d, $J = 3.78$ Hz, 1H), 2.52 (s, 3H), 1.34 (s, 9H). ^{13}C NMR (500 MHz, CDCl_3 , 300 K), δ (ppm): 190.18, 147.96, 142.41, 137.25, 132.30, 48.22, 30.85, 26.79.

1-(5-(decylthio)thiophen-2-yl)ethan-1-one (CD36). Silica gel column chromatography having eluent as *n*-hexane and ethyl acetate of 10:1 (v/v). Light brown solid. Yield: 280.5 mg, 94% (**Ni B-1**); 271.6 mg, 91% (**Pd B-1**). ESI-MS m/z $[\text{M} + \text{H}]^+ = 299.0127$ (calculated for $\text{C}_{16}\text{H}_{26}\text{OS}_2$, 299.0093). ^1H NMR (500 MHz, CDCl_3 , 300 K): δ (ppm): 7.52 (d, 1H, $J = 3.90$ Hz), 6.96 (d, 1H, $J = 3.91$ Hz), 2.95 (t, 2H, $J = 7.38$ Hz), 2.50 (s, 3H), 1.64-1.71 (m, 2H), 1.37-1.41 (m, 2H), 1.25 (s, 12H), 0.87 (t, 3H, $J = 6.90$ Hz). ^{13}C NMR (500 MHz, CDCl_3 , 300 K), δ (ppm): 189.73, 148.42, 144.38, 132.97, 129.42, 37.49, 32.00, 29.63, 29.58, 29.40, 29.34, 29.20, 28.71, 26.44, 22.79, 14.22.

5-(decylthio)-2-methylpyrimidin-4-ol (CD37). Silica gel column chromatography having eluent as *n*-hexane and ethyl acetate of 10:1 (v/v). White solid. Yield: 259.8 mg, 92% (**Ni B-1**); 240.0 mg, 85% (**Pd B-1**). ESI-MS m/z $[\text{M} + \text{H}]^+ = 283.0015$ (calculated for $\text{C}_{15}\text{H}_{26}\text{N}_2\text{OS}$, 283.0078). ^1H NMR (500 MHz, CDCl_3 , 300 K): δ (ppm): 13.31 (br, 1H), 6.10 (s, 1H), 2.94 (t, $J = 7.37$ Hz, 2H), 2.43 (s, 3H), 1.68-1.71 (m, 2H), 1.41-1.43 (m, 2H), 1.25 (b, 12H), 0.87 (t, $J = 6.85$

Hz, 3H). ^{13}C NMR (500 MHz, CDCl_3 , 300 K), δ (ppm): 171.38, 164.24, 158.11, 104.58, 32.01, 30.66, 29.65, 29.59, 29.41, 29.23, 29.00, 28.77, 22.79, 21.62, 14.22.

4-(pyridin-4-ylthio)phenol (CD38). Silica gel column chromatography having eluent as *n*-hexane and ethyl acetate of 5:1 (v/v). Light brown solid. Yield: 203.1 mg, 92% (**Ni B-1**); 174.8 mg, 86% (**Pd B-1**). ESI-MS m/z $[\text{M} + \text{H}]^+ = 204.0067$ (calculated for $\text{C}_{11}\text{H}_9\text{NOS}$, 204.0024). ^1H NMR (500 MHz, CDCl_3 , 300 K): δ (ppm): 8.38 (br, 2H), 7.35 (t, $J = 8.03$ Hz, 2H), 7.17 (d, $J = 7.43$ Hz, 1H), 7.02 (d, $J = 7.63$ Hz, 2H), 6.76 (d, $J = 6.11$ Hz, 2H). ^{13}C NMR (500 MHz, CDCl_3 , 300 K), δ (ppm): 165.00, 154.14, 151.40, 130.34, 125.59, 120.95, 112.34.

1-(4-(pyridin-4-ylthio)phenyl)ethan-1-one (CD39).⁶³ Silica gel column chromatography having eluent as *n*-hexane and ethyl acetate of 5:1 (v/v). Light grey solid. Yield: 217.8 mg, 95% (**Ni B-1**); 204.0 mg, 89% (**Pd B-1**). ESI-MS m/z $[\text{M} + \text{H}]^+ = 230.0157$ (calculated for $\text{C}_{13}\text{H}_{11}\text{NOS}$, 230.0086). ^1H NMR (500 MHz, CDCl_3 , 300 K): δ (ppm): 8.42 (s, 2H), 7.97 (d, 2H, $J = 8.31$ Hz), 7.56 (d, 2H, $J = 8.31$ Hz), 7.06 (s, 2H), 2.62 (s, 3H). ^{13}C NMR (500 MHz, CDCl_3 , 300 K), δ (ppm): 197.15, 149.96, 147.92, 137.28, 137.11, 133.50, 129.57, 122.51, 26.75.

4-((4-nitrophenyl)thio)pyridine (CD40).⁶⁴ Silica gel column chromatography having eluent as *n*-hexane and ethyl acetate of 5:1 (v/v). Light brown solid. Yield: 216.0 mg, 93% (**Ni B-1**); 209.0 mg, 90% (**Pd B-1**). ESI-MS m/z $[\text{M} + \text{H}]^+ = 233.059$ (calculated for $\text{C}_{11}\text{H}_8\text{N}_2\text{O}_2\text{S}$, 233.0042). ^1H NMR (500 MHz, CDCl_3 , 300 K): δ (ppm): 8.11 (d, $J = 9.43$ Hz, 2H), 7.40 (d, $J = 8.70$ Hz, 2H), 6.60 (d, $J = 9.44$ Hz, 2H), 6.46 (d, $J = 8.69$ Hz, 2H). ^{13}C NMR (500 MHz, CDCl_3 , 300 K), δ (ppm): 154.36, 146.22, 138.04, 126.24, 117.42, 110.37.

4-(pyridin-4-ylthio)benzotrile (CD41).¹⁸ Silica gel column chromatography having eluent as *n*-hexane and ethyl acetate of 5:1 (v/v). White solid. Yield: 203.7 mg, 96% (**Ni B-1**);

191.0 mg, 90% (**Pd B-1**). ESI-MS m/z $[M + H]^+ = 213.0107$ (calculated for $C_{12}H_8N_2S$, 213.0043). 1H NMR (500 MHz, $CDCl_3$, 300 K): δ (ppm): 8.47 (d, $J = 5.47$ Hz, 1H), 7.66 (d, $J = 8.39$ Hz, 1H), 7.53 (d, $J = 8.36$ Hz, 1H), 7.10 (d, $J = 6.09$ Hz, 1H). ^{13}C NMR (500 MHz, $CDCl_3$, 300 K), δ (ppm): 150.20, 146.49, 138.40, 133.21, 133.07, 123.30, 118.14, 112.42.

3.7 Supporting Information

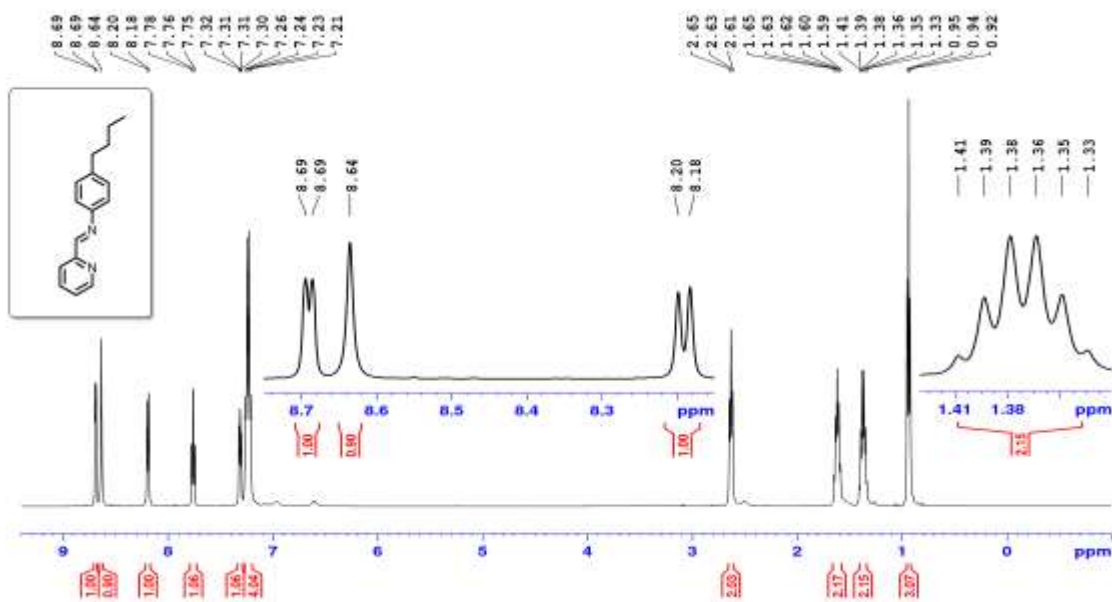


Figure 3.5. 1H NMR spectrum of ligand **1a**.

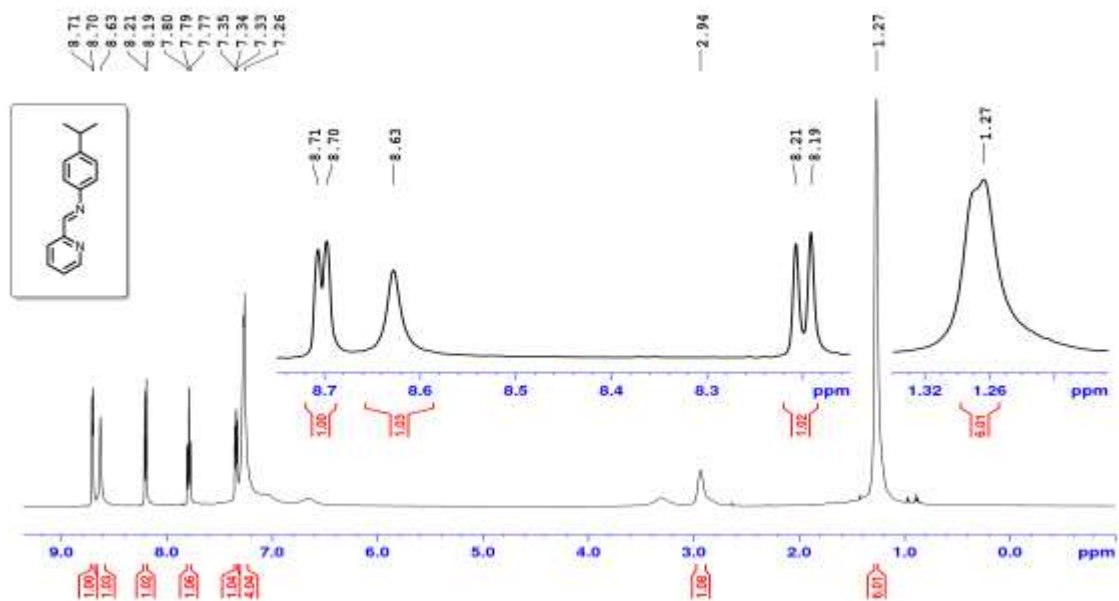


Figure 3.6. ¹H NMR spectrum of ligand **1b**.

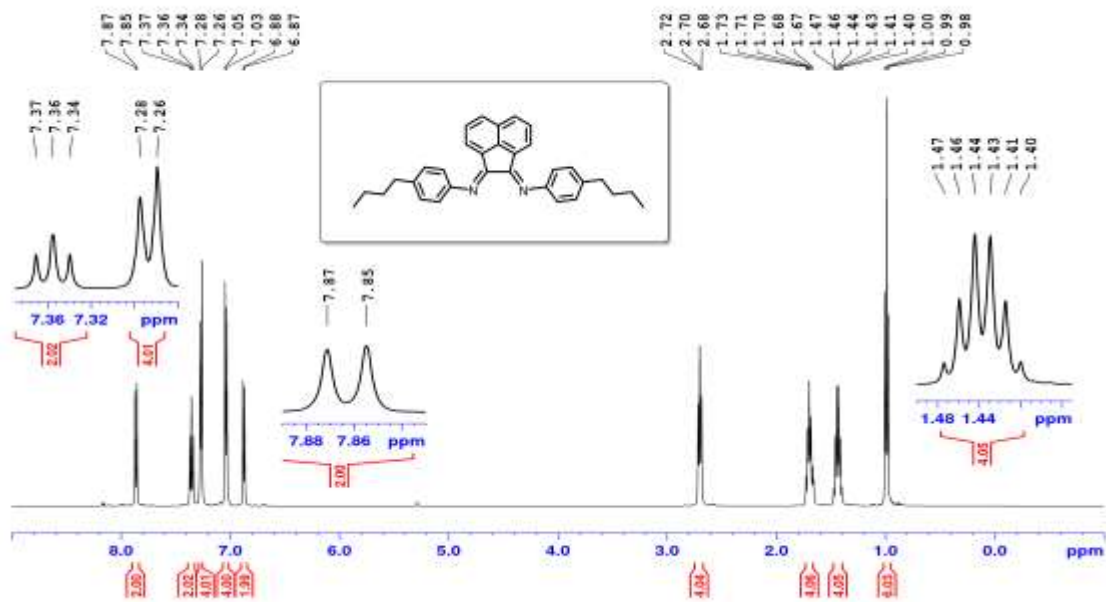


Figure 3.7. ¹H NMR spectrum of ligand **1c**.

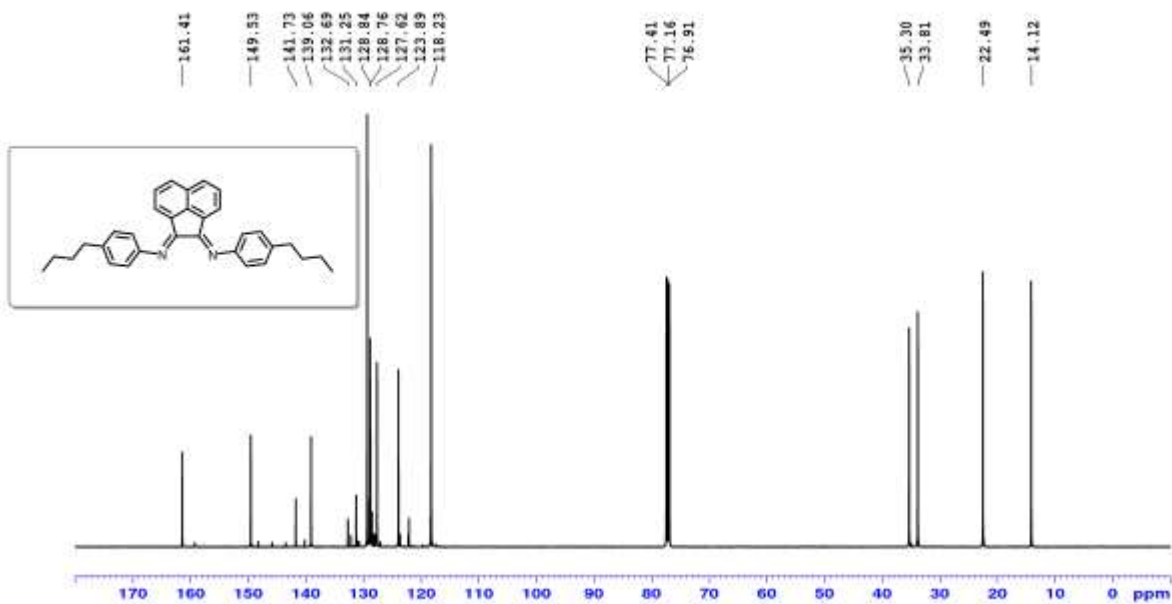


Figure 3.8. ^{13}C NMR spectrum of ligand **1c**.

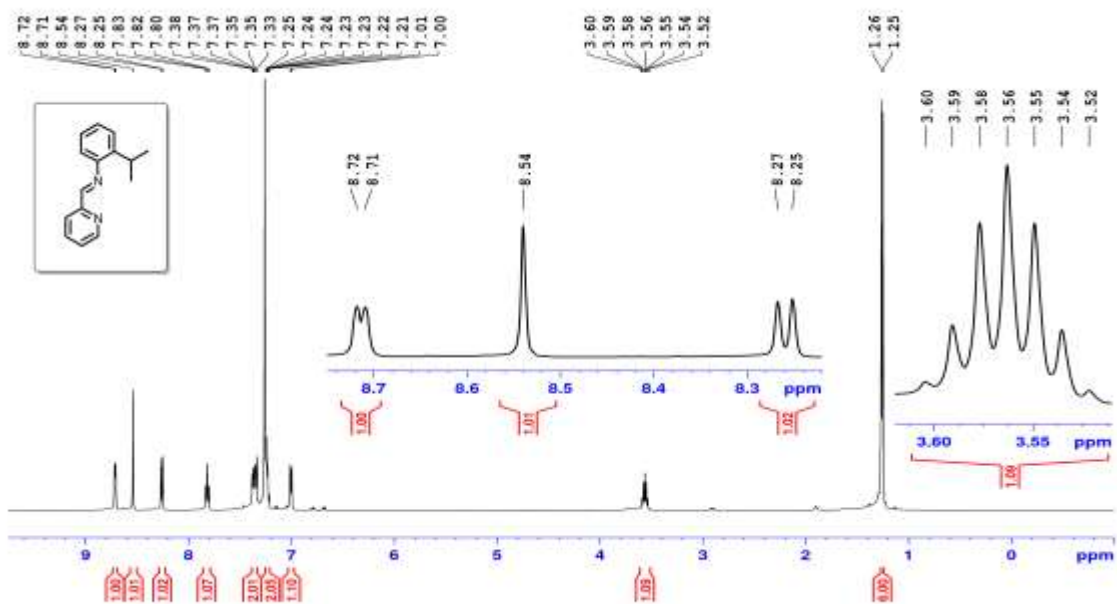


Figure 3.9. ^1H NMR spectrum of ligand **1d**.

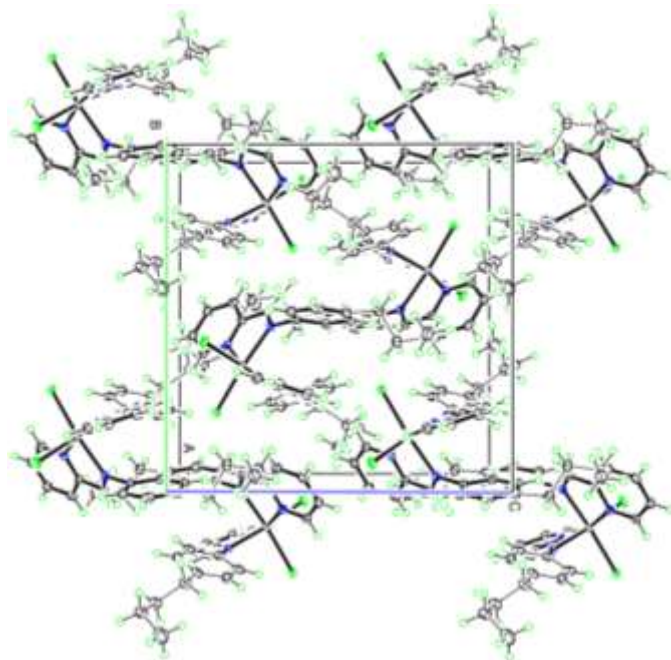


Figure 3.10. Unit cell representation of complex **Ni A-1** (Positional disorder with dashed bonds).

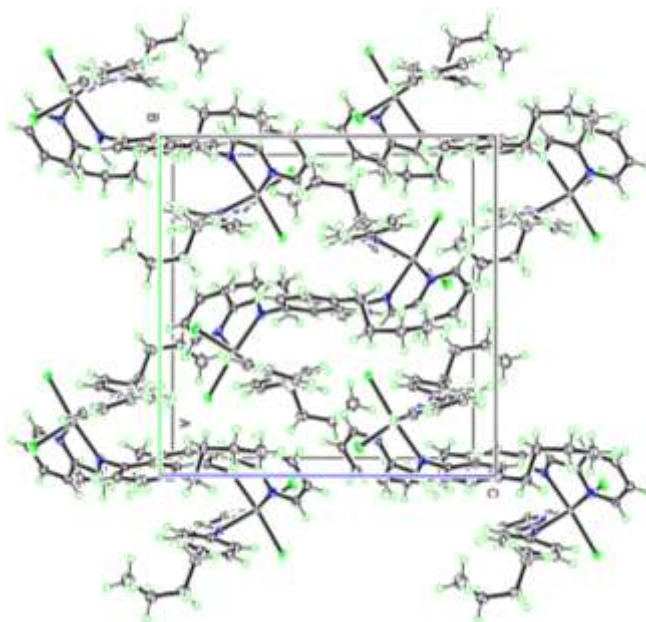


Figure 3.11. Unit cell representation of complex **Ni A-1** (Positional disorder with solid bonds).

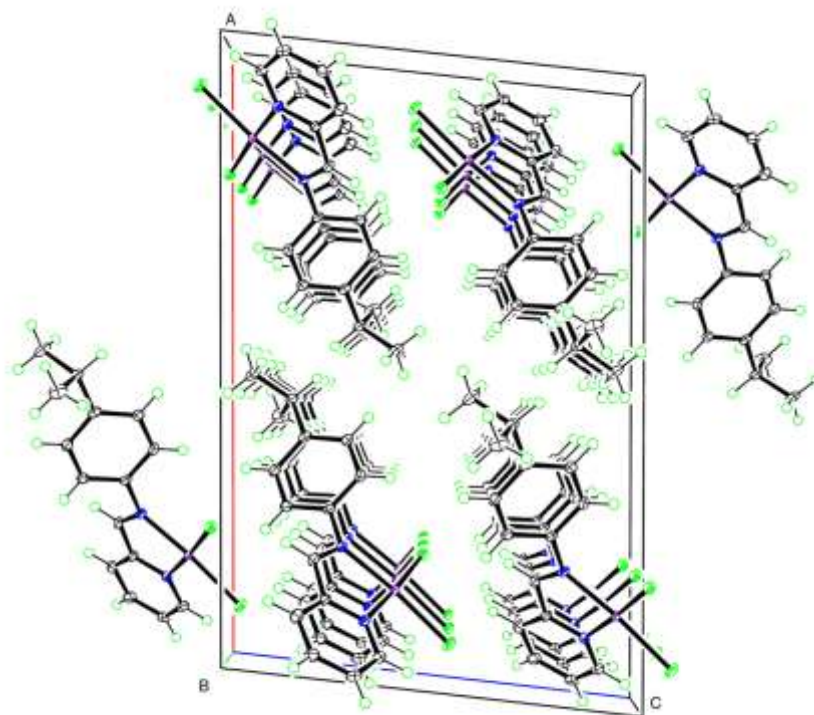


Figure 3.12. Unit cell representation of complex **Pd A-1**.

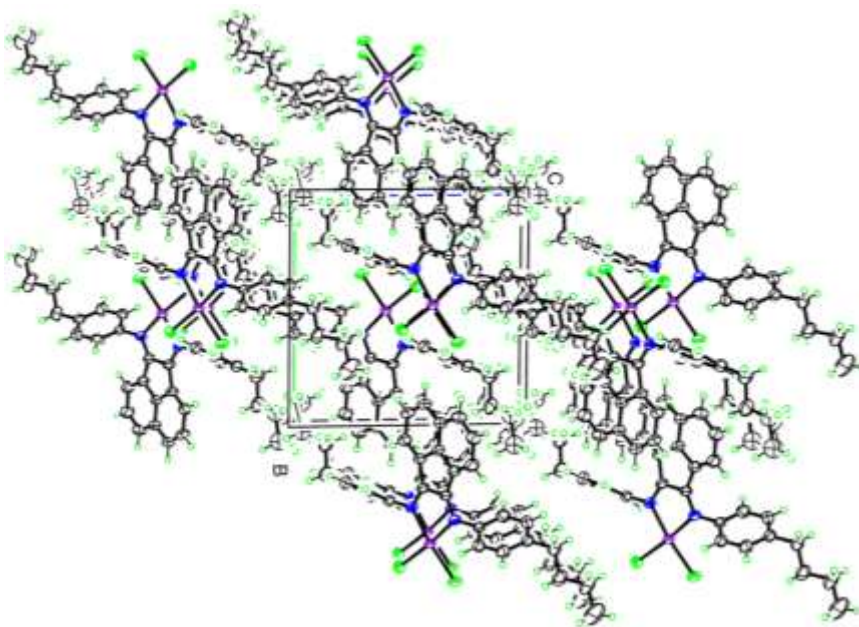


Figure 3.13. Unit cell representation of complex **Pd B-1**.

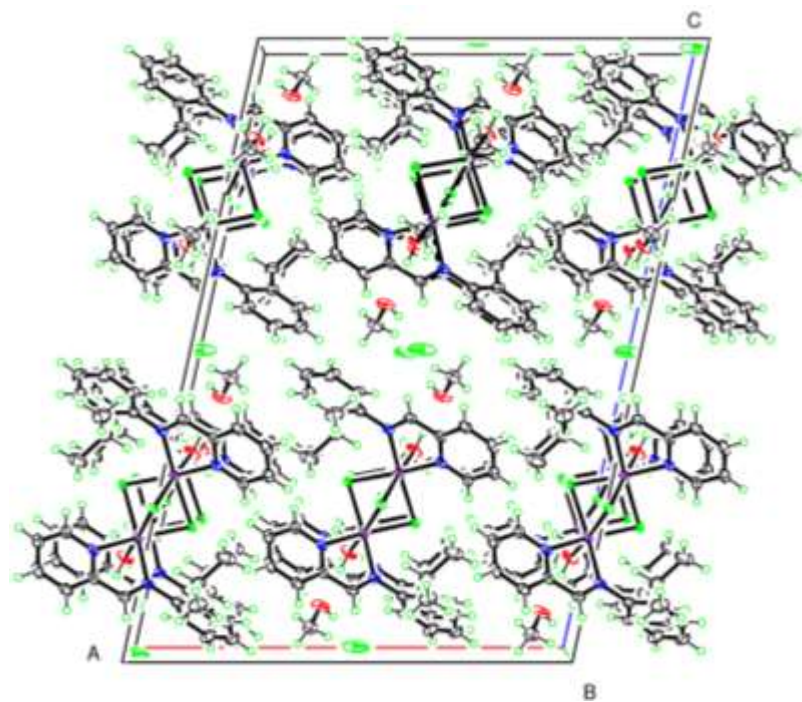


Figure 3.14. Unit cell representation of complex Ni B-1.

Table 3.3. Crystal data, data collection and refinement for complex **Ni A-1** and **Pd A-1**.

CCDC	2038719	2038722
Complexes	Ni A-1	Pd A-1
Crystallized from	CH ₃ OH	DMSO
Chemical formula	C ₃₂ H ₃₆ Cl ₂ N ₄ Ni	C ₁₅ H ₁₆ Cl ₂ N ₂ Pd
Formula weight [g mol ⁻¹]	606.26	401.60
Crystal color, habit	Yellow, Tablet	Orange, Plate
Crystal size (mm ³)	0.50 × 0.25 × 0.07	0.70 × 0.64 × 0.08
T (K)	100	100
Crystal system	Monoclinic	Monoclinic
Space group	<i>P2₁/c</i>	<i>P2₁/c</i>
a, b, c (Å)	13.952 (4), 14.687 (5), 14.567 (6)	19.833 (6), 5.9500 (18), 13.250 (4)
α, β, γ (°)	β = 93.406 (8)	β = 96.399 (8)
V (Å ³)	2979.7 (18)	1553.9 (8)
Z	4	4
D _x (Mg m ⁻³)	1.351	1.717
μ (Mo-Kα) (mm ⁻¹)	0.86	1.53
F (000), θ range (°)	1272, 2.4–30.5	800, 3.1–30.5
No. of measured, independent and observed [<i>I</i> > 2σ(<i>I</i>)] reflections	91886, 9100, 7220	30945, 4762, 4030
<i>R</i> _{int}	0.056	0.058
Δρ _{max} , Δρ _{min} (e Å ⁻³)	0.66, -0.55	0.61, -1.04
No. of parameters	385	184
Refinement R[<i>F</i> ² > 2σ(<i>F</i> ²)], wR(<i>F</i> ²), <i>S</i>	0.038, 0.084, 1.07	0.035, 0.068, 1.08

Table 3.4. Crystal data, data collection and refinement for complex **Pd B-1** and **Ni B-1**.

CCDC	2038721	2038720
Complexes	Pd B-1	Ni B-1
Crystallized from	DMSO	CH ₃ OH
Chemical formula	C ₃₂ H ₃₂ Cl ₂ N ₂ Pd	C ₃₂ H ₄₀ Cl ₃ N ₄ Ni ₂ O ₂ ·2(CH ₄ O)·Cl
Formula weight [g mol ⁻¹]	621.89	835.98
Crystal color, habit	Orange, Tablet	Green, Fragment
Crystal size (mm ³)	0.36 × 0.34 × 0.12	0.54 × 0.34 × 0.16
T (K)	250	100
Crystal system	Triclinic	Monoclinic
Space group	$\bar{1}$ <i>P1</i>	<i>C2/c</i>
a, b, c (Å)	10.101 (4), 12.023 (4), 12.119 (4)	18.633 (5), 8.056 (3), 26.341 (7)
α, β, γ (°)	90.332 (9), 96.382 (8), 97.934 (12)	β = 102.394 (12)
V (Å ³)	1448.3 (8)	3861.9 (19)
Z	2	4
D _x (Mg m ⁻³)	1.426	1.438
μ (Mo-Kα) (mm ⁻¹)	0.85	1.29
F (000), θ range (°)	636, 2.5–27.5	1744, 2.5–30.2
No. of measured, independent and observed [<i>I</i> > 2σ(<i>I</i>)] reflections	25778, 6617, 5385	54385, 5913, 4527
<i>R</i> _{int}	0.047	0.087
Δρ _{max} , Δρ _{min} (e Å ⁻³)	0.48, -0.51	0.75, -0.93
No. of parameters	335	233
Refinement R[<i>F</i> ² > 2σ(<i>F</i> ²)], wR(<i>F</i> ²), <i>S</i>	0.047, 0.079, 1.12	0.040, 0.109, 1.14

Table 3.5. Selected bond lengths and angles for complexes **Ni A-1** and **Ni B-1**.

Complex	Selected bond distances (Å)	Selected bond angles [°]
Ni A-1	Ni1—N3 2.0825 (15), Ni1—N1 2.0847 (15), Ni1—N4 2.1481 (15), Ni1—N2 2.1549 (15), Ni1—C11 2.3709 (7), Ni1—C12 2.3962 (8)	N1—Ni1—N2 78.13 (6), N3—Ni1—N2 97.85 (6), N3—Ni1—N4 77.44 (6), N1—Ni1—N4 91.38 (6), C11—Ni1—C12 97.00 (3)
Ni B-1	Ni—N1 2.0683 (19), Ni—N8 2.0863 (19), Ni—C11 2.3949 (8), Ni—C11 ⁱ 2.4189 (8), Ni—C12 2.4352 (8), Ni—Ni ⁱ 2.9809 (9)	N1—Ni—N8 79.02 (8), N8—Ni—C11 95.62 (6), N1—Ni—C11 ⁱ 97.53 (6), C11—Ni—C11 ⁱ 87.83 (3), N1—Ni—C12 90.87 (6), N8—Ni—C12 95.25 (5), C11—Ni—C12 85.22 (2), C11 ⁱ —Ni—C12 84.70 (2), Ni ⁱ —C12—Ni 75.47 (3)

Table 3.6. Selected bond lengths and angles for complexes **Pd A-1** and **Pd B-1**.

Complex	Selected bond distances (Å): Pd1—N1, Pd1—N2, Pd1—Cl2, Pd1—Cl1	Selected bond angles [°]: N1—Pd1—N2, N1—Pd1—Cl2, N2—Pd1—Cl2, N1—Pd1—Cl1, N2—Pd1—Cl1, Cl2—Pd1—Cl1
Pd A-1	2.028 (2), 2.039 (2), 2.2820 (8), 2.2886 (8)	80.62 (8), 176.38 (6), 95.91 (6), 93.58 (6), 173.95 (6), 89.86 (3)
Pd B-1	2.052 (3), 2.046 (2), 2.2694 (10), 2.2734 (10)	81.22 (10), 173.82 (7), 94.30 (8), 94.65 (7), 173.35 (8), 90.20 (4)

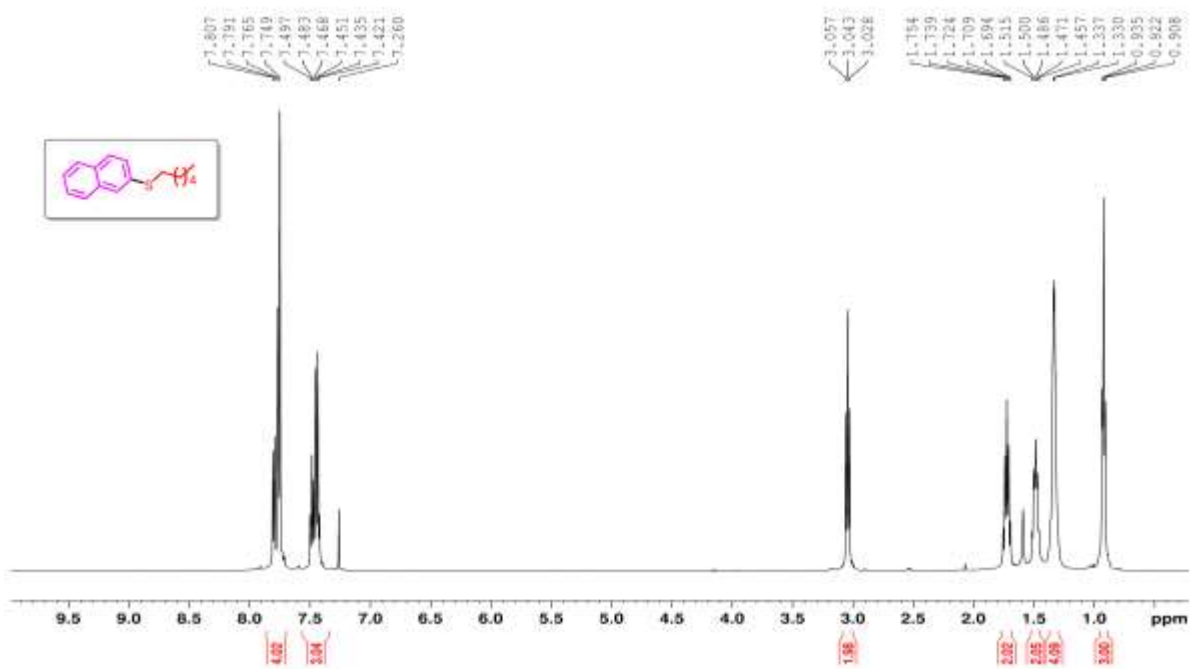


Figure 3.15. ^1H NMR spectrum of **CD1**.

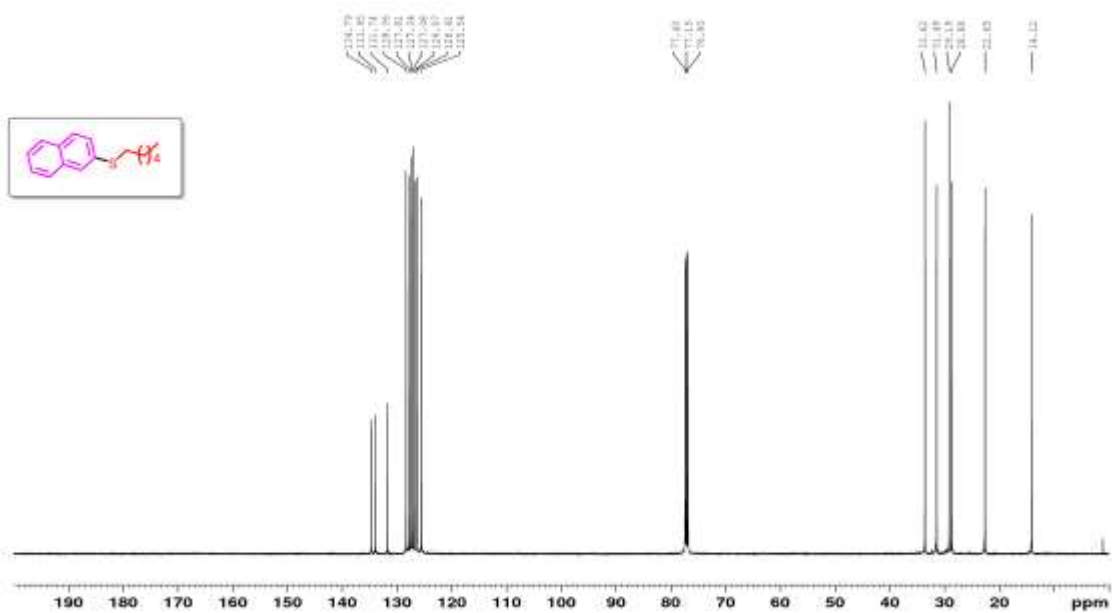


Figure 3.16. ^{13}C NMR spectrum of **CD1**.

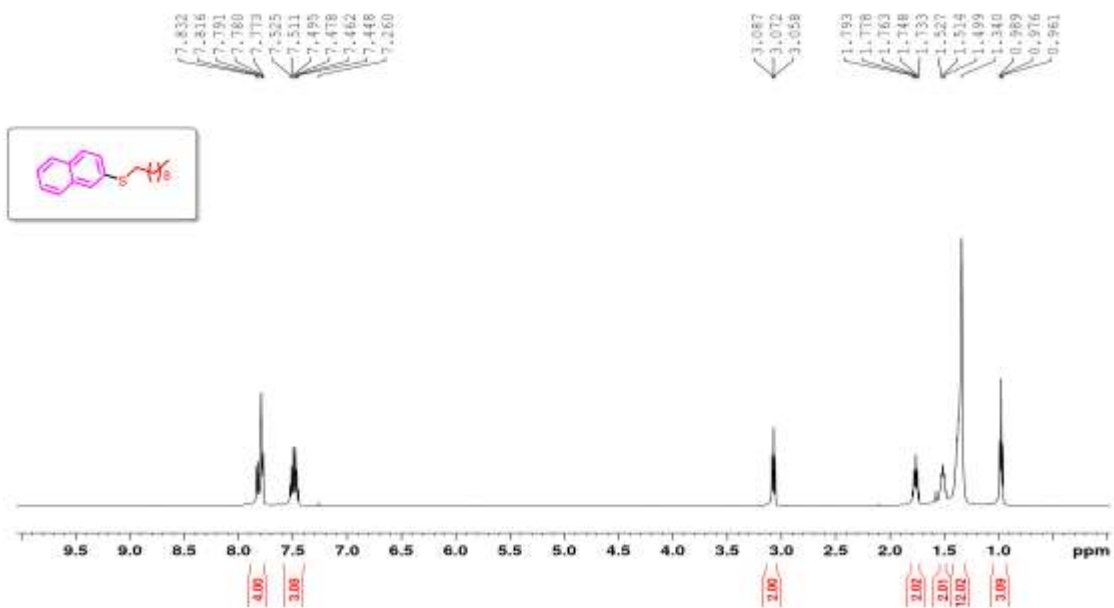


Figure 3.17. ¹H NMR spectrum of CD2.

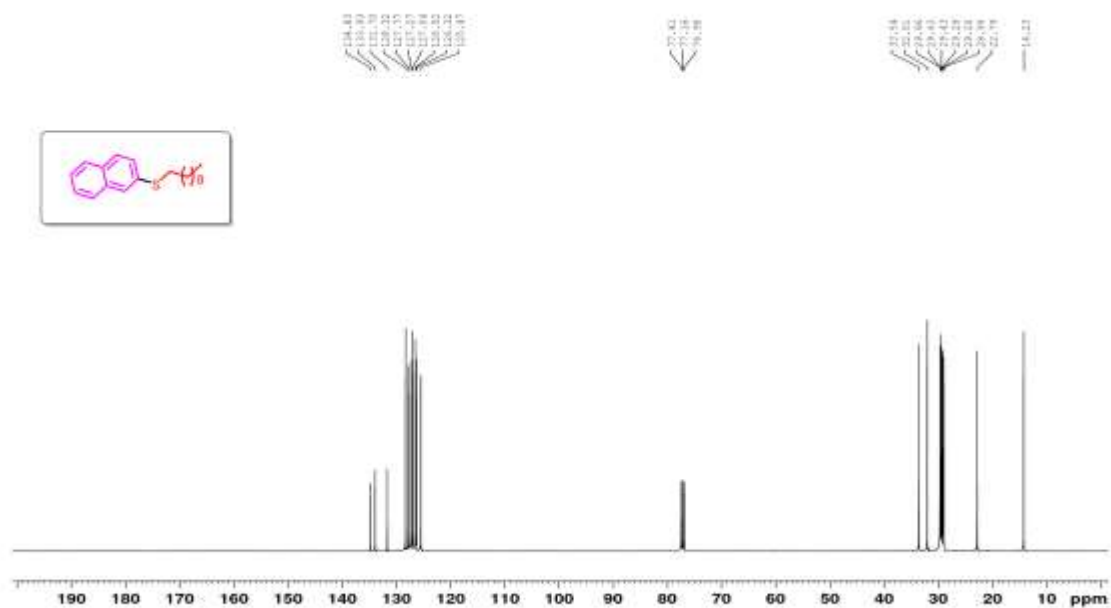


Figure 3.18. ¹³C NMR spectrum of CD2.

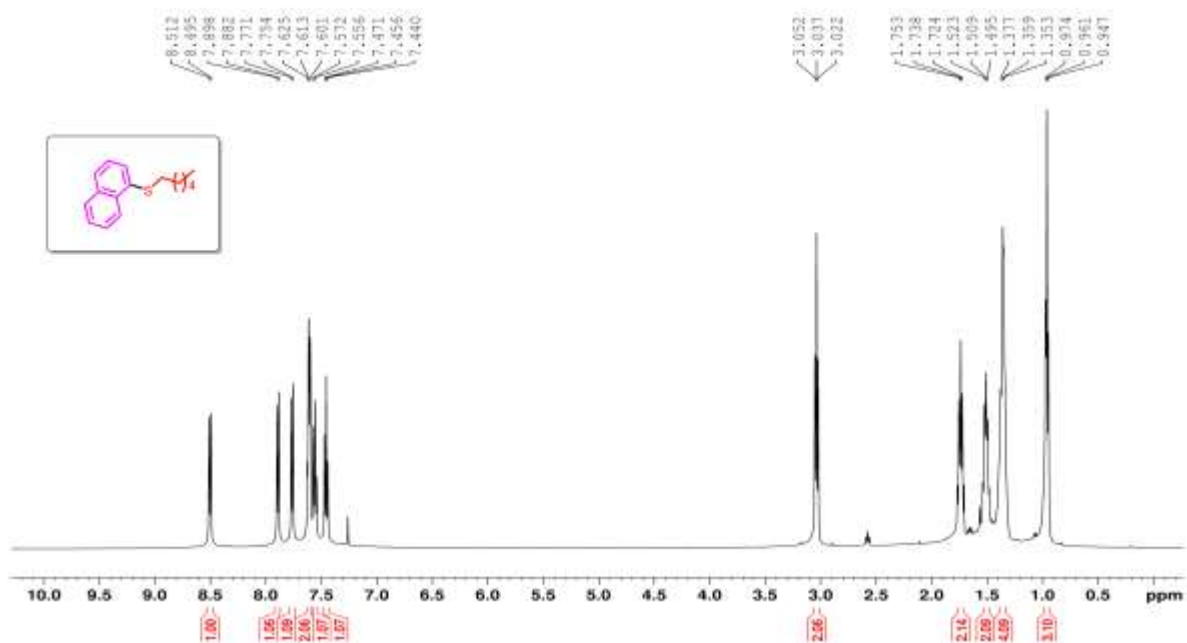


Figure 3.19. ¹H NMR spectrum of CD3.

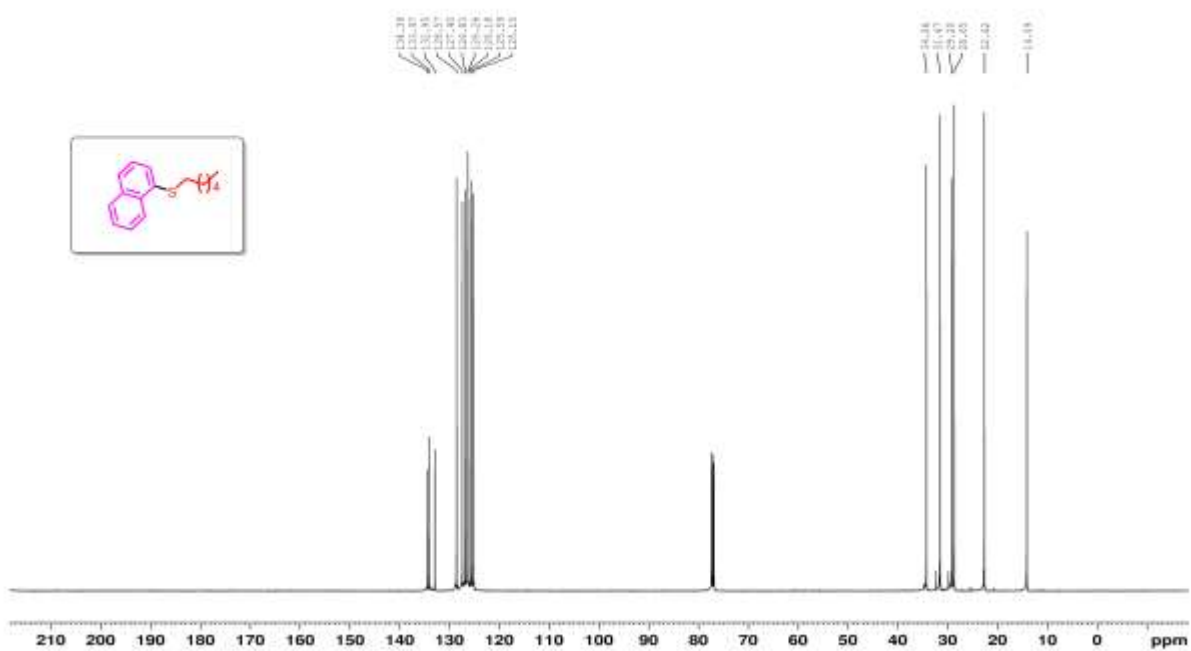


Figure 3.20. ¹³C NMR spectrum of CD3.

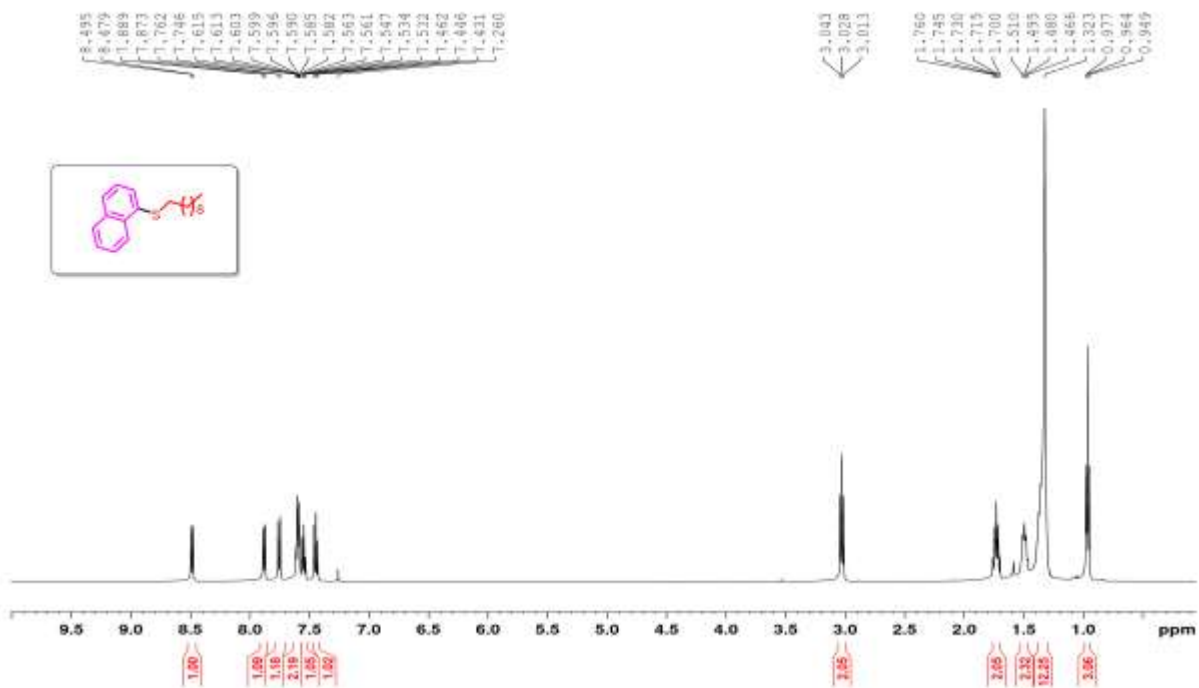
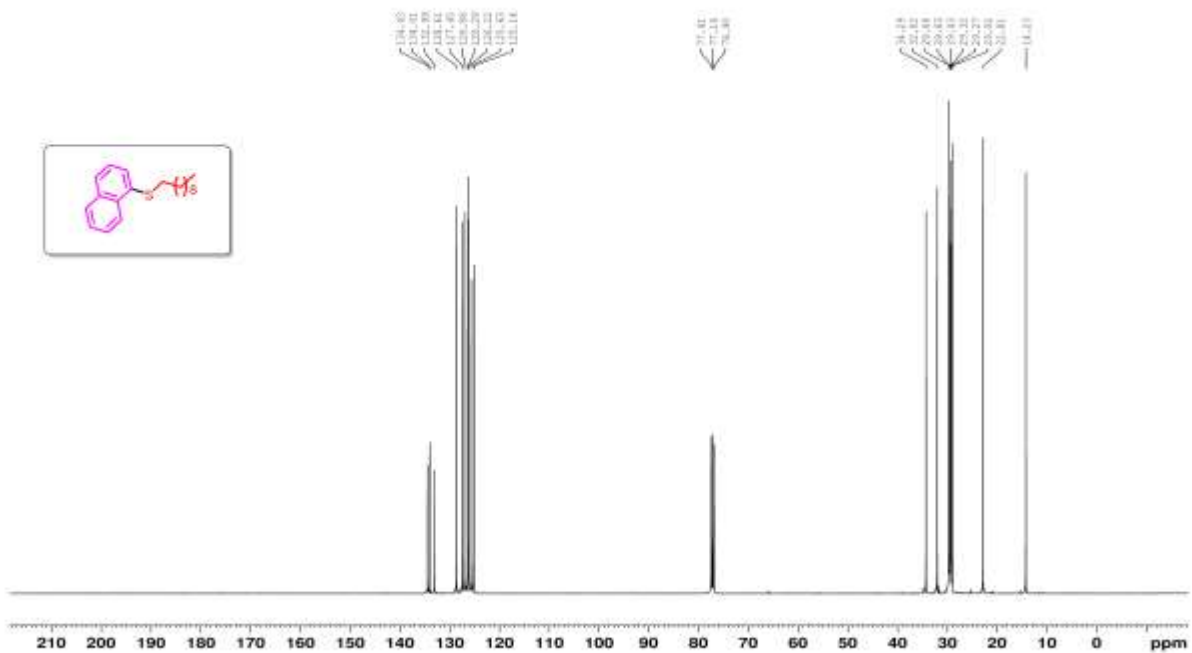


Figure 3.21. ¹H NMR spectrum of CD4.



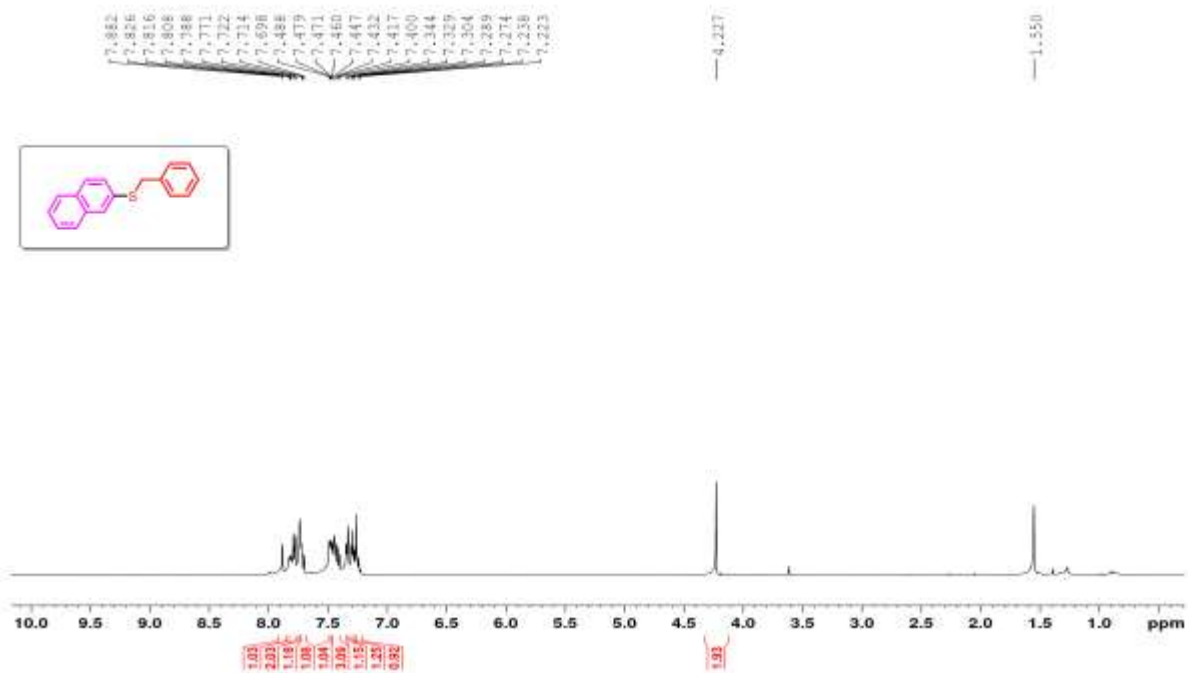


Figure 3.23. ^1H NMR spectrum of CD5.

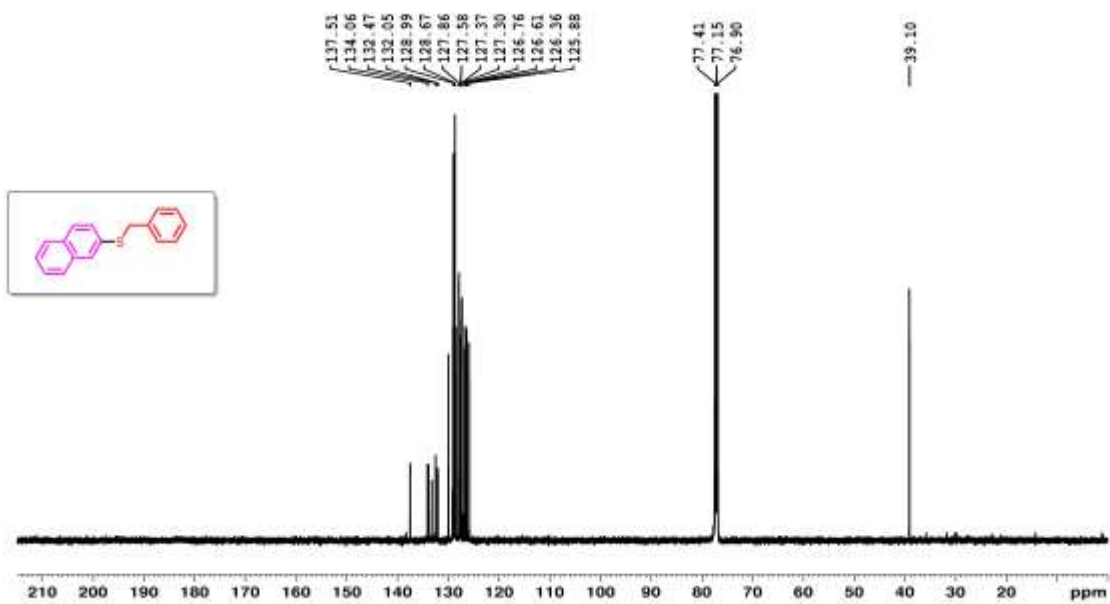


Figure 3.24. ^{13}C NMR spectrum of CD5.

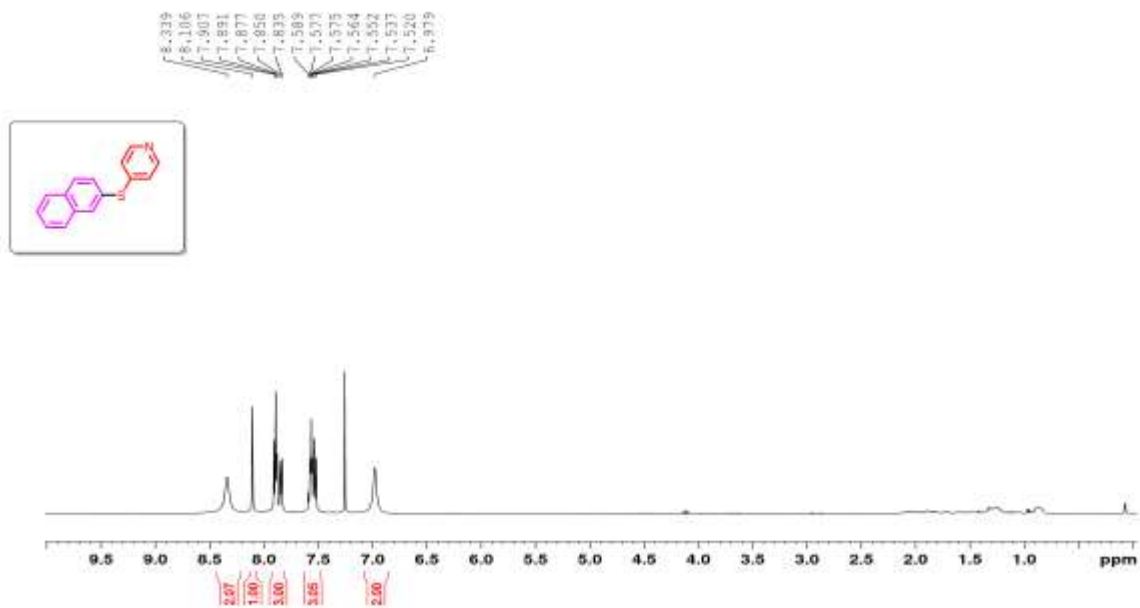


Figure 3.27. ¹H NMR spectrum of CD7.

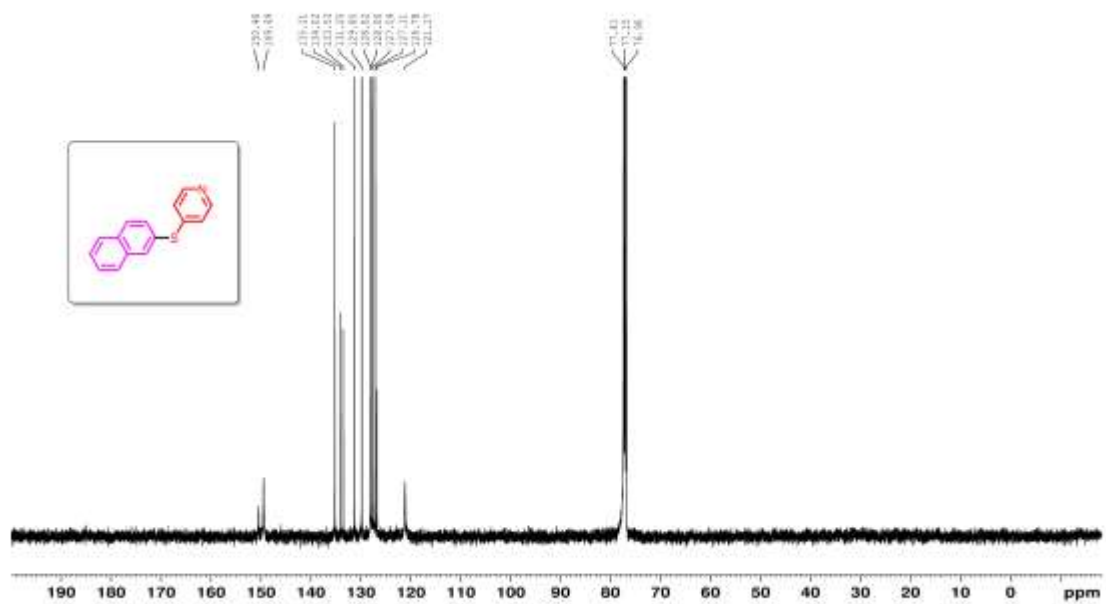


Figure 3.28. ¹³C NMR spectrum of CD7.

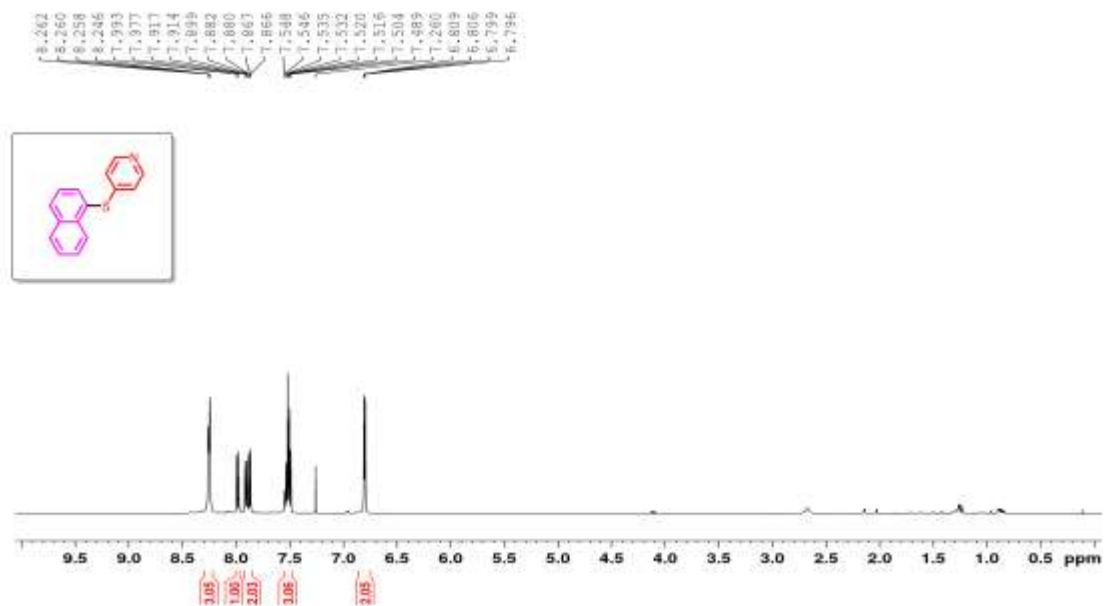


Figure 3.29. ^1H NMR spectrum of CD8.

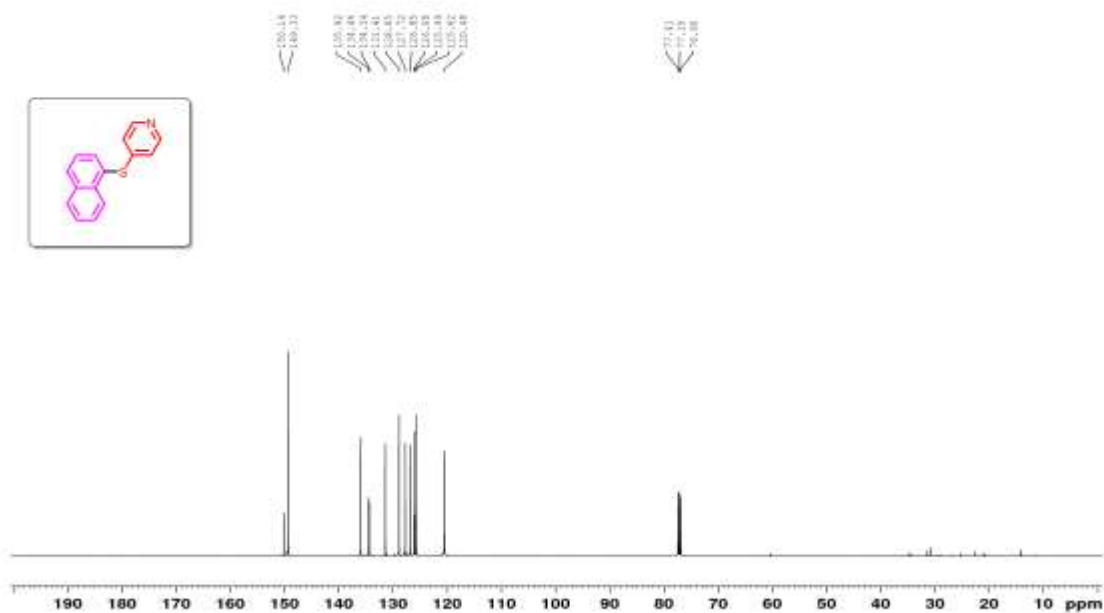


Figure 3.30. ^{13}C NMR spectrum of CD8.

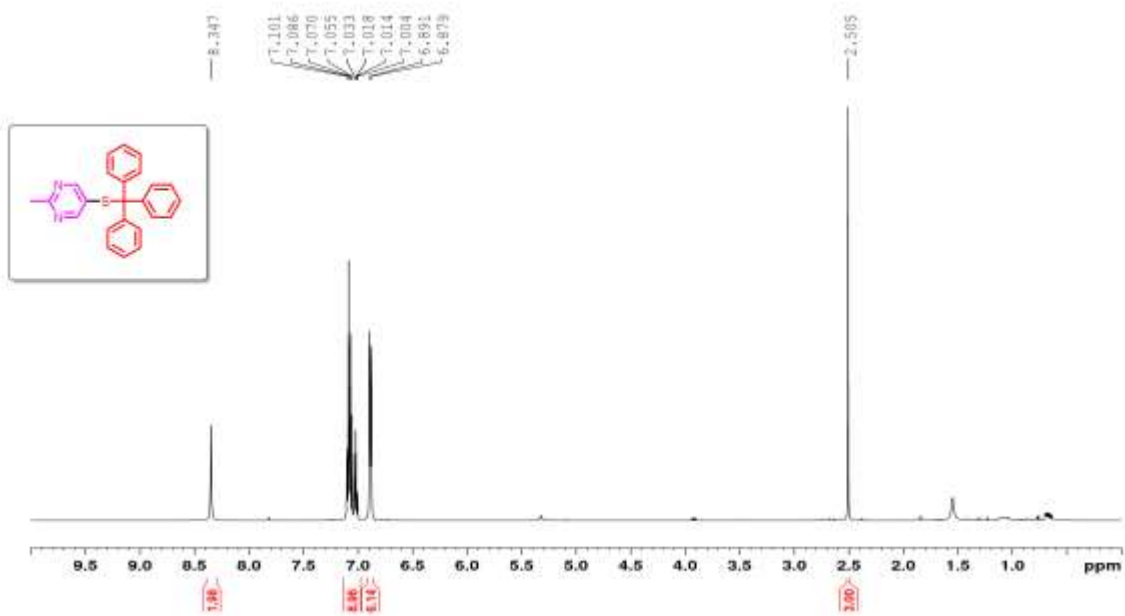


Figure 3.31. ^1H NMR spectrum of CD9.

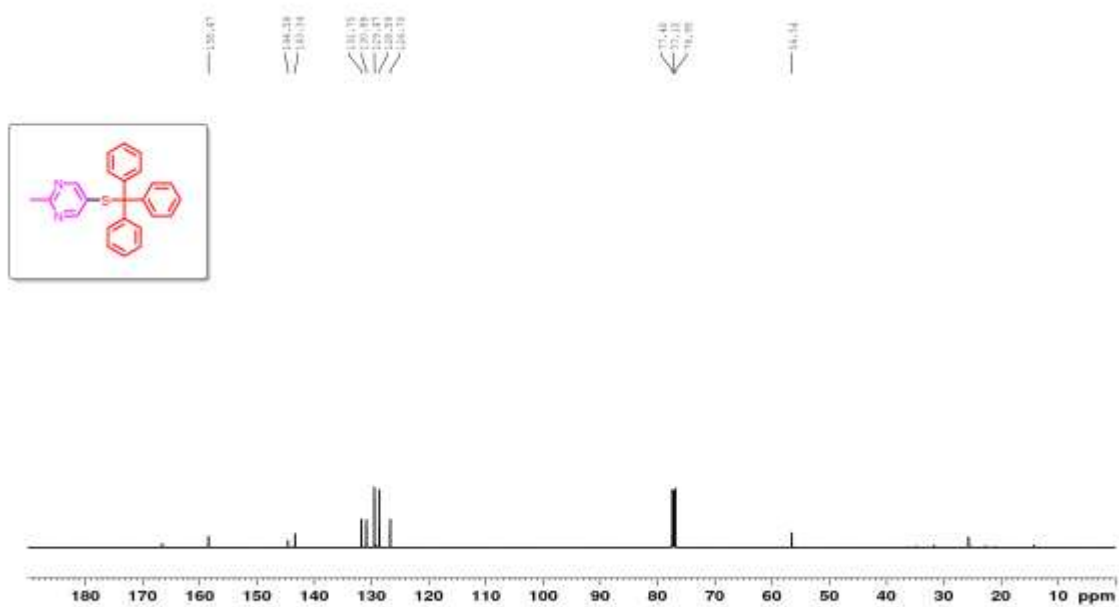


Figure 3.32. ^{13}C NMR spectrum of CD9.

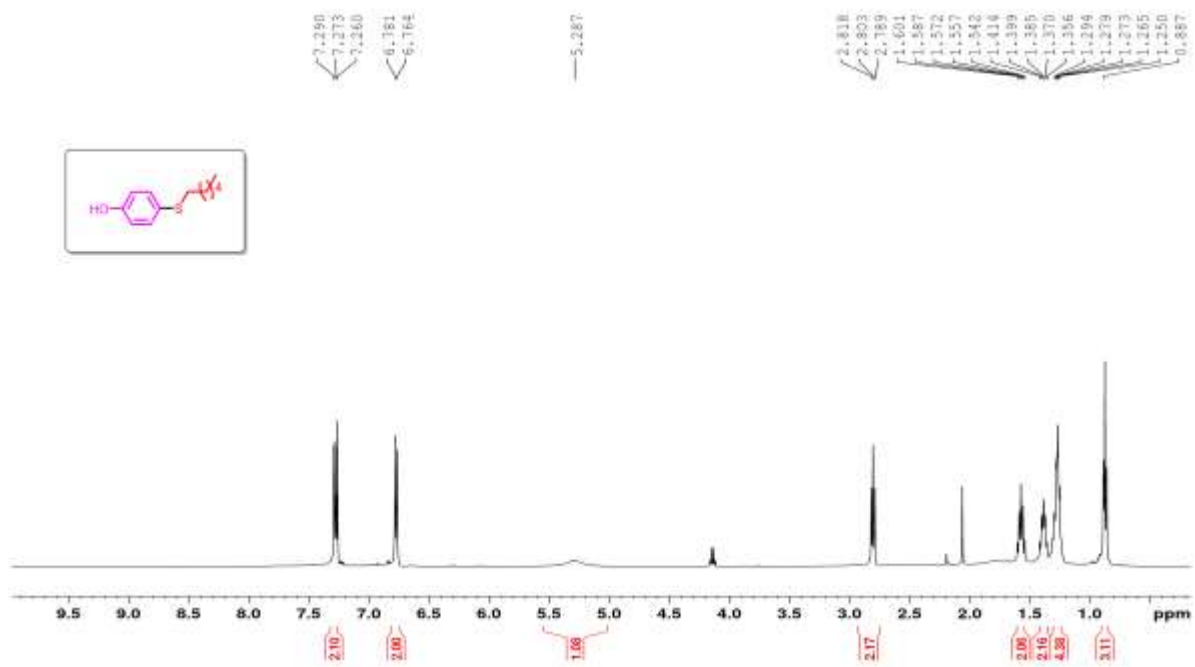


Figure 3.33. ¹H NMR spectrum of CD10.

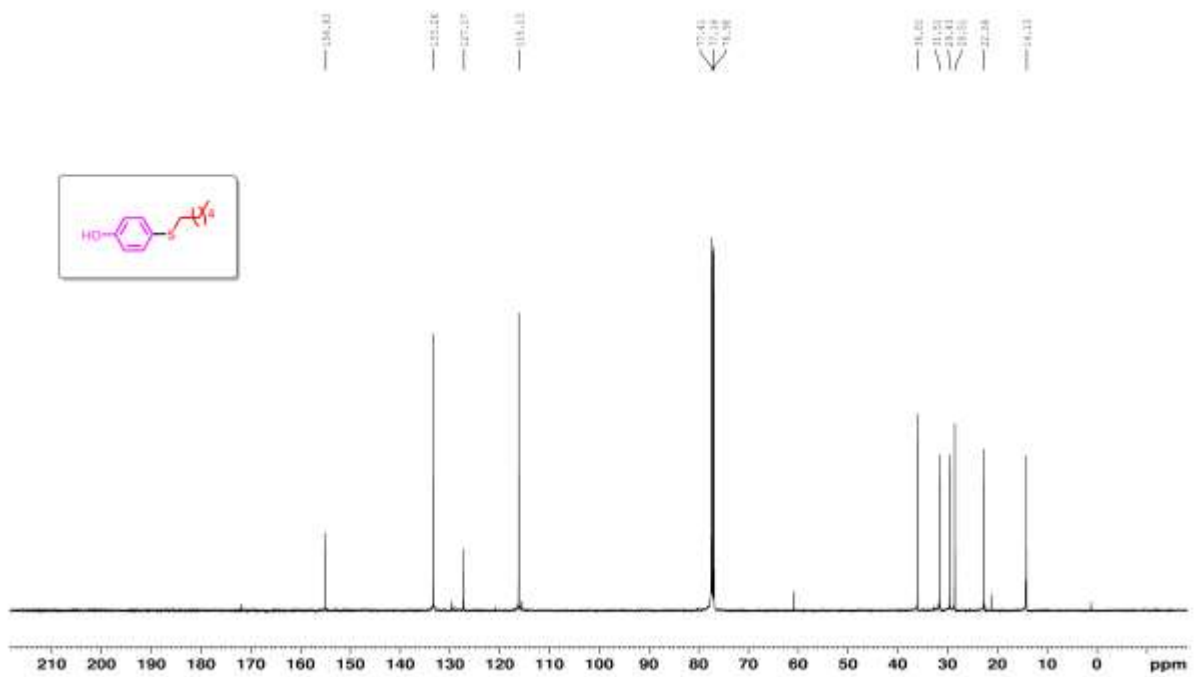


Figure 3.34. ¹³C NMR spectrum of CD10.

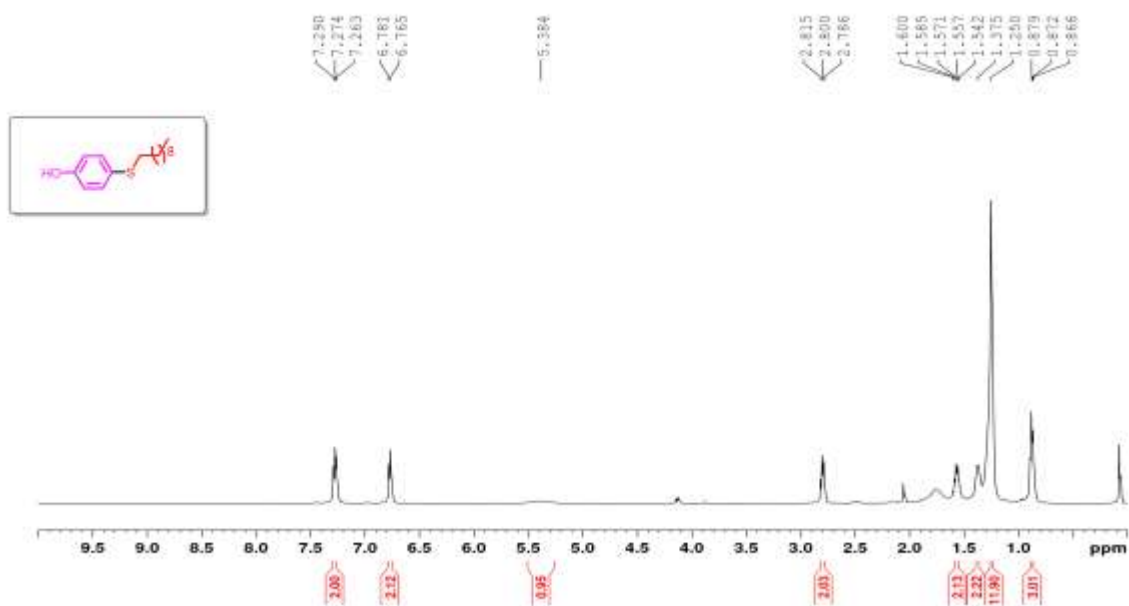


Figure 3.35. ^1H NMR spectrum of **CD11**.

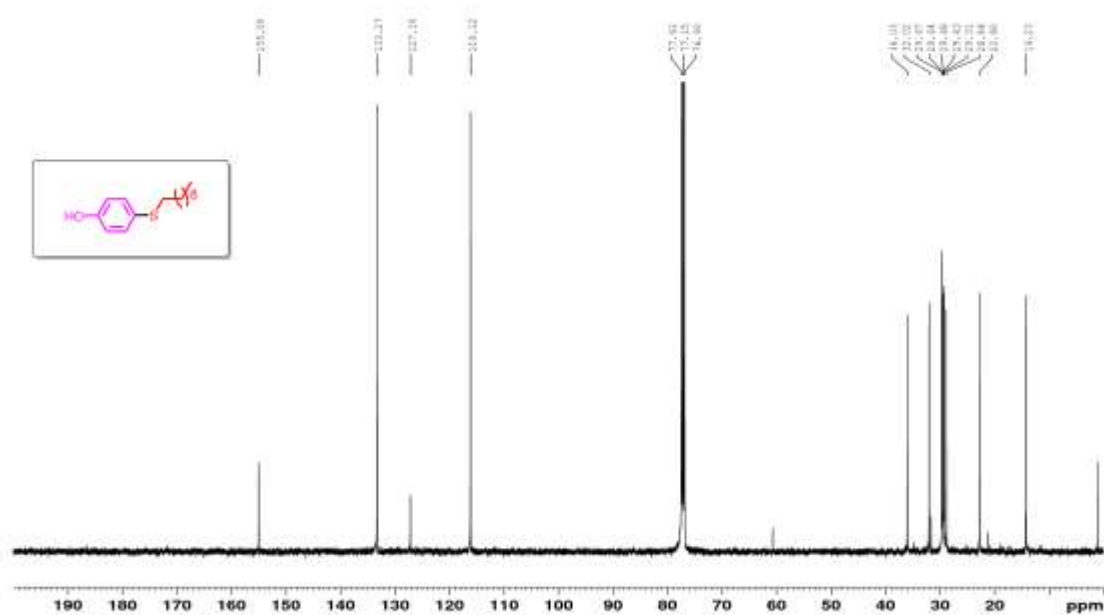


Figure 3.36. ^{13}C NMR spectrum of **CD11**.

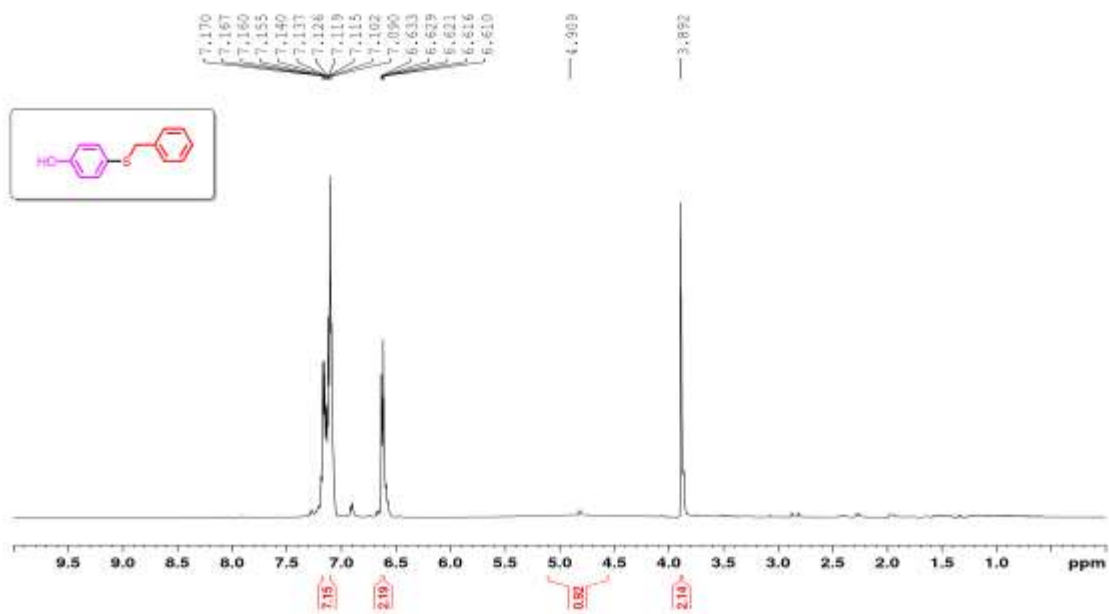


Figure 3.37. ^1H NMR spectrum of **CD12**.

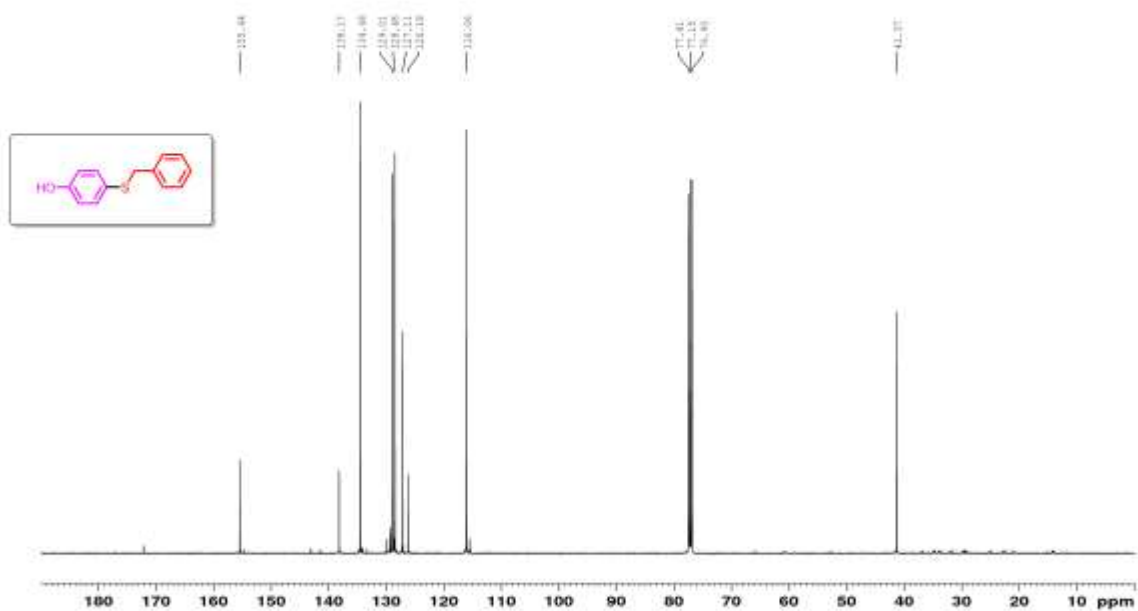


Figure 3.38. ^{13}C NMR spectrum of **CD12**.

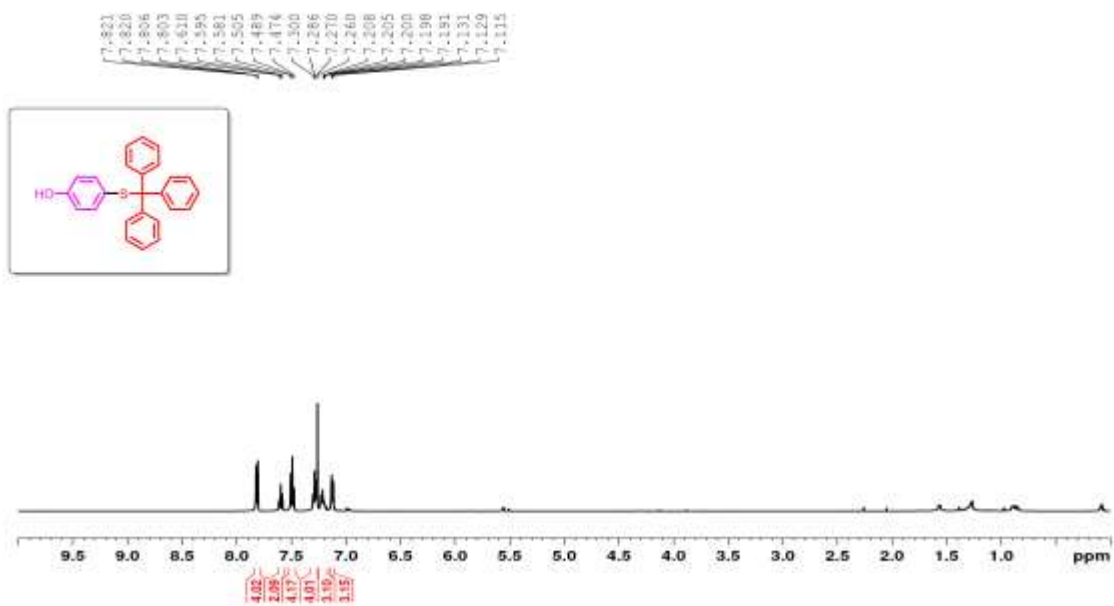


Figure 3.39. ¹H NMR spectrum of **CD13**.

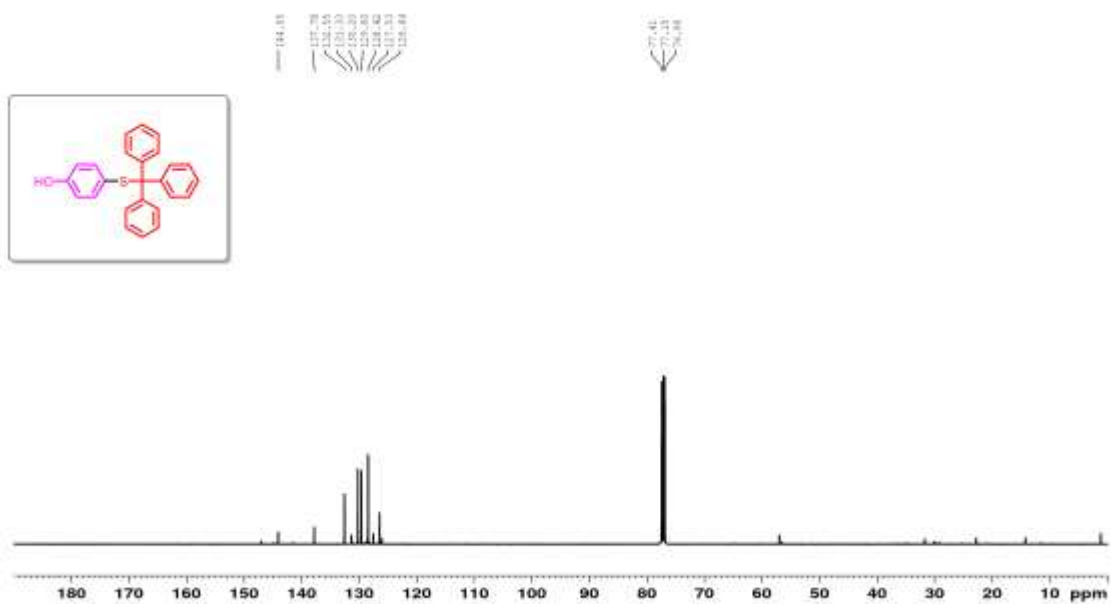


Figure 3.40. ¹³C NMR spectrum of **CD13**.

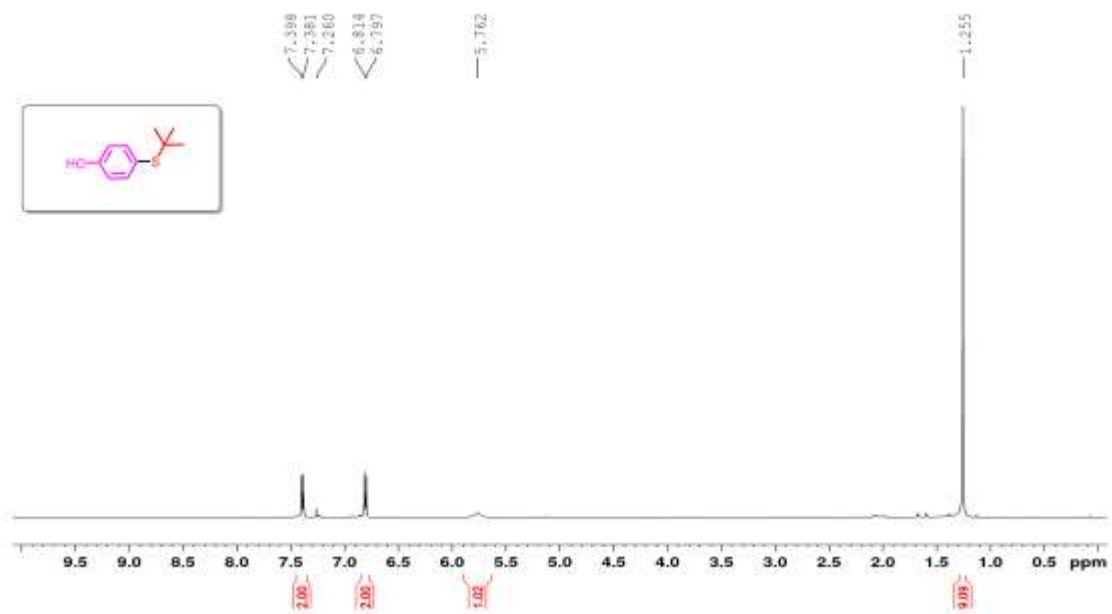


Figure 3.41. ^1H NMR spectrum of **CD14**.

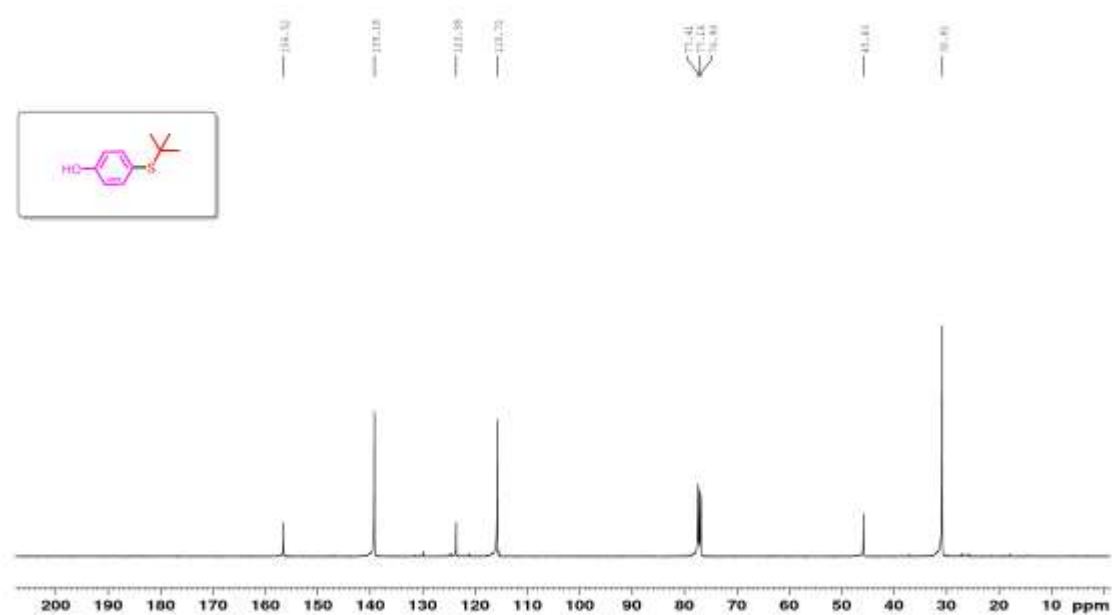


Figure 3.42. ^{13}C NMR spectrum of **CD14**.

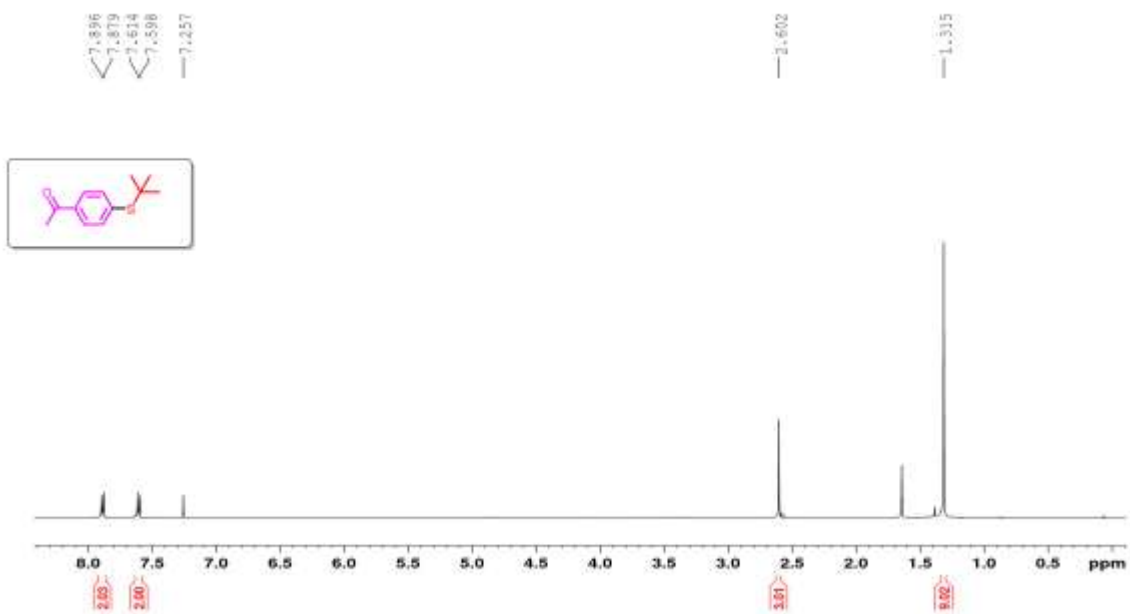


Figure 3.43. ¹H NMR spectrum of **CD15**.

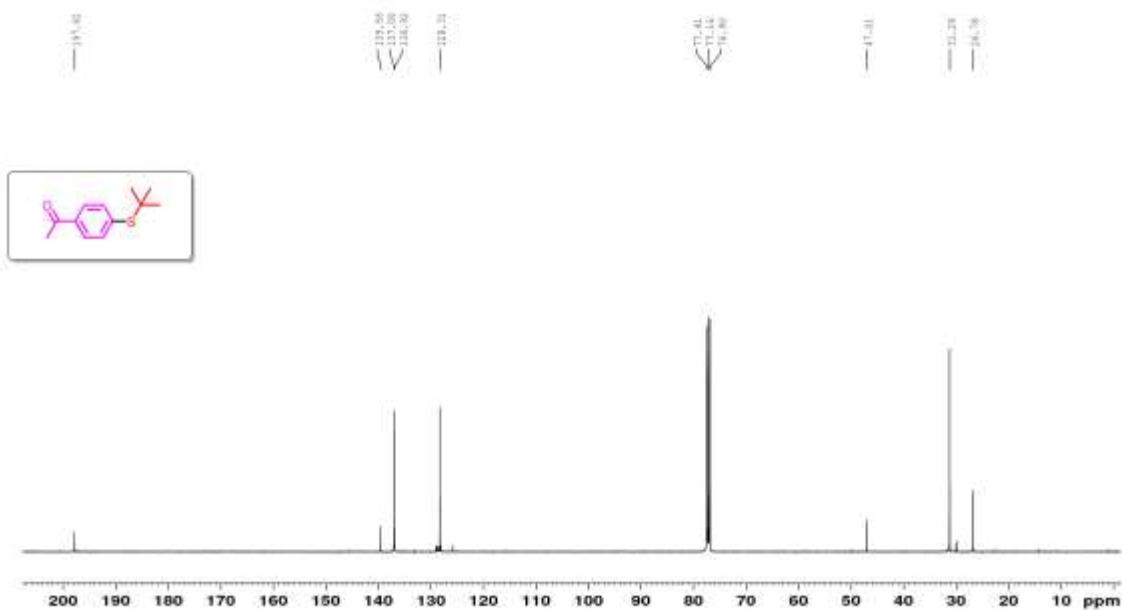


Figure 3.44. ¹³C NMR spectrum of **CD15**

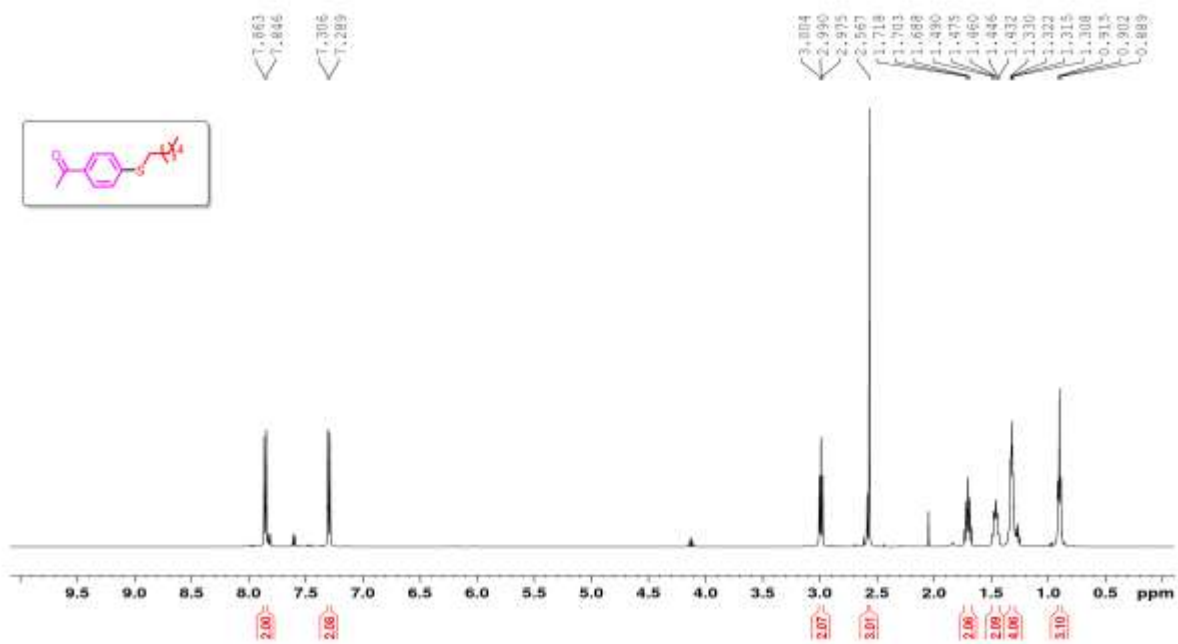


Figure 3.45. ¹H NMR spectrum of CD16.

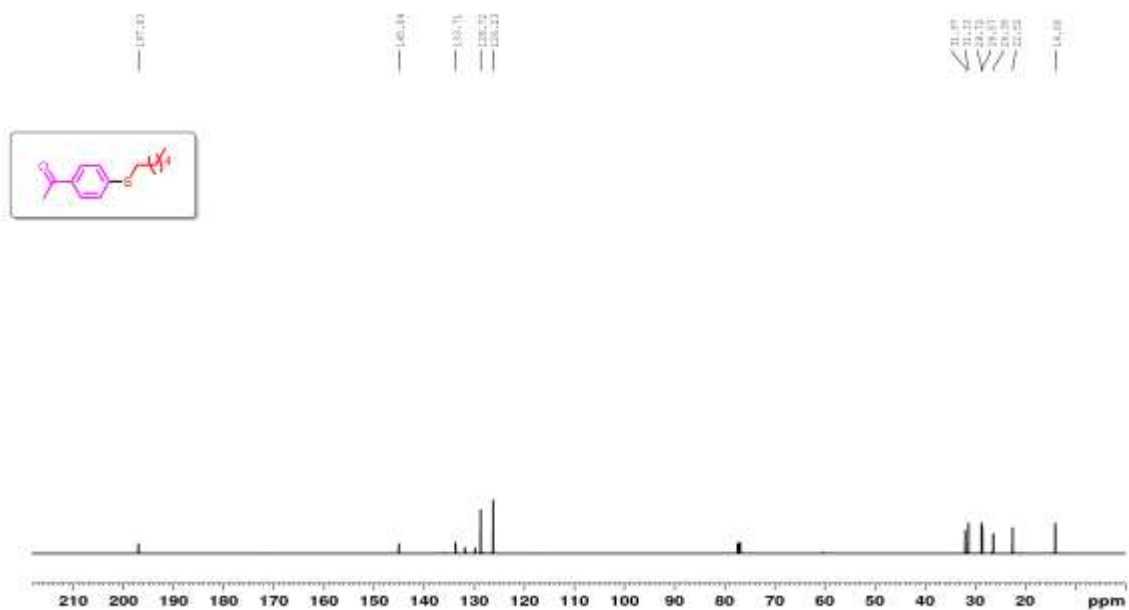


Figure 3.46. ¹³C NMR spectrum of CD16.

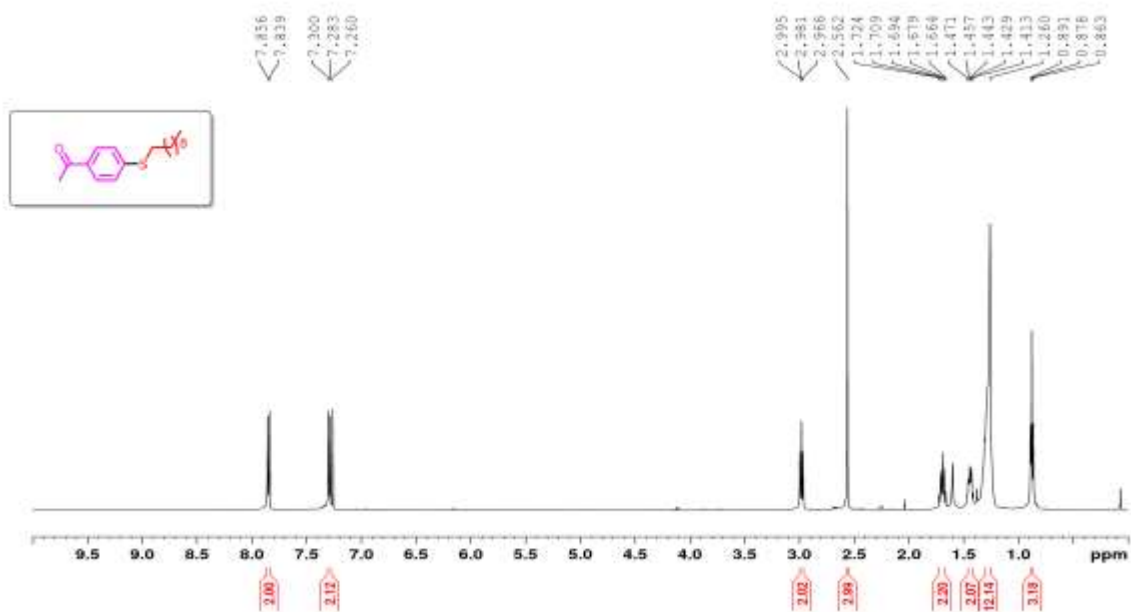


Figure 3.47. ¹H NMR spectrum of CD17.

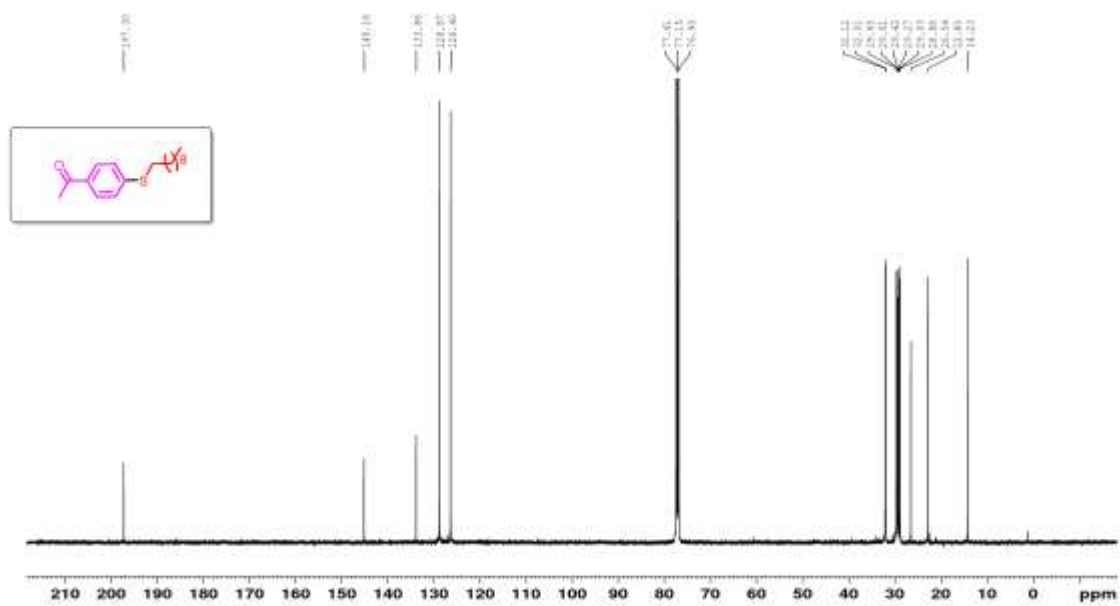


Figure 3.48. ¹³C NMR spectrum of CD17.

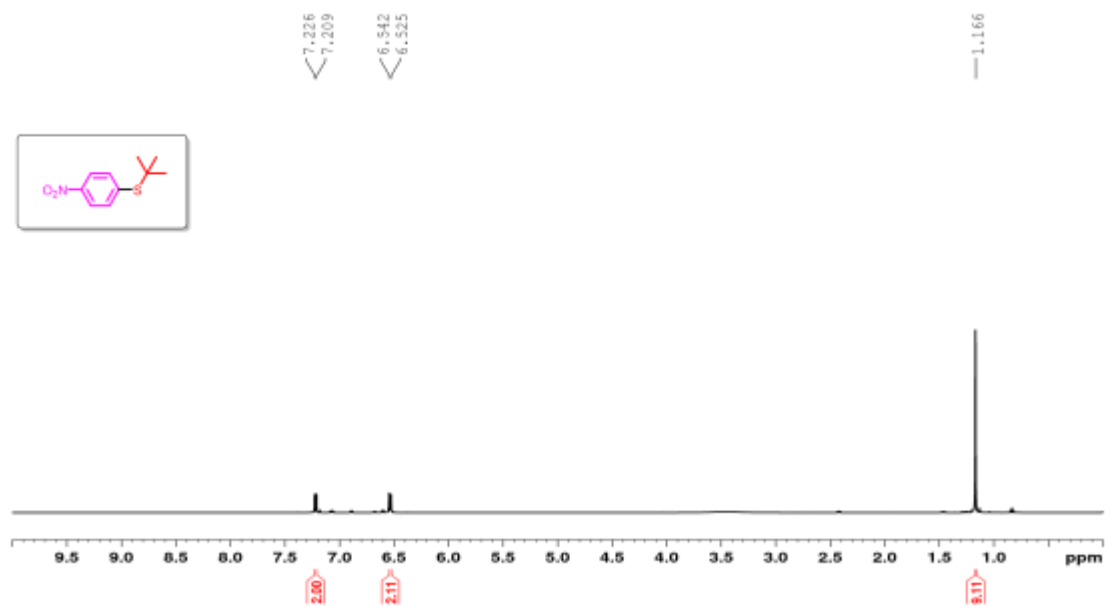


Figure 3.49. ^1H NMR spectrum of **CD18**.

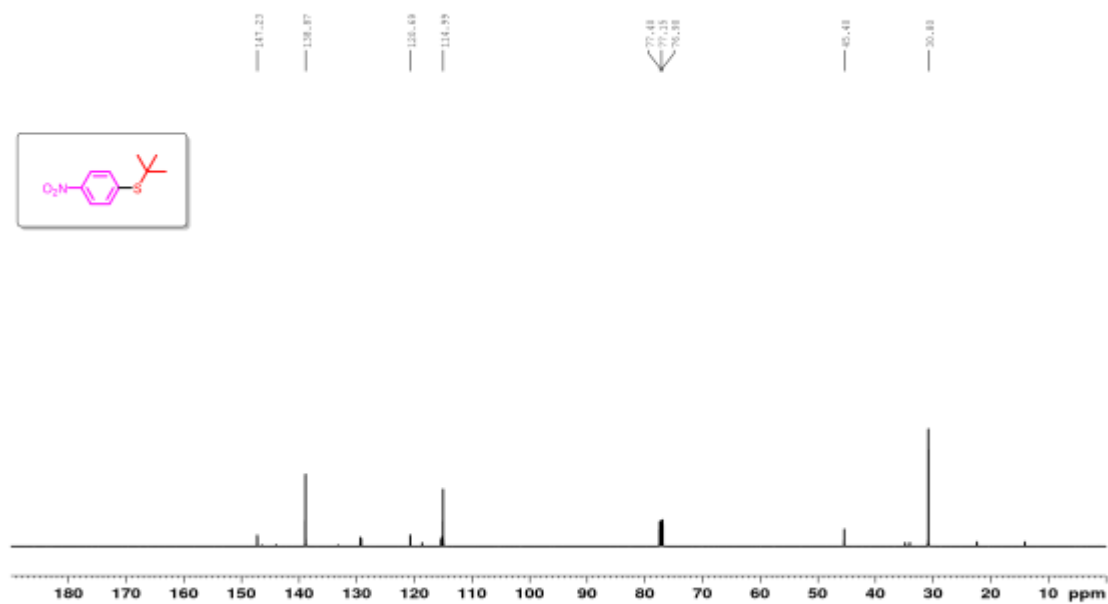


Figure 3.50. ^{13}C NMR spectrum of **CD18**.

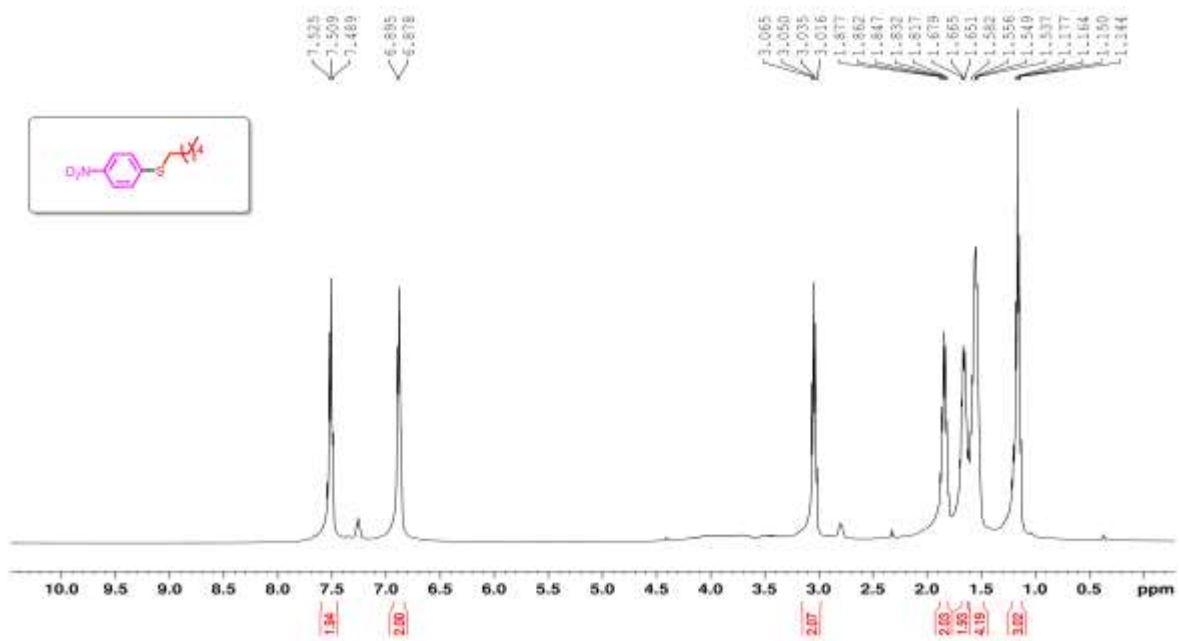


Figure 3.51. ¹H NMR spectrum of CD19.

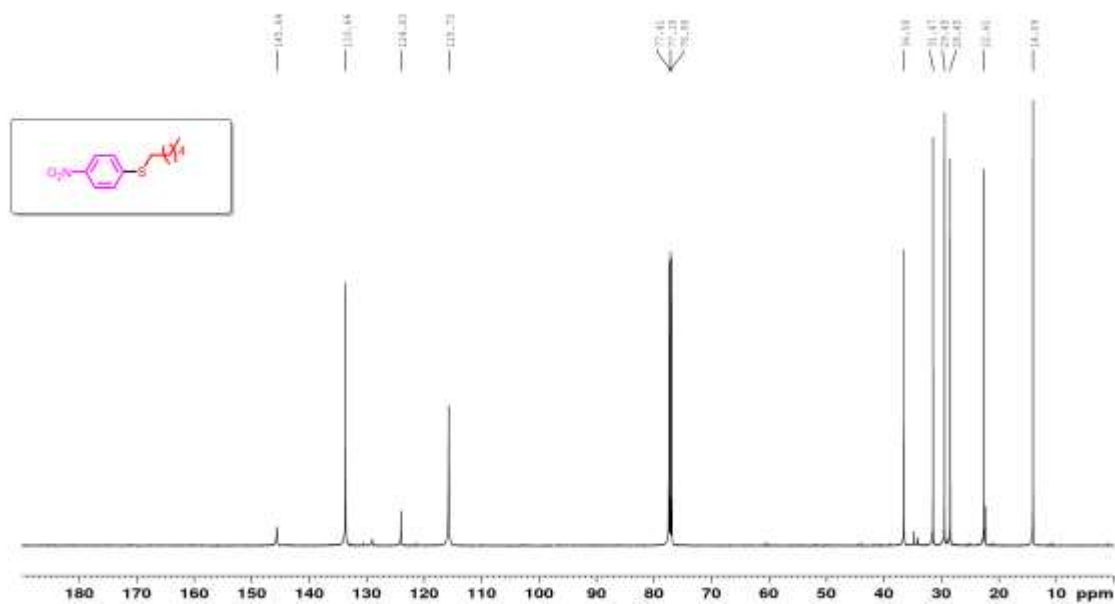


Figure 3.52. ¹³C NMR spectrum of CD19.

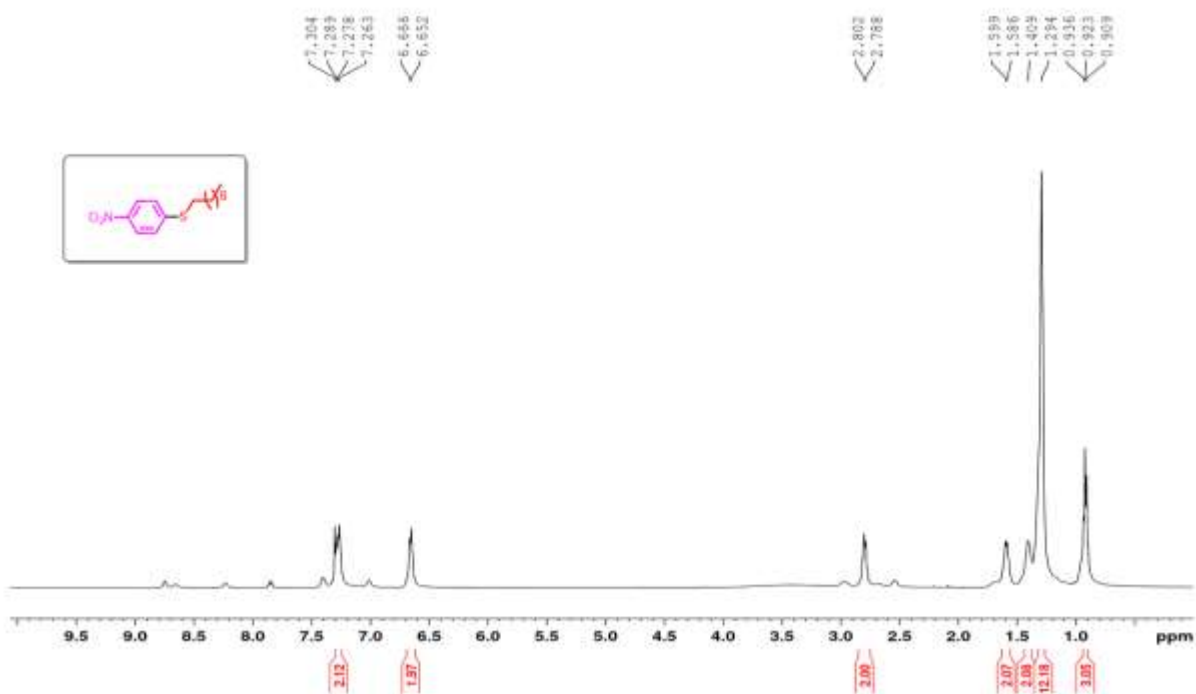


Figure 3.53. ¹H NMR spectrum of CD20.

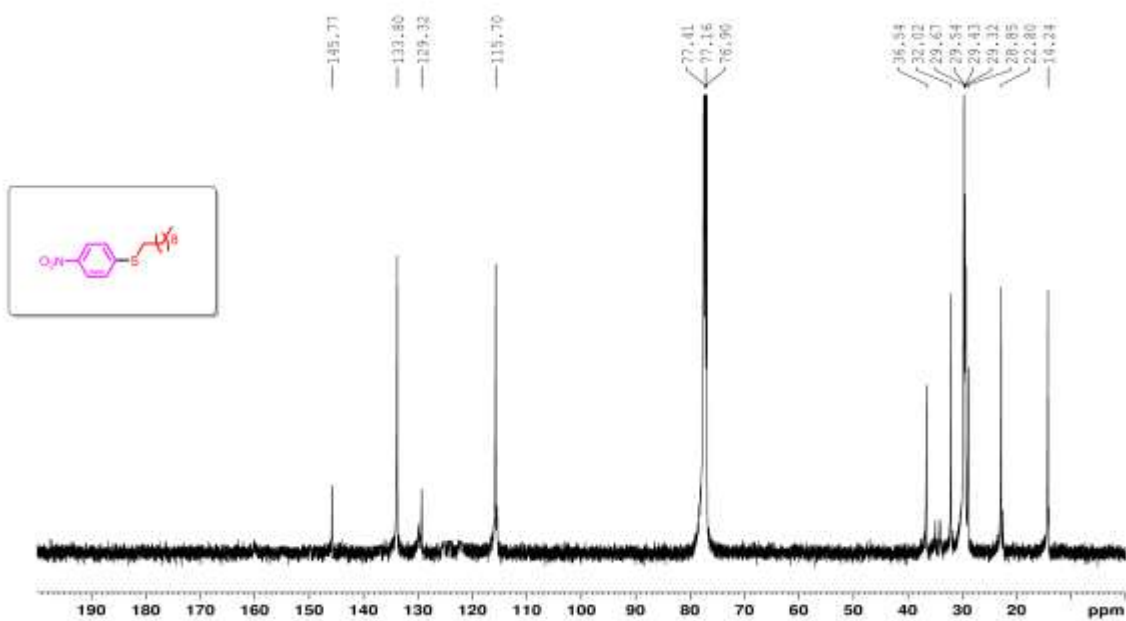


Figure 3.54. ¹³C NMR spectrum of CD20.

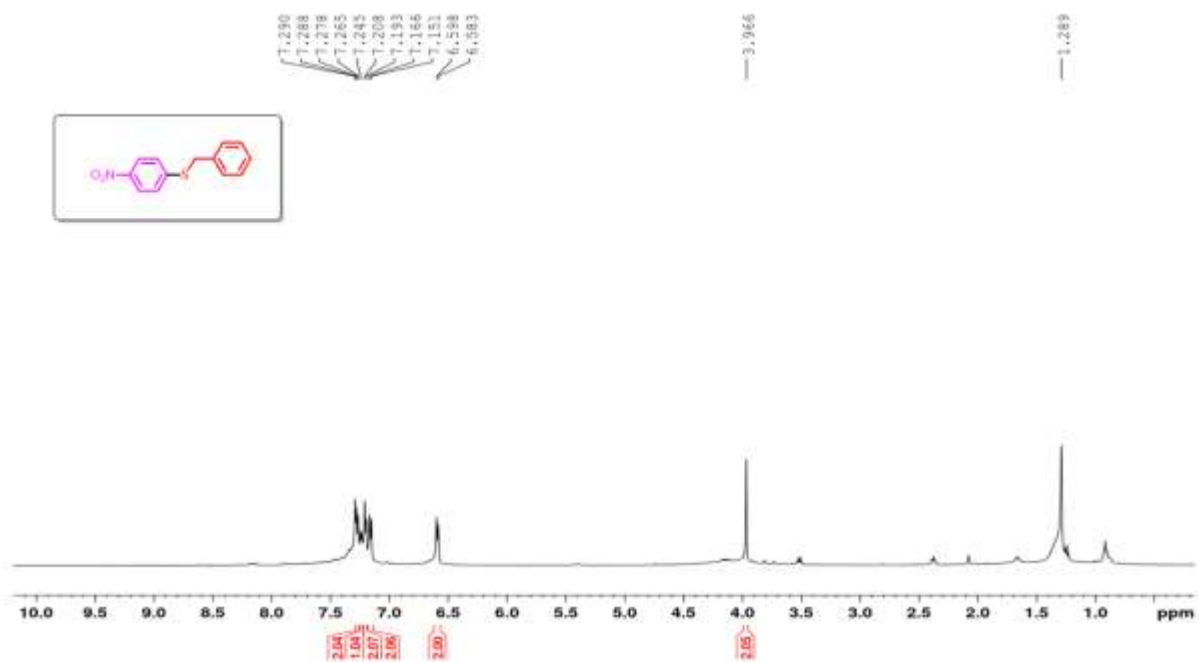


Figure 3.55. ^1H NMR spectrum of CD21.

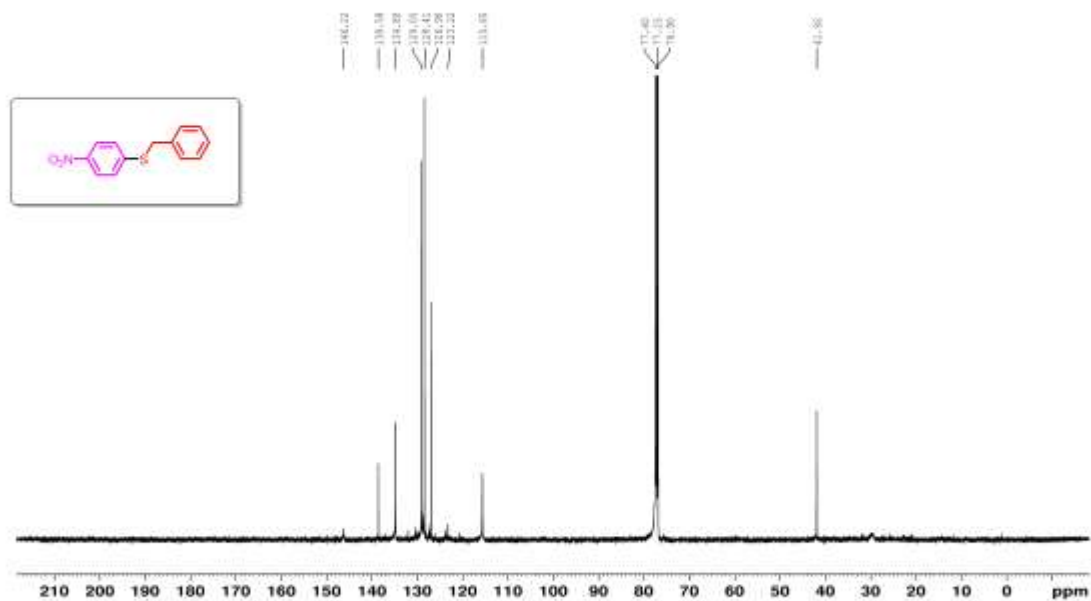


Figure 3.56. ^{13}C NMR spectrum of CD21.

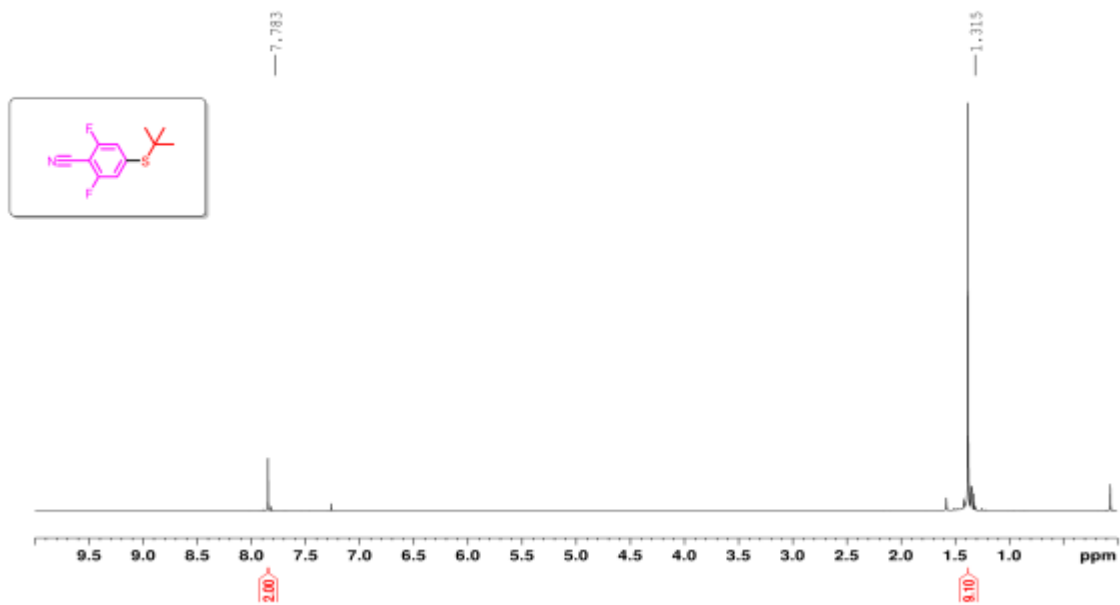


Figure 3.57. ^1H NMR spectrum of **CD22**.

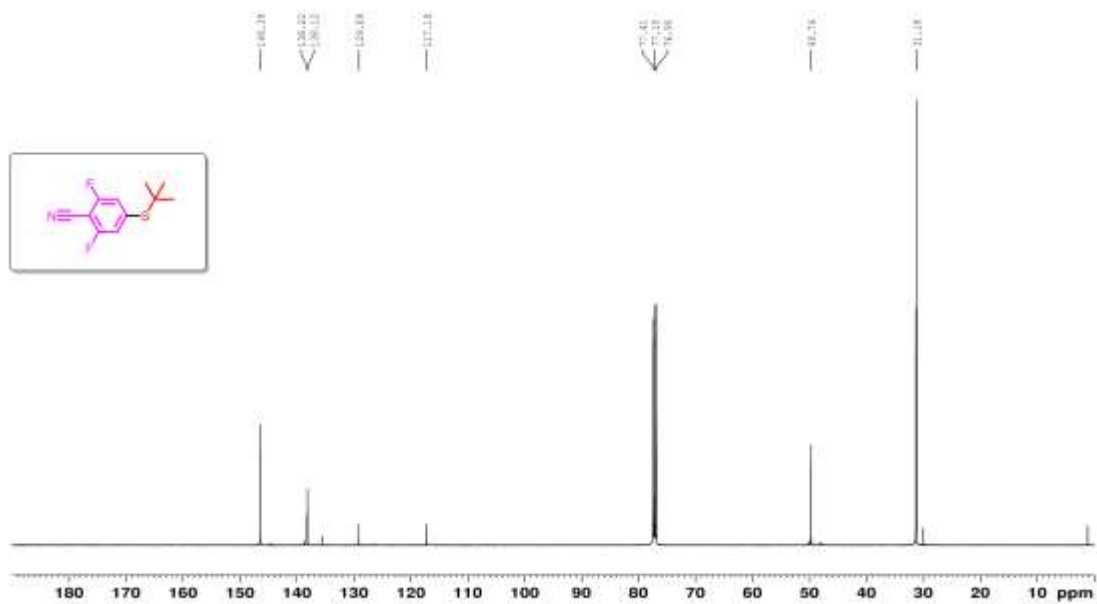


Figure 3.58. ^{13}C NMR spectrum of **CD22**.

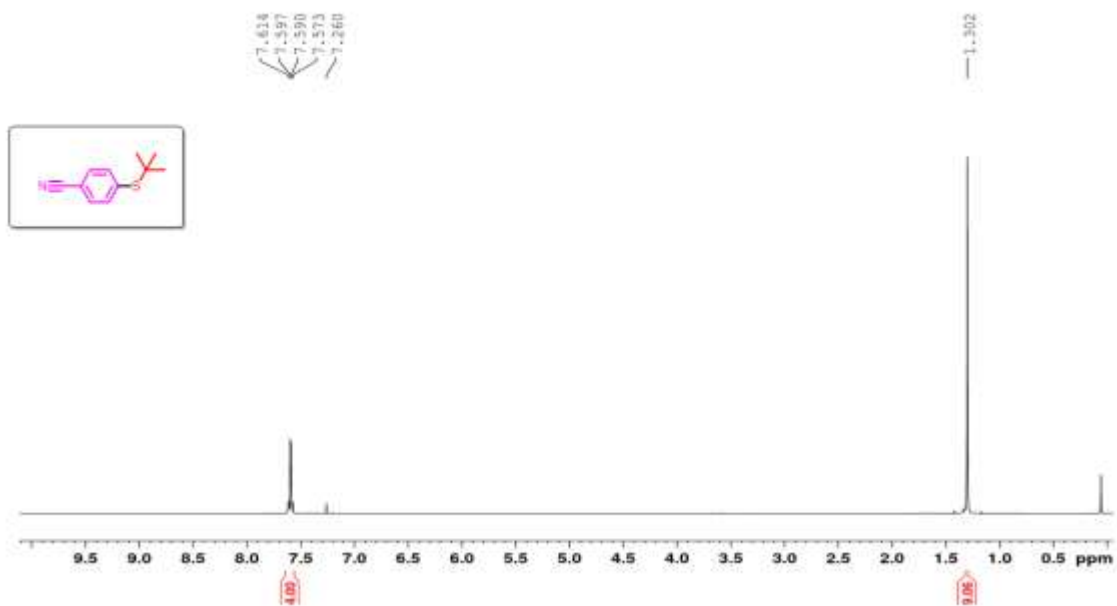


Figure 3.59. ^1H NMR spectrum of CD23.

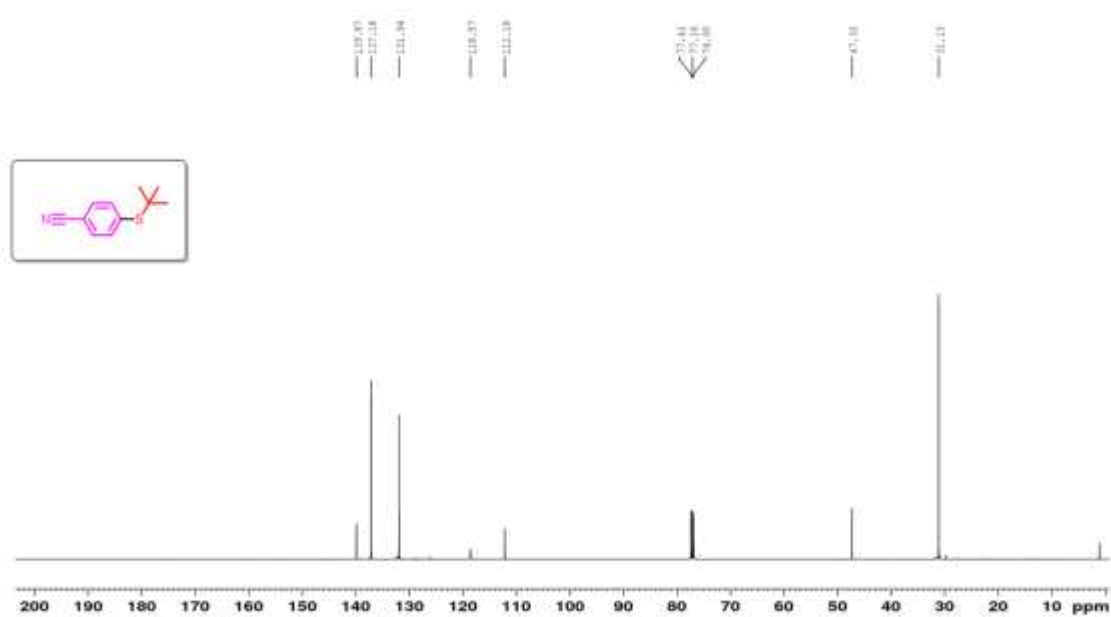


Figure 3.60. ^{13}C NMR spectrum of CD23.

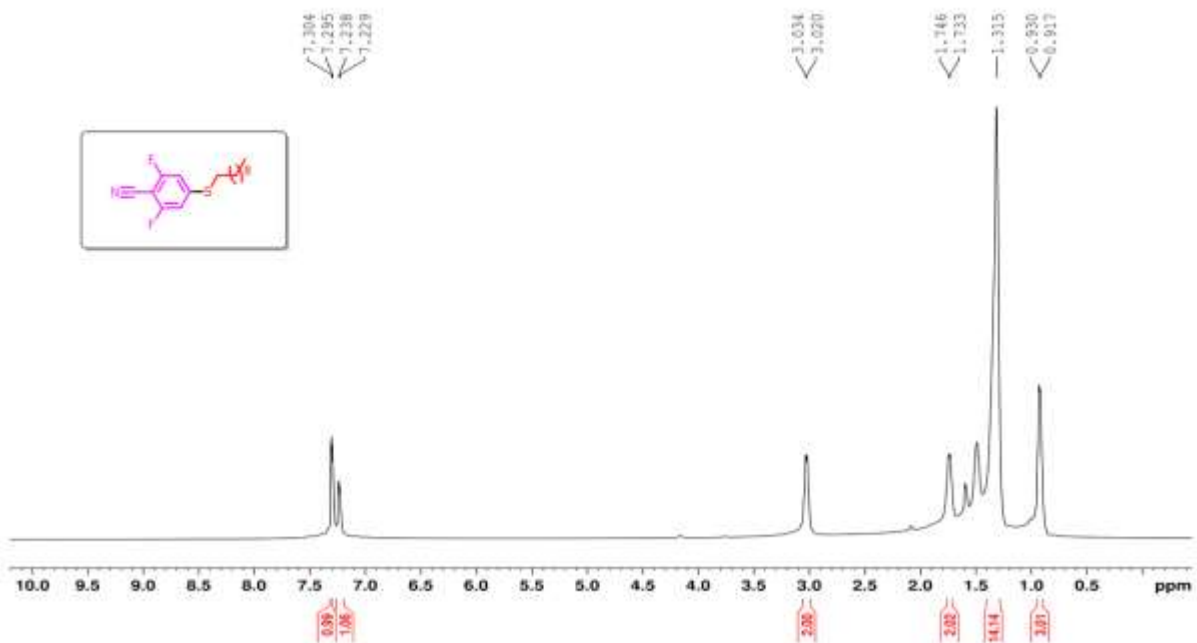


Figure 3.61. ^1H NMR spectrum of CD24.

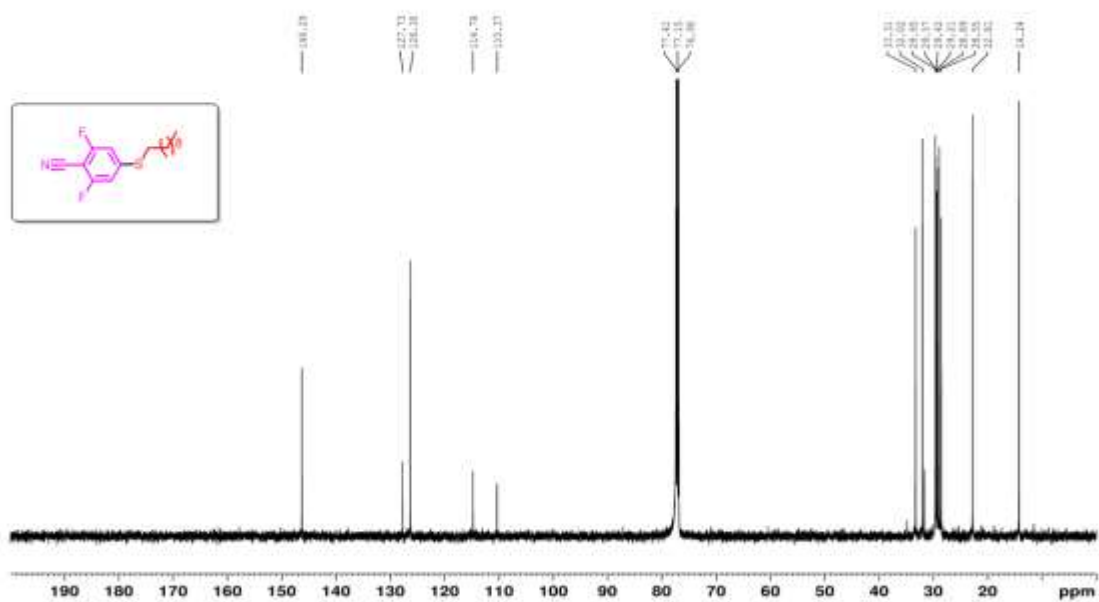


Figure 3.62. ^{13}C NMR spectrum of CD24.

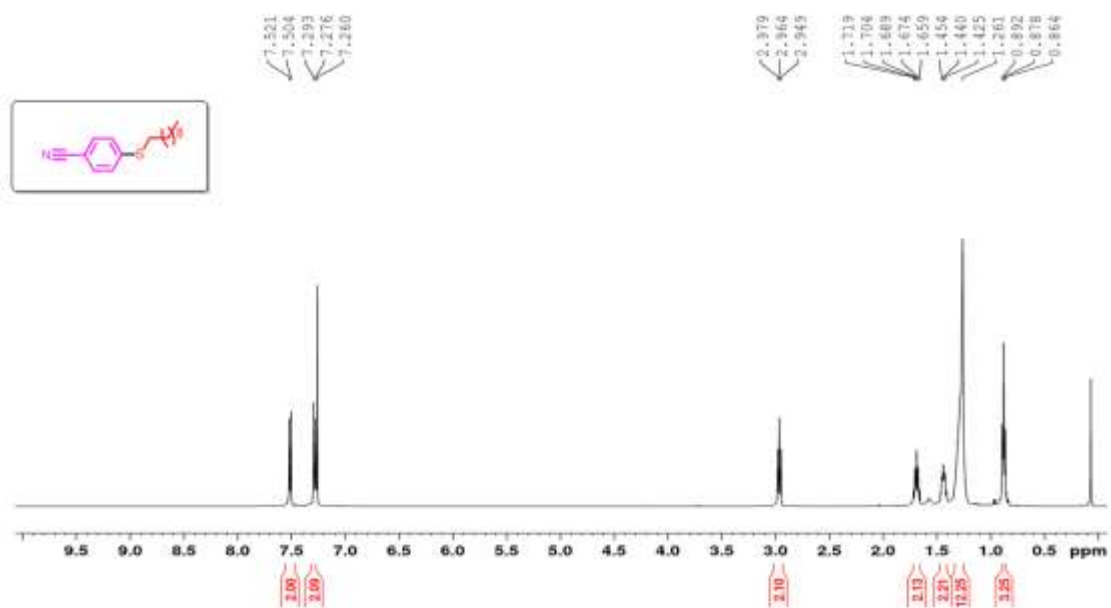


Figure 3.63. ^1H NMR spectrum of CD25.

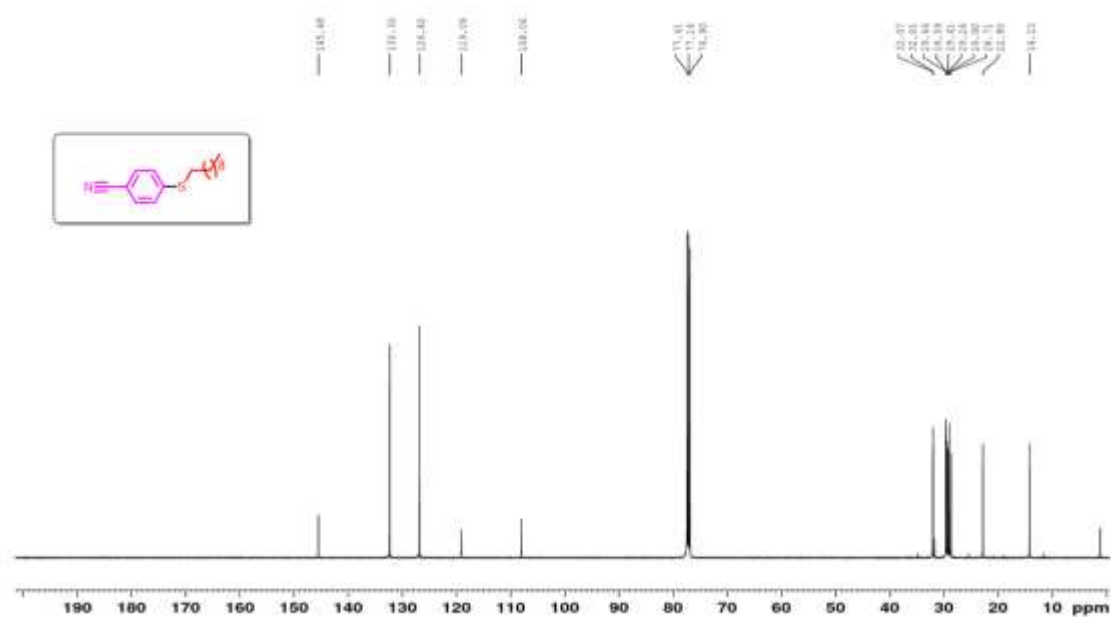


Figure 3.64. ^{13}C NMR spectrum of CD25.

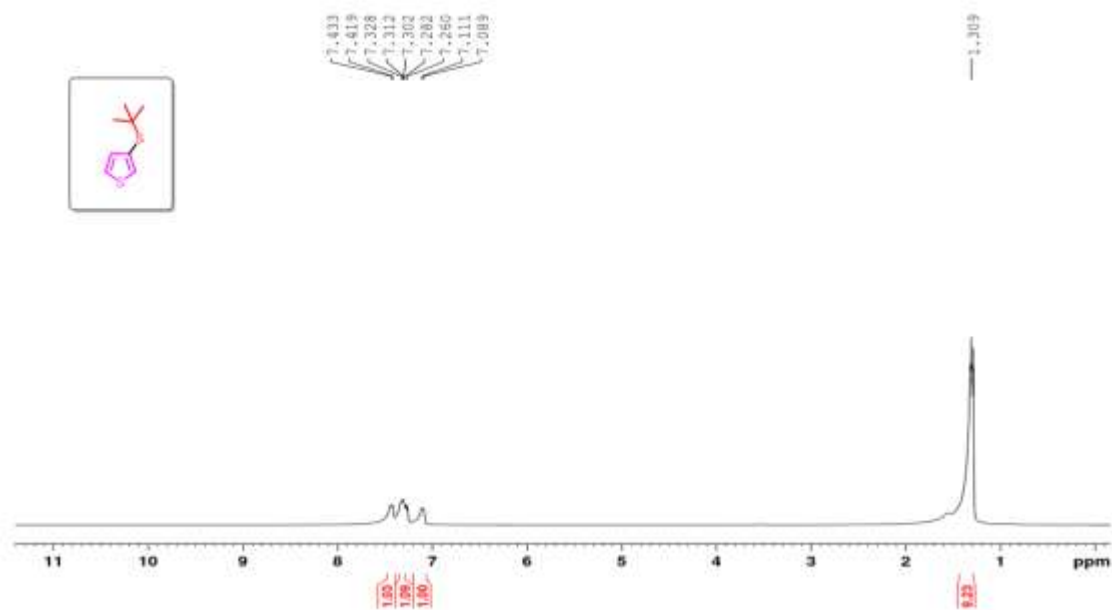


Figure 3.65. ^1H NMR spectrum of CD26.

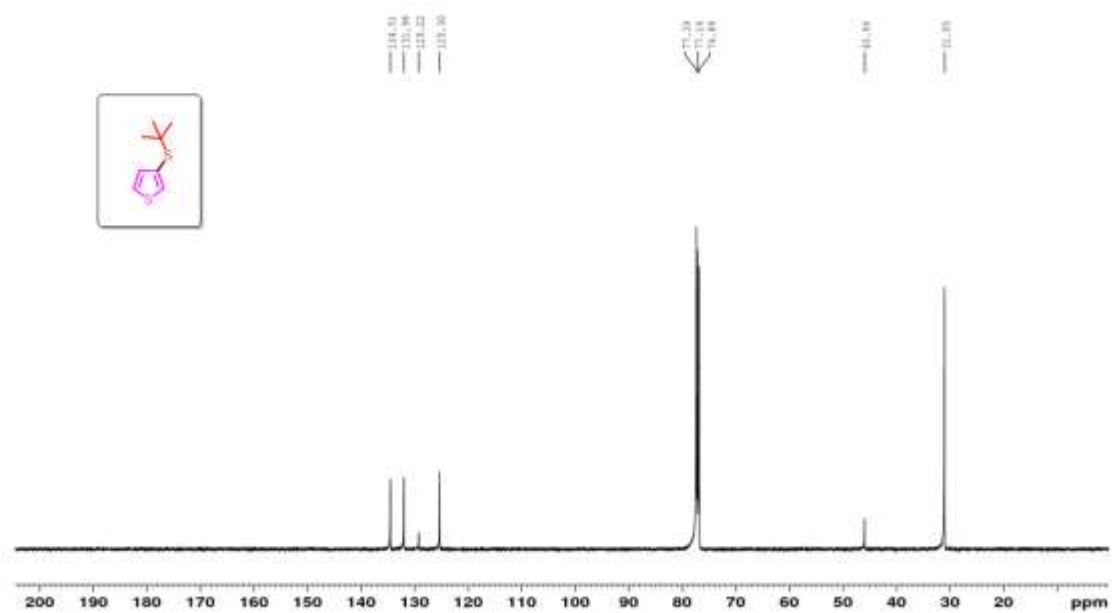


Figure 3.66. ^{13}C NMR spectrum of CD26.

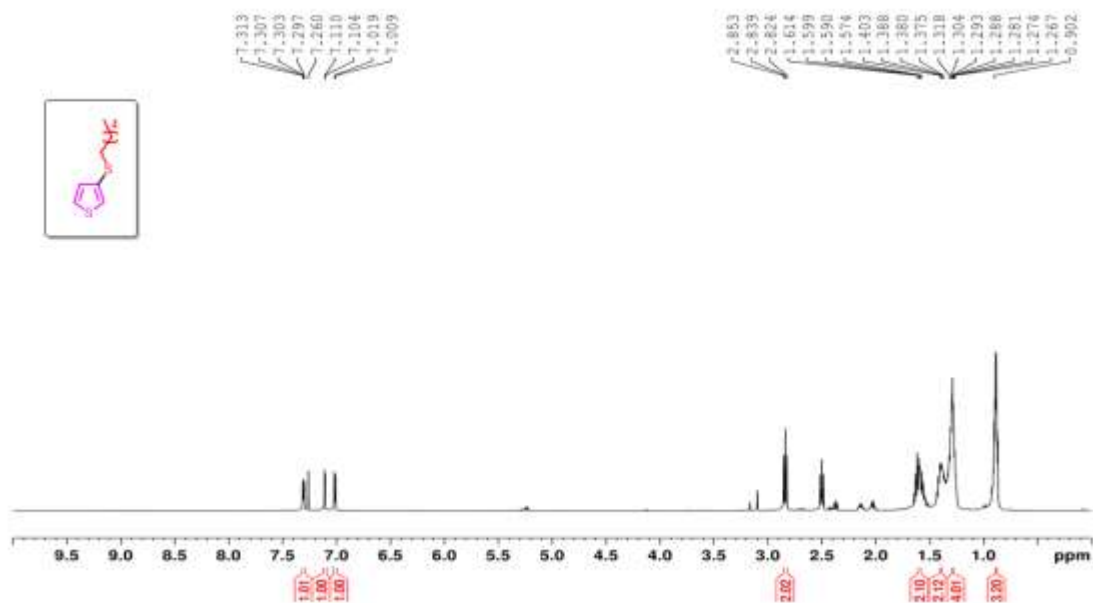


Figure 3.67. ¹H NMR spectrum of CD27.

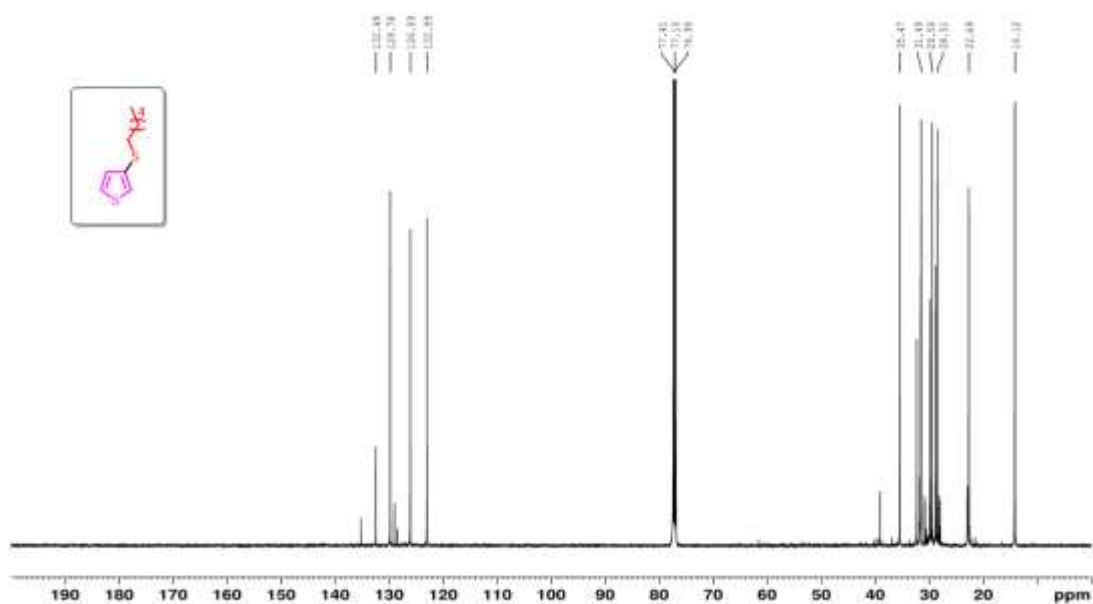


Figure 3.68. ¹³C NMR spectrum of CD27.

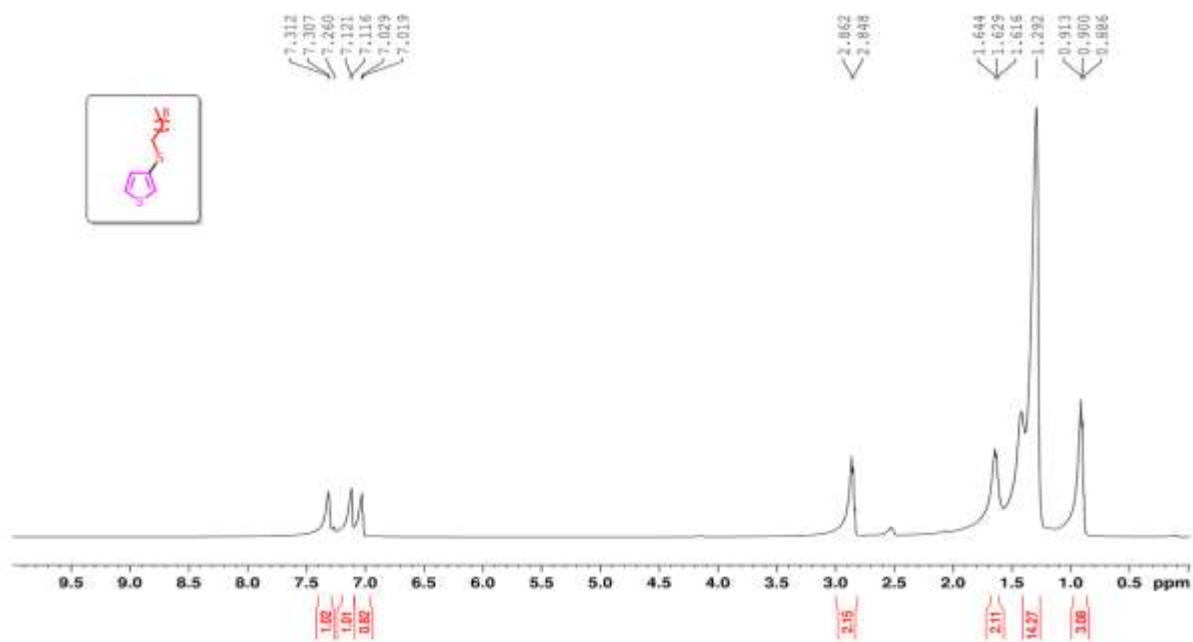


Figure 3.69. ¹H NMR spectrum of **CD28**.

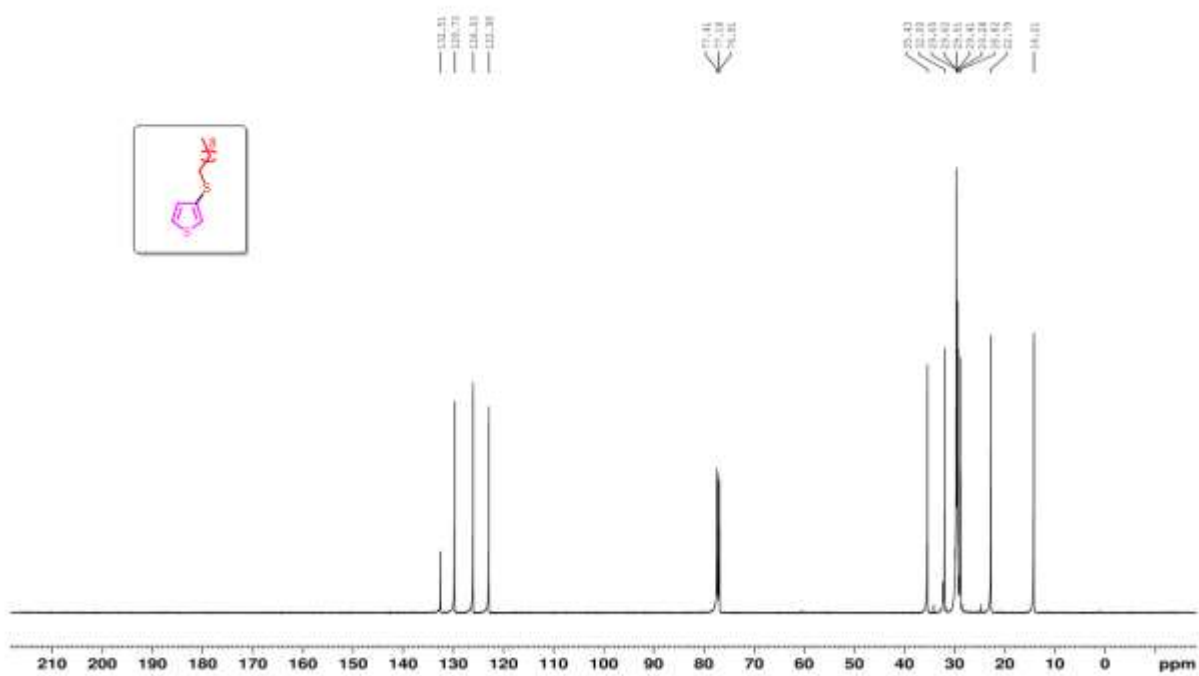


Figure 3.70. ¹³C NMR spectrum of **CD28**.

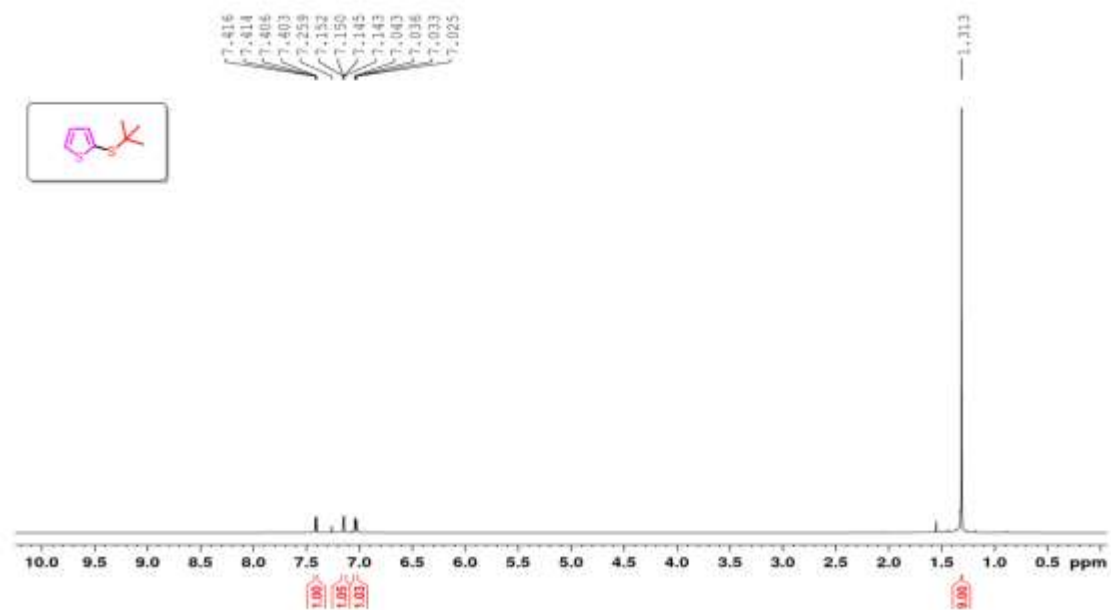


Figure 3.71. ^1H NMR spectrum of CD29.

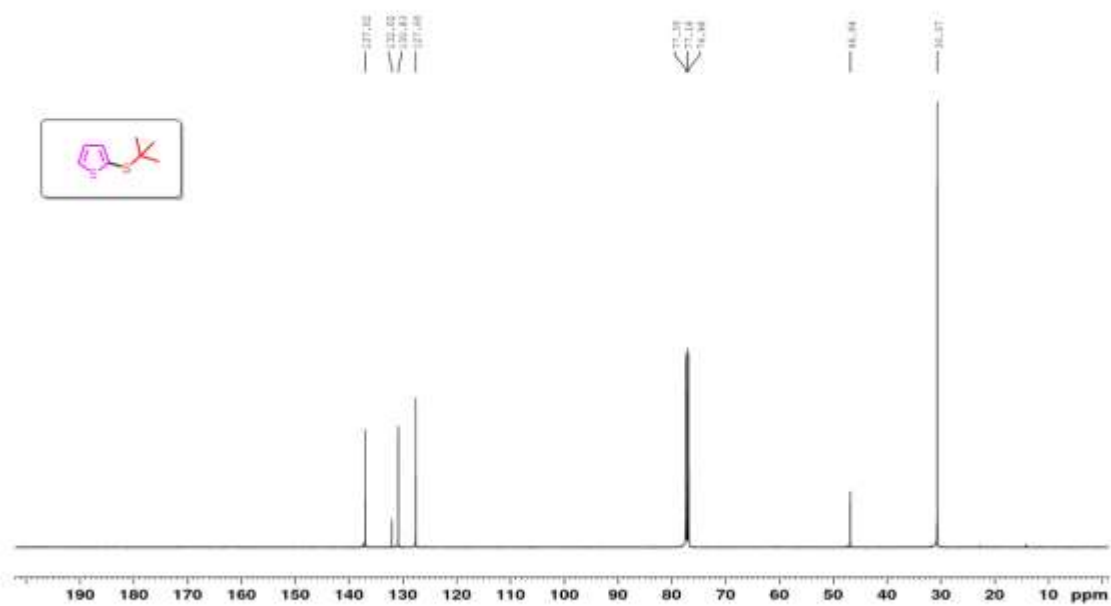


Figure 3.72. ^{13}C NMR spectrum of CD29.

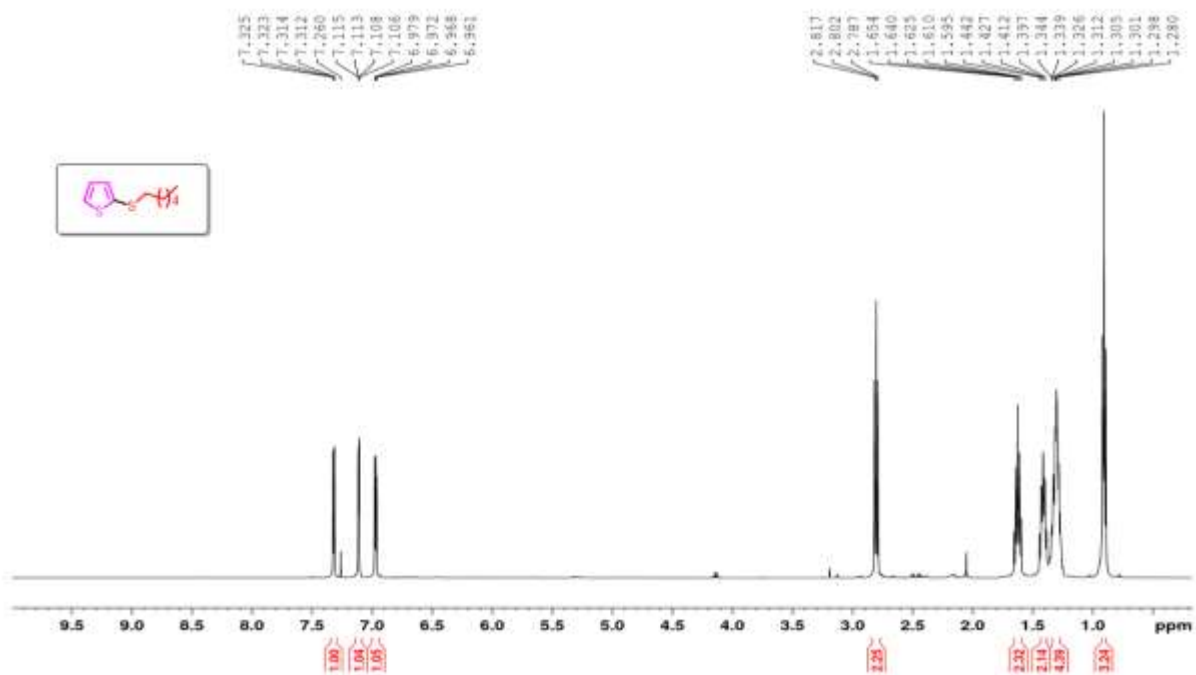


Figure 3.73. ^1H NMR spectrum of CD30.

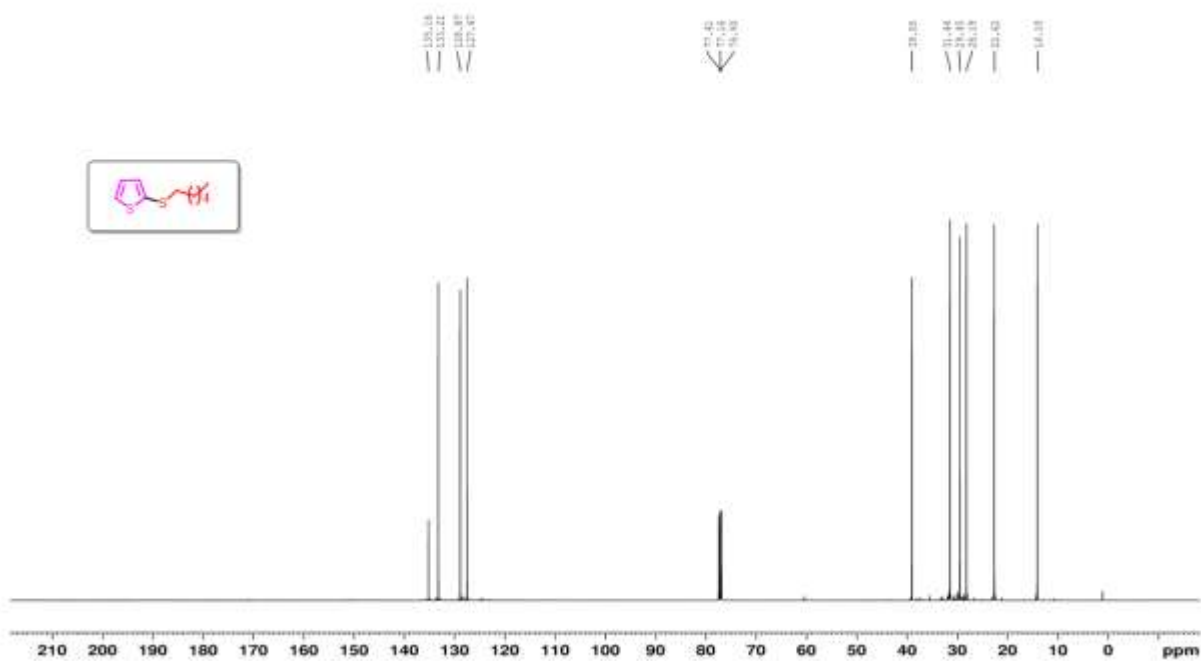


Figure 3.74. ^{13}C NMR spectrum of CD30.

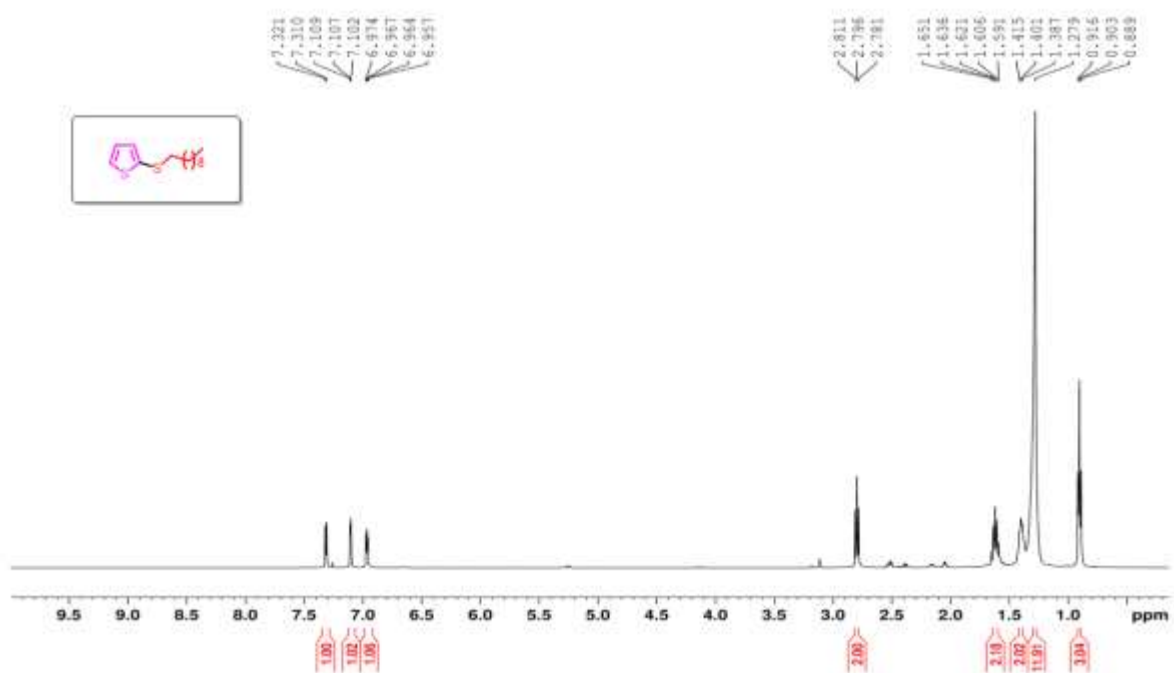


Figure 3.75. ^1H NMR spectrum of CD31.

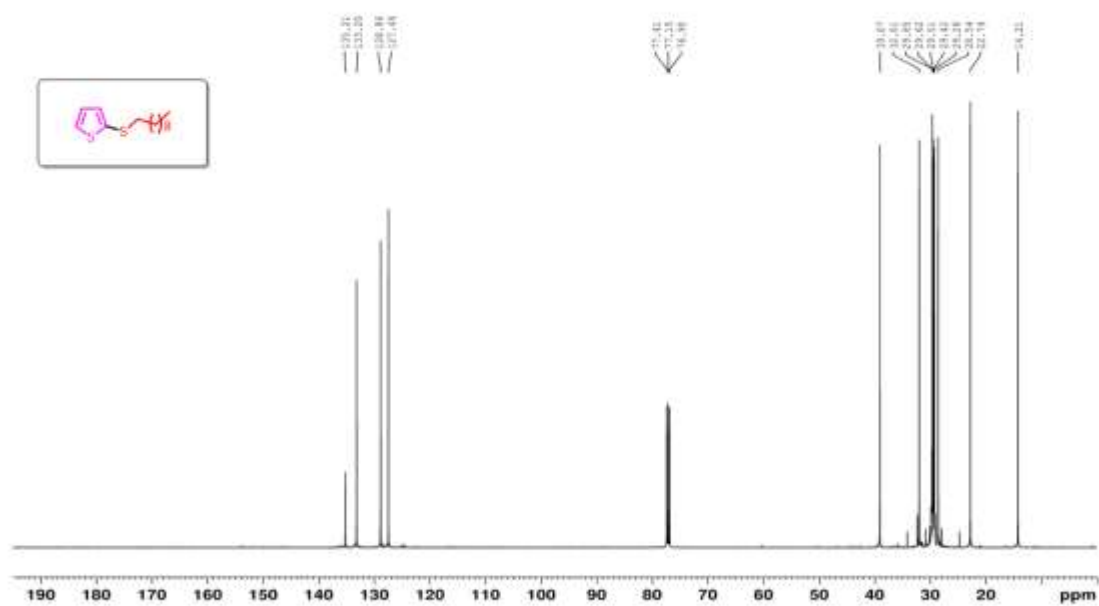


Figure 3.76. ^{13}C NMR spectrum of CD31.

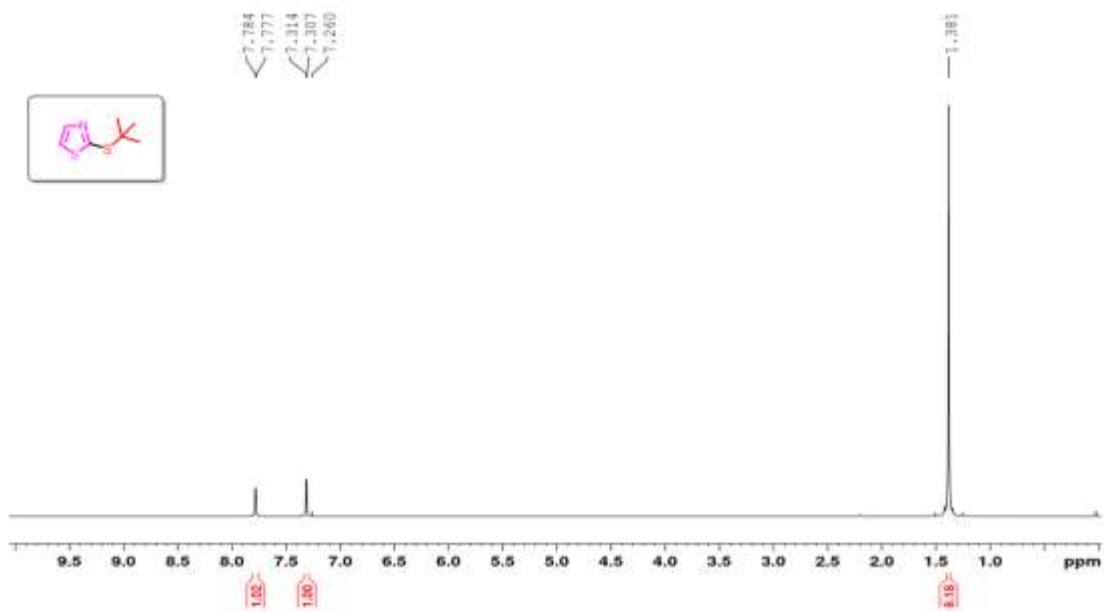


Figure 3.77. ^1H NMR spectrum of CD32.

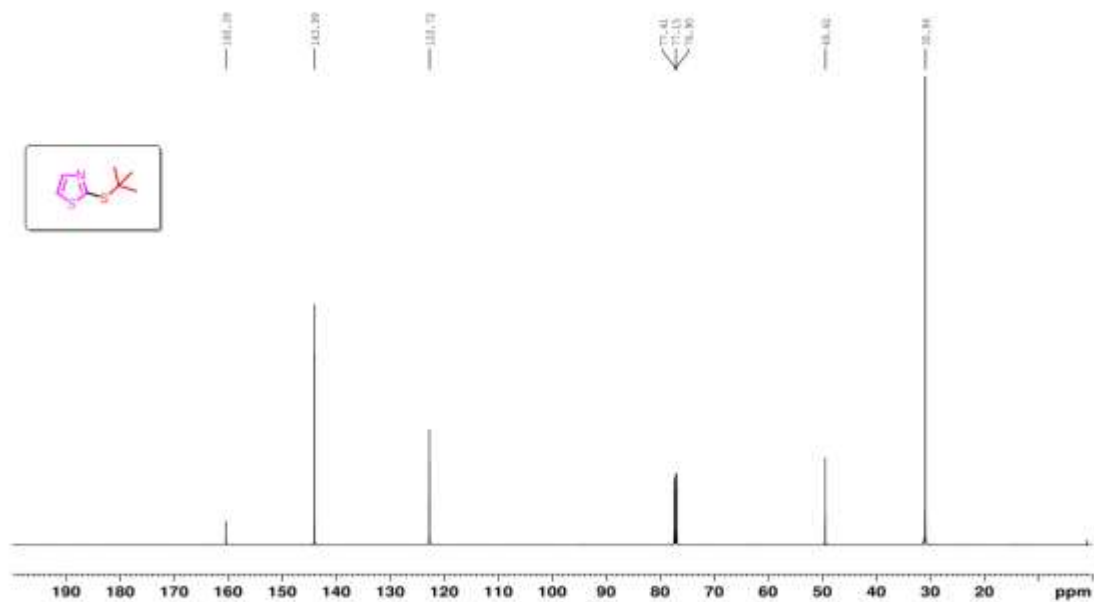


Figure 3.78. ^{13}C NMR spectrum of CD32.

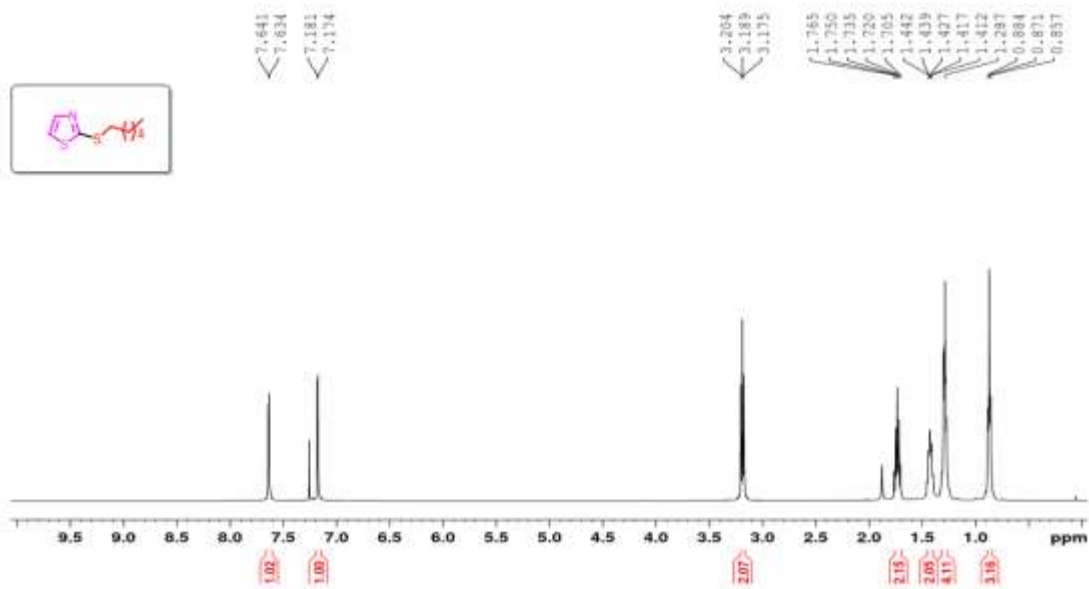


Figure 3.79. ^1H NMR spectrum of CD33.

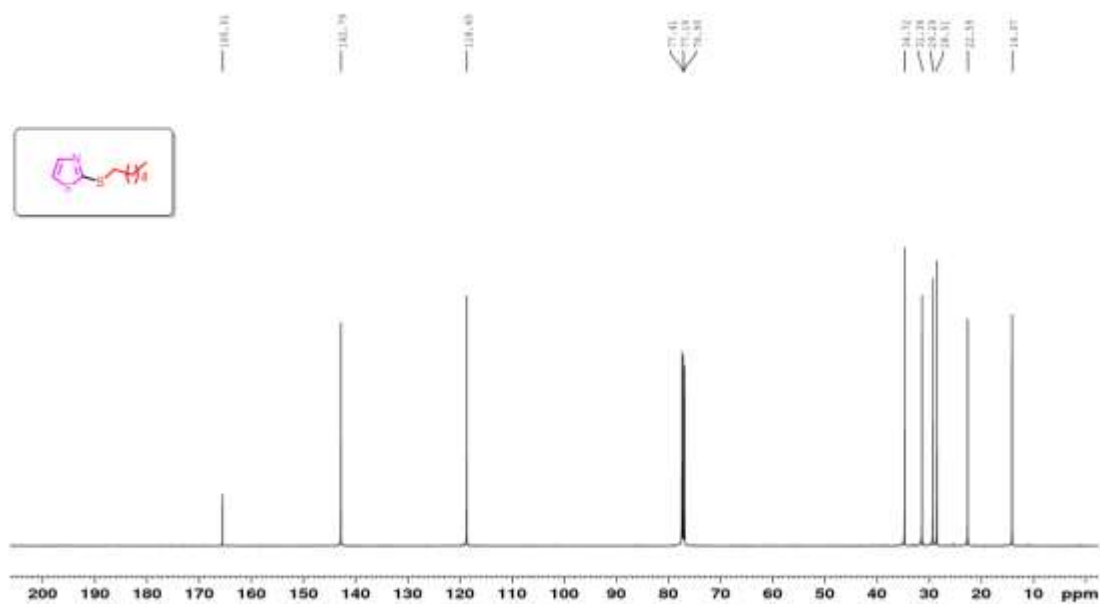


Figure 3.80. ^{13}C NMR spectrum of CD33.

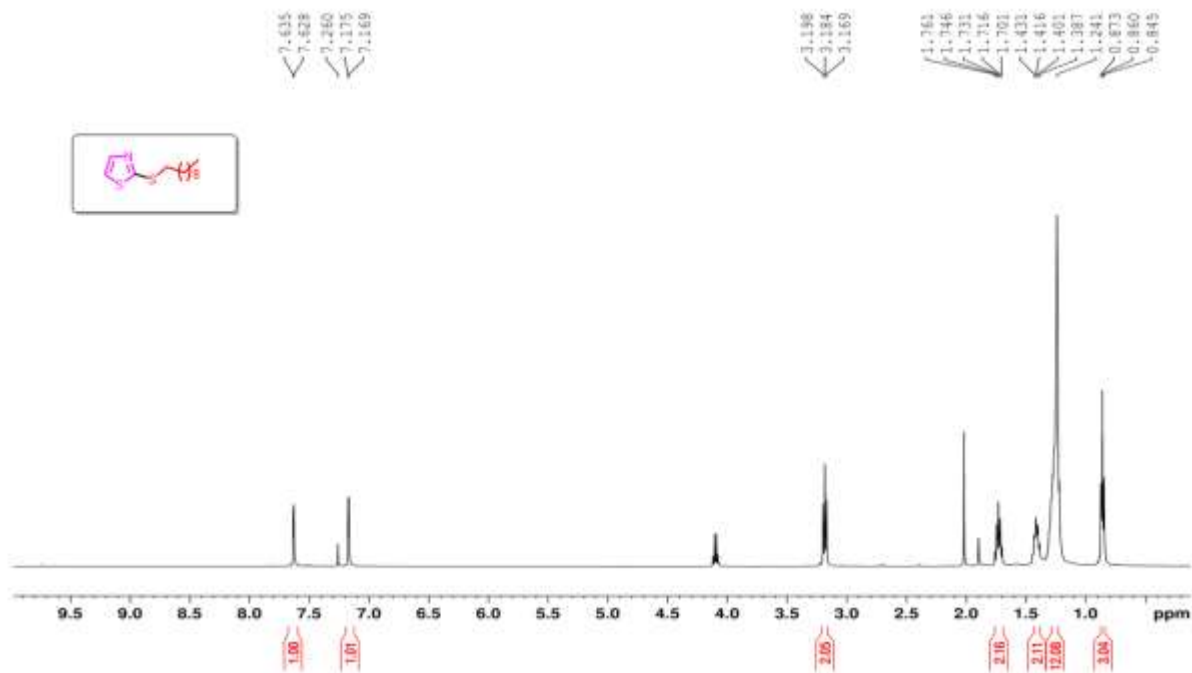


Figure 3.81. ¹H NMR spectrum of CD34.

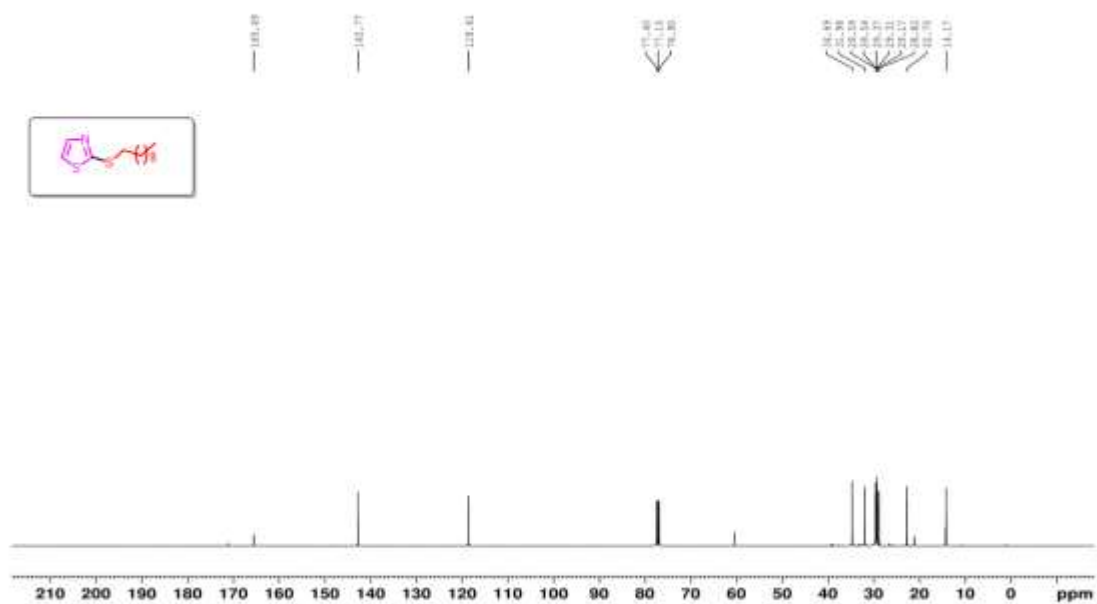


Figure 3.82. ¹³C NMR spectrum of CD34.

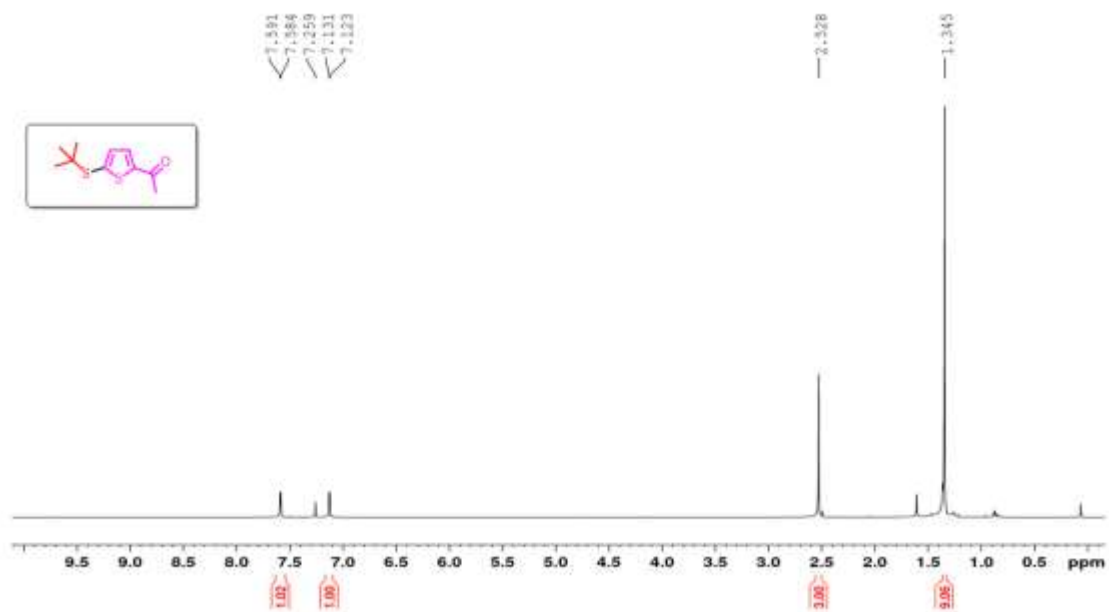


Figure 3.83. ^1H NMR spectrum of CD35.

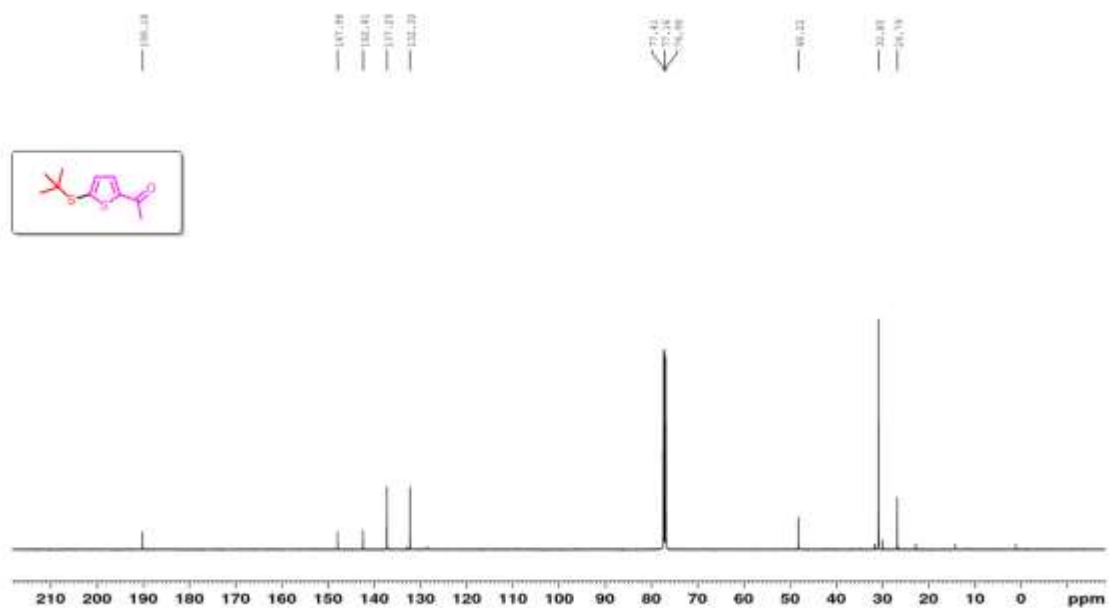


Figure 3.84. ^{13}C NMR spectrum of CD35.

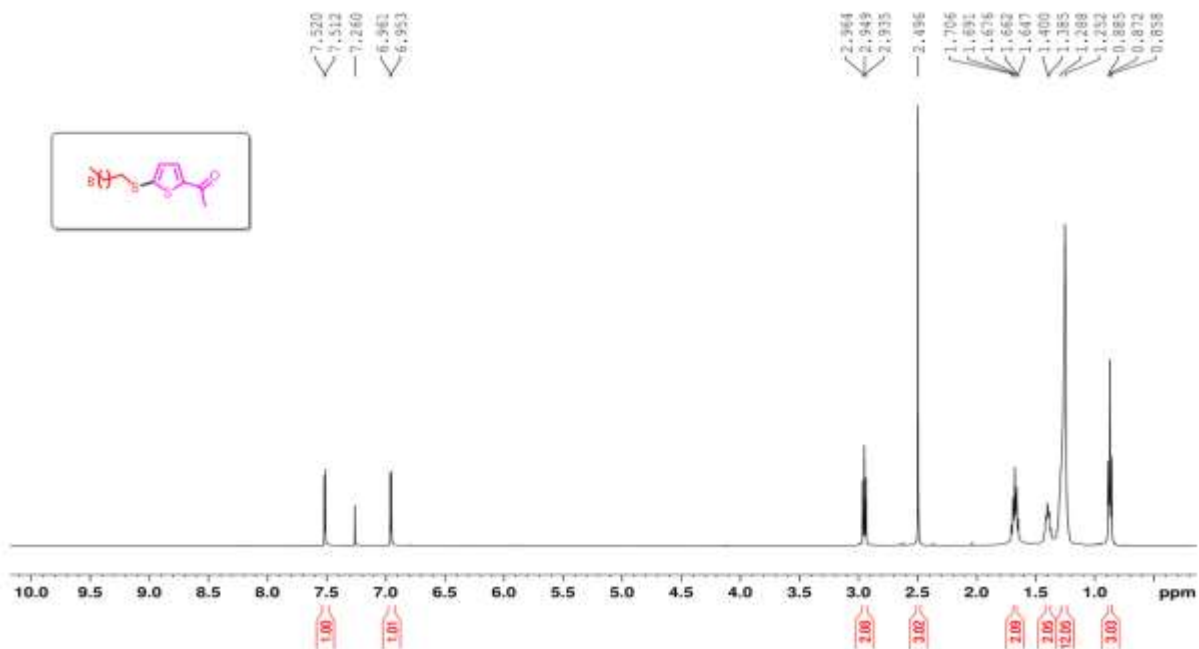


Figure 3.85. ¹H NMR spectrum of CD36.

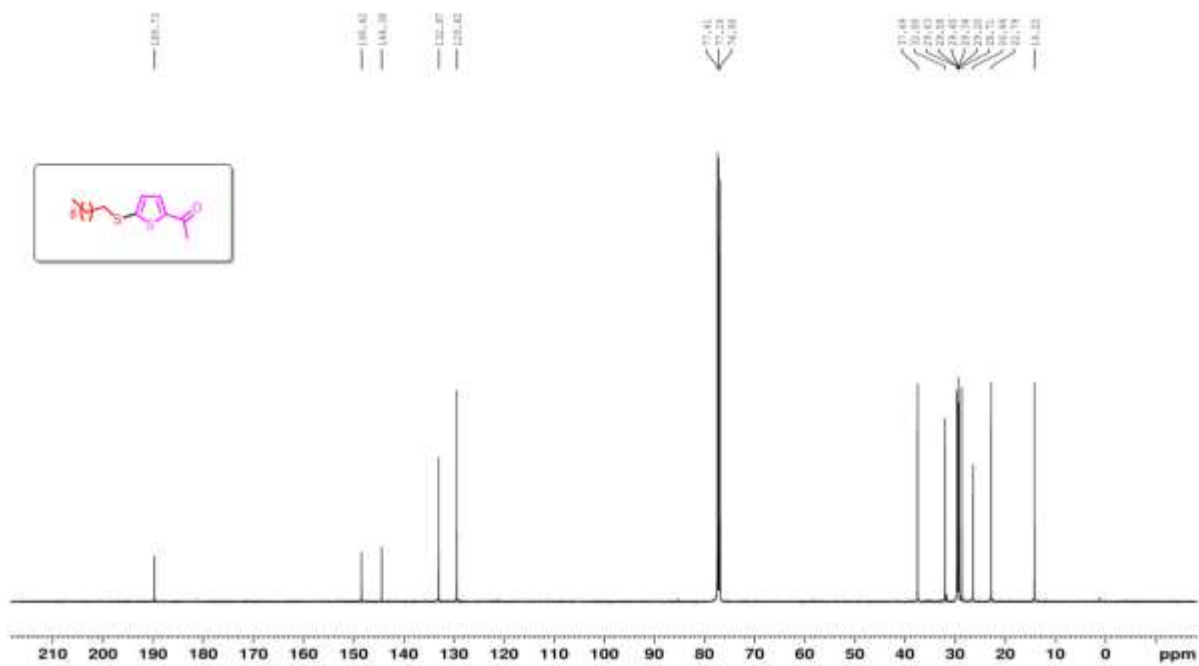


Figure 3.86. ¹³C NMR spectrum of CD36.

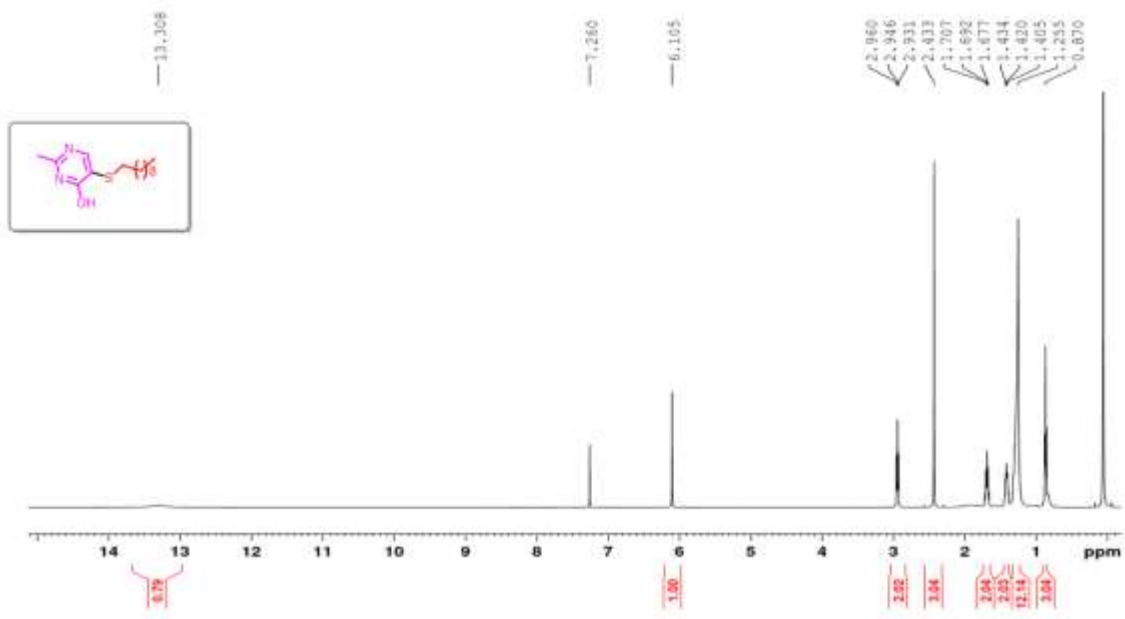


Figure 3.87. ^1H NMR spectrum of CD37.

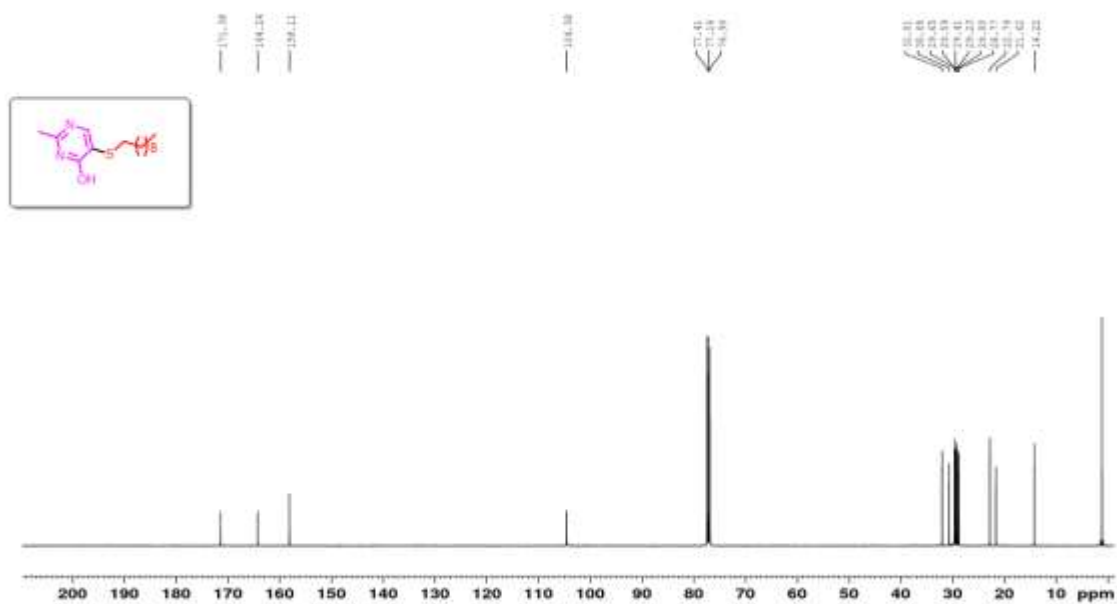


Figure 3.88. ^{13}C NMR spectrum of CD37.

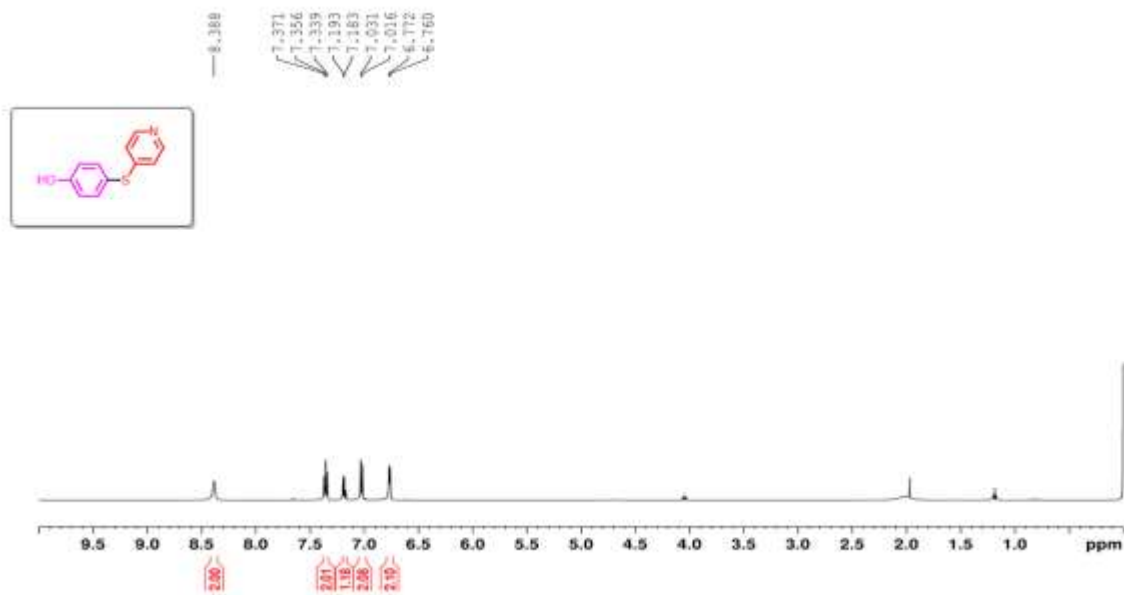


Figure 3.89. ^1H NMR spectrum of **CD38**.

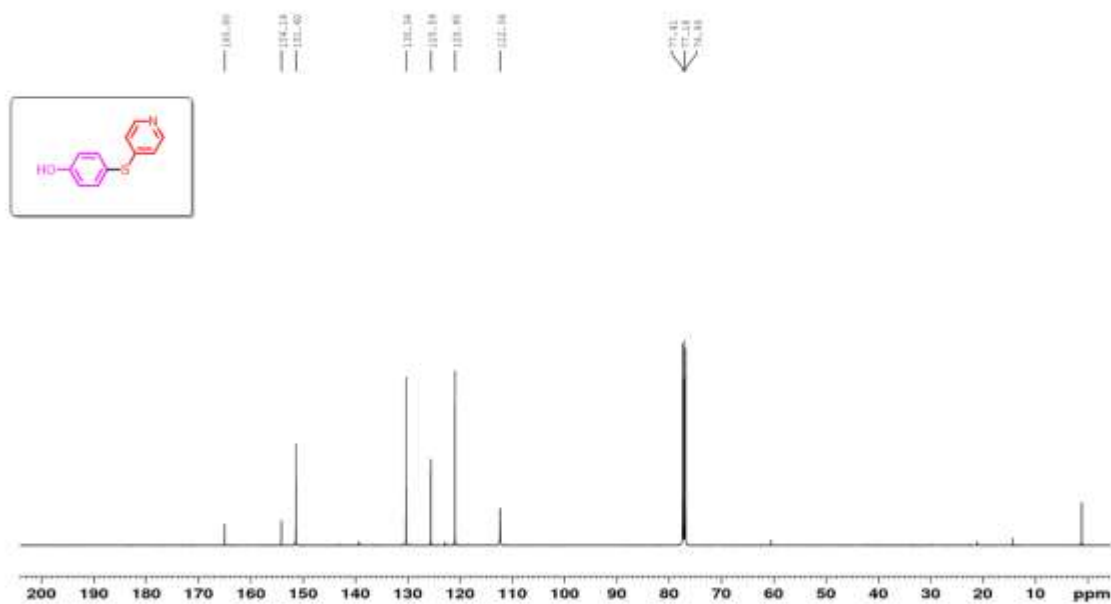


Figure 3.90. ^{13}C NMR spectrum of **CD38**.

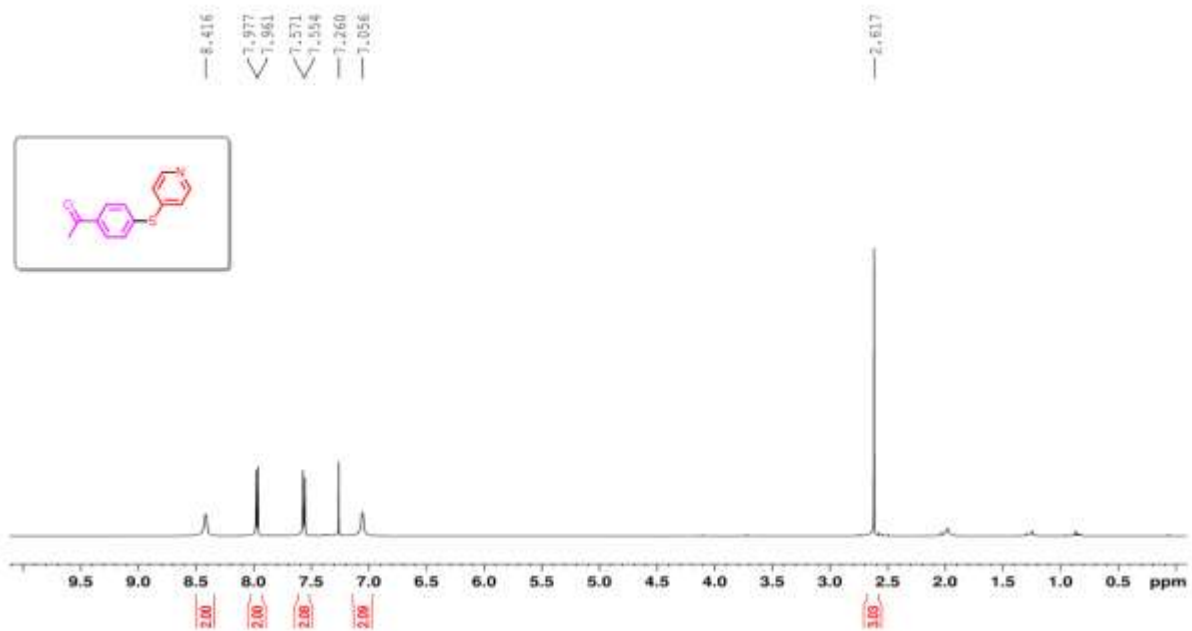


Figure 3.91. ^1H NMR spectrum of CD39.

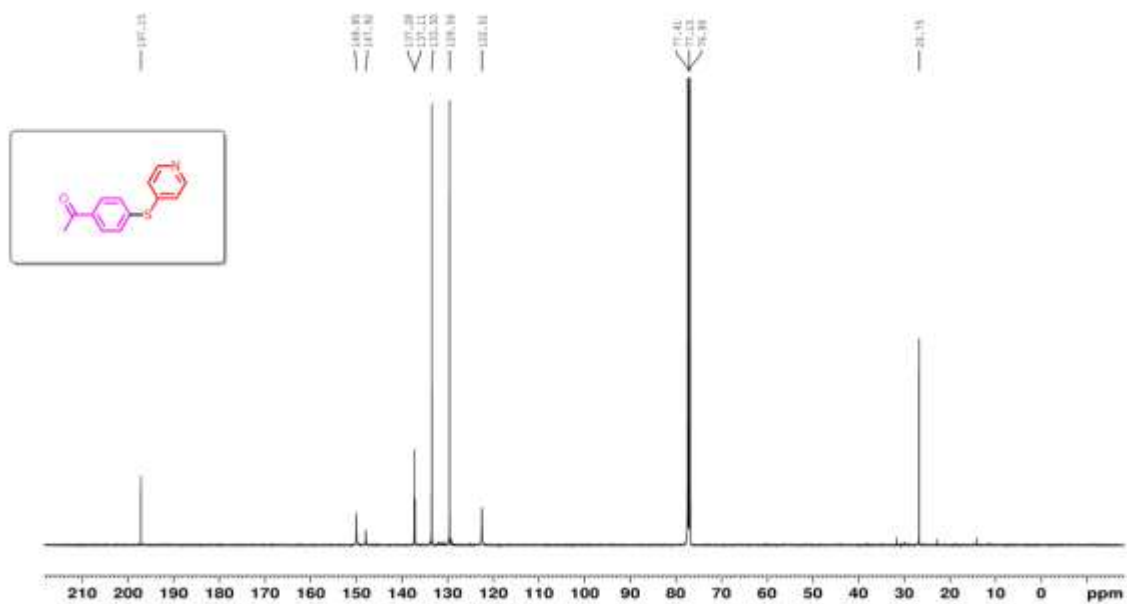


Figure 3.92. ^{13}C NMR spectrum of CD39.

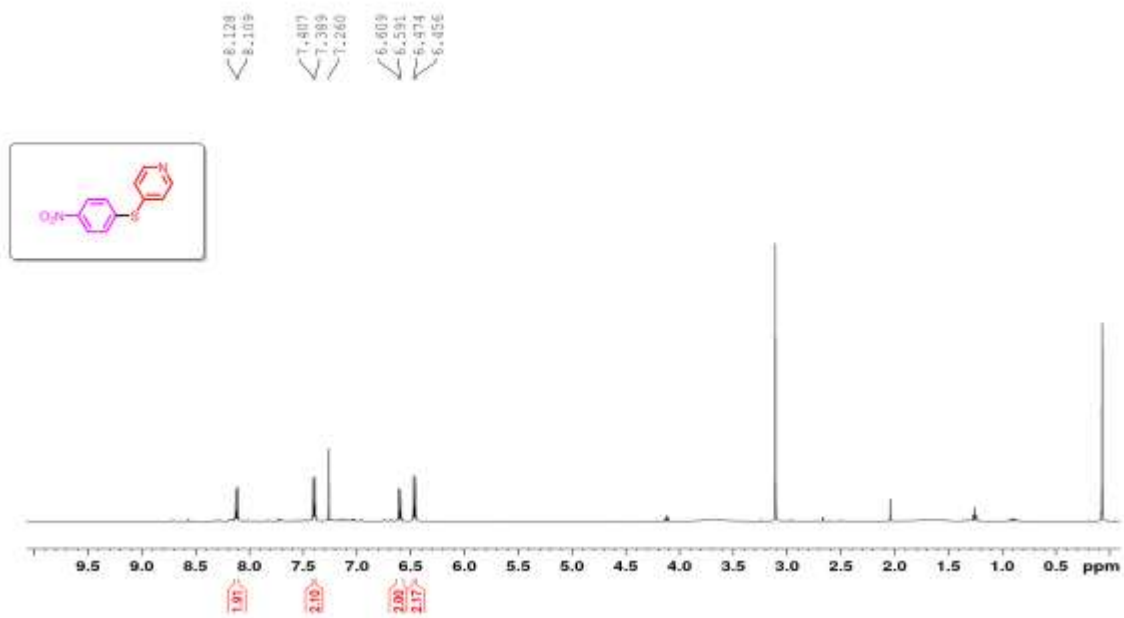


Figure 3.93. ^1H NMR spectrum of CD40.

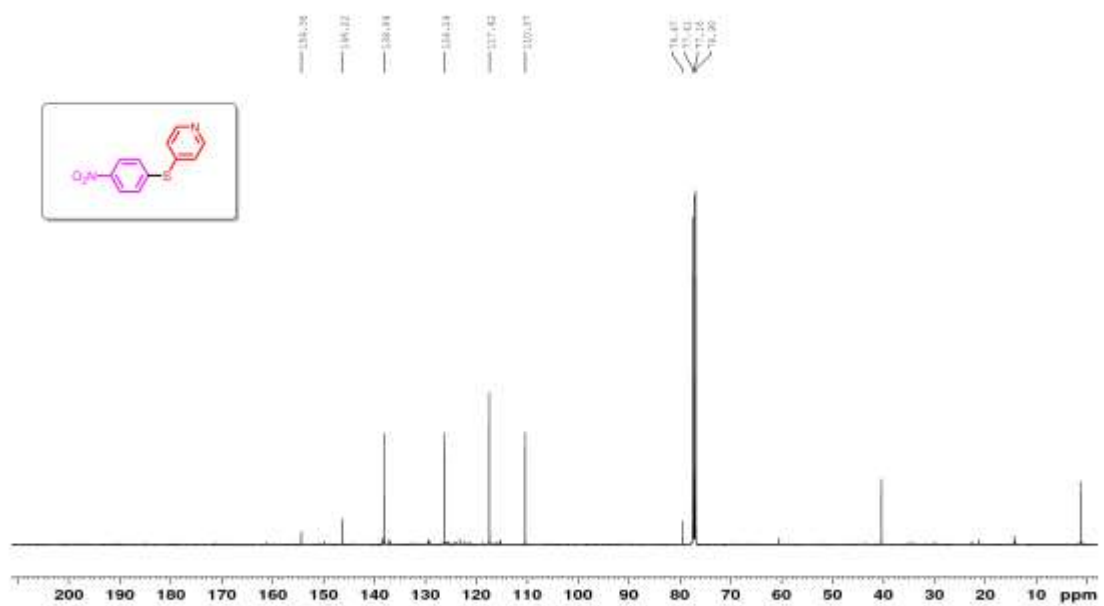


Figure 3.94. ^{13}C NMR spectrum of CD40.

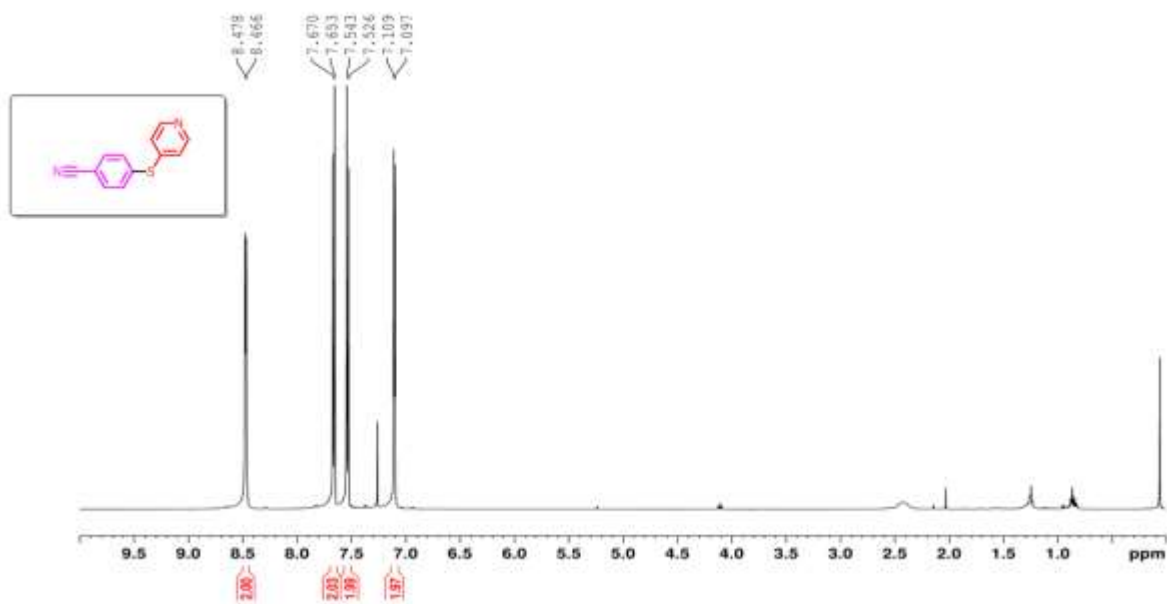


Figure 3.95. ^1H NMR spectrum of CD41.

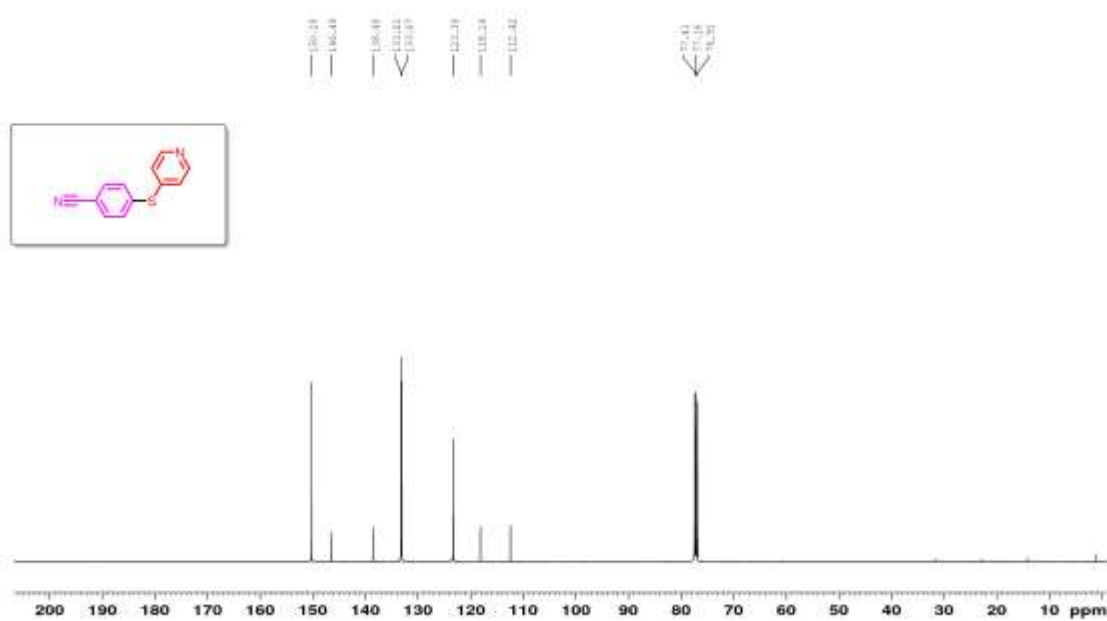


Figure 3.96. ^{13}C NMR spectrum of CD41.

3.8 References

- (1) Hartwig, J. F. Carbon–Heteroatom Bond-Forming Reductive Eliminations of Amines, Ethers, and Sulfides. *Acc. Chem. Res.* **1998**, *31*, 852-860.
- (2) Hartwig, J. F. Carbon–heteroatom bond formation catalysed by organometallic complexes. *Nature* **2008**, *455*, 314-322.
- (3) Jiang, M.; Li, H.; Yang, H.; Fu, H. Room-Temperature Arylation of Thiols: Breakthrough with Aryl Chlorides. *Angew. Chem., Int. Ed.* **2017**, *56*, 874-879.
- (4) Lee, C.-F.; Liu, Y.-C.; Badsara, S. S. Transition-Metal-Catalyzed C–S Bond Coupling Reaction. *Chem. - Asian J.* **2014**, *9*, 706-722.
- (5) Migita, T.; Shimizu, T.; Asami, Y.; Shiobara, J.-i.; Kato, Y.; Kosugi, M. The Palladium Catalyzed Nucleophilic Substitution of Aryl Halides by Thiolate Anions. *Bull. Chem. Soc. Jpn.* **1980**, *53*, 1385-1389.
- (6) Masanori, K.; Toshimi, O.; Masahiro, T.; Hiroshi, S.; Toshihiko, M. Palladium-catalyzed Reaction of Stannyl Sulfide with Aryl Bromide. Preparation of Aryl Sulfide. *Bull. Chem. Soc. Jpn.* **1985**, *58*, 3657-3658.
- (7) Alvaro, E.; Hartwig, J. F. Resting State and Elementary Steps of the Coupling of Aryl Halides with Thiols Catalyzed by Alkylbisphosphine Complexes of Palladium. *J. Am. Chem. Soc.* **2009**, *131*, 7858-7868.
- (8) Scattolin, T.; Senol, E.; Yin, G.; Guo, Q.; Schoenebeck, F. Site-Selective C–S Bond Formation at C–Br over C–OTf and C–Cl Enabled by an Air-Stable, Easily Recoverable, and Recyclable Palladium(I) Catalyst. *Angew. Chem., Int. Ed.* **2018**, *57*, 12425-12429.
- (9) Hartwig, J. F. Evolution of a Fourth Generation Catalyst for the Amination and Thioetherification of Aryl Halides. *Acc. Chem. Res.* **2008**, *41*, 1534-1544.
- (10) Mann, G.; Baranano, D.; Hartwig, J. F.; Rheingold, A. L.; Guzei, I. A. Carbon–Sulfur Bond-Forming Reductive Elimination Involving sp-, sp²-, and sp³-Hybridized Carbon. Mechanism, Steric Effects, and Electronic Effects on Sulfide Formation. *J. Am. Chem. Soc.* **1998**, *120*, 9205-9219.
- (11) Fernández-Rodríguez, M. A.; Shen, Q.; Hartwig, J. F. A General and Long-Lived Catalyst for the Palladium-Catalyzed Coupling of Aryl Halides with Thiols. *J. Am. Chem. Soc.* **2006**, *128*, 2180-2181.

- (12) Fernández-Rodríguez, M. A.; Shen, Q.; Hartwig, J. F. Highly Efficient and Functional-Group-Tolerant Catalysts for the Palladium-Catalyzed Coupling of Aryl Chlorides with Thiols. *Chem. - Eur. J.* **2006**, *12*, 7782-7796.
- (13) Valente, C.; Pompeo, M.; Sayah, M.; Organ, M. G. Carbon-Heteroatom Coupling Using Pd-PEPSI Complexes. *Org. Process Res. Dev.* **2014**, *18*, 180-190.
- (14) Xu, J.; Liu, R. Y.; Yeung, C. S.; Buchwald, S. L. Monophosphine Ligands Promote Pd-Catalyzed C-S Cross-Coupling Reactions at Room Temperature with Soluble Bases. *ACS Catal.* **2019**, *9*, 6461-6466.
- (15) Bastug, G.; Nolan, S. P. Carbon-Sulfur Bond Formation Catalyzed by [Pd(IPr*OMe)(cin)Cl] (cin = cinnamyl). *J. Org. Chem.* **2013**, *78*, 9303-9308.
- (16) Fernández-Rodríguez, M. A.; Hartwig, J. F. A General, Efficient, and Functional-Group-Tolerant Catalyst System for the Palladium-Catalyzed Thioetherification of Aryl Bromides and Iodides. *J. Org. Chem.* **2009**, *74*, 1663-1672.
- (17) Mohammadinezhad, A.; Akhlaghinia, B. CoII immobilized on an aminated magnetic metal-organic framework catalyzed C-N and C-S bond forming reactions: a journey for the mild and efficient synthesis of arylamines and arylsulfides. *New J. Chem.* **2019**, *43*, 15525-15538.
- (18) Wang, Y.; Deng, L.; Wang, X.; Wu, Z.; Wang, Y.; Pan, Y. Electrochemically Promoted Nickel-Catalyzed Carbon-Sulfur Bond Formation. *ACS Catal.* **2019**, *9*, 1630-1634.
- (19) Venkanna, G. T.; Arman, H. D.; Tonzetich, Z. J. Catalytic C-S Cross-Coupling Reactions Employing Ni Complexes of Pyrrole-Based Pincer Ligands. *ACS Catal.* **2014**, *4*, 2941-2950.
- (20) Gehrtz, P. H.; Geiger, V.; Schmidt, T.; Sršan, L.; Fleischer, I. Cross-Coupling of Chloro(hetero)arenes with Thiolates Employing a Ni(0)-Precatalyst. *Org. Lett.* **2019**, *21*, 50-55.
- (21) Zhang, J.; Medley, C. M.; Krause, J. A.; Guan, H. Mechanistic Insights into C-S Cross-Coupling Reactions Catalyzed by Nickel Bis(phosphinite) Pincer Complexes. *Organometallics* **2010**, *29*, 6393-6401.
- (22) Sikari, R.; Sinha, S.; Das, S.; Saha, A.; Chakraborty, G.; Mondal, R.; Paul, N. D. Achieving Nickel Catalyzed C-S Cross-Coupling under Mild Conditions Using Metal-Ligand Cooperativity. *J. Org. Chem.* **2019**, *84*, 4072-4085.
- (23) Jones, K. D.; Power, D. J.; Bierer, D.; Gericke, K. M.; Stewart, S. G. Nickel Phosphite/Phosphine-Catalyzed C-S Cross-Coupling of Aryl Chlorides and Thiols. *Org. Lett.* **2018**, *20*, 208-211.

- (24) Xu, X.-B.; Liu, J.; Zhang, J.-J.; Wang, Y.-W.; Peng, Y. Nickel-Mediated Inter- and Intramolecular C–S Coupling of Thiols and Thioacetates with Aryl Iodides at Room Temperature. *Org. Lett.* **2013**, *15*, 550-553.
- (25) Oderinde, M. S.; Frenette, M.; Robbins, D. W.; Aquila, B.; Johannes, J. W. Photoredox Mediated Nickel Catalyzed Cross-Coupling of Thiols With Aryl and Heteroaryl Iodides via Thiyl Radicals. *J. Am. Chem. Soc.* **2016**, *138*, 1760-1763.
- (26) Kabir, M. S.; Lorenz, M.; Van Linn, M. L.; Namjoshi, O. A.; Ara, S.; Cook, J. M. A Very Active Cu-Catalytic System for the Synthesis of Aryl, Heteroaryl, and Vinyl Sulfides. *J. Org. Chem.* **2010**, *75*, 3626-3643.
- (27) Panova, Y. S.; Kashin, A. S.; Vorobev, M. G.; Degtyareva, E. S.; Ananikov, V. P. Nature of the Copper-Oxide-Mediated C–S Cross-Coupling Reaction: Leaching of Catalytically Active Species from the Metal Oxide Surface. *ACS Catal.* **2016**, *6*, 3637-3643.
- (28) Uyeda, C.; Tan, Y.; Fu, G. C.; Peters, J. C. A New Family of Nucleophiles for Photoinduced, Copper-Catalyzed Cross-Couplings via Single-Electron Transfer: Reactions of Thiols with Aryl Halides Under Mild Conditions (0 °C). *J. Am. Chem. Soc.* **2013**, *135*, 9548-9552.
- (29) Timpa, S. D.; Pell, C. J.; Ozerov, O. V. A Well-Defined (POCOP)Rh Catalyst for the Coupling of Aryl Halides with Thiols. *J. Am. Chem. Soc.* **2014**, *136*, 14772-14779.
- (30) Reddy, V. P.; Swapna, K.; Kumar, A. V.; Rao, K. R. Indium-Catalyzed C–S Cross-Coupling of Aryl Halides with Thiols. *J. Org. Chem.* **2009**, *74*, 3189-3191.
- (31) Guo, F.-J.; Sun, J.; Xu, Z.-Q.; Kühn, F. E.; Zang, S.-L.; Zhou, M.-D. C-S cross-coupling of aryl halides with alkyl thiols catalyzed by in-situ generated nickel(II) N-heterocyclic carbene complexes. *Catal. Commun.* **2017**, *96*, 11-14.
- (32) Lan, M.-T.; Wu, W.-Y.; Huang, S.-H.; Luo, K.-L.; Tsai, F.-Y. Reusable and efficient CoCl₂·6H₂O/cationic 2,2'-bipyridyl system-catalyzed S-arylation of aryl halides with thiols in water under air. *RSC Adv.* **2011**, *1*, 1751-1755.
- (33) Liu, Y.; Huang, B.; Cao, X.; Wu, D.; Wan, J.-P. Synthesis of heteroaryl containing sulfides via enaminone ligand assisted, copper-catalyzed C–S coupling reactions of heteroaryl thiols and aryl halides. *RSC Adv.* **2014**, *4*, 37733-37737.
- (34) Talukder, M. M.; Cue, J. M. O.; Miller, J. T.; Gamage, P. L.; Aslam, A.; McCandless, G. T.; Biewer, M. C.; Stefan, M. C. Ligand Steric Effects of α -Diimine Nickel(II) and Palladium(II) Complexes in the Suzuki–Miyaura Cross-Coupling Reaction. *ACS Omega* **2020**, *5*, 24018-24032.

- (35) Gates, D. P.; Svejda, S. A.; Oñate, E.; Killian, C. M.; Johnson, L. K.; White, P. S.; Brookhart, M. Synthesis of Branched Polyethylene Using (α -Diimine)nickel(II) Catalysts: Influence of Temperature, Ethylene Pressure, and Ligand Structure on Polymer Properties. *Macromolecules* **2000**, *33*, 2320-2334.
- (36) Rhinehart, J. L.; Brown, L. A.; Long, B. K. A Robust Ni(II) α -Diimine Catalyst for High Temperature Ethylene Polymerization. *J. Am. Chem. Soc.* **2013**, *135*, 16316-16319.
- (37) Zhong, L.; Li, G.; Liang, G.; Gao, H.; Wu, Q. Enhancing Thermal Stability and Living Fashion in α -Diimine–Nickel-Catalyzed (Co)polymerization of Ethylene and Polar Monomer by Increasing the Steric Bulk of Ligand Backbone. *Macromolecules* **2017**, *50*, 2675-2682.
- (38) Popeney, C.; Guan, Z. Ligand Electronic Effects on Late Transition Metal Polymerization Catalysts. *Organometallics* **2005**, *24*, 1145-1155.
- (39) Falivene, L.; Credendino, R.; Poater, A.; Petta, A.; Serra, L.; Oliva, R.; Scarano, V.; Cavallo, L. SambVca 2. A Web Tool for Analyzing Catalytic Pockets with Topographic Steric Maps. *Organometallics* **2016**, *35*, 2286-2293.
- (40) Falivene, L.; Cao, Z.; Petta, A.; Serra, L.; Poater, A.; Oliva, R.; Scarano, V.; Cavallo, L. Towards the online computer-aided design of catalytic pockets. *Nat. Chem.* **2019**, *11*, 872-879.
- (41) Marcone, J. E.; Moloy, K. G. Kinetic Study of Reductive Elimination from the Complexes (Diphosphine)Pd(R)(CN). *J. Am. Chem. Soc.* **1998**, *120*, 8527-8528.
- (42) Crumpton-Bregel, D. M.; Goldberg, K. I. Mechanisms of C–C and C–H Alkane Reductive Eliminations from Octahedral Pt(IV): Reaction via Five-Coordinate Intermediates or Direct Elimination? *J. Am. Chem. Soc.* **2003**, *125*, 9442-9456.
- (43) Gallardo, I.; Guirado, G.; Marquet, J. Electrochemical Synthesis of Alkyl Nitroaromatic Compounds. *J. Org. Chem.* **2003**, *68*, 631-633.
- (44) Yang, C.; Williams, J. M. Palladium-Catalyzed Cyanation of Aryl Bromides Promoted by Low-Level Organotin Compounds. *Org. Lett.* **2004**, *6*, 2837-2840.
- (45) Shi, Y.; Guo, H.; Qin, M.; Wang, Y.; Zhao, J.; Sun, H.; Wang, H.; Wang, Y.; Zhou, X.; Facchetti, A.; Lu, X.; Zhou, M.; Guo, X. Imide-Functionalized Thiazole-Based Polymer Semiconductors: Synthesis, Structure–Property Correlations, Charge Carrier Polarity, and Thin-Film Transistor Performance. *Chem. Mater.* **2018**, *30*, 7988-8001.

- (46) McCulloch, B.; Ho, V.; Hoarfrost, M.; Stanley, C.; Do, C.; Heller, W. T.; Segalman, R. A. Polymer Chain Shape of Poly(3-alkylthiophenes) in Solution Using Small-Angle Neutron Scattering. *Macromolecules* **2013**, *46*, 1899-1907.
- (47) Cui, C.; Wong, W.-Y.; Li, Y. Improvement of open-circuit voltage and photovoltaic properties of 2D-conjugated polymers by alkylthio substitution. *Energy Environ. Sci.* **2014**, *7*, 2276-2284.
- (48) Sheldrick, G. M. SHELXT-Integrated Space-Group and Crystalstructure Determination. *Acta Crystallogr., Sect. A: Found. Adv.* **2015**, *71*, 3-8.
- (49) Sheldrick, G. M. Crystal Structure Refinement with SHELXL. *Acta Crystallogr., Sect. C: Struct. Chem.* **2015**, *71*, 3-8.
- (50) Sreenath, K.; Yuan, Z.; Macias-Contreras, M.; Ramachandran, V.; Clark, R. J.; Zhu, L. Dual Role of Acetate in Copper(II) Acetate Catalyzed Dehydrogenation of Chelating Aromatic Secondary Amines: A Kinetic Case Study of Copper-Catalyzed Oxidation Reactions. *Eur. J. Inorg. Chem.* **2016**, *2016*, 3728-3743.
- (51) Song, G.; Guo, L.; Du, Q.; Kong, W.; Li, W.; Liu, Z. Highly active mono and bis-ligated iminopyridyl nickel catalysts for 1-hexene reactions. *J. Organomet. Chem.* **2018**, *858*, 1-7.
- (52) Sorribes, I.; Corma, A. Nanolayered cobalt–molybdenum sulphides (Co–Mo–S) catalyse borrowing hydrogen C–S bond formation reactions of thiols or H₂S with alcohols. *Chem. Sci.* **2019**, *10*, 3130-3142.
- (53) Ren, X.; Tang, S.; Li, L.; Li, J.; Liang, H.; Li, G.; Yang, G.; Li, H.; Yuan, B. Surfactant-Type Catalyst for Aerobic Oxidative Coupling of Hydrazine with Thiol in Water. *J. Org. Chem.* **2019**, *84*, 8683-8690.
- (54) Vantourout, J. C.; Miras, H. N.; Isidro-Llobet, A.; Sproules, S.; Watson, A. J. B. Spectroscopic Studies of the Chan–Lam Amination: A Mechanism-Inspired Solution to Boronic Ester Reactivity. *J. Am. Chem. Soc.* **2017**, *139*, 4769-4779.
- (55) Ko, J.; Ham, J.; Yang, I.; Chin, J.; Nam, S.-J.; Kang, H. A simple one-pot synthesis of hydroxylated and carboxylated aryl alkyl sulfides from various bromobenzenes. *Tetrahedron Lett.* **2006**, *47*, 7101-7106.
- (56) Wang, L.; Zhou, W.-Y.; Chen, S.-C.; He, M.-Y.; Chen, Q. A Highly Efficient Palladium-Catalyzed One-Pot Synthesis of Unsymmetrical Aryl Alkyl Thioethers under Mild Conditions in Water. *Adv. Synth. Catal.* **2012**, *354*, 839-845.
- (57) Gholinejad, M. One-Pot Copper-Catalysed Thioetherification of Aryl Halides Using Alcohols and Lawesson's Reagent in Diglyme. *Eur. J. Org. Chem.* **2015**, *2015*, 4162-4167.

- (58) Zhao, J.-N.; Kayumov, M.; Wang, D.-Y.; Zhang, A. Transition-Metal-Free Aryl–Heteroatom Bond Formation via C–S Bond Cleavage. *Org. Lett.* **2019**, *21*, 7303-7306.
- (59) Jouffroy, M.; Kelly, C. B.; Molander, G. A. Thioetherification via Photoredox/Nickel Dual Catalysis. *Org. Lett.* **2016**, *18*, 876-879.
- (60) Di Maria, F.; Olivelli, P.; Gazzano, M.; Zanelli, A.; Biasiucci, M.; Gigli, G.; Gentili, D.; D'Angelo, P.; Cavallini, M.; Barbarella, G. A Successful Chemical Strategy To Induce Oligothiophene Self-Assembly into Fibers with Tunable Shape and Function. *J. Am. Chem. Soc.* **2011**, *133*, 8654-8661.
- (61) Oyaizu, K.; Iwasaki, T.; Tsukahara, Y.; Tsuchida, E. Linear Ladder-Type π -Conjugated Polymers Composed of Fused Thiophene Ring Systems. *Macromolecules* **2004**, *37*, 1257-1270.
- (62) Yonekura, K.; Yoshimura, Y.; Akehi, M.; Tsuchimoto, T. A Heteroarylamine Library: Indium-Catalyzed Nucleophilic Aromatic Substitution of Alkoxyheteroarenes with Amines. *Adv. Synth. Catal.* **2018**, *360*, 1159-1181.
- (63) Liu, B.; Lim, C.-H.; Miyake, G. M. Visible-Light-Promoted C–S Cross-Coupling via Intermolecular Charge Transfer. *Journal of the American Chemical Society* **2017**, *139*, 13616-13619.
- (64) Moser, D.; Duan, Y.; Wang, F.; Ma, Y.; O'Neill, M. J.; Cornella, J. Selective Functionalization of Aminoheterocycles by a Pyrylium Salt. *Angew. Chem., Int. Ed.* **2018**, *57*, 11035-11039.

CHAPTER 4

IMINOPYRIDINE-BASED α -DIIMINE NICKEL(II) AND PALLADIUM(II)

COMPLEXES IN DIRECT C-H BOND ARYLATION OF FIVE-MEMBERED

HETEROAROMATICS

Authors: Md Muktadir Talukder, Justin T. Miller, John Michael O. Cue, Chinthaka M Udamulle,
Michael C. Biewer, and Mihaela C. Stefan*

The Department of Chemistry and Biochemistry, BE26

The University of Texas at Dallas

800 West Campbell Road

Richardson, Texas 75080-3021

Manuscript titled "Iminopyridine-Based α -Diimine Nickel (II) and Palladium (II) Complexes in Direct C-H Bond Arylation of Five-Membered Heteroaromatics" in preparation.

4.1 Abstract

Transition metal-catalyzed direct C-H bond arylation has been studied for synthesizing structurally diverse and valuable functionalized (hetero)aryl building blocks. Nonetheless, air- and moisture sensitivity along with harsh reaction settings significantly reduce the efficacy of this atom economical and cost-effective synthetic tool. Herein, we have developed highly air- and moisture stable iminopyridine-based α -diimine Nickel (II) and Palladium (II) complexes in direct C-H bond arylation of thiazole and thiophene derivatives. Steric features of the synthesized complexes were investigated for evaluating the catalytic performance. Under aerobic conditions and lower temperatures, both Ni and Pd catalytic systems manifested broader substrate scope and functional group tolerance. Particularly, a series of biheteroaryl and π -conjugated poly(hetero)arenes were synthesized from different five-membered heteroaromatics including 3,4-ethylenedioxythiophene (EDOT). Moreover, catalytic systems afforded good to excellent yields having low catalyst loading (0.1-0.4 mol%). Consequently, α -diimine-based systems have the potential to be employed in direct C-H arylation for producing valuable functional materials.

4.2 Introduction

Direct C-H bond arylation of heteroaromatics through transition metal catalytic systems has recently drawn notable recognition.¹⁻⁴ Compared to traditional Negishi, Suzuki, or Stille cross-coupling for making biaryl building blocks, direct arylation offers atom-economical and facile synthetic tools.³⁻⁶ Consequently, this synthetic tool has emerged as the most desirable method for synthesizing biaryl building blocks. Five-membered heteroaryl moieties containing biaryl building blocks are essential in organic field-effect transistors (OFETs),⁷ organic solar cells (OSC),⁸ and organic light-emitting diodes (OLEDs).⁹

Compared to other transition metal-catalyzed systems, palladium-based systems for direct C-H bond arylation have been extensively studied over the last decade.¹⁰⁻²⁸ However, the environmental and financial costs associated with the Pd-systems has led the researcher to explore more sustainable choices. In this aspect, Ni-based systems are gaining popularity.²⁹⁻³² Nonetheless, a major portion of Pd and Ni-catalyzed systems are air- and moisture sensitive.^{10, 16, 18, 29-31, 33} Moreover, both Pd and Ni-systems often require *in situ* catalyst generation from expensive precursors.^{16, 19, 30-33} Furthermore, these systems greatly suffer from high catalyst loading (5 – 10 mol%),^{10-11, 19, 29-31, 33} longer reaction time (12 – 36 h),^{10-13, 15-16, 27-29, 33} high temperature (100 – 150 °C),^{10, 12-17, 27-31, 33} and time-consuming synthesis of ligands.²

Transition metal catalysts containing *N*-heterocyclic carbene (NHC) ligands have been widely studied in direct arylation because of their tunable sterics and electron-rich environment. Particularly, the higher steric bulk is perceived to be advantageous in the catalytic performance.^{1-2, 25, 27-28} Transition metal catalysts based on α -diimine ligand frameworks have the potential to diversify the sterics for developing more efficient catalytic systems in direct arylation. Brookhart-type α -diimine transition metal catalysts have transformed the olefin polymerization field. High thermal stability, high air- and moisture stability, structural versatility, and facile synthesis have attracted researchers to employ this catalytic system in other fields.^{12-14, 34-36} Moreover, steric and electronic characteristics are highly adaptable by attaching different valuable groups in the ligand frameworks.^{34, 37-38} Inadequate research has been identified with the α -diimine-based Pd catalysts; however, there is no report with Ni-based systems in direct arylation.¹²⁻¹⁴

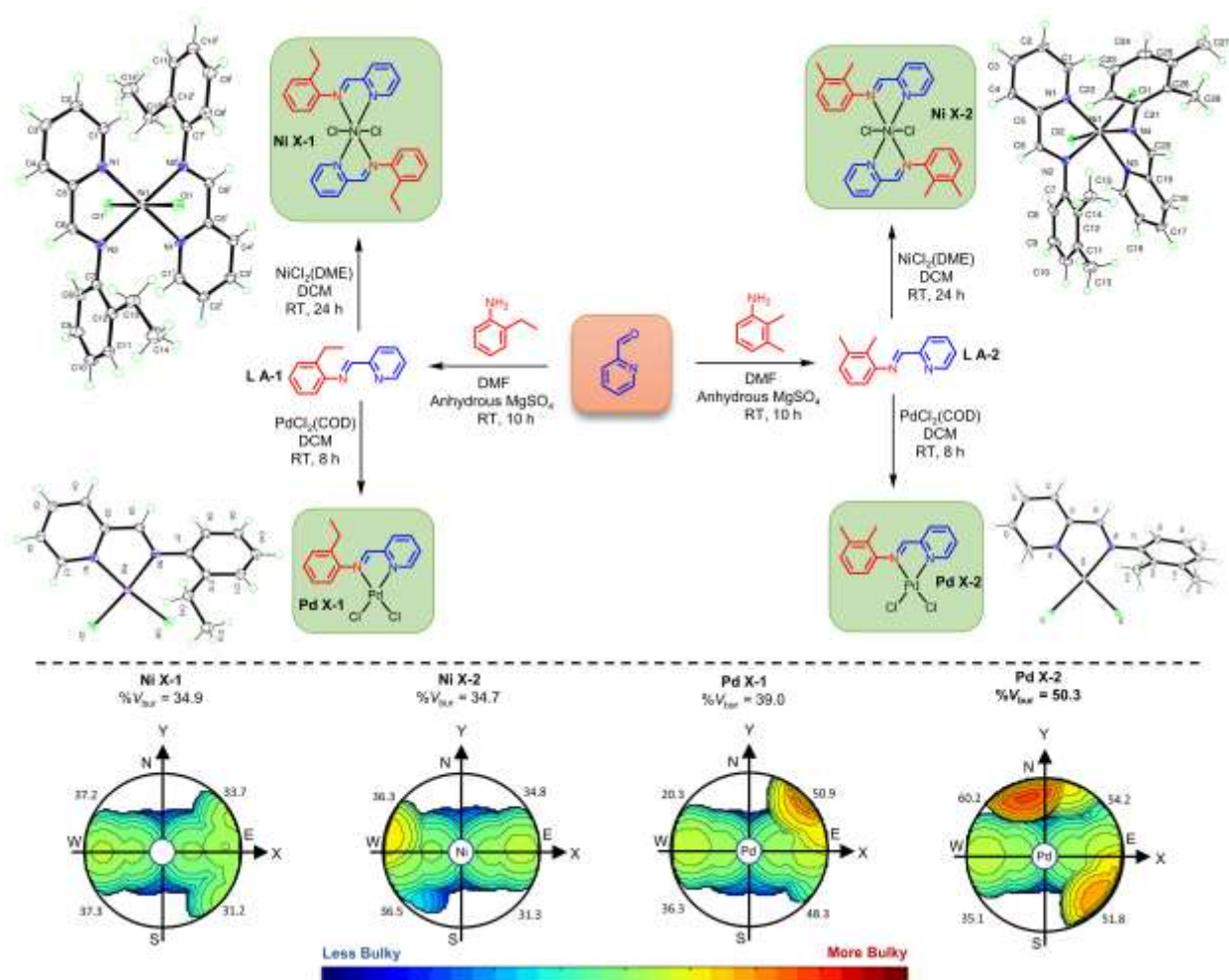
Herein, we report the first application of iminopyridine-based α -diimine Ni (II) and Pd (II) complexes in direct C-H bond arylation of five-membered heteroaromatics. The variation in the

sterics was analyzed and correlated with the reaction performance by synthesizing four Ni (II) and Pd (II) complexes from two iminopyridine ligands. For investigating the substrate scope, different five-membered rings, including thiazole and thiophene units, are applied for synthesizing biheteroaryl as well as π -conjugated poly(hetero)arenes with numerous aryl halides. Various reactive groups originating from both five-membered rings, and aryl halides are coupled for examining the functional group tolerance.

4.3 Results and Discussion

4.3.1 Synthesis and Characterization of α -Diimine Nickel (II) and Palladium (II) Complexes

Synthesis of the complexes and ORTEP diagrams are shown in Scheme 4.1. By adopting a previously published procedure, two ligands and four complexes were synthesized.³⁴ For this purpose, 2-pyridinecarboxaldehyde was reacted with 2-ethylaniline, and 2,3-dimethylaniline for synthesizing the ligands **LA-1** and **LA-2**, respectively. For the Ni (II) complexes, **Ni X-1** and **Ni X-2**, both ligands were reacted with one equivalent of NiCl₂(DME). Correspondingly, Pd (II) complexes, **Pd X-1** and **Pd X-2** were synthesized by reacting one equivalent of PdCl₂(COD) with the ligands. Both **Ni X-1** and **Ni X-2** exhibit a distorted octahedral geometry having two free chlorine atoms and four nitrogen atoms from two unit of ligands are directly coordinated with the nickel center. For **Ni X-2**, there is positionally disordered solvent that appears to be acetonitrile (which was used for crystallization). Meanwhile, a distorted square planar geometry is displayed for **Pd X-1** and **Pd X-2** with two nitrogen atoms directly coordinated with the Pd center possessing two free chlorine atoms. Crystal data collection, unit cell representations selected bond angles, and distances are provided in the supporting information.

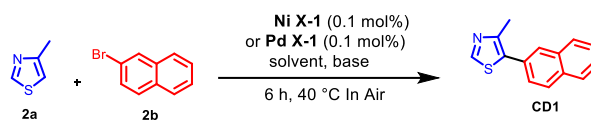


Scheme 4.1. Synthesis, ORTEP diagrams, percent buried volume, and topographic steric maps of the α -diimine Ni(II) and Pd(II) Complexes.

4.3.2 Optimization of Reaction Conditions in Direct C-H Bond Arylation

Ni X-1 and **Pd X-1** are applied for establishing the Ni- and Pd-based catalytic systems, respectively. For this purpose, the reaction of 4-methylthiazole (**2a**), and 2-bromonaphthalene (**2b**) was analyzed with 0.1 mol% of the complexes for obtaining the most suitable base, solvent, and acid combination (Table 4.1). In the first twelve experiments (Table 4.1, entry 1-12), we applied pivalic acid (PivOH) and altered the base and solvent for optimizing the conditions. **Ni X-1**

Table 4.1. Optimization of base, solvent, and acid^a



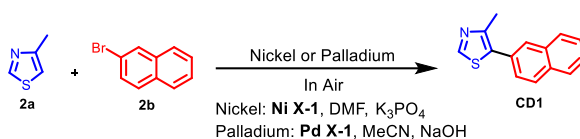
entry	base	solvent	acid	yield (%) ^b (Ni X-1 / Pd X-1)
1	K ₂ CO ₃	DMF	PivOH	51 / 39
2	K ₃ PO ₄	DMF	PivOH	68 / 55
3	NaOH	DMF	PivOH	43 / 51
4	K ₂ CO ₃	H ₂ O	PivOH	34 / 49
5	K ₃ PO ₄	H ₂ O	PivOH	40 / 46
6	NaOH	H ₂ O	PivOH	57 / 51
7	K ₂ CO ₃	MeCN	PivOH	58 / 51
8	K ₃ PO ₄	MeCN	PivOH	42 / 58
9	NaOH	MeCN	PivOH	19 / 76
10	K ₂ CO ₃	1,4-dioxane	PivOH	53 / 71
11	K ₃ PO ₄	1,4-dioxane	PivOH	47 / 43
12	NaOH	1,4-dioxane	PivOH	56 / 66
13	K ₃ PO ₄	DMF	PhCOOH	53 / 45
14	NaOH	MeCN	PhCOOH	48 / 37

^aReaction conditions: 4-methylthiazole (1.5 mmol), 2-acetyl-5-bromothiophene (1 mmol), base (1.5 mmol), 0.1 mol% of **Ni X-1** or **Pd X-1**, solvent (6 mL), PivOH (0.2 mmol) for 6 h at 40 °C. ^bIsolated yields from column chromatography.

afforded the best yields having K₃PO₄ and DMF (Table 4.1, entry 2). On the other hand, NaOH, and MeCN produced the highest yield for **Pd X-1** (Table 4.1, entry 9). Subsequently, additional two experiments were performed with benzoic acid; however, the yields for both catalytic systems did not improve.

Another set of experiments were carried out for screening the reaction time, temperature, and the catalyst loading (Table 4.2). Keeping the catalyst loading at 0.1 mol%, three experiments were conducted by altering the temperature from 60-100 °C for six hours (Table 4.2, entry 1-3). The yields for **Ni X-1** increased by raising the temperature from 40 to 80 °C; however, decreased

Table 4.2. Optimization of time, concentration of complex, and temperature^a



entry	time	com (mol%)	temp (°C)	yield (%) ^b (Ni X-1 / Pd X-1)
1	6	0.1	60	76 / 88
2	6	0.1	80	85 / 77
3	6	0.1	100	78 / -
5	6	0.2	60	- / 82
6	8	0.1	60	- / 96
7	10	0.1	60	- / 78
8	4	0.1	60	- / 71
9	6	0.2	80	91 / -
10	6	0.3	80	82 / -
11	8	0.2	80	78 / -
12	4	0.2	80	80 / -

^aReaction conditions: 4-methylthiazole (1.5 mmol), 2-acetyl-5-bromothiophene (1 mmol), base (1.5 mmol), **Ni X-1** or **Pd X-1**, solvent (6 mL), PivOH (0.2 mmol). ^bIsolated yields from column chromatography. Entry 5-8 for only **Pd X-1**; entry 9-12 for **Ni X-1** only.

at 100 °C (Table 4.2, entry 1-3). Meanwhile, **Pd X-1** experienced an increase in yield at 60 °C but decreased upon increasing the temperature at 80 °C (Table 4.2, entry 1 & 2). Increasing the catalyst loading to 0.2 mol%, the yield did not improve for **Pd X-1** (Table 4.2, entry 5). Moreover, the highest yield was recorded by increasing the reaction time to eight hours having 0.1 mol% of complex **Pd X-1** (Table 4.2, entry 6). Similar variations were performed for **Ni X-1**; however, the best yields were recorded by utilizing catalyst loading of 0.2 mol% for six hours at 80 °C (Table 4.2, entry 8).

4.3.3 Evaluation of catalytic performance

Arylated thiazoles are essential building blocks found in the biologically active natural products, drug molecules, agrochemicals, and novel optical materials.¹⁰⁻¹¹ We have synthesized seven compounds from the 4-methylthiazole unit by applying four complexes (Figure 4.1).

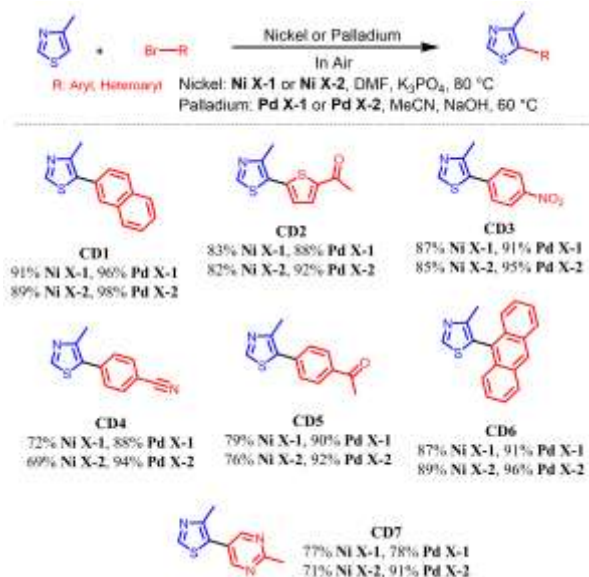


Figure 4.1. Evaluation of catalytic performance.

Different aryl and heteroaryl bromides including nitrile, acetyl, and nitro functionalities were introduced for making the diaryl compounds. **Pd X-2** afforded excellent yields (91-98%), whereas **Pd X-1** provided good yields (78-96%). In addition, both **Ni X-1** and **Ni X-2** presented similar but lower yields (69-91%). For instance, introducing a bulky naphthalene unit for making the compound CD1, all the complexes produced nearly excellent yields. However, introducing reactive functionalities such as acetyl, nitro, and nitrile, the yields for **Pd X-1**, and **Pd X-2** were better than the **Ni X-1**, and **Ni X-2** (Scheme 2, CD2-CD5). These observations are also noticeable in compound CD6 and CD7 containing a bulkier anthracene and heteroaryl rings, respectively.

Percent buried volume (%V_{Bur}) has gained popularity for analyzing the reaction outcomes.^{34,39-40} For investigating the differences in the catalytic performance, we have generated percent buried volume (%V_{Bur}) and topographic steric map of the synthesized α -diimine complexes from SambVca 2.1, a free web application designed by Falivene et al (Scheme 4.1).⁴⁰ **Pd X-2** exhibits the highest buried volume (%V_{Bur} = 50.3) among the complexes. **Pd X-1** provides improved buried volume than the remaining two Ni complexes, **Ni X-1** and **Ni X-2**. Additionally, both Pd complexes have a more desirable ligand bite angle than the Ni counterparts (Table 4.5 & 4.6). Consequently, in the seven synthesized compounds, Pd catalytic systems have generated nearly excellent yields compared to the Ni systems managing satisfactory yields. Higher steric bulk promotes catalytic performance in direct arylation.^{1-2, 25, 27-28} Moreover, a wider ligand bite angle is perceived to be advantageous in the transition metal-catalyzed C-C cross-coupling.^{34, 41} Accordingly, **Pd X-2**, with the highest buried volume, has outperformed the remaining complexes.

4.3.4 Expansion of Substrate Scope: Thiophene Derivatives

We decided to continue our efforts for the expansion of substrate scope. Based on the catalytic performance from Figure 4.1, we decided to apply **Ni X-1** and **Ni X-1** as Pd and Ni-catalyzed systems, respectively. In this purpose, different thiophene derivatives were applied for direct C-H bond arylation with various aryl and heteroaryl bromides (Figure 4.2). Aryl or heteroaryl thiophene building blocks have gained much recognition because of their unique physical or biological properties.⁴² Here, we have synthesized eight compounds carrying mono- or di-functionalities including acetyl, nitro, aldehyde, and nitrile groups. Notably, **Pd X-2** provided

much higher yields (89-97%) than the catalytic system containing **Ni X-1** (71-89%). For instance, bulky naphthalene units are incorporated with 2-substituted thiophene rings for making CD8 and

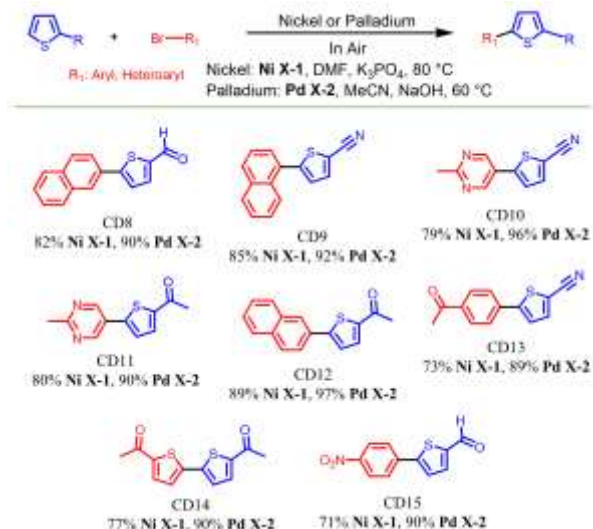


Figure 4.2. Expansion of substrate scope: thiophene derivatives.

CD9. In both compounds possessing reactive aldehyde or nitrile group did not reduce the catalytic performance of **Pd X-2** (90-92%), whereas the **Ni X-1** provided lower yields (82-85%). Biheteroaryls are another class of biaryl compounds that presents essential substructures in biologically active compounds.⁴³ Moreover, low reactivity and the poisoning of the transition metal species by heteroatoms remains a persistent challenge in direct arylation for the coupling of heteroarenes and heteroaryl halides.⁴⁴ In this interest to recognize the efficacy of our catalytic systems, we have employed 5-bromo-2-methylpyrimidine for synthesizing biheteroaryl compounds CD10 and CD11. Still, **Pd X-2** maintained excellent yields (90-96%), whereas **Ni X-1** afforded much lower yields (79-80%). Moreover, the thiophene ring containing acetyl functionality was successfully coupled with a bulky naphthalene ring in CD12. Furthermore, three biaryl compounds possessing two reactive functional groups were synthesized for observing the

effectiveness of both catalytic systems (Figure 4.2, CD-13-CD15). Introducing two functional groups did not reduce the catalytic performance appreciably for **Pd X-2** (89-90%); however, Ni X-1 continued to afford lesser yields (71-77%).

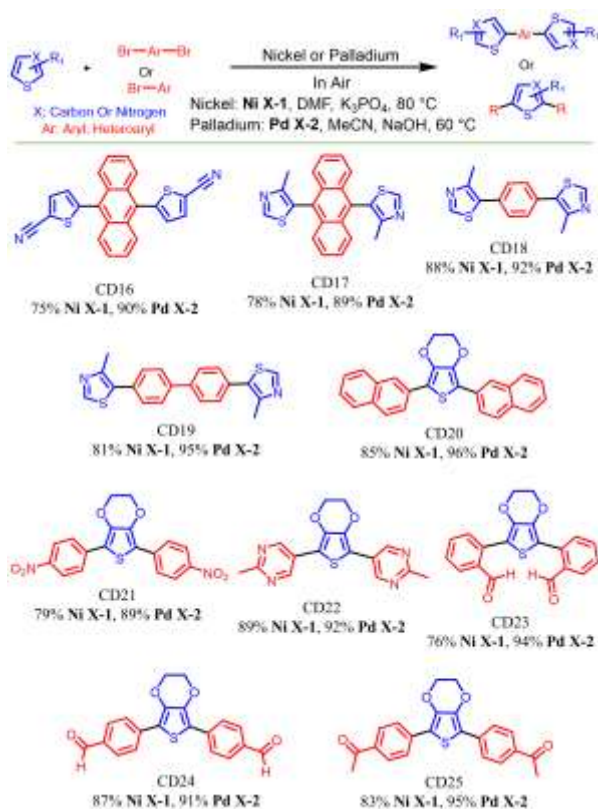


Figure 4.3. Expansion of substrate scope: π -conjugated monomers

4.3.5 Extension of Substrate Scope: π -Conjugated Monomers

π -conjugated poly(hetero)arenes are widely studied functional materials for electrochromic and optoelectronic device fabrication.⁴² Here, we have synthesized π -conjugated poly(hetero)aryl compounds through double direct C-H bond arylation from five-membered heteroaromatics. Anthracene is a valuable supramolecular building block that provides a low electronic bandgap in OLED application.⁴⁵ We have applied both **Ni X-1** and **Pd X-2** for synthesizing anthracene-based

poly(hetero)aryl compounds possessing thiazole or thiophene units (Figure 4.3, CD16 & CD17). Moreover, 1,4-dibromobenzene and 4,4'-dibromo-1,1'-biphenyl were successfully applied for producing the π -conjugated building blocks holding biologically active thiazole units (Figure 4.3, CD18 & CD19). Then, we devoted our efforts to synthesize valuable functional materials from 3,4-ethylenedioxythiophene (EDOT). Traditionally, EDOT-based monomers are prepared by employing Kumada, Stille, Suzuki, and Heck cross-coupling reactions. Nonetheless, these methods are not atom economical and require time-consuming additional synthetic steps.⁵⁻⁶ We have introduced direct C-H arylation of EDOT for making six valuable π -conjugated monomers including acetyl, nitro, and aldehyde functionalities (Figure 4.3, CD20-CD25). In those compounds, **Pd X-2** presented approximately excellent yields (89-96%), whereas **Ni X-1** afforded lesser but satisfactory yields (79-89%). Especially, the *ortho* and *para* aldehyde group did not significantly affect the catalytic performance of **Pd X-2**, which continued to deliver excellent yields (91-94%). Notably, all these compounds were synthesized by precipitation method which significantly circumvented the time-consuming column chromatography.

4.4 Conclusion

We have demonstrated direct C-H bond arylation of various thiazole and thiophene derivatives through iminopyridine-based α -diimine nickel (II) and palladium (II) complexes. Steric attributes of the complexes were correlated to the reaction outcomes by generating percent buried volumes and topographic steric maps. Both Ni and Pd catalytic systems were applied for investigating the substrate scope in producing biaryl building blocks holding various reactive functionalities. Moreover, valuable biheteroaryl compounds were successfully synthesized without degrading catalytic performance. Notably, π -conjugated poly(hetero)arenes were prepared

from five-membered heteroaromatics maintaining satisfactory to excellent yields. Consequently, α -diimine frameworks have the potentiality to deliver transition metal-catalyzed systems as an alternative to other ligand-based counterparts.

4.5 Experimental

4.5.1 General Materials and Methods

All the required chemicals were obtained from Sigma-Aldrich or Fisher Scientific and employed without additional purification unless specified. a 500 MHz Bruker AVANCE III spectrometer was operated having chloroform as the reference solvent for obtaining the ^1H NMR and ^{13}C NMR spectra. Synthesized α -diimine complexes were characterized by elemental analysis from utilizing Thermo FLASH 2000 CHN elemental analyzer. For collecting the ESI-MS data, a Waters ACQUITY UPLC M-Class was employed. To generate the percent buried volume and topographic steric maps of the synthesized α -diimine complexes, SambVca 2.1, a web tool, was used. All the reactions except for the synthesis of the α -diimine complexes were performed in air.

4.5.2 Single-Crystal XRD Data Characterization

A Bruker Kappa D8 Quest CPAD diffractometer having an Incoatec microfocus Mo $K\alpha$ radiation source ($\lambda = 0.71073 \text{ \AA}$) was implemented for acquiring the single-crystal X-ray diffraction data. In addition, an Oxford Cryosystems cooler was applied including a Photon 100 CMOS detector. Bruker APEX3 graphical interface and Bruker SAINT were applied for achieving the data reduction and cell refinement. Moreover, Bruker XPREP and SADABS were used to estimate the space group and multi-scan absorption correction, respectively. To solve and refine the structure, SHELXTL (intrinsic phasing method)⁴⁶ and SHELXL2017⁴⁷ were applied,

respectively. The publCIF and ORTEP-3 used for the preparation of the crystallographic Information File (CIF).

4.5.3 Steric Map and Percent Buried Volume

For obtaining the percent buried volumes (%/Bur) and topographic steric maps of the synthesized α -diimine complexes, SambVca 2.1 was applied.⁴⁰ The web address for this freely available software is <https://www.molnac.unisa.it/OMtools/sambvca2.1/index.html>. CIF files of the synthesized α -diimine complexes or converted XYZ files were uploaded in that software having a mesh of 0.1 Å, bond radii scaled by 1.17, and the radius of the sphere as 3.5 Å.

4.5.4. Synthesis of Iminopyridine Ligand *N*-(2-ethylphenyl)-1-(pyridin-2-yl)methanimine (**L A-1**)

The ligand **L A-1** was synthesized by adopting a procedure.³⁴ In a one-neck 100 mL flask, 2-pyridinecarboxaldehyde (3.0 mL, 0.032 mol) and 2-ethylaniline (3.88 g, 0.032 mol) were mixed having anhydrous MgSO₄ (120 mg, 1 mmol), and DMF (40 mL) as a solvent. The reaction mixture was stirred for ten hours at room temperature. After that, three extractions were performed with 40 mL of ethyl acetate and 40 mL of distilled water. After drying the ethyl acetate layer with anhydrous MgSO₄, the crude product was obtained by concentrating with the rotary evaporator. The final pure product was collected by employing silica gel column chromatography having *n*-hexane as an eluent. The product was isolated as dark-orange oil (Yield = 5.24 g, 77.86 %). ESI-MS m/z $[M + H]^+$ = 211.0104 (calculated for C₁₄H₁₄N₂, 211.0139). ¹H NMR (500 MHz, CDCl₃, 300 K): δ (ppm): 8.70 (d, J = 4.15 Hz, 1H), 8.55 (s, 1H), 8.25 (d, J = 7.85 Hz, 1H), 7.78 (t, J = 7.65 Hz, 1H), 7.34 (t, J = 6.05 Hz, 1H), 7.19 – 7.27 (m, 3H), 7.02 (d, J = 7.35 Hz, 1H), 2.83 (q, J = 7.45 Hz, 2H), 1.22 (t, J = 7.55 Hz, 3H).

4.5.5 Synthesis of Iminopyridine Ligand *N*-(2,3-dimethylphenyl)-1-(pyridin-2-yl)methanimine (L A-2)⁴⁸

The ligand **L A-2** was synthesized by employing the above procedure having from the reaction between 2-pyridinecarboxaldehyde (3.0 mL, 0.032 mol) and 2,3-dimethylaniline (3.88 g, 0.032 mol). The pure product was isolated as dark-yellow oil (Yield = 6.01 g, 89.35 %). ESI-MS m/z $[M+H]^+$ = 211.0183 (calculated for $C_{14}H_{14}N_2$ = 211.0139). 1H NMR (500 MHz, $CDCl_3$, 300 K), δ (ppm): 8.70 (d, J = 4.2 Hz, 1H), 8.51 (s, 1H), 8.27 (d, J = 7.9 Hz, 1H), 7.81 (t, J = 7.55 Hz, 1H), 7.36 (q, J = 3.7, 1H), 7.14 (t, J = 7.60 Hz, 1H), 7.08 (d, J = 7.35 Hz, 1H), 6.88 (d, J = 7.60 Hz, 1H), 2.33 (d, J = 3.50 Hz, 6H).

4.5.6 Synthesis of the Iminopyridine Bis-Ligated Nickel(II) Complex (Ni X-1)

Complex **Ni X-1** was synthesized by adopting a procedure. $NiCl_2(DME)$ (219.72 mg, 1 mmol) was transferred to a one-neck 50 mL flask having a magnetic stirrer. Before adding the ligand **L A-1** (420.56 mg, 2 mmol) dissolved in dichloromethane (20 mL), the flask was purged with nitrogen. After stirring at room temperature for 24 hours, the precipitated solid was filtered and subsequently washed with petroleum ether (40 mL) and hexane (40 mL). The pure product was isolated as a light green solid after drying under vacuum for 24 hours (Yield = 480.17 mg, 87.28 %). Elemental analysis: calculated for $C_{28}H_{28}Cl_2N_4Ni$: C, 61.13; H, 5.13; N, 10.18. Found: C, 61.23; H, 5.01; N, 10.27. Acetonitrile was applied as a solvent for growing the single crystal for XRD analysis. A saturated solution of the complex was formed, and it was slowly evaporated over one week. Crystal size: $0.18 \times 0.16 \times 0.16$ mm³; crystal shape: fragment; crystal color: yellow.

4.5.7 Synthesis of the Iminopyridine Bis-Ligated Nickel(II) Complex (Ni X-2)

The complex **Ni X-2** was synthesized by employing the above procedure having the reaction between NiCl₂(DME) (219.72 mg, 1 mmol) and the ligand **L A-2** (420.56 mg, 2 mmol). Dark-green solid (Yield = 427.50 mg, 78.20 %). Elemental analysis: calculated for C₂₈H₂₈Cl₂N₄Ni: C, 61.13; H, 5.13; N, 10.18. Found: C, 61.02; H, 5.21; N, 10.06. Acetonitrile was applied as a solvent for growing the single crystal for XRD analysis. A saturated solution of the complex was formed, and it was slowly evaporated over one week. Crystal size: 0.14 × 0.14 × 0.02 mm³; crystal shape: plate; crystal color: yellow.

4.5.8 Synthesis of the Iminopyridine Palladium(II) Complex (Pd X-1)

Complex **Pd X-1** was synthesized by adopting a procedure. PdCl₂(cod) (200 mg, 0.7 mmol) was transferred to a one-neck 50 mL flask having a magnetic stirrer. Before adding the ligand **L A-1** (210.28 mg, 1 mmol) dissolved in dichloromethane (20 mL), the flask was purged with nitrogen. After stirring at room temperature for 8 hours, the precipitated solid was filtered and subsequently washed with petroleum ether (40 mL) and hexane (40 mL). The pure product was isolated as a light orange solid after drying under vacuum for 24 hours (Yield = 355.4 mg, 92.14 %). Elemental analysis: calculated for C₁₄H₁₄Cl₂N₂Pd: C, 43.38; H, 3.64; N, 7.23. Found: C, 43.49; H, 3.57; N, 7.31. Dimethylformamide was applied as a solvent for growing the single crystal for XRD analysis. A saturated solution of the complex was formed, and it was slowly evaporated over one week. Crystal size: 0.49 × 0.12 × 0.02 mm³; crystal shape: blade; crystal color: orange.

4.5.9 Synthesis of the Iminopyridine Palladium(II) Complex (Pd X-2)

The complex **Pd X-2** was synthesized by employing the above procedure having the reaction between PdCl₂(cod) (200 mg, 0.7 mmol) and the ligand **L A-2** (210.28 mg, 1 mmol).

Orange solid (Yield = 345.45 mg, 89.50 %). Elemental analysis: calculated for C₁₄H₁₄Cl₂N₂Pd: C, 43.38; H, 3.64; N, 7.23. Found: C, 43.41; H, 3.72; N, 7.16. Dimethylformamide was applied as a solvent for growing the single crystal for XRD analysis. A saturated solution of the complex was formed, and it was slowly evaporated over one week. Crystal size: 0.20 × 0.16 × 0.12 mm³; crystal shape: block; crystal color: orange.

4.5.10 General Procedure for Nickel-Catalyzed Direct Arylation

All the reactions were performed in air. A 25 mL one-neck round bottom flask was equipped with a condenser. For the single C-H activation, the reaction setup was maintained with heteroaryl derivative (1.5 mmol), aryl halide (1 mmol), DMF (6 mL), K₃PO₄ (1.5 mmol), 0.2 mol% of Ni X-1 or Ni X-2, and PivOH (0.2 mmol). The reaction mixture was stirred for six hours at 80 °C. For the double C-H activation with bis-halogenated aromatics, the reaction setup was maintained with heteroaryl derivative (2.5 mmol), aryl halide (1 mmol), DMF (6 mL), K₃PO₄ (3 mmol), 0.4 mol% of Ni X-1, and PivOH (0.4 mmol). The reaction mixture was stirred for six hours at 80 °C. For the double C-H activation with mono-halogenated aromatics, the reaction setup was maintained with heteroaryl derivative (1 mmol), aryl halide (2.5 mmol), DMF (6 mL), K₃PO₄ (3 mmol), 0.4 mol% of Ni X-1, and PivOH (0.4 mmol). The reaction mixture was stirred for six hours at 80 °C. After that, the reaction mixture was cooled to the room temperature and it was poured into a 100 mL beaker containing 40 mL of water. Three extractions were carried out with 20 mL of ethyl acetate and 20 mL of water. The ethyl acetate layer was dried over anhydrous MgSO₄ and concentrated through rotary evaporation for obtaining the crude product. The pure product was obtained by either precipitation or using silica gel (200–300 mesh) column chromatography.

4.5.11 General Procedure for Palladium-Catalyzed Direct Arylation

All the reactions were performed in air. A 25 mL one-neck round bottom flask was equipped with a condenser. For the single C-H activation, the reaction setup was maintained with heteroaryl derivative (1.5 mmol), aryl halide (1 mmol), MeCN (6 mL), NaOH (1.5 mmol), 0.1 mol% of **Pd X-1** or **Pd X-2**, and PivOH (0.2 mmol). The reaction mixture was stirred for eight hours at 60 °C. For the double C-H activation with bis-halogenated aromatics, the reaction setup was maintained with heteroaryl derivative (2.5 mmol), aryl halide (1 mmol), MeCN (6 mL), NaOH (3 mmol), 0.2 mol% of **Pd X-2**, and PivOH (0.4 mmol). The reaction mixture was stirred for eight hours at 60 °C. For the double C-H activation with mono-halogenated aromatics, the reaction setup was maintained with heteroaryl derivative (1 mmol), aryl halide (2.5 mmol), MeCN (6 mL), NaOH (3 mmol), 0.2 mol% of **Pd X-2**, and PivOH (0.4 mmol). The reaction mixture was stirred for eight hours at 60 °C. After that, the reaction mixture was cooled to the room temperature and it was poured into a 100 mL beaker containing 40 mL of water. Three extractions were carried out with 20 mL of ethyl acetate and 20 mL of water. The ethyl acetate layer was dried over anhydrous MgSO₄ and concentrated through rotary evaporation for obtaining the crude product. The pure product was obtained by either precipitation or using silica gel (200–300 mesh) column chromatography.

4.6 Characterization of the Synthesized Direct Arylated Compounds

4-methyl-5-(naphthalen-2-yl)thiazole (CD1). Silica gel column chromatography having eluent as *n*-hexane and ethyl acetate of 10:1 (v/v). Colorless oil. Yield: 205.1 mg, 91% (**Ni X-1**); 200.5 mg, 89% (**Ni X-2**); 216.3 mg, 96% (**Pd X-1**); 220.80 mg, 98% (**Pd X-2**). ESI-MS *m/z* [M + H]⁺ = 226.0021 (calculated for C₁₄H₁₁NS, 226.0087). ¹H NMR (500 MHz, CDCl₃, 300 K): δ

(ppm): 8.73 (s, 1H), 7.91 – 7.86 (m, 4H), 7.56 – 7.51 (m, 3H), 2.61 (s, 3H). ¹³C NMR (500 MHz, CDCl₃, 300 K), δ (ppm): 150.56, 148.85, 133.32, 132.71, 132.08, 129.42, 128.48, 128.40, 128.07, 127.80, 127.16, 126.76, 126.61, 30.93.

1-(5-(4-methylthiazol-5-yl)thiophen-2-yl)ethan-1-one (CD2). Silica gel column chromatography having eluent as *n*-hexane and ethyl acetate of 10:1 (v/v). Light brown solid. Yield: 185.3 mg, 99% (**Ni X-1**); 183.2 mg, 82% (**Ni X-1**); 196.5 mg, 96% (**Pd X-1**); 205.4 mg, 92% (**Pd X-2**). ESI-MS m/z [M + H]⁺ = 224.0035 (calculated for C₁₀H₉NOS₂, 224.0047). ¹H NMR (500 MHz, CDCl₃, 300 K): δ (ppm): 8.65 (s, 1H), 7.60 (d, *J* = 4 Hz, 1H), 7.12 (d, *J* = 4 Hz, 1H), 2.63 (s, 3H), 2.53 (s, 3H). ¹³C NMR (500 MHz, CDCl₃, 300 K), δ (ppm): 190.43, 151.09, 150.81, 144.20, 141.83, 132.85, 127.55, 125.16, 26.65, 17.03.

4-methyl-5-(4-nitrophenyl)thiazole (CD3).¹⁴ Silica gel column chromatography having eluent as *n*-hexane and ethyl acetate of 10:1 (v/v). Colorless oil. Yield: 191.6 mg, 87% (**Ni X-1**); 187.2 mg, 85% (**Ni X-2**); 200.4 mg, 91% (**Pd X-1**); 209.2 mg, 95% (**Pd X-2**). ESI-MS m/z [M + H]⁺ = 221.0121 (calculated for C₁₀H₈N₂O₂S, 221.0147). ¹H NMR (500 MHz, CDCl₃, 300 K): δ (ppm): 8.76 (s, 1H), 8.25 (d, *J* = 10 Hz, 2H), 7.59 (d, *J* = 10 Hz, 2H), 2.57 (s, 3H). ¹³C NMR (500 MHz, CDCl₃, 300 K), δ (ppm): 151.89, 150.46, 147.14, 138.88, 129.87, 129.81, 124.09, 16.48.

4-(4-methylthiazol-5-yl)benzotrile (CD4).²⁷ Silica gel column chromatography having eluent as *n*-hexane and ethyl acetate of 10:1 (v/v). Light brown oil. Yield: 144.1 mg, 72% (**Ni X-1**); 138.1 mg, 69% (**Ni X-2**); 176.2 mg, 88% (**Pd X-1**); 188.2 mg, 94% (**Pd X-2**). ESI-MS m/z [M + H]⁺ = 201.0101 (calculated for C₁₁H₈N₂S, 201.0059). ¹H NMR (500 MHz, CDCl₃, 300 K): δ (ppm): 8.74 (s, 1H) 7.69 (d, *J* = 10 Hz, 2H), 7.54 (d, *J* = 5 Hz, 2H), 2.55 (s, 3H). ¹³C NMR (500

MHz, CDCl₃, 300 K), δ (ppm): 151.63, 150.08, 136.90, 132.56, 130.17, 129.77, 118.50, 111.58, 16.39.

1-(4-(4-methylthiazol-5-yl)phenyl)ethan-1-one (CD5).²⁷ Silica gel column chromatography having eluent as *n*-hexane and ethyl acetate of 10:1 (v/v). Light yellow oil. Yield: 171.6 mg, 79% (**Ni X-1**); 165.1 mg, 76% (**Ni X-2**); 195.5 mg, 90% (**Pd X-1**); 199.9 mg, 92% (**Pd X-2**). ESI-MS m/z $[M + H]^+ = 218.0109$ (calculated for C₁₂H₁₁NOS, 218.0123). ¹H NMR (500 MHz, CDCl₃, 300 K): δ (ppm): 8.70 (s, 1H), 7.97 (d, $J = 5$ Hz, 2H), 7.50 (d, $J = 10$ Hz, 2H), 2.59 (s, 3H), 2.54 (s, 3H). ¹³C NMR (500 MHz, CDCl₃, 300 K), δ (ppm): 197.28, 151.17, 149.59, 136.83, 136.22, 130.90, 129.29, 128.77, 26.64, 16.38.

5-(anthracen-9-yl)-4-methylthiazole (CD6). Silica gel column chromatography having eluent as *n*-hexane and ethyl acetate of 10:1 (v/v). Light yellow solid. Yield: 239.5 mg, 87% (**Ni X-1**); 245.1 mg, 89% (**Ni X-2**); 250.5 mg, 91% (**Pd X-1**); 264.3 mg, 96% (**Pd X-2**). ESI-MS m/z $[M + H]^+ = 276.0019$ (calculated for C₁₈H₁₃NS, 276.0026). ¹H NMR (500 MHz, CDCl₃, 300 K): δ (ppm): 9.03 (s, 1H), 8.57 (s, 1H), 8.06 (d, $J = 8$ Hz, 2H), 7.66 (d, $J = 8.5$ Hz, 2H), 7.51 – 7.44 (m, 4H), 2.16 (s, 3H). ¹³C NMR (500 MHz, CDCl₃, 300 K), δ (ppm): 152.99, 152.55, 131.84, 131.44, 128.80, 128.76, 126.60, 125.93, 125.92, 124.67, 15.50.

4-methyl-5-(2-methylpyrimidin-5-yl)thiazole (CD7). Silica gel column chromatography having eluent as *n*-hexane and ethyl acetate of 10:1 (v/v). Colorless oily liquid. Yield: 147.2 mg, 77% (**Ni X-1**); 135.7 mg, 71% (**Ni X-2**); 149.1 mg, 78% (**Pd X-1**); 174.1 mg, 91% (**Pd X-2**). ESI-MS m/z $[M + H]^+ = 192.0128$ (calculated for C₉H₉N₃S, 192.0113). ¹H NMR (500 MHz, CDCl₃, 300 K): δ (ppm): 8.77 (s, 1H), 8.70 (s, 2H), 2.77 (s, 3H), 2.52 (s, 3H). ¹³C NMR (500 MHz, CDCl₃, 300 K), δ (ppm): 167.55, 156.51, 151.89, 150.78, 124.65, 123.64, 25.89, 15.99.

5-(naphthalen-2-yl)thiophene-2-carbaldehyde (CD8).⁴⁹ Silica gel column chromatography having eluent as *n*-hexane and ethyl acetate of 10:1 (v/v). Light yellow solid. Yield: 195.4 mg, 82% (**Ni X-1**); 214.4 mg, 90% (**Pd X-2**). ESI-MS m/z $[M + H]^+ = 239.0152$ (calculated for C₁₅H₁₀OS, 239.0123). ¹H NMR (500 MHz, CDCl₃, 300 K): δ (ppm): 9.92 (s, 1H), 8.15 (s, 1H), 7.90 – 7.88 (m, 2H), 7.86 – 7.84 (m, 1H), 7.78 – 7.75 (m, 2H) 7.54 – 7.52 (m, 3H). ¹³C NMR (500 MHz, CDCl₃, 300 K), δ (ppm): 182.87, 154.48, 142.72, 137.56, 133.73, 133.51, 130.54, 129.16, 128.54, 127.95, 127.16, 127.14, 125.79, 124.51, 124.13.

5-(naphthalen-1-yl)thiophene-2-carbonitrile (CD9).¹² Silica gel column chromatography having eluent as *n*-hexane and ethyl acetate of 10:1 (v/v). Light yellow solid. Yield: 200.1 mg, 85% (**Ni X-1**); 216.4 mg, 92% (**Pd X-2**). ESI-MS m/z $[M + H]^+ = 236.0083$ (calculated for C₁₅H₉NS, 236.0089). ¹H NMR (500 MHz, CDCl₃, 300 K): δ (ppm): 8.18 (d, $J = 10$ Hz, 1H), 7.92 - 7.89 (m, 2H), 7.62 (d, $J = 5$ Hz, 1H), 7.58 – 7.49 (m, 4H), 7.22 (d, $J = 5$ Hz, 1H). ¹³C NMR (500 MHz, CDCl₃, 300 K), δ (ppm): 163.90, 147.90, 137.42, 133.97, 131.58, 131.43, 129.76, 129.45, 128.61, 128.45, 128.21, 126.99, 126.41, 125.43, 125.35.

5-(2-methylpyrimidin-5-yl)thiophene-2-carbonitrile (CD10). Silica gel column chromatography having eluent as *n*-hexane and ethyl acetate of 10:1 (v/v). Light brown solid. Yield: 158.9 mg, 79% (**Ni X-1**); 193.2 mg, 96% (**Pd X-2**). ESI-MS m/z $[M + H]^+ = 202.0074$ (calculated for C₁₀H₇N₃S, 202.0039). ¹H NMR (500 MHz, CDCl₃, 300 K): δ (ppm): 8.84 (s, 2H), 7.65 (d, $J = 5$ Hz, 1H), 7.33 (d, $J = 5$ Hz, 1H), 2.77 (s, 3H). ¹³C NMR (500 MHz, CDCl₃, 300 K), δ (ppm): 168.91, 154.19, 144.01, 138.59, 124.94, 123.90, 113.63, 110.50, 25.97.

1-(5-(2-methylpyrimidin-5-yl)thiophen-2-yl)ethan-1-one (CD11). Silica gel column chromatography having eluent as *n*-hexane and ethyl acetate of 10:1 (v/v). Light brown solid.

Yield: 174.6 mg, 80% (**Ni X-1**); 196.4 mg, 90% (**Pd X-2**). ESI-MS m/z $[M + H]^+ = 219.0128$ (calculated for $C_{11}H_{10}N_2OS$, 219.0176). 1H NMR (500 MHz, $CDCl_3$, 300 K): δ (ppm): 8.87 (s, 2H), 7.68 (d, $J = 5$ Hz, 1H), 7.36 (d, $J = 5$ Hz, 1H), 2.76 (s, 3H), 2.57 (s, 3H). ^{13}C NMR (500 MHz, $CDCl_3$, 300 K), δ (ppm): 190.39, 168.40, 154.05, 145.12, 144.75, 133.33, 125.44, 124.83, 26.77, 25.96.

1-(5-(naphthalen-2-yl)thiophen-2-yl)ethan-1-one (CD12).⁵⁰ Silica gel column chromatography having eluent as *n*-hexane and ethyl acetate of 20:1 (v/v). Light brown solid. Yield: 224.5 mg, 89% (**Ni X-1**); 244.7 mg, 97% (**Pd X-2**). ESI-MS m/z $[M + H]^+ = 253.0081$ (calculated for $C_{16}H_{12}OS$, 253.0048). 1H NMR (500 MHz, $CDCl_3$, 300 K): δ (ppm): 8.13 (s, 1H), 7.87 (d, $J = 5$ Hz, 2H), 7.85 – 7.83 (m, 1H), 7.76 – 7.74 (m, 1H), 7.69 (d, $J = 5$ Hz, 1H), 7.52 – 7.50 (m, 2H), 7.44 (d, $J = 5$ Hz, 1H), 2.59 (s, 3H). ^{13}C NMR (500 MHz, $CDCl_3$, 300 K), δ (ppm): 190.66, 152.96, 143.38, 133.64, 133.56, 130.84, 129.05, 128.47, 127.92, 127.04, 126.95, 125.47, 124.33, 124.16, 26.74.

5-(4-acetylphenyl)thiophene-2-carbonitrile (CD13).⁵¹ Silica gel column chromatography having eluent as *n*-hexane and ethyl acetate of 30:1 (v/v). Light orange solid. Yield: 165.9 mg, 73% (**Ni X-1**); 202.2 mg, 89% (**Pd X-2**). ESI-MS m/z $[M + H]^+ = 228.0063$ (calculated for $C_{13}H_9NOS$, 228.0071). 1H NMR (500 MHz, $CDCl_3$, 300 K): δ (ppm): 7.99 (d, $J = 10$ Hz, 2H), 7.67 (d, $J = 10$ Hz, 2H), 7.61 (d, $J = 5$ Hz, 1H), 7.37 (d, $J = 5$ Hz, 1H), 2.62 (s, 3H). ^{13}C NMR (500 MHz, $CDCl_3$, 300 K), δ (ppm): 197.12, 150.12, 138.55, 137.47, 136.46, 129.42, 126.53, 124.68, 114.08, 109.83, 26.74.

1,1'-([2,2'-bithiophene]-5,5'-diyl)bis(ethan-1-one) (CD14).⁵² Pure product was obtained by precipitation method. *n*-hexane was added to a concentrated dichloromethane solution followed

by filtering and washing with *n*-hexane. Light red solid. Yield: 192.7 mg, 77% (**Ni X-1**); 225.2 mg, 90% (**Pd X-2**). ESI-MS m/z $[M + H]^+ = 251.0064$ (calculated for $C_{12}H_{10}O_2S_2$, 251.0078). 1H NMR (500 MHz, $CDCl_3$, 300 K): δ (ppm): 7.60 (d, $J = 5$ Hz, 2H), 7.29 (d, $J = 5$ Hz, 2H), 2.56 (s, 6H). ^{13}C NMR (500 MHz, $CDCl_3$, 300 K), δ (ppm): 190.46, 144.44, 144.14, 133.27, 126.10, 26.76.

5-(4-nitrophenyl)thiophene-2-carbaldehyde (CD15). Pure product was obtained by precipitation method. *n*-hexane was added to a concentrated dichloromethane solution followed by filtering and washing with *n*-hexane. Light orange solid. Yield: 165.6 mg, 71% (**Ni X-1**); 209.9 mg, 90% (**Pd X-2**). ESI-MS m/z $[M + H]^+ = 234.0254$ (calculated for $C_{11}H_7NO_3S$, 234.0187). 1H NMR (500 MHz, $CDCl_3$, 300 K): δ (ppm): 9.95 (s, 1H), 8.29 (d, $J = 10$ Hz, 2H), 7.84 – 7.80 (m, 3H), 7.54 (d, $J = 5$ Hz, 1H). ^{13}C NMR (500 MHz, $CDCl_3$, 300 K), δ (ppm): 182.83, 150.54, 148.08, 144.73, 139.21, 137.12, 127.15, 126.44, 124.72.

5,5'-(anthracene-9,10-diyl)bis(thiophene-2-carbonitrile) (CD16). Pure product was obtained by precipitation method. *n*-hexane was added to a concentrated dichloromethane solution followed by filtering and washing with *n*-hexane. Light orange solid. Yield: 294.3 mg, 75% (**Ni X-1**); 353.2 mg, 90% (**Pd X-2**). ESI-MS m/z $[M + H]^+ = 237.0033$ (calculated for $C_{24}H_{12}N_2S_2$, 237.0067). 1H NMR (500 MHz, $CDCl_3$, 300 K): δ (ppm): 7.87 (d, $J = 5$ Hz, 2H), 7.78 – 7.76 (m, 4H), 7.51 – 7.49 (m, 4H), 7.25 (t, $J = 5$ Hz, 2H). ^{13}C NMR (500 MHz, $CDCl_3$, 300 K), δ (ppm): 146.74, 137.88, 131.17, 130.23, 128.23, 126.93, 126.11, 113.99, 111.67.

9,10-bis(4-methylthiazol-5-yl)anthracene (CD17). Pure product was obtained by precipitation method. *n*-hexane was added to a concentrated dichloromethane solution followed by filtering and washing with *n*-hexane. Light orange solid. Yield: 290.5 mg, 78% (**Ni X-1**); 331.5 mg, 89% (**Pd X-2**). ESI-MS m/z $[M + H]^+ = 373.0169$ (calculated for $C_{22}H_{16}N_2S_2$, 373.0132). 1H

NMR (500 MHz, CDCl₃, 300 K): δ (ppm): 9.06 (s, 2H), 7.74 – 7.71 (m, 4H), 7.47 – 7.45 (m, 4H), 2.23 (s, 3H), 2.19 (s, 3H). ¹³C NMR (500 MHz, CDCl₃, 300 K), δ (ppm): 153.23, 153.20, 152.76, 152.66, 131.49, 126.54, 126.39, 15.61, 15.54.

1,4-bis(4-methylthiazol-5-yl)benzene (CD18).¹⁰ Pure product was obtained by precipitation method. *n*-hexane was added to a concentrated dichloromethane solution followed by filtering and washing with *n*-hexane. Light red solid. Yield: 239.6 mg, 88% (**Ni X-1**); 250.5 mg, 92% (**Pd X-2**). ESI-MS m/z [M + H]⁺ = 273.0112 (calculated for C₁₄H₁₂N₂S₂, 273.0147). ¹H NMR (500 MHz, CDCl₃, 300 K): δ (ppm): 8.70 (s, 2H), 7.50 (s, 4H), 2.58 (s, 6H). ¹³C NMR (500 MHz, CDCl₃, 300 K), δ (ppm): 150.64, 149.00, 131.71, 131.36, 129.62, 16.32.

4,4'-bis(4-methylthiazol-5-yl)-1,1'-biphenyl (CD19). Pure product was obtained by precipitation method. *n*-hexane was added to a concentrated dichloromethane solution followed by filtering and washing with *n*-hexane. Light red solid. Yield: 282.2 mg, 81% (**Ni X-1**); 331.0 mg, 95% (**Pd X-2**). ESI-MS m/z [M + H]⁺ = 349.0061 (calculated for C₂₀H₁₆N₂S₂, 349.0097). ¹H NMR (500 MHz, CDCl₃, 300 K): δ (ppm): 8.71 (s, 2H), 7.68 (d, *J* = 10 Hz, 4H), 7.54 (d, *J* = 10 Hz, 4H), 2.60 (s, 6H). ¹³C NMR (500 MHz, CDCl₃, 300 K), δ (ppm): 150.54, 148.87, 139.93, 131.65, 131.46, 129.90, 127.42, 16.37.

5,7-di(naphthalen-2-yl)-2,3-dihydrothieno[3,4-b][1,4]dioxine (CD20). Pure product was obtained by precipitation method. *n*-hexane was added to a concentrated dichloromethane solution followed by filtering and washing with *n*-hexane. Light green solid. Yield: 335.3 mg, 85% (**Ni X-1**); 378.7 mg, 96% (**Pd X-2**). ESI-MS m/z [M + H]⁺ = 395.0078 (calculated for C₂₆H₁₈O₂S, 395.0056). ¹H NMR (500 MHz, CDCl₃, 300 K): δ (ppm): 8.27 (s, 2H), 7.92 – 7.92 (m, 2H), 7.88 – 7.81 (m, 6H), 7.50 – 7.43 (m, 4H), 4.44 (s, 4H). ¹³C NMR (500 MHz, CDCl₃, 300 K), δ (ppm):

139.24, 133.79, 132.36, 130.60, 128.30, 128.20, 127.79, 126.47, 125.84, 124.70, 124.58, 116.00, 64.79.

5,7-bis(4-nitrophenyl)-2,3-dihydrothieno[3,4-b][1,4]dioxine (CD21).⁵ Pure product was obtained by precipitation method. *n*-hexane was added to a concentrated dichloromethane solution followed by filtering and washing with *n*-hexane. Dark orange solid. Yield: 303.6 mg, 79% (**Ni X-1**); 342.1 mg, 89% (**Pd X-2**). ESI-MS m/z $[M + H]^+ = 385.0205$ (calculated for $C_{18}H_{12}N_2O_6S$, 385.0118). 1H NMR (500 MHz, $CDCl_3$, 300 K): δ (ppm): 8.24 (d, $J = 5$ Hz, 4H), 7.91 (d, $J = 10$ Hz, 4H), 4.47 (s, 4H).

5,7-bis(2-methylpyrimidin-5-yl)-2,3-dihydrothieno[3,4-b][1,4]dioxine (CD22). Pure product was obtained by precipitation method. *n*-hexane was added to a concentrated dichloromethane solution followed by filtering and washing with *n*-hexane. Light yellow solid. Yield: 290.4 mg, 89% (**Ni X-1**); 300.2 mg, 92% (**Pd X-2**). ESI-MS m/z $[M + H]^+ = 327.0092$ (calculated for $C_{16}H_{14}N_4O_2S$, 327.0075). 1H NMR (500 MHz, $CDCl_3$, 300 K): δ (ppm): 8.95 (s, 4H), 4.40 (s, 4H), 2.74 (s, 6H). ^{13}C NMR (500 MHz, $CDCl_3$, 300 K), δ (ppm): 165.88, 153.45, 140.07, 124.08, 109.82, 64.72, 25.74.

2,2'-(2,3-dihydrothieno[3,4-b][1,4]dioxine-5,7-diyl)dibenzaldehyde (CD23). Pure product was obtained by precipitation method. *n*-hexane was added to a concentrated dichloromethane solution followed by filtering and washing with *n*-hexane. Dark orange solid. Yield: 266.2 mg, 76% (**Ni X-1**); 329.3 mg, 94% (**Pd X-2**). ESI-MS m/z $[M + H]^+ = 351.0251$ (calculated for $C_{20}H_{14}O_4S$, 351.0187). 1H NMR (500 MHz, $CDCl_3$, 300 K): δ (ppm): 10.16 (s, 2H), 8.03 (d, $J = 5$ Hz, 2H), 7.66 (t, $J = 5$ Hz, 2H), 7.54 – 7.49 (m, 4H), 4.25 (s, 4H). ^{13}C NMR (500

MHz, CDCl₃, 300 K), δ (ppm): 192.03, 138.77, 134.65, 134.00, 133.86, 131.25, 128.57, 128.05, 114.04, 64.83.

4,4'-(2,3-dihydrothieno[3,4-b][1,4]dioxine-5,7-diyl)dibenzaldehyde (CD24).⁵³ Pure product was obtained by precipitation method. *n*-hexane was added to a concentrated dichloromethane solution followed by filtering and washing with *n*-hexane. Light orange solid. Yield: 304.8 mg, 87% (**Ni X-1**); 318.8 mg, 91% (**Pd X-2**). ESI-MS m/z $[M + H]^+ = 312.0210$ (calculated for C₂₀H₁₄O₄S, 351.0187). ¹H NMR (500 MHz, CDCl₃, 300 K): δ (ppm): 9.99 (s, 2H), 7.93 (d, $J = 10$ Hz, 4H), 7.88 (d, $J = 10$ Hz, 4H), 4.45 (s, 4H). ¹³C NMR (500 MHz, CDCl₃, 300 K), δ (ppm): 191.57, 140.71, 138.67, 134.61, 130.35, 126.36, 116.53, 64.82.

1,1'-((2,3-dihydrothieno[3,4-b][1,4]dioxine-5,7-diyl)bis(4,1-phenylene))bis(ethan-1-one) (CD25). Pure product was obtained by precipitation method. *n*-hexane was added to a concentrated dichloromethane solution followed by filtering and washing with *n*-hexane. Light orange solid. Yield: 314.1 mg, 83% (**Ni X-1**); 359.5 mg, 95% (**Pd X-2**). ESI-MS m/z $[M + H]^+ = 379.0048$ (calculated for C₂₂H₁₈O₄S, 379.0083). ¹H NMR (500 MHz, CDCl₃, 300 K): δ (ppm): 7.97 (d, $J = 10$ Hz, 4H), 7.86 (d, $J = 10$ Hz, 4H), 4.44 (s, 4H), 2.62 (s, 6H). ¹³C NMR (500 MHz, CDCl₃, 300 K), δ (ppm): 197.42, 140.33, 137.40, 135.16, 128.98, 125.93, 116.20, 64.78, 26.65.

4.7 Supporting Information

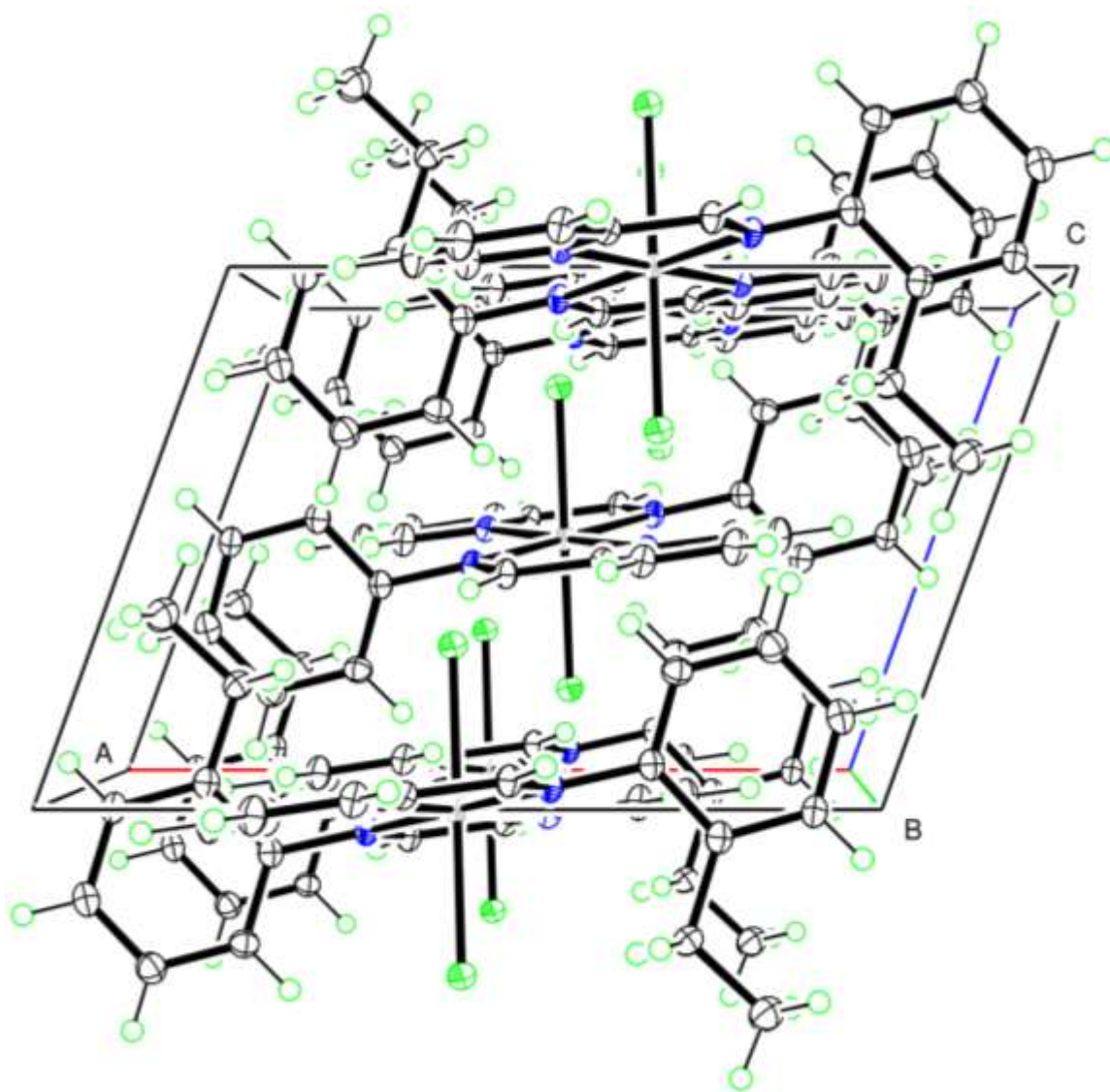


Figure 4.6. Unit cell representation of complex **Ni X-1**.

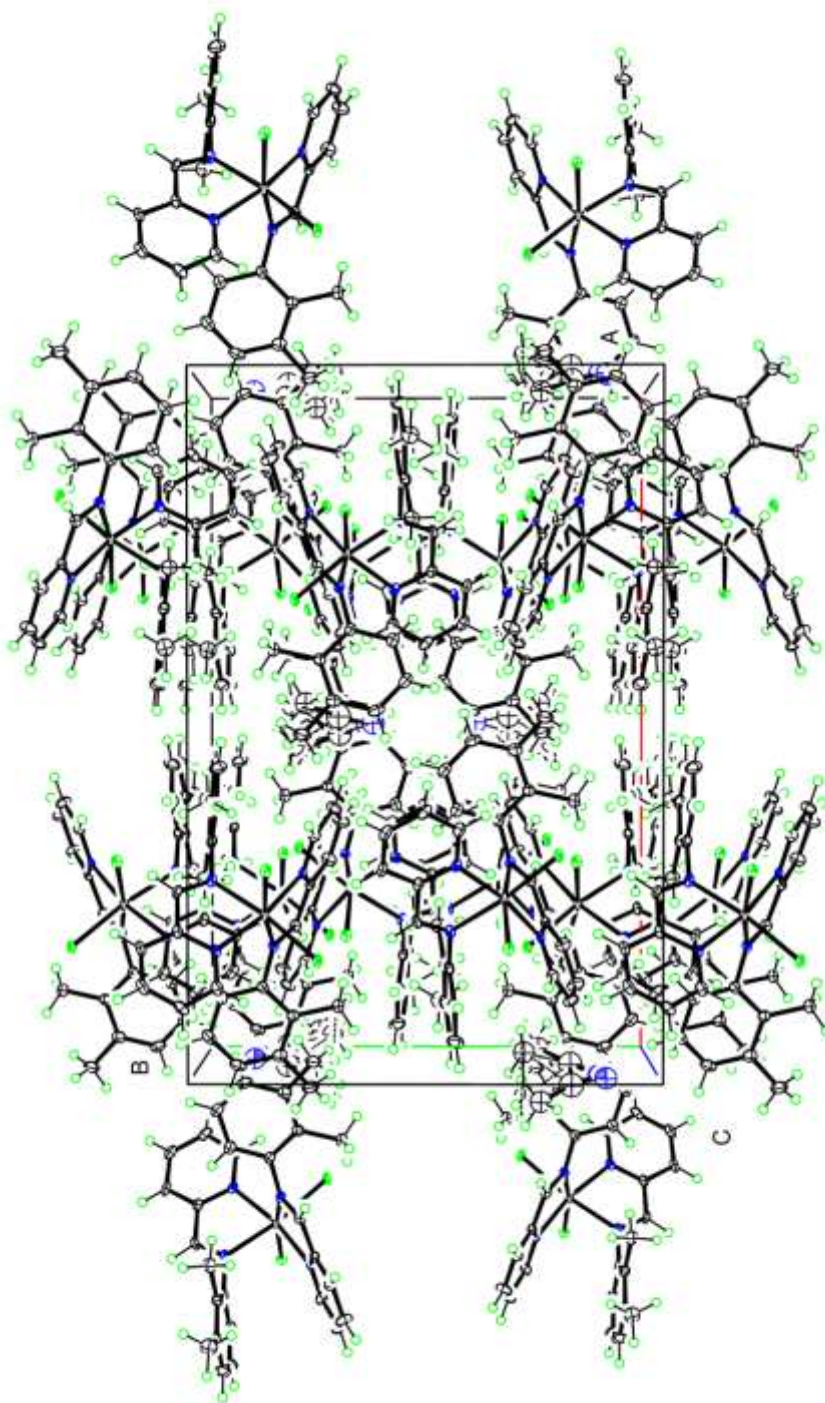


Figure 4.7. Unit cell representation of complex **Ni X-2**.

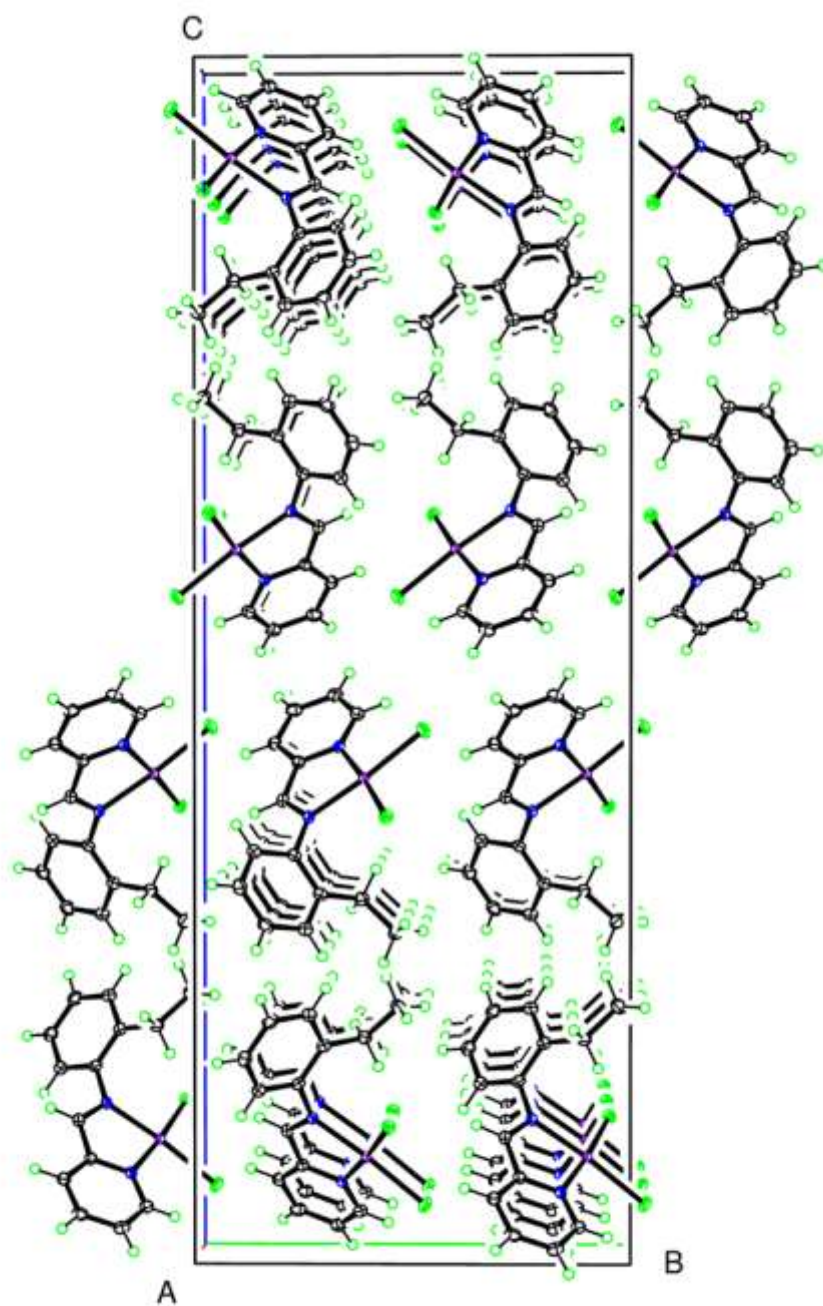


Figure 4.8. Unit cell representation of complex **Pd X-1**.

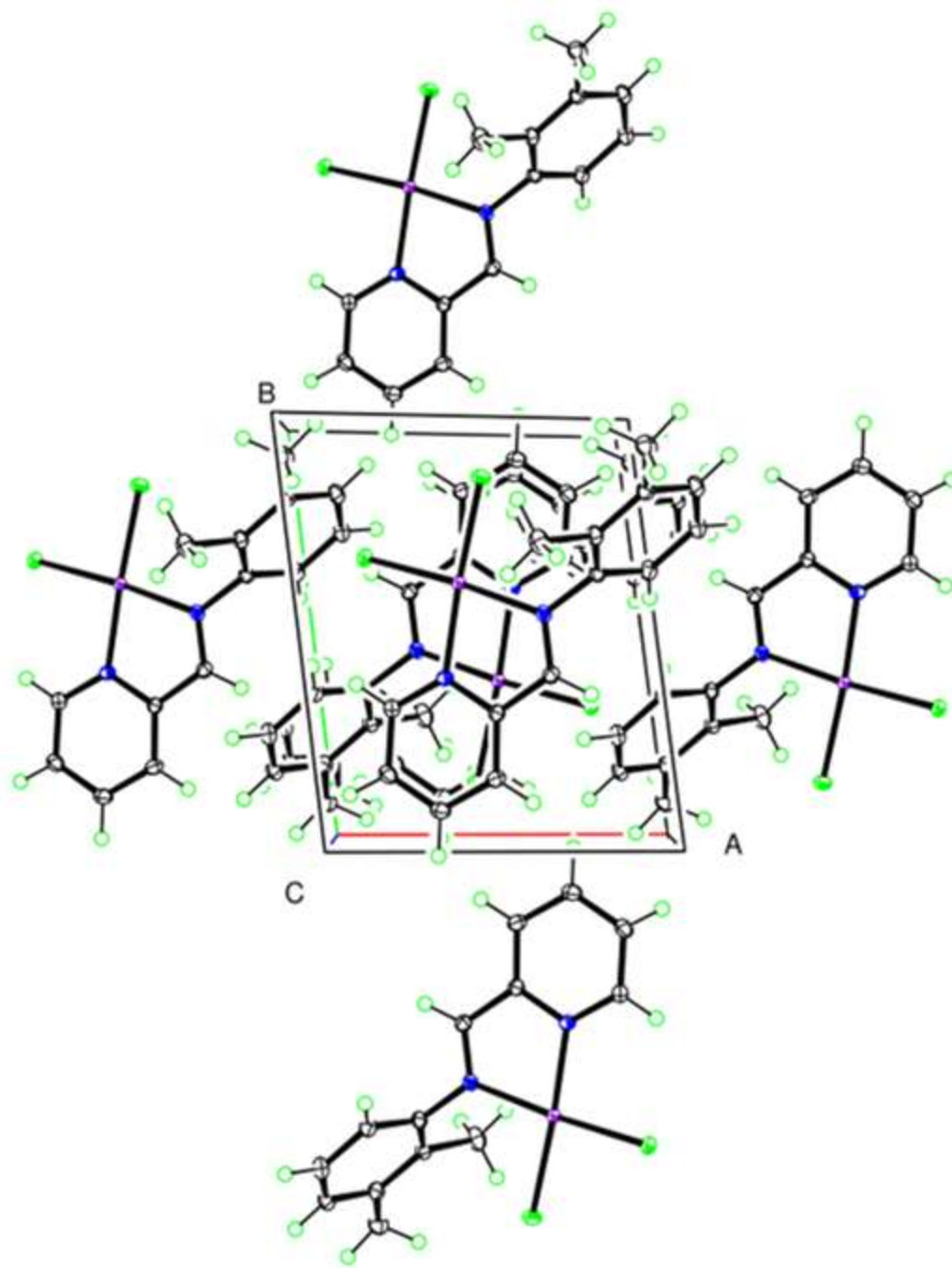


Figure 4.9. Unit cell representation of complex **Pd X-2**.

Table 4.3. Crystal data, data collection and refinement for complex Ni X-1 and Ni X-2.

Complexes	Ni X-1	Ni X-2
Crystallized from	CH ₃ CN	CH ₃ CN
Chemical formula	C ₂₈ H ₂₈ Cl ₂ N ₄ Ni	C ₂₈ H ₂₈ Cl ₂ N ₄ Ni·0.601(C ₂ H ₃ N)
Formula weight [g mol ⁻¹]	550.15	574.84
Crystal color, habit	Yellow, Fragment	Yellow, Plate
Crystal size (mm ³)	0.18 × 0.16 × 0.16	0.14 × 0.14 × 0.02
T (K)	100	100
Crystal system	Monoclinic	Orthorhombic
Space group	<i>P2₁/c</i>	<i>Pbcn</i>
a, b, c (Å)	12.196 (3), 13.347 (3), 8.298 (2)	23.142 (8), 15.323 (5), 15.564 (4)
α, β, γ (°)	β = 109.844 (11)	
V (Å ³)	1270.7 (6)	5519 (3)
Z	2	8
D _x (Mg m ⁻³)	1.438	1.384
μ (Mo-Kα) (mm ⁻¹)	1.00	0.92
F (000), θ range (°)	572, 2.3–30.5	2394, 2.6–30.5
No. of measured, independent and observed [I > 2σ(I)] reflections	46578, 3876, 3538	136290, 8429, 7736
R _{int}	0.035	0.097
Δρ _{max} , Δρ _{min} (e Å ⁻³)	0.71, -0.39	0.94, -1.00
No. of parameters	161	342
Refinement R[F ² > 2σ(F ²)], wR(F ²), S	0.029, 0.074, 1.08	0.081, 0.158, 1.31

Table 4.4. Crystal data, data collection and refinement for complex **Pd X-1** and **Pd X-2**.

Complexes	Pd X-1	Pd X-2
Crystallized from	DMF	DMF
Chemical formula	C ₁₄ H ₁₄ Cl ₂ N ₂ Pd	C ₁₄ H ₁₄ Cl ₂ N ₂ Pd
Formula weight [g mol ⁻¹]	387.57	387.57
Crystal color, habit	Orange, Blade	Orange, Block
Crystal size (mm ³)	0.49 × 0.12 × 0.02	0.20 × 0.16 × 0.12
T (K)	100	100
Crystal system	Orthorhombic	Triclinic,
Space group	<i>Pbca</i>	$P\bar{1}$
a, b, c (Å)	5.7395 (17), 13.363 (3), 36.945 (9)	7.935 (2), 9.451 (3), 10.083 (3)
α, β, γ (°)		97.771 (12), 105.521 (10), 95.285 (11)
V (Å ³)	2833.4 (13)	715.4 (4)
Z	8	2
D _x (Mg m ⁻³)	1.817	1.799
μ (Mo-Kα) (mm ⁻¹)	1.67	1.66
F (000), θ range (°)	1536, 3.1–30.5	384, 2.2–30.5
No. of measured, independent and observed [I > 2σ(I)] reflections	63373, 4329, 3652	16360, 4349, 4017
R _{int}	0.040	0.036
Δρ _{max} , Δρ _{min} (e Å ⁻³)	0.97, -0.83	0.55, -0.77
No. of parameters	174	175
Refinement R[F ² > 2σ(F ²)], wR(F ²), S	0.030, 0.063, 1.19	0.024, 0.052, 1.06

Table 4.5. Selected bond lengths and angles for complexes **Ni A-1** and **Ni B-1**.

Complex	Selected bond distances (Å)	Selected bond angles [°]
Ni X-1	Ni1—N1 ⁱ 2.1133 (11), Ni1—N1 2.1133 (11), Ni1—N2 ⁱ 2.1380 (12), Ni1—N2 2.1380 (11), Ni1—Cl1 2.3889 (7), Ni1—Cl1 ⁱ 2.3890 (7)	N1—Ni1—N2 78.15 (5), N1 ⁱ — Ni1—N2 101.85 (5), N1 ⁱ —Ni1— N2 ⁱ 78.15 (5), N1—Ni1—N2 ⁱ 101.85 (5), Cl1—Ni1—Cl1 ⁱ 179.999 (15)
Ni X-2	Ni1—N1 2.082 (3), Ni1—N3 2.092 (3), Ni1—N2 2.127 (3), Ni1—N4 2.128 (3), Ni1—Cl1 2.3893 (10), Ni1—Cl2 2.4239 (10)	N1—Ni1—N2 77.95 (11), N3— Ni1—N2 89.36 (10), N3—Ni1— N4 78.18 (10), N1—Ni1—N4 99.13 (10), Cl1—Ni1—Cl2 92.66 (3)

Table 4.6. Selected bond lengths and angles for complexes **Pd A-1** and **Pd B-1**.

Complex	Selected bond distances (Å):	Selected bond angles [°]:
	Pd1—N1, Pd1—N2, Pd1—Cl2, Pd1—Cl1	N1—Pd1—N2, N1—Pd1—Cl2, N2—Pd1—Cl2, N1—Pd1—Cl1, N2—Pd1—Cl1, Cl2—Pd1—Cl1
Pd X-1	2.025 (2), 2.045 (2), 2.2894 (8), 2.2879 (8)	80.89 (9), 174.53 (6), 94.71 (7), 93.56 (6), 174.31 (6), 90.76 (3)
Pd X-2	2.0221 (16), 2.0305 (16), 2.2727 (8), 2.2945 (7)	80.27 (6), 174.73 (5), 94.94 (5), 94.71 (5), 173.69 (5), 90.21 (2)

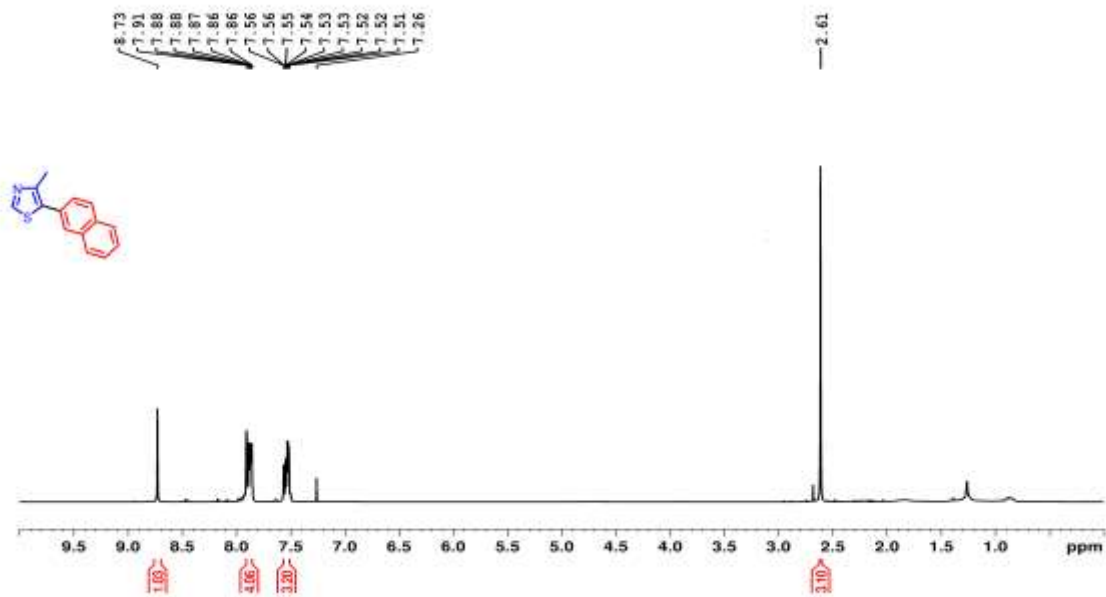


Figure 4.10. ^1H NMR spectrum of **CD1**.

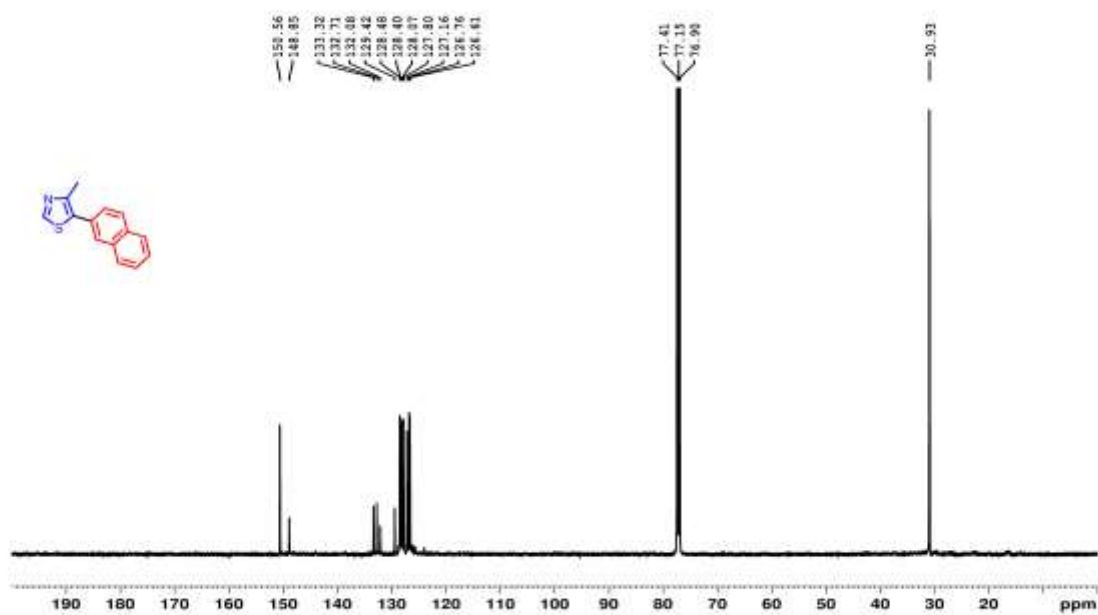


Figure 4.11. ^{13}C NMR spectrum of **CD1**.

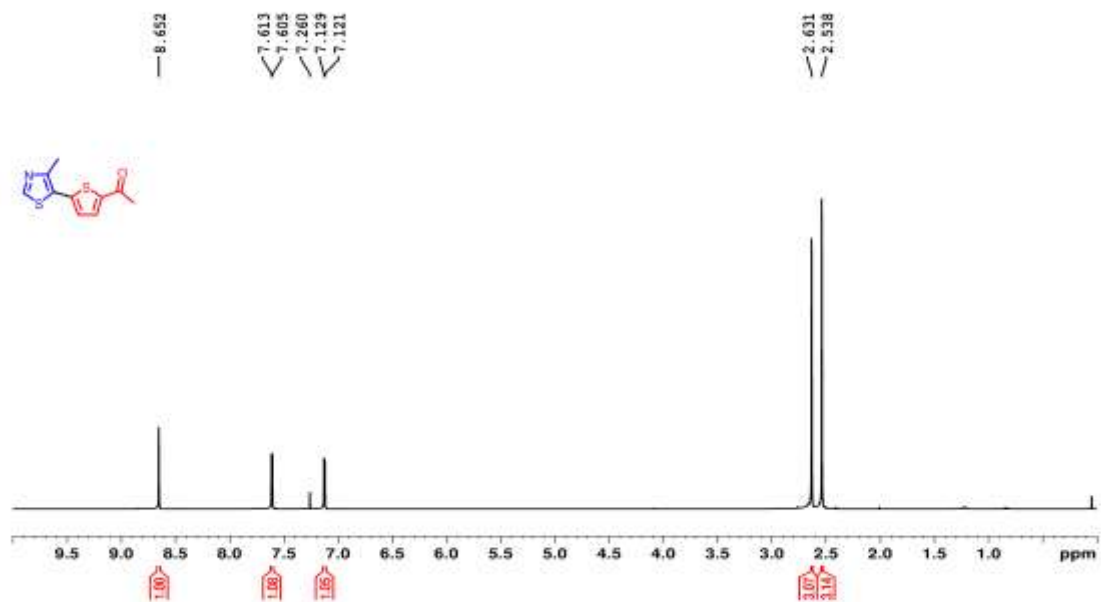


Figure 4.12. ^1H NMR spectrum of **CD2**.

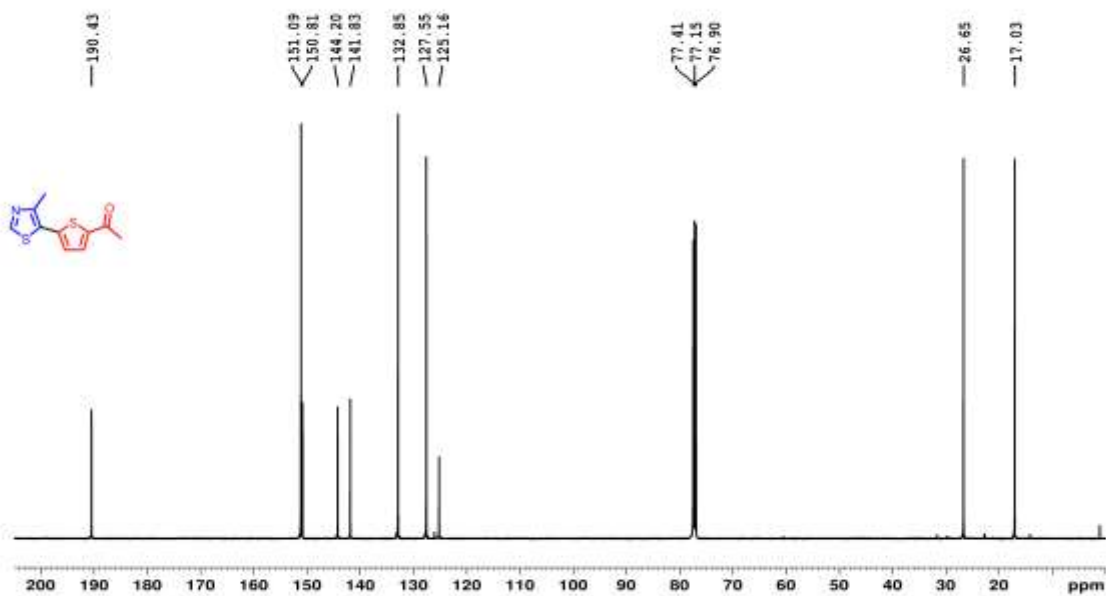


Figure 4.13. ^{13}C NMR spectrum of **CD2**.

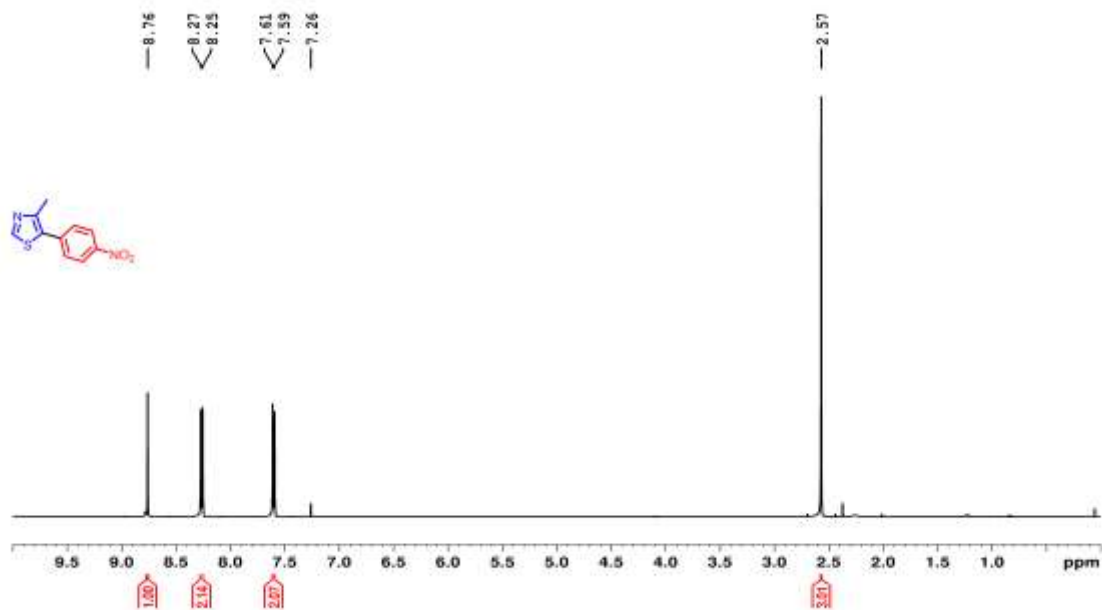


Figure 4.14. ^1H NMR spectrum of **CD3**.

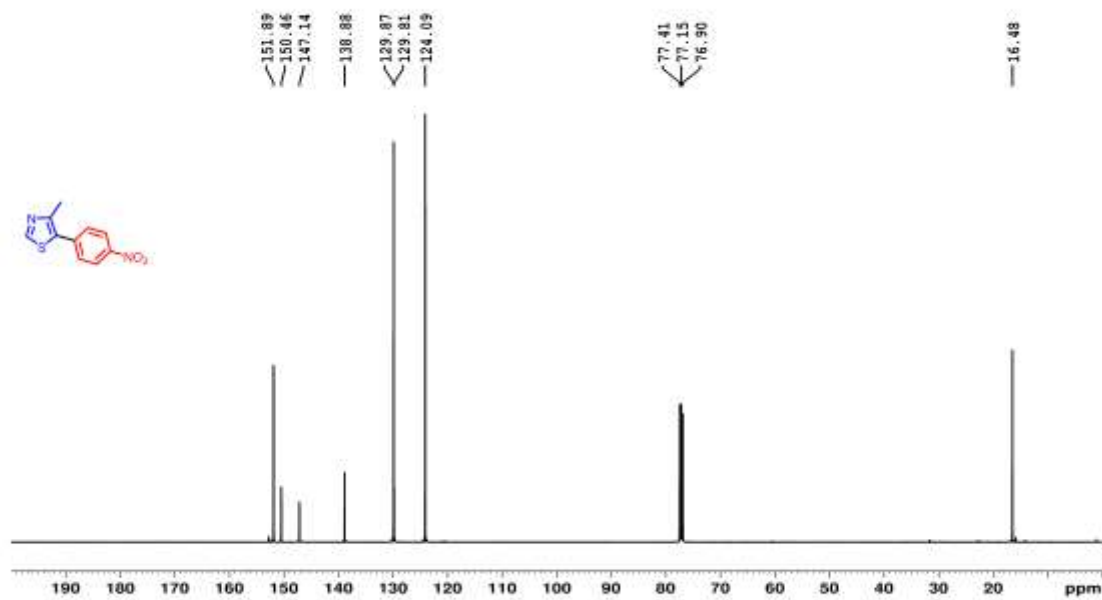


Figure 4.15. ^{13}C NMR spectrum of **CD3**.

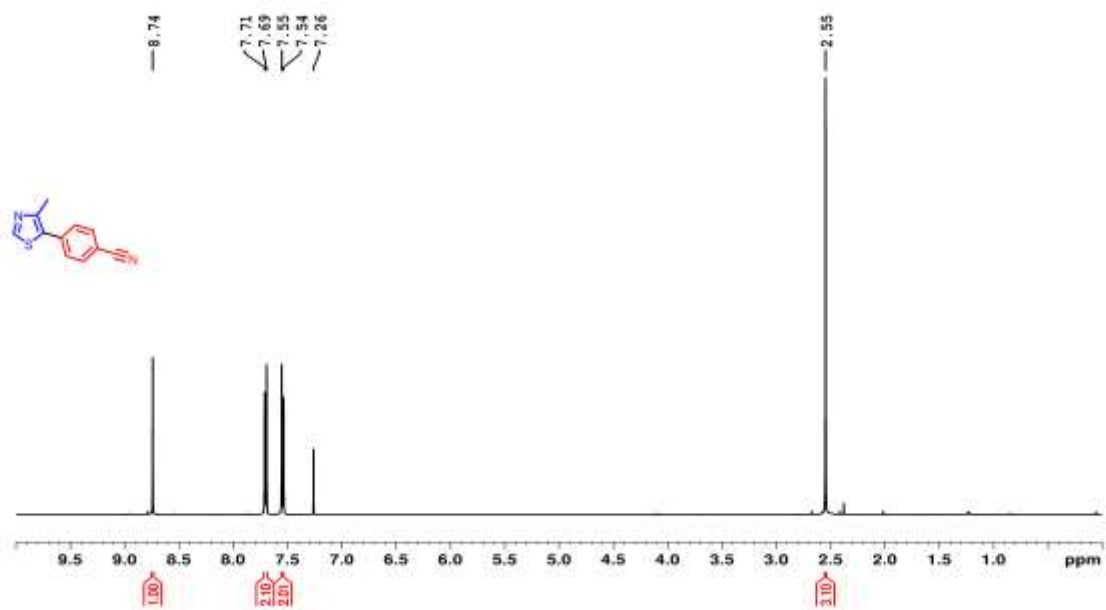


Figure 4.16. ^1H NMR spectrum of **CD4**.

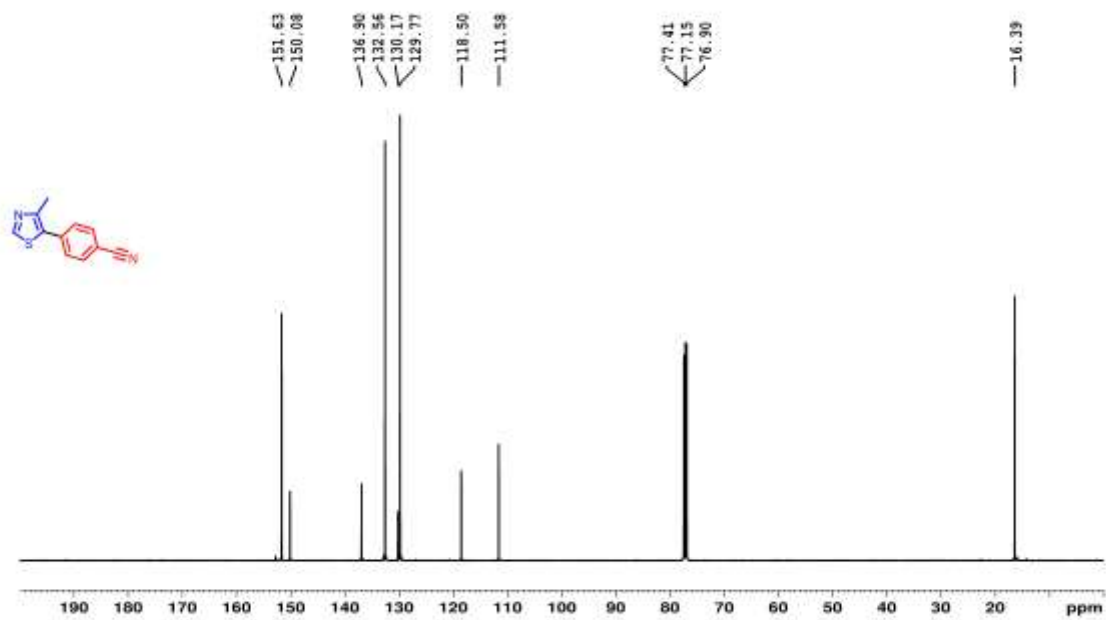


Figure 4.17. ^{13}C NMR spectrum of **CD4**.

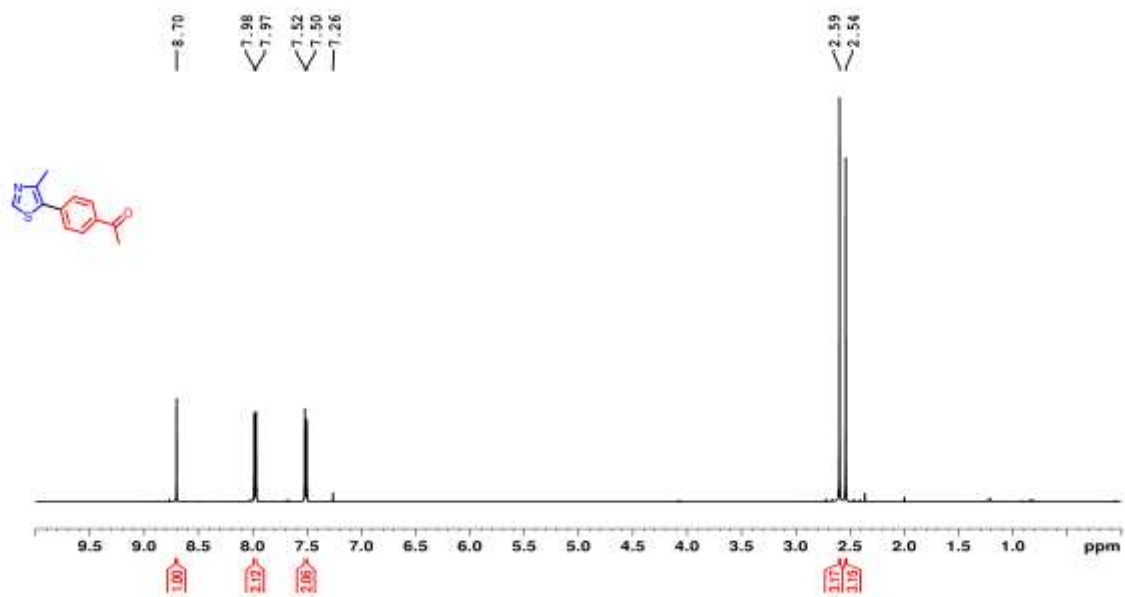


Figure 4.18. ^1H NMR spectrum of **CD5**.

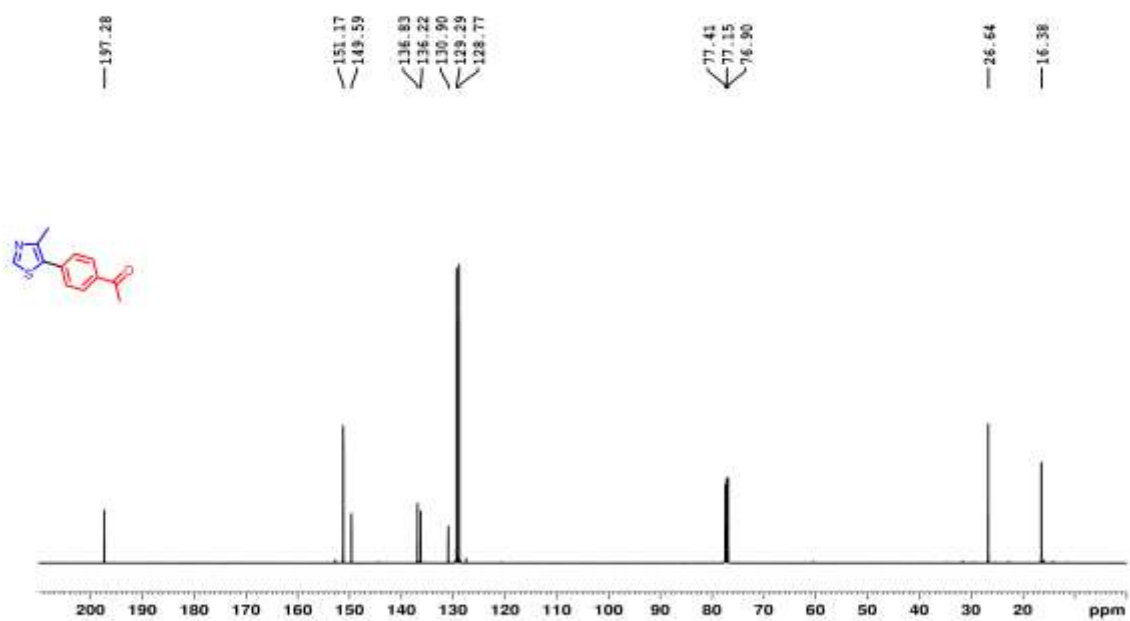


Figure 4.19. ^{13}C NMR spectrum of **CD5**.

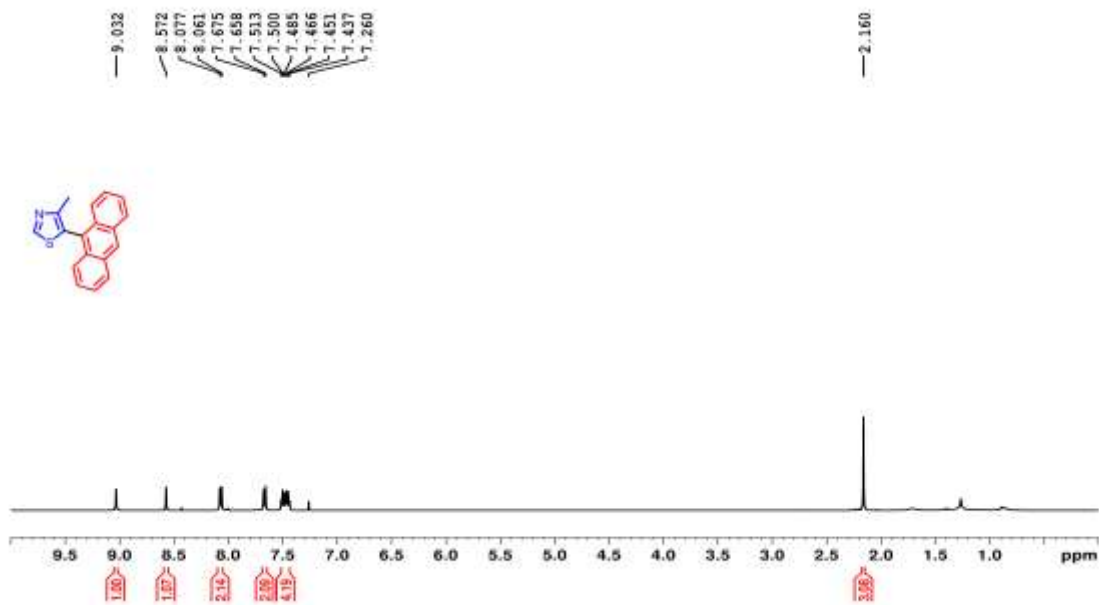


Figure 4.20. ^1H NMR spectrum of CD6.

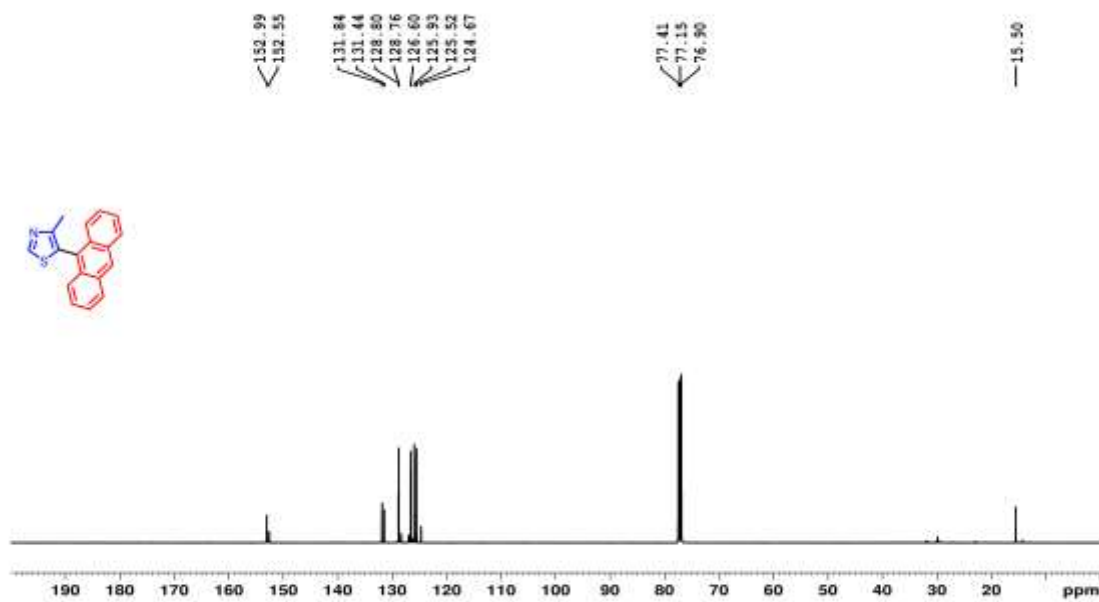


Figure 4.21. ^{13}C NMR spectrum of CD6.

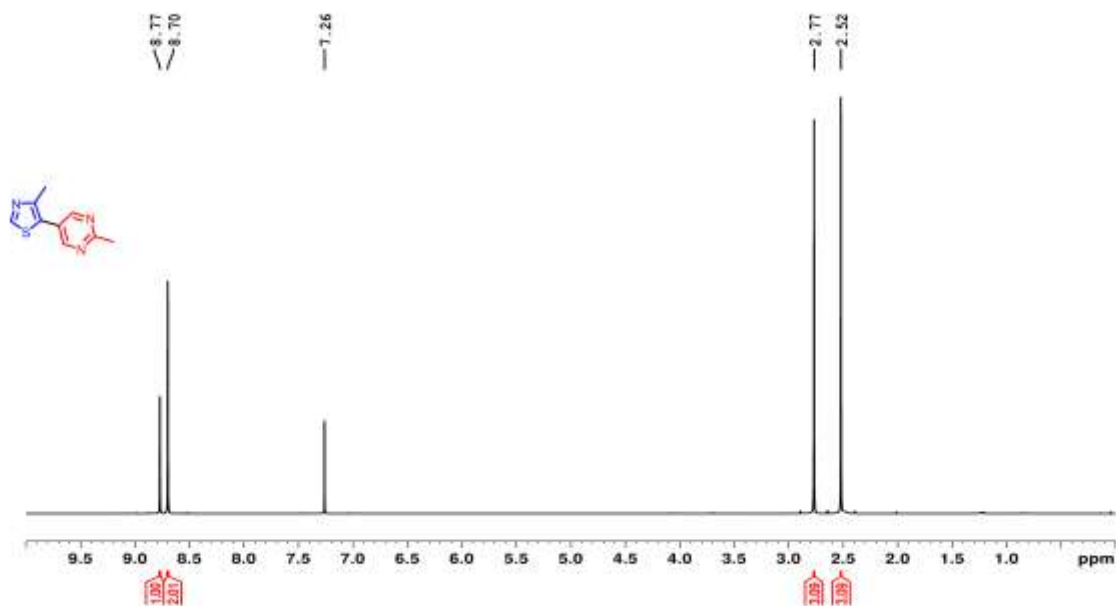


Figure 4.22. ^1H NMR spectrum of **CD7**.

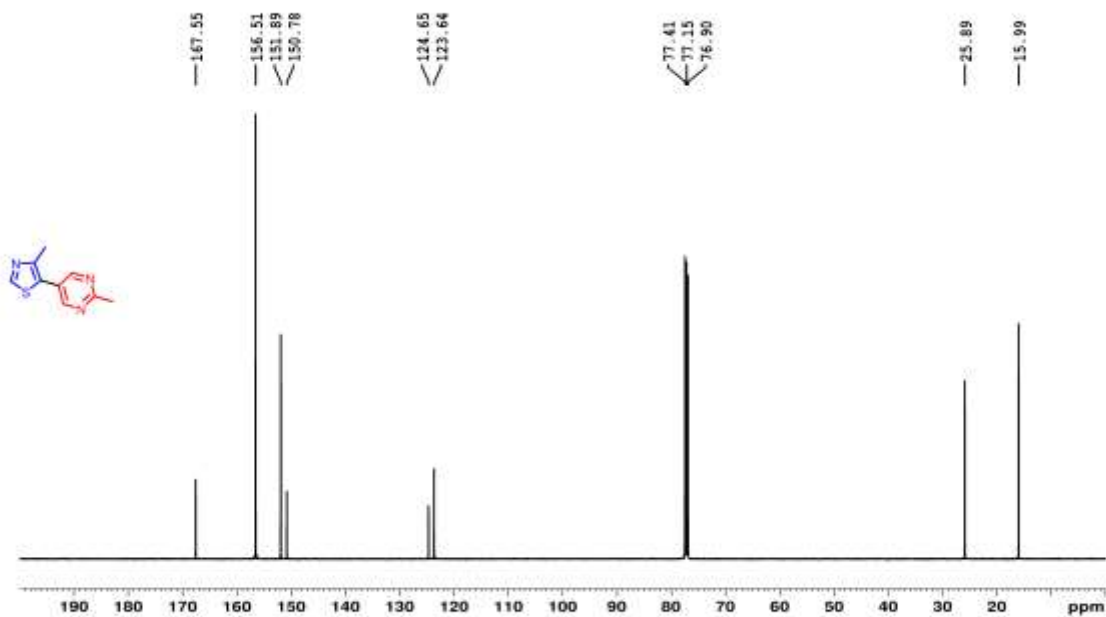


Figure 4.23. ^{13}C NMR spectrum of **CD7**.

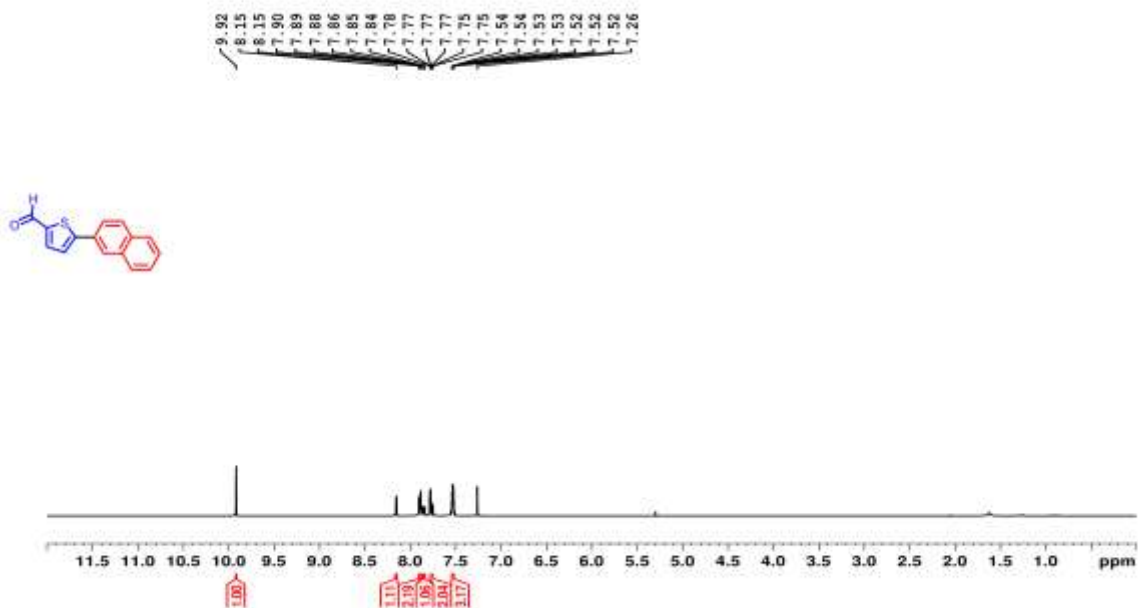


Figure 4.24. ^1H NMR spectrum of **CD8**.

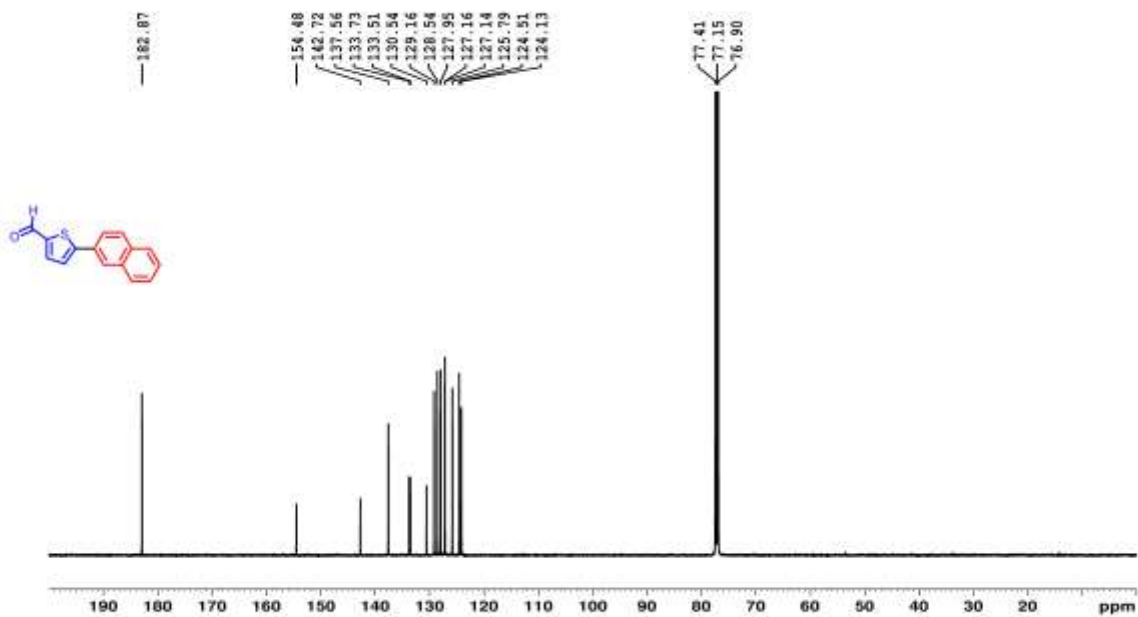


Figure 4.25. ^{13}C NMR spectrum of **CD8**.

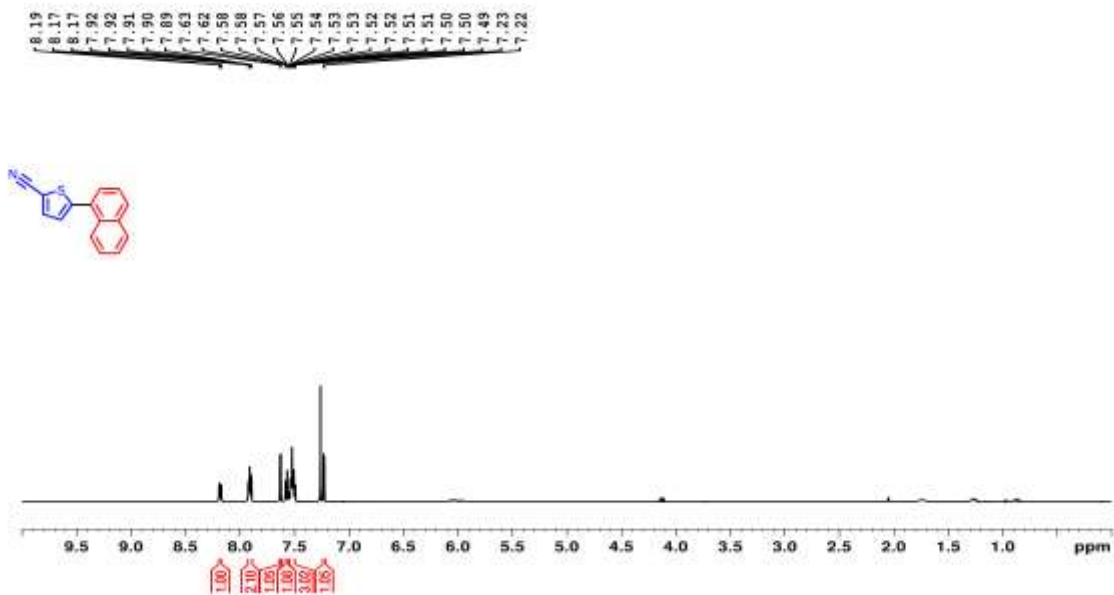


Figure 4.26. ^1H NMR spectrum of **CD9**.

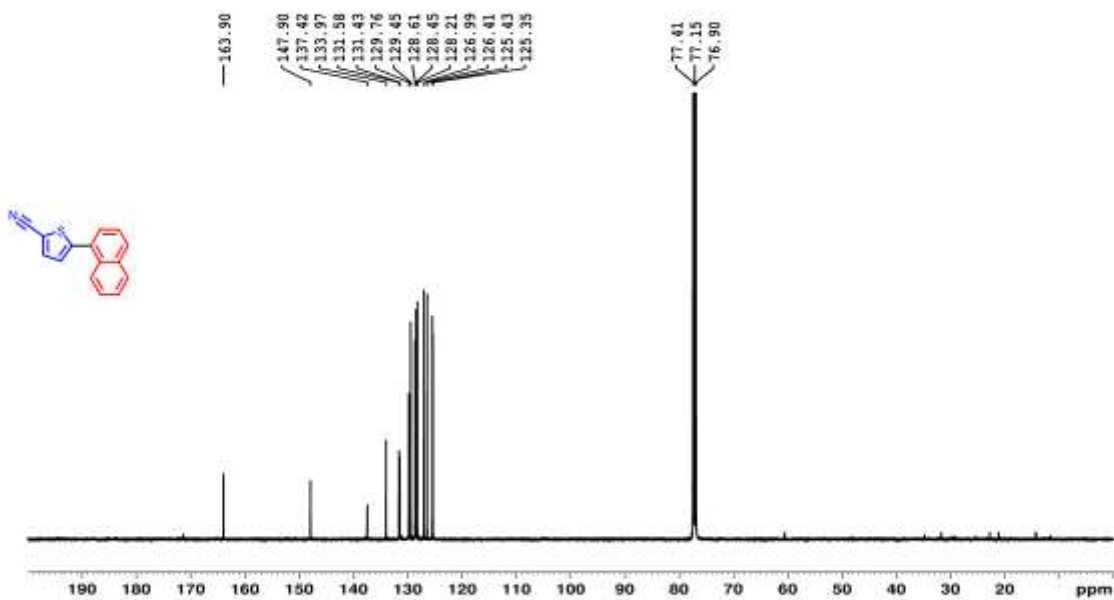


Figure 4.27. ^{13}C NMR spectrum of **CD9**.

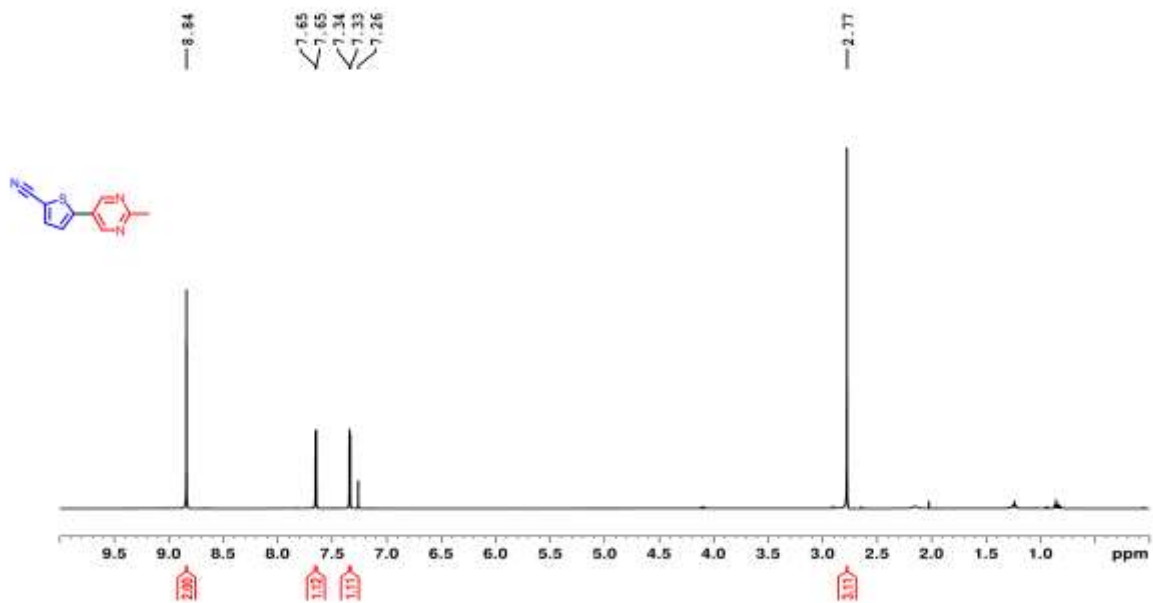


Figure 4.28. ^1H NMR spectrum of **CD10**.

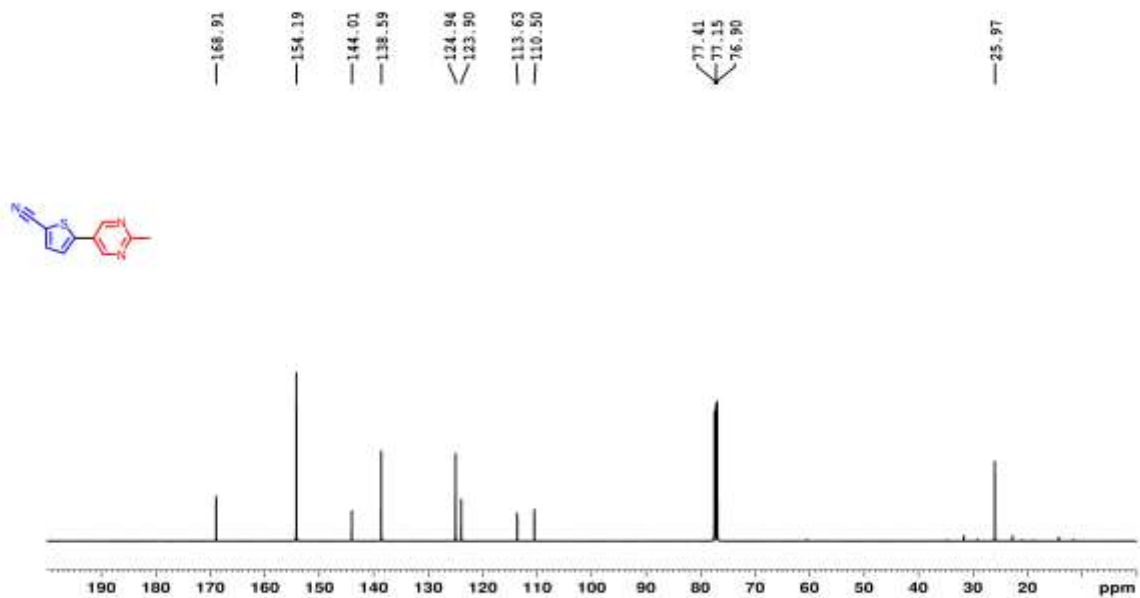


Figure 4.29. ^{13}C NMR spectrum of **CD10**.

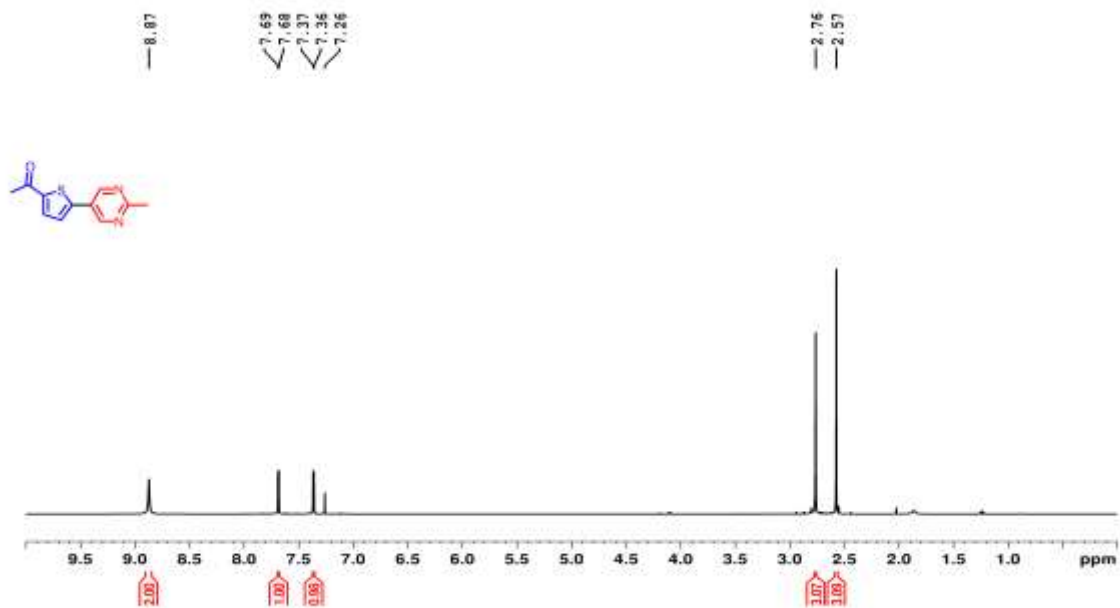


Figure 4.30. ^1H NMR spectrum of **CD11**.

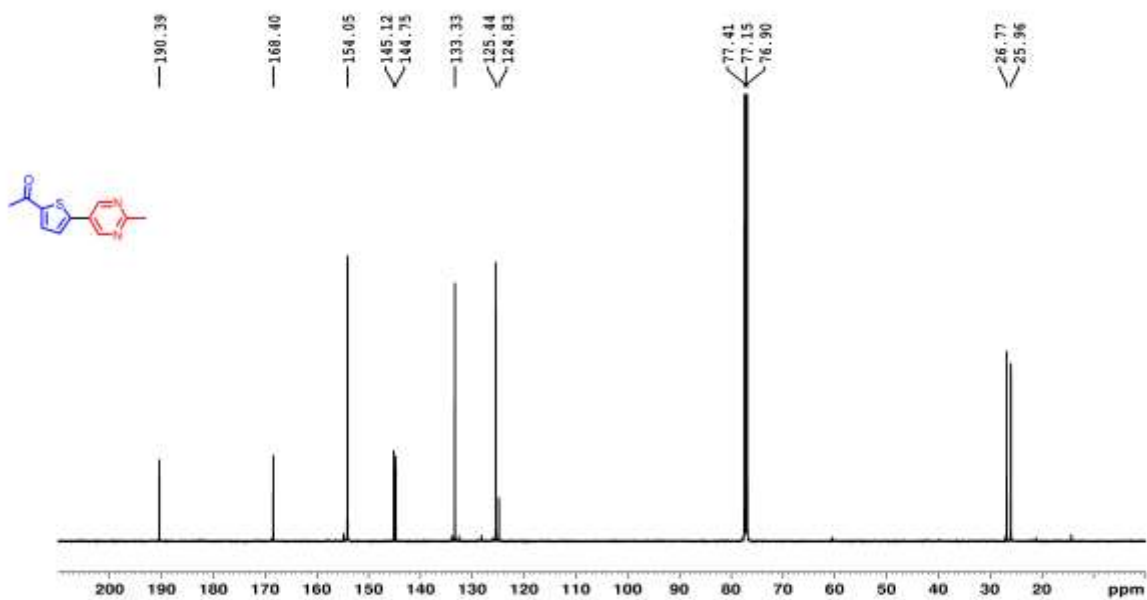


Figure 4.31. ^{13}C NMR spectrum of **CD11**.

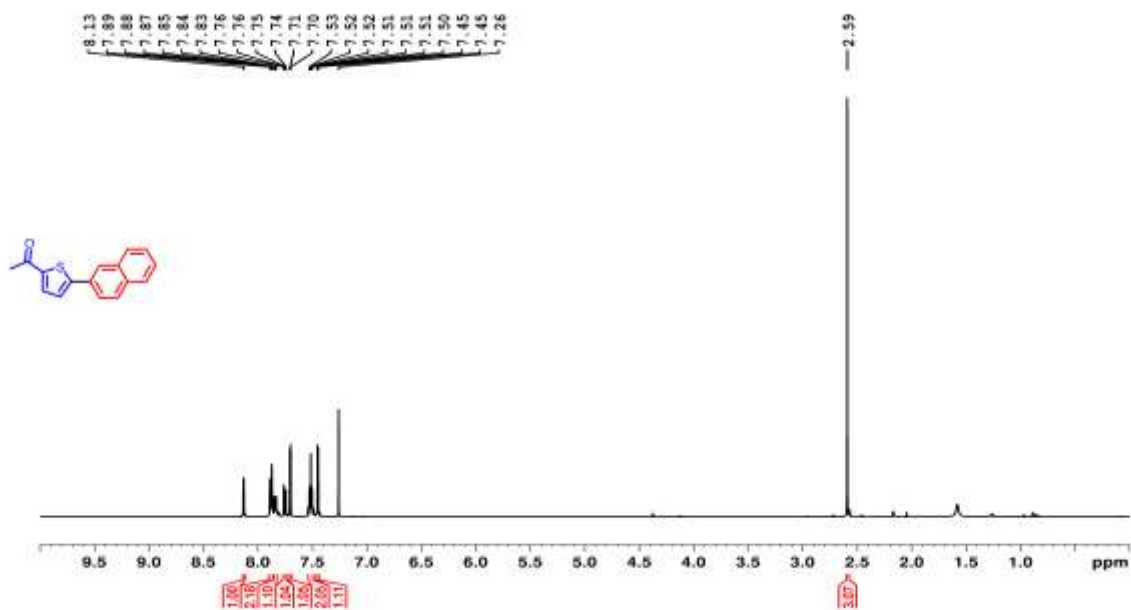


Figure 4.32. ¹H NMR spectrum of CD12.

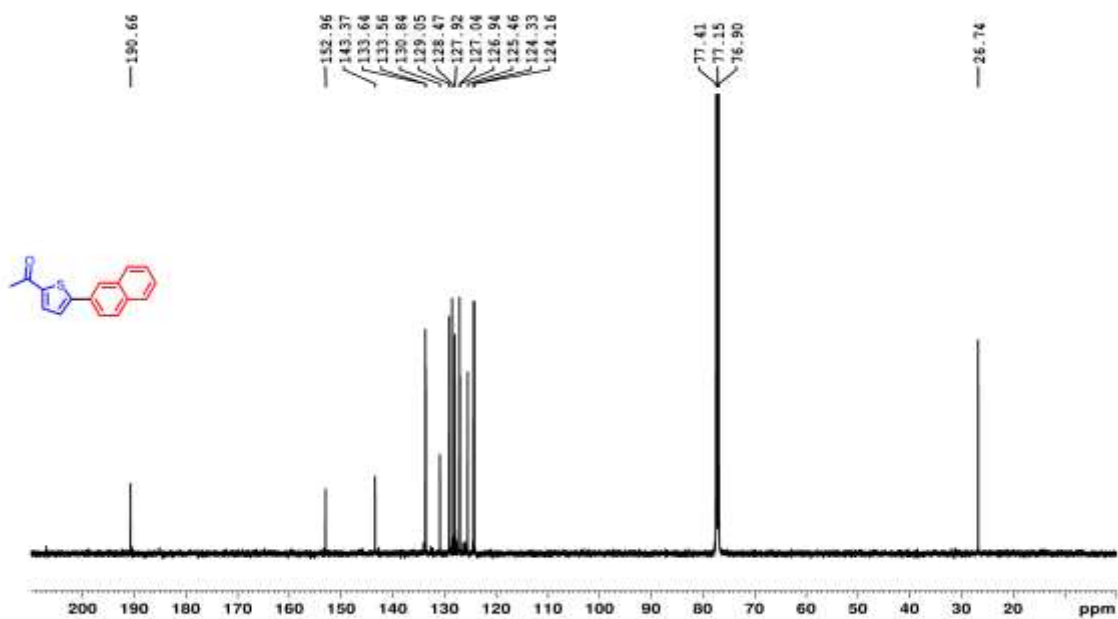


Figure 4.33. ¹³C NMR spectrum of CD12.

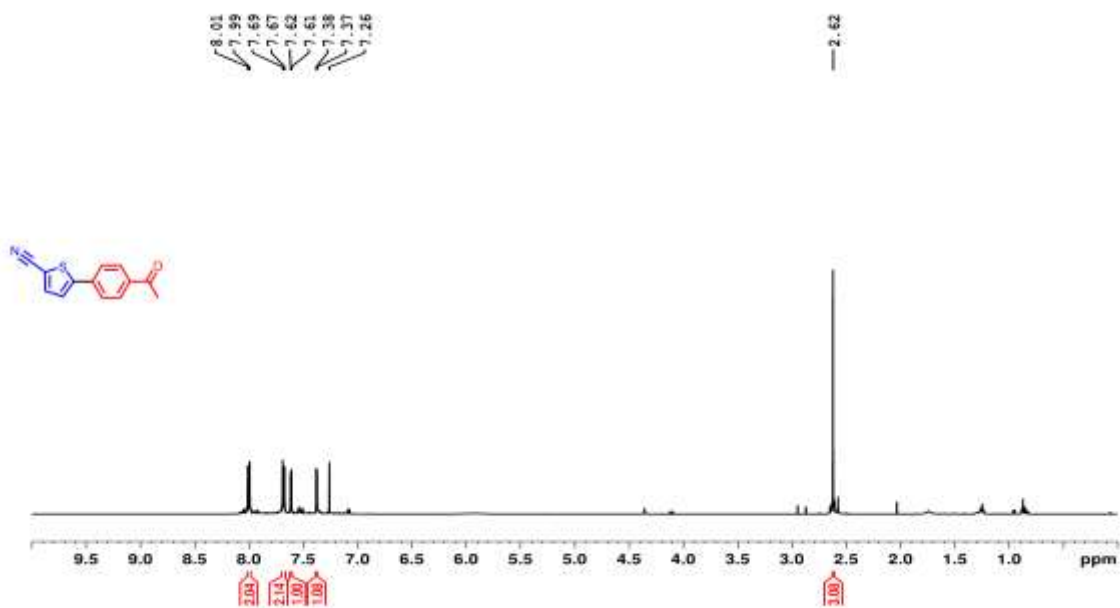


Figure 4.34. ^1H NMR spectrum of **CD13**.

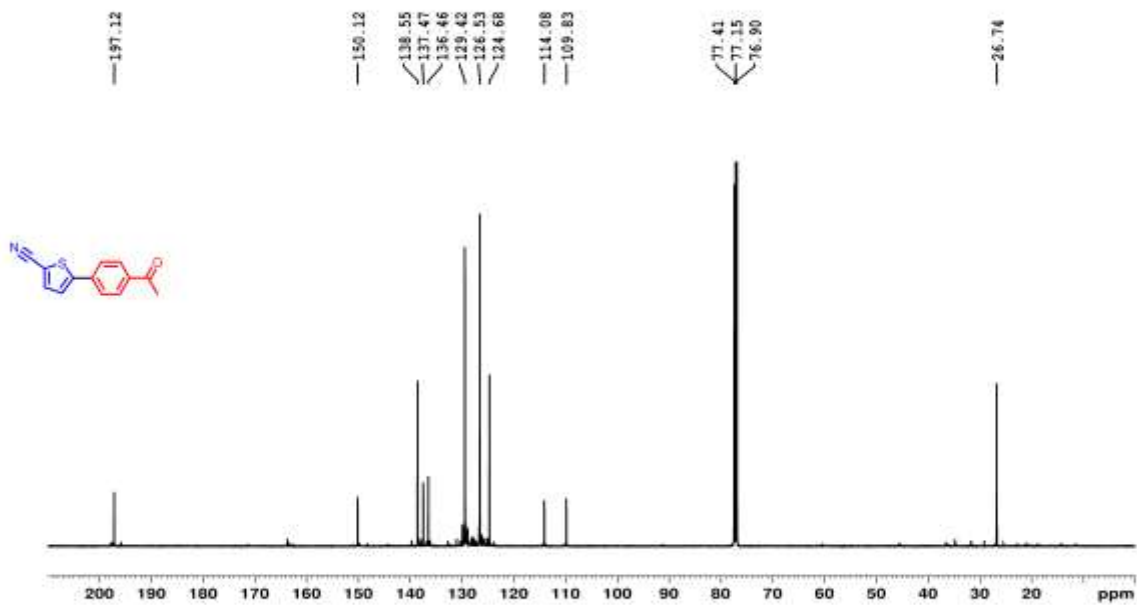


Figure 4.35. ^{13}C NMR spectrum of **CD13**.

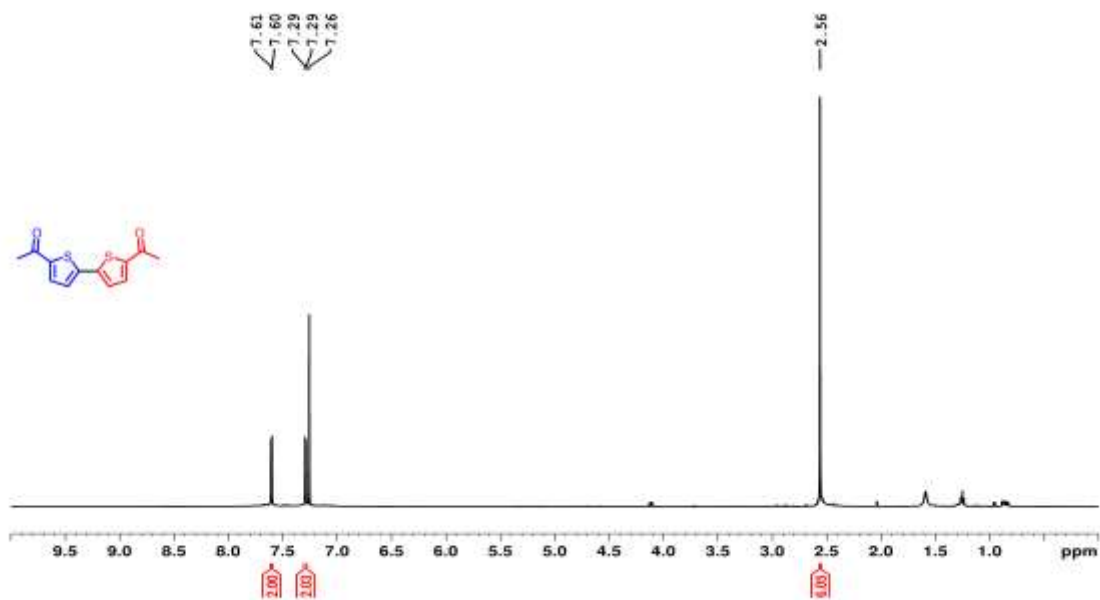


Figure 4.36. ^1H NMR spectrum of **CD14**.

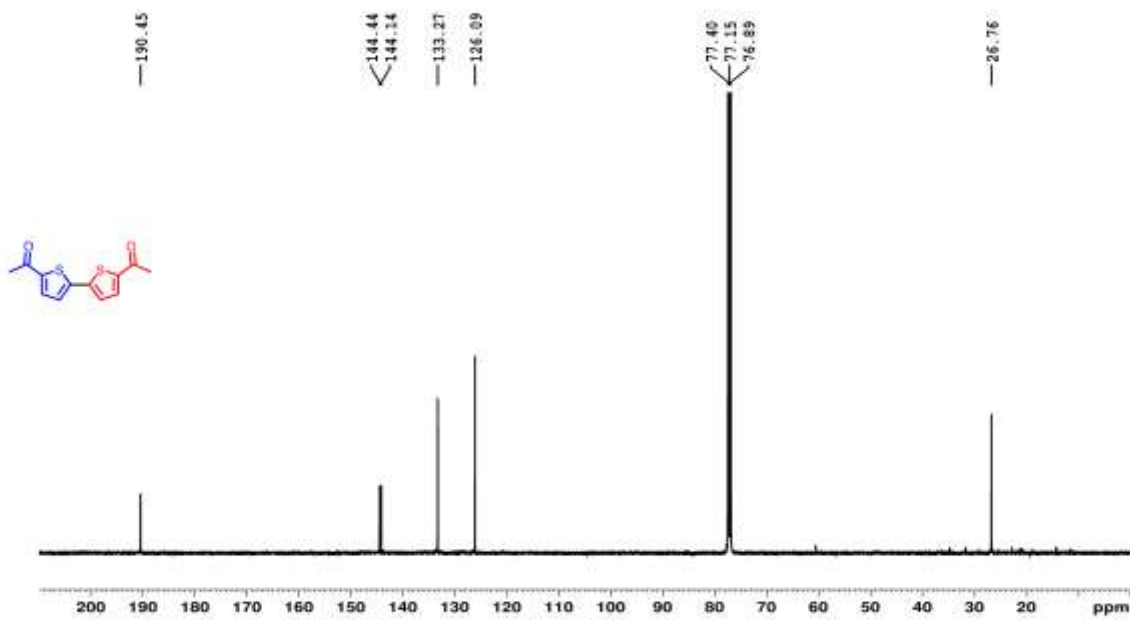


Figure 4.37. ^{13}C NMR spectrum of **CD14**.

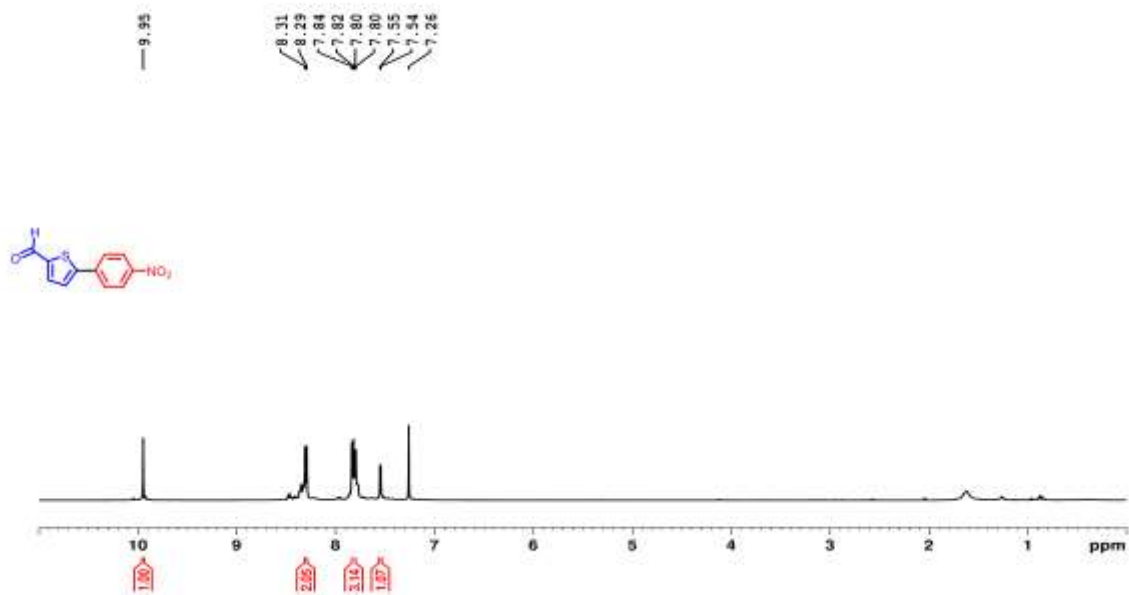


Figure 4.38. ¹H NMR spectrum of **CD15**.

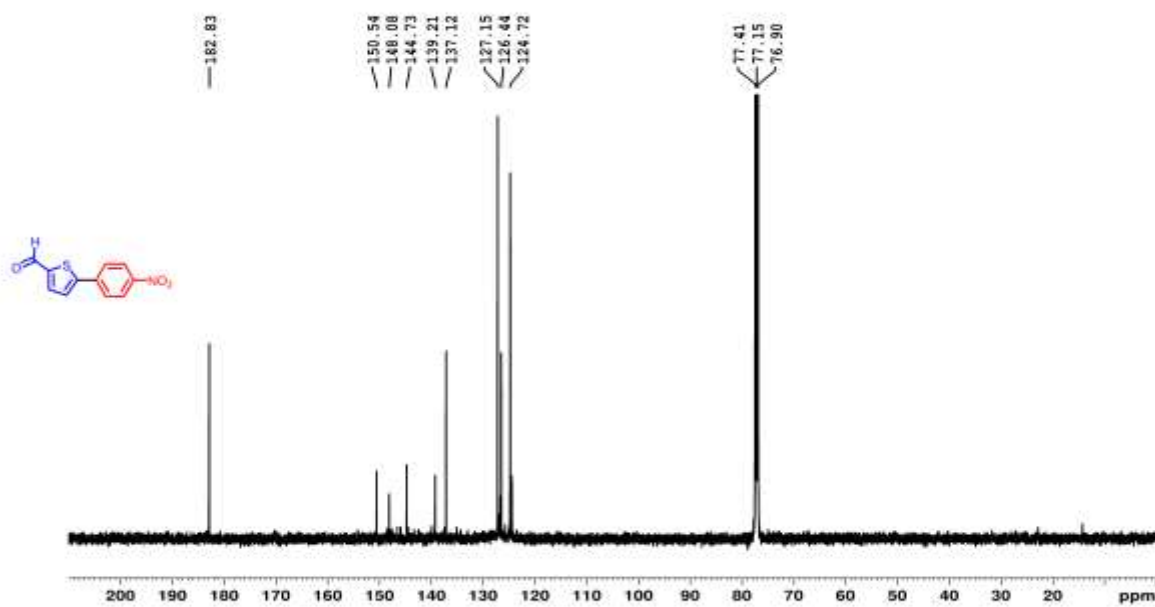


Figure 4.39. ¹³C NMR spectrum of **CD15**.

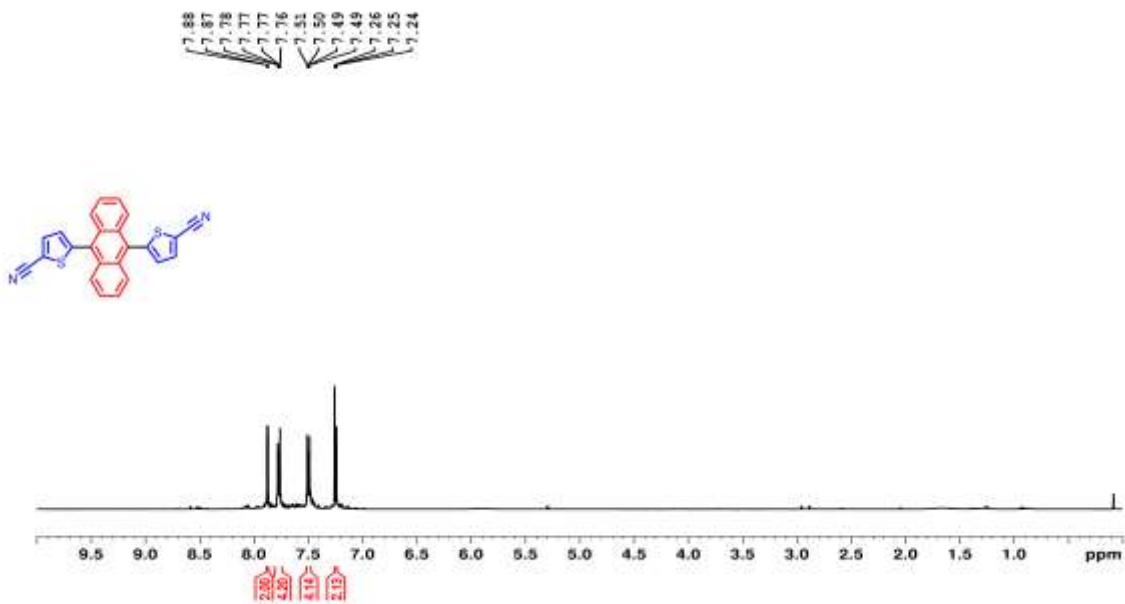


Figure 4.40. ^1H NMR spectrum of CD16.

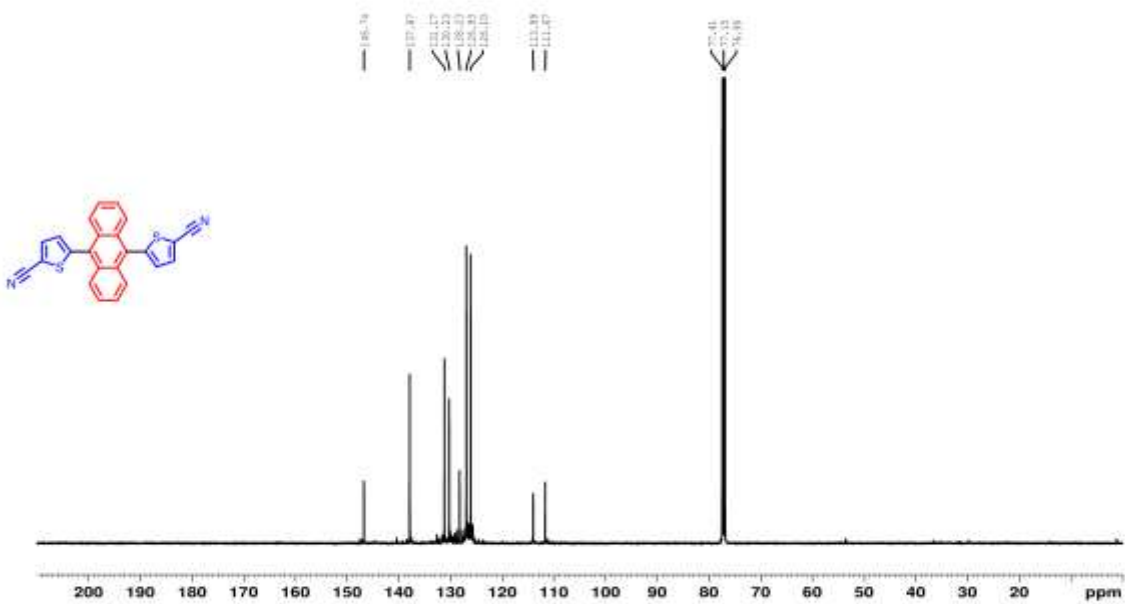


Figure 4.41. ^{13}C NMR spectrum of CD16.

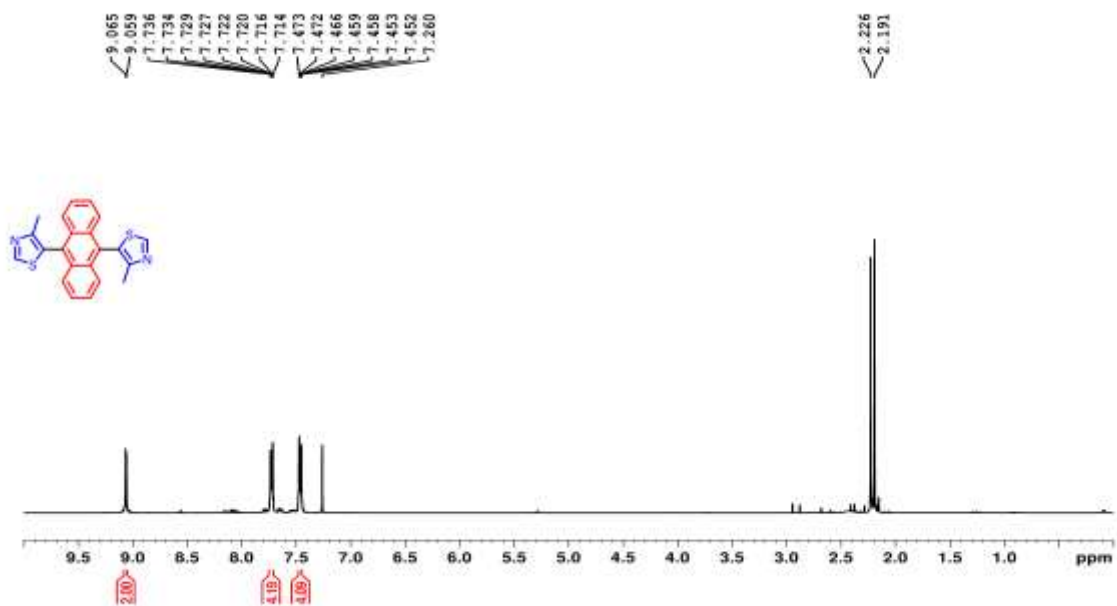


Figure 4.42. ^1H NMR spectrum of CD17.

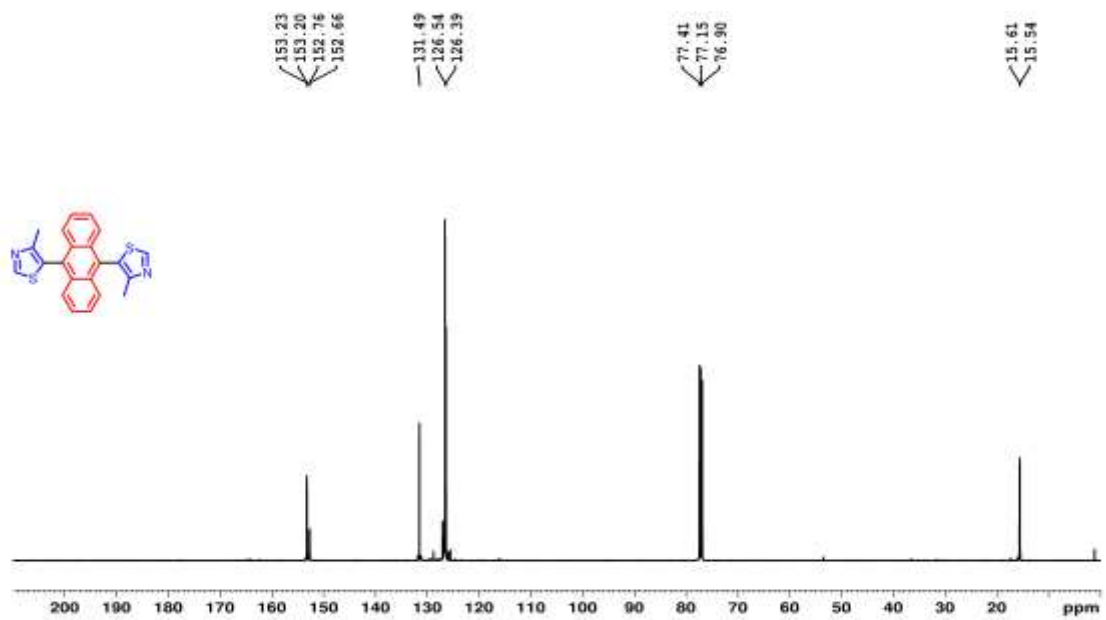


Figure 4.43. ^{13}C NMR spectrum of CD17.

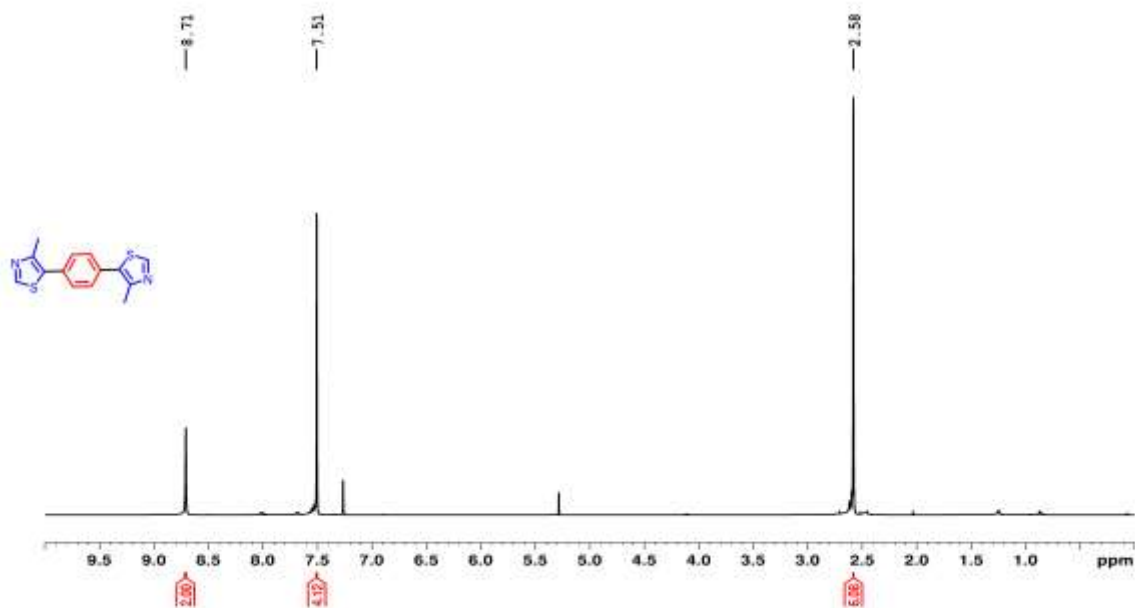


Figure 4.44. ^1H NMR spectrum of **CD18**.

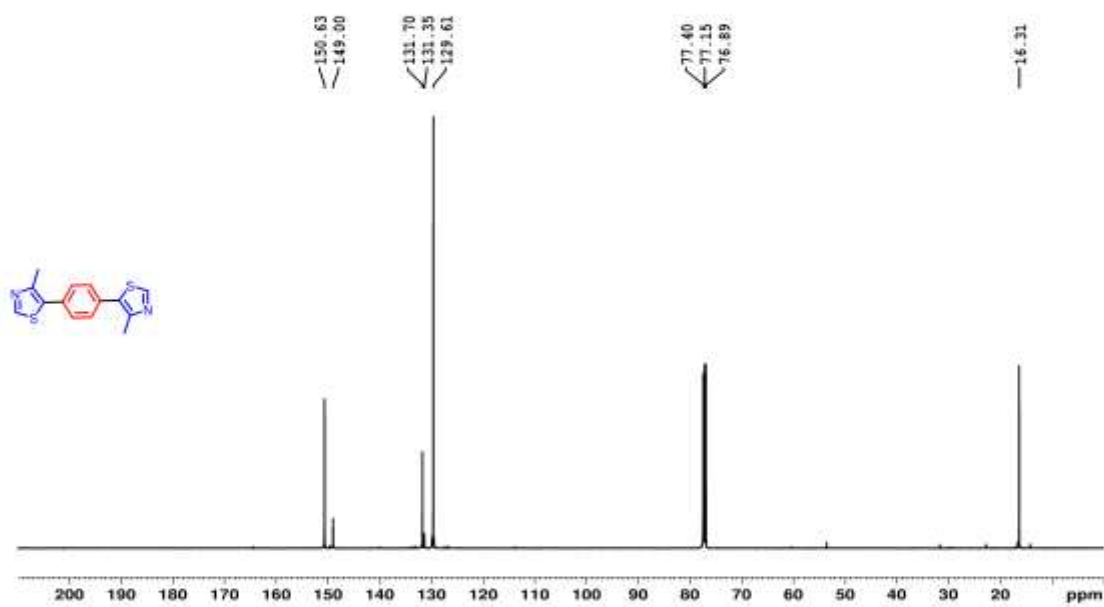


Figure 4.45. ^{13}C NMR spectrum of **CD18**.

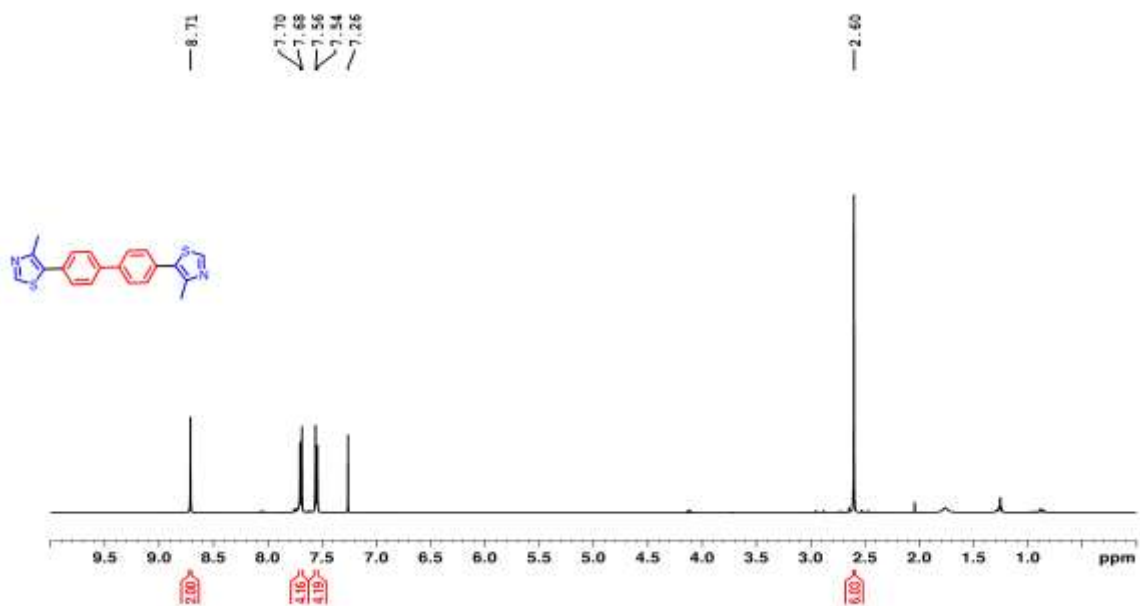


Figure 4.46. ^1H NMR spectrum of **CD19**.

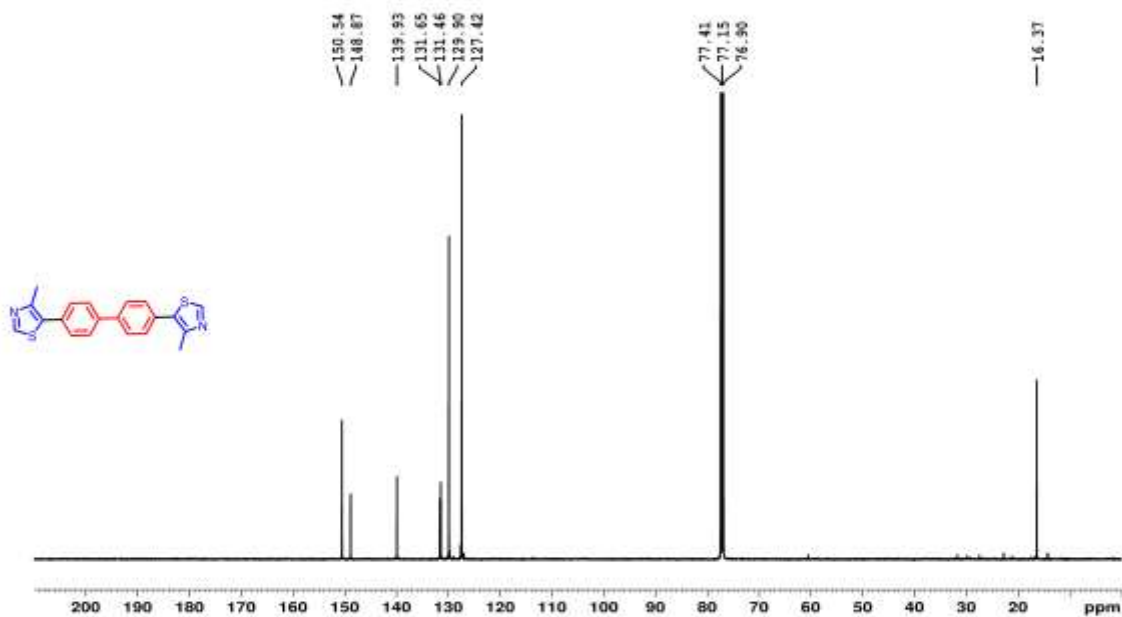


Figure 4.47. ^{13}C NMR spectrum of **CD19**.

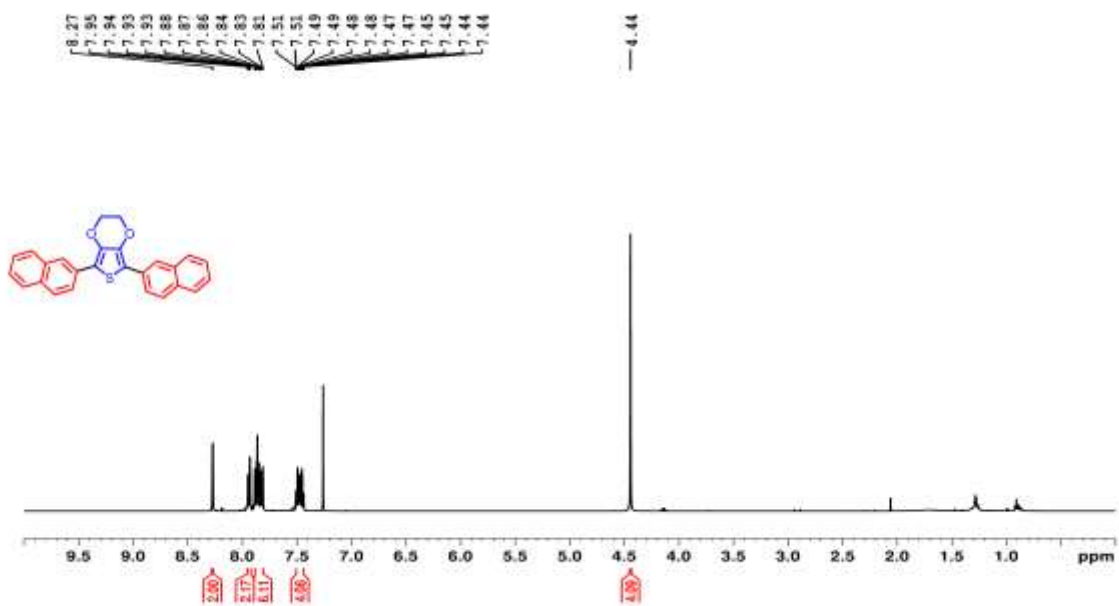


Figure 4.48. ¹H NMR spectrum of **CD20**.

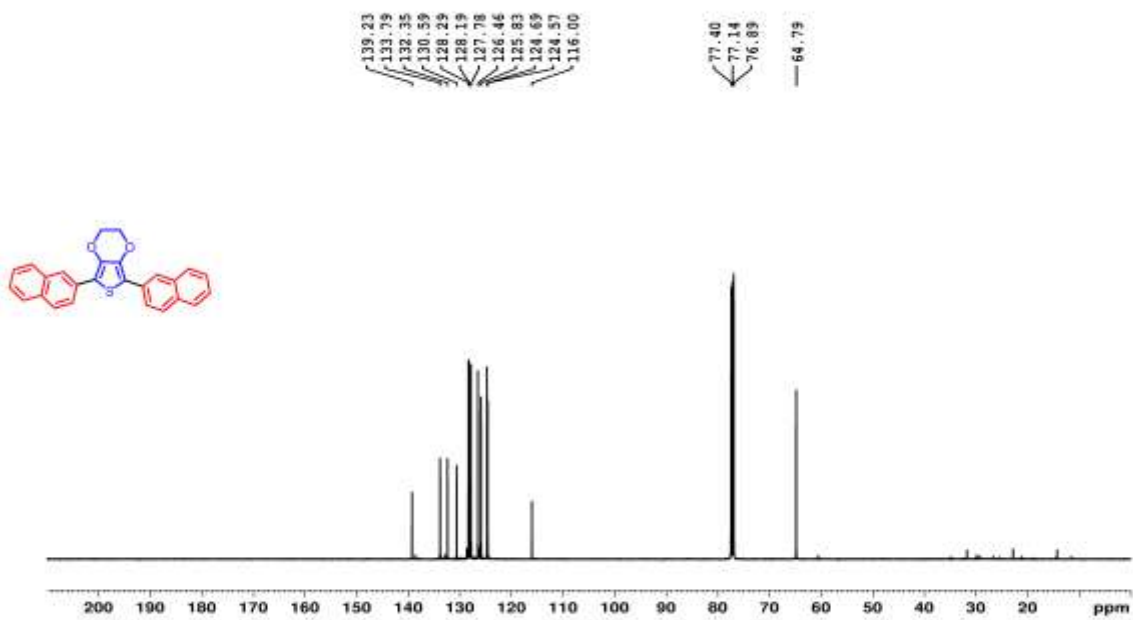


Figure 4.49. ¹³C NMR spectrum of **CD20**.

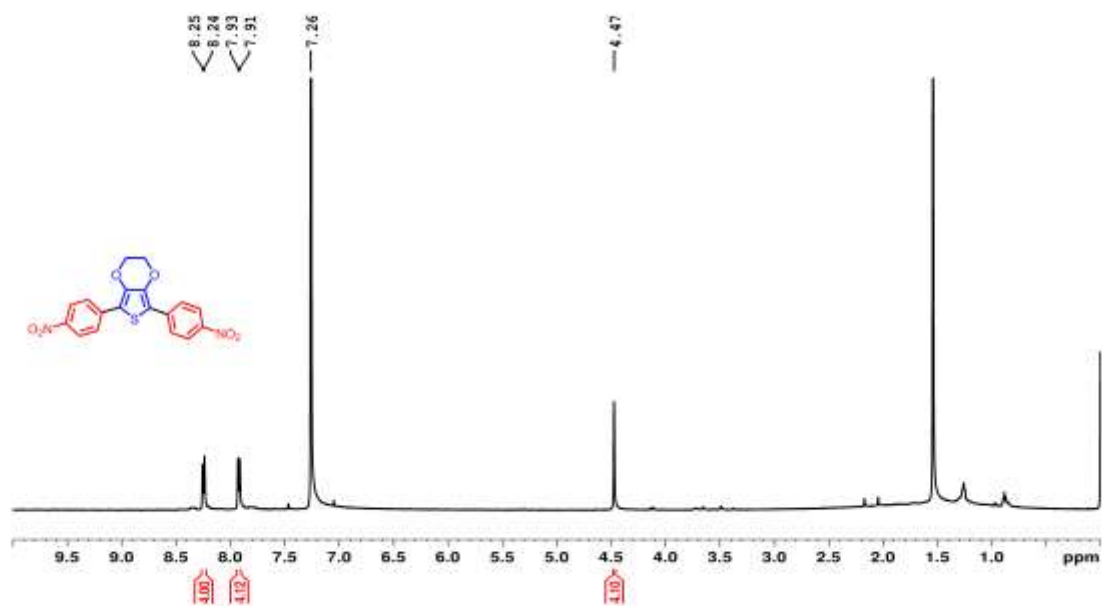


Figure 4.50. ^1H NMR spectrum of **CD21**.

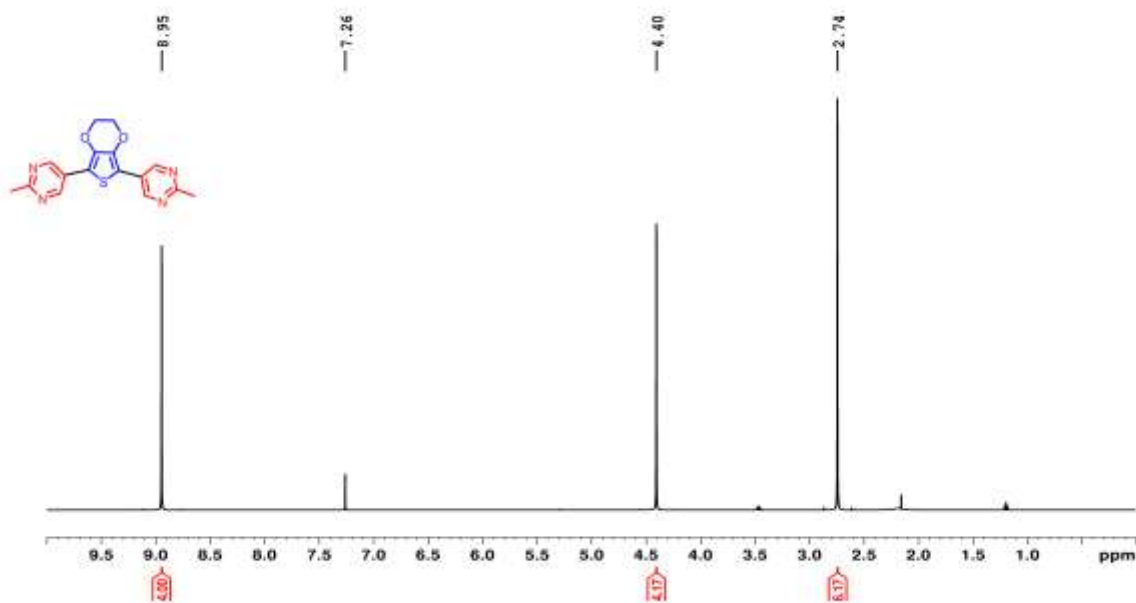


Figure 4.51. ^1H NMR spectrum of **CD22**.

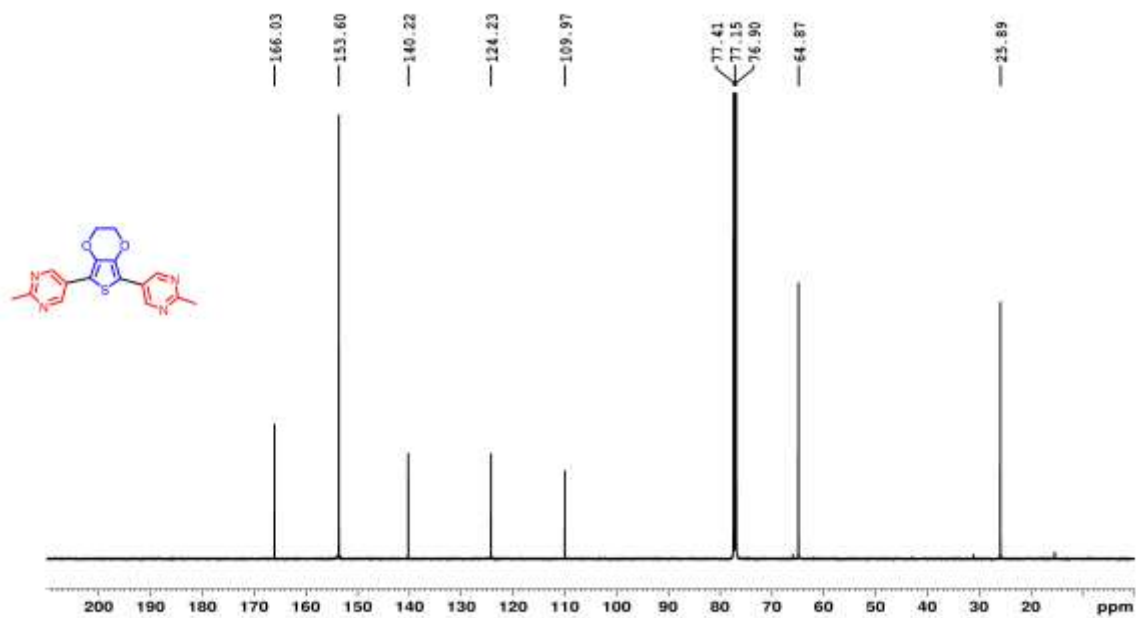


Figure 4.52. ^{13}C NMR spectrum of **CD22**.

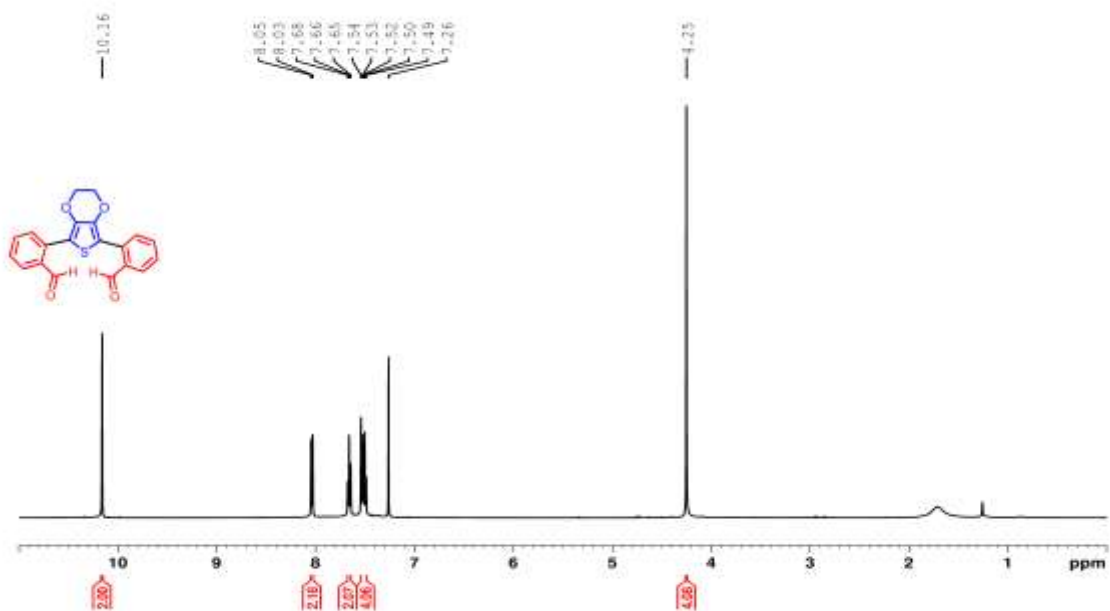


Figure 4.53. ^1H NMR spectrum of **CD23**.

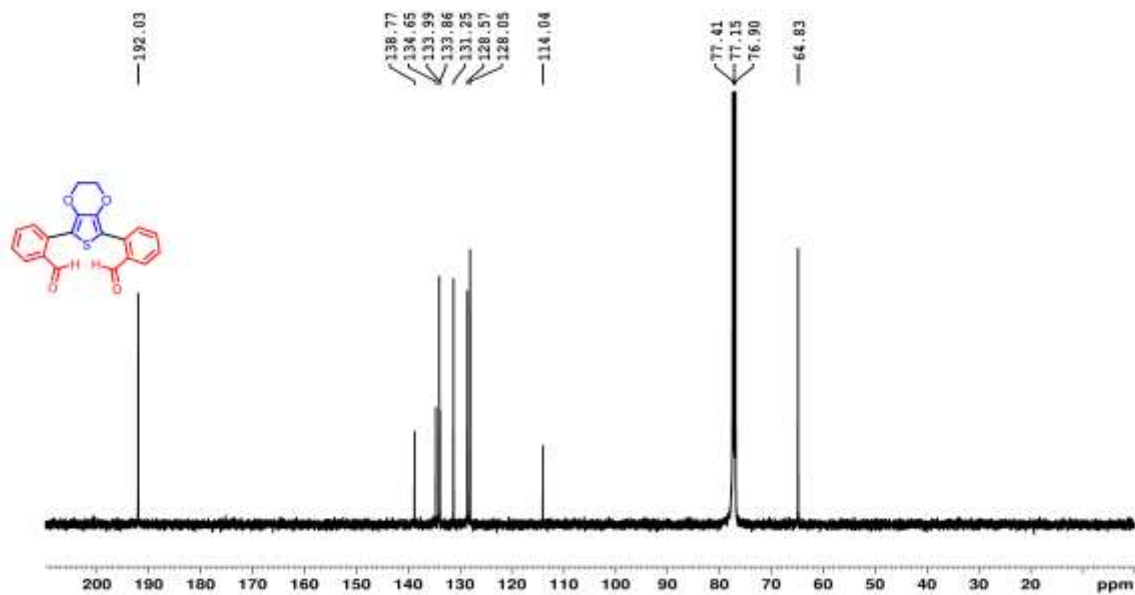


Figure 4.54. ^{13}C NMR spectrum of **CD23**.

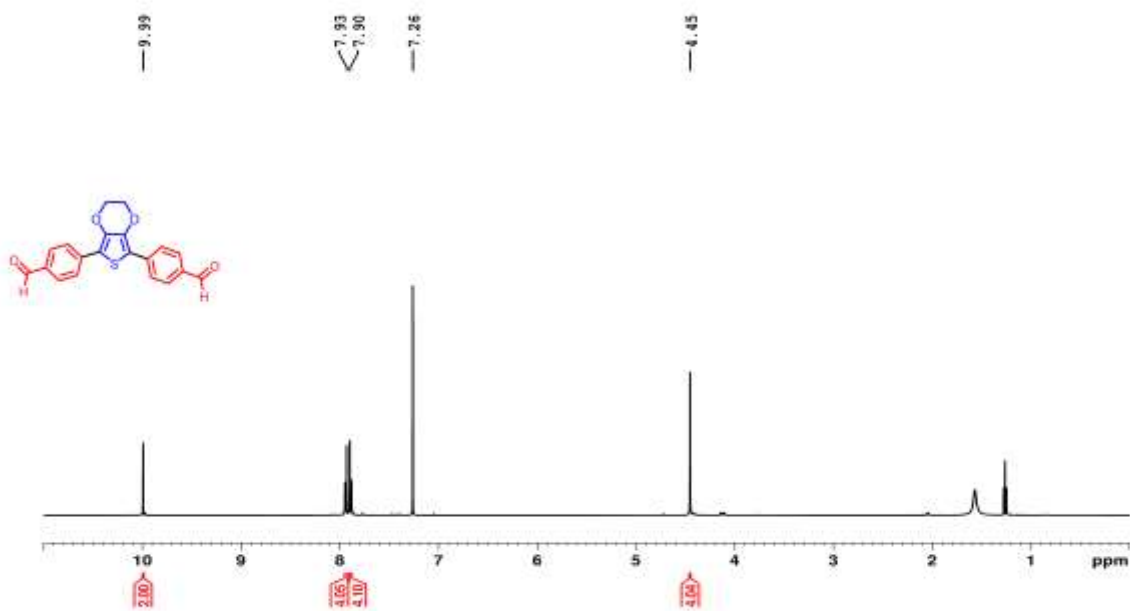


Figure 4.55. ^1H NMR spectrum of **CD24**.

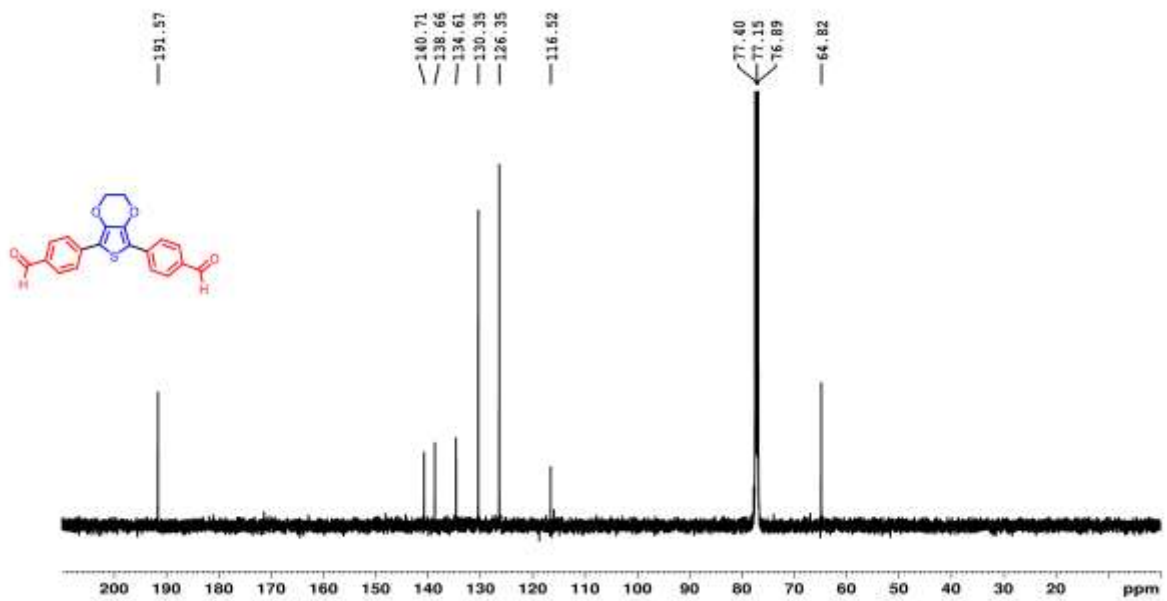


Figure 4.56. ^{13}C NMR spectrum of CD24.

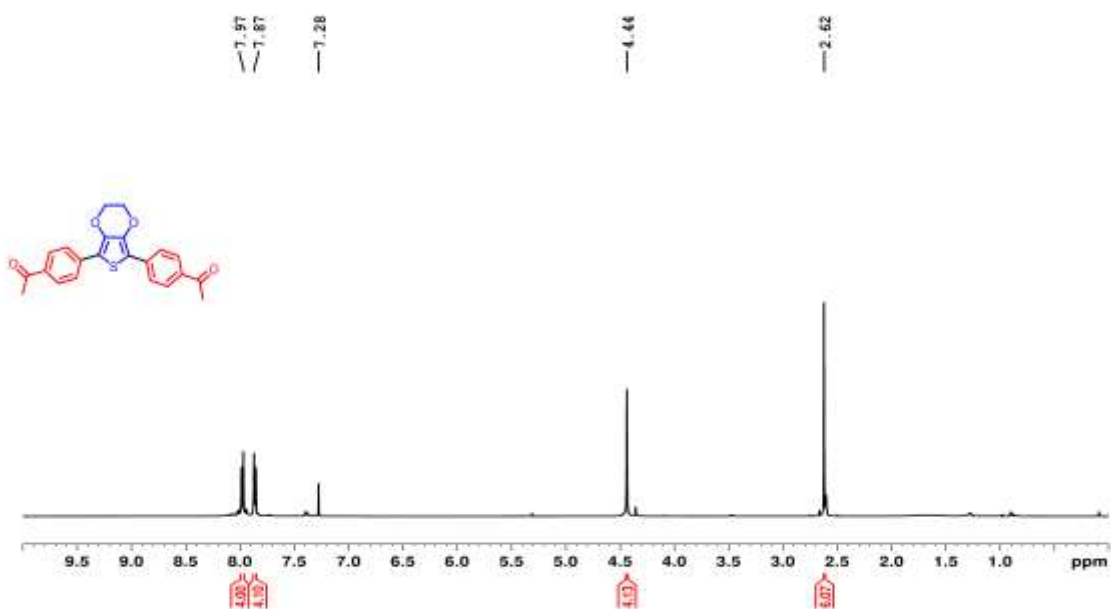


Figure 4.57. ^1H NMR spectrum of CD25.

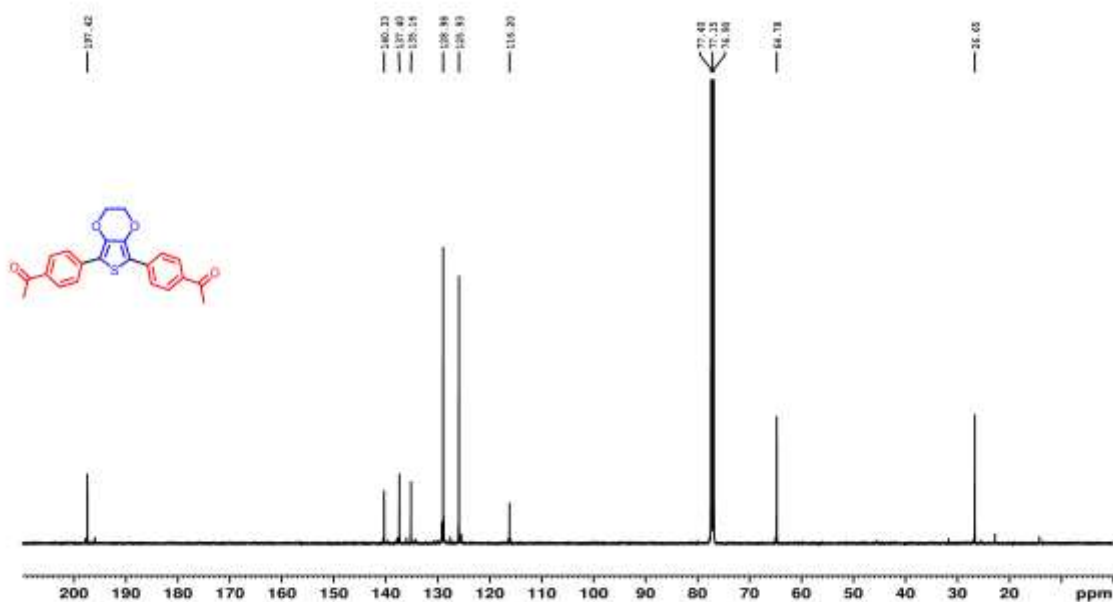


Figure 4.58. ^{13}C NMR spectrum of **CD25**.

4.8 References

- (1) Alberico, D.; Scott, M. E.; Lautens, M. Aryl–Aryl Bond Formation by Transition-Metal-Catalyzed Direct Arylation. *Chem. Rev.* **2007**, *107*, 174-238.
- (2) Zhao, Q.; Meng, G.; Nolan, S. P.; Szostak, M. N-Heterocyclic Carbene Complexes in C–H Activation Reactions. *Chem. Rev.* **2020**, *120*, 1981-2048.
- (3) Mainville, M.; Leclerc, M. Direct (Hetero)arylation: A Tool for Low-Cost and Eco-Friendly Organic Photovoltaics. *ACS Appl. Polym. Mater.* **2020**.
- (4) Mercier, L. G.; Leclerc, M. Direct (Hetero)Arylation: A New Tool for Polymer Chemists. *Acc. Chem. Res.* **2013**, *46*, 1597-1605.
- (5) Amaladass, P.; Clement, J. A.; Mohanakrishnan, A. K. Pd-mediated C–H arylation of EDOT and synthesis of push–pull systems incorporating EDOT. *Tetrahedron* **2007**, *63*, 10363-10371.

- (6) Liu, C.-Y.; Zhao, H.; Yu, H.-h. Efficient Synthesis of 3,4-Ethylenedioxythiophene (EDOT)-Based Functional π -Conjugated Molecules through Direct C–H Bond Arylations. *Org. Lett.* **2011**, *13*, 4068-4071.
- (7) Allard, S.; Forster, M.; Souharce, B.; Thiem, H.; Scherf, U. Organic semiconductors for solution-processable field-effect transistors (OFETs). *Angew. Chem., Int. Ed. Engl.* **2008**, *47*, 4070-98.
- (8) Koumura, N.; Wang, Z.-S.; Mori, S.; Miyashita, M.; Suzuki, E.; Hara, K. Alkyl-Functionalized Organic Dyes for Efficient Molecular Photovoltaics. *J. Am. Chem. Soc.* **2006**, *128*, 14256-14257.
- (9) Fell, V. H. K.; Findlay, N. J.; Breig, B.; Forbes, C.; Inigo, A. R.; Cameron, J.; Kanibolotsky, A. L.; Skabara, P. J. Effect of end group functionalisation of small molecules featuring the fluorene–thiophene–benzothiadiazole motif as emitters in solution-processed red and orange organic light-emitting diodes. *J. Mater. Chem. C* **2019**, *7*, 3934-3944.
- (10) Liu, X.-W.; Shi, J.-L.; Yan, J.-X.; Wei, J.-B.; Peng, K.; Dai, L.; Li, C.-G.; Wang, B.-Q.; Shi, Z.-J. Regioselective Arylation of Thiazole Derivatives at 5-Position via Pd Catalysis under Ligand-Free Conditions. *Org. Lett.* **2013**, *15*, 5774-5777.
- (11) Turner, G. L.; Morris, J. A.; Greaney, M. F. Direct Arylation of Thiazoles on Water. *Angew. Chem., Int. Ed.* **2007**, *46*, 7996-8000.
- (12) Ouyang, J.-S.; Li, Y.-F.; Shen, D.-S.; Ke, Z.; Liu, F.-S. Bulky α -diimine palladium complexes: highly efficient for direct C–H bond arylation of heteroarenes under aerobic conditions. *Dalton Trans.* **2016**, *45*, 14919-14927.
- (13) Chen, F.-M.; Huang, F.-D.; Yao, X.-Y.; Li, T.; Liu, F.-S. Direct C–H heteroarylation by an acenaphthyl-based α -diimine palladium complex: improvement of the reaction efficiency for bi(hetero)aryls under aerobic conditions. *Org. Chem. Front.* **2017**, *4*, 2336-2342.
- (14) Chen, F.-M.; Lu, D.-D.; Hu, L.-Q.; Huang, J.; Liu, F.-S. Camphyl-based α -diimine palladium complexes: highly efficient precatalysts for direct arylation of thiazoles in open-air. *Org. Biomol. Chem.* **2017**, *15*, 5731-5736.
- (15) Jafarpour, F.; Rahiminejadan, S.; Hazrati, H. Triethanolamine-Mediated Palladium-Catalyzed Regioselective C-2 Direct Arylation of Free NH-Pyrroles. *J. Org. Chem.* **2010**, *75*, 3109-3112.

- (16) Roy, D.; Mom, S.; Royer, S.; Lucas, D.; Hierso, J.-C.; Doucet, H. Palladium-Catalyzed Direct Arylation of Heteroaromatics with Activated Aryl Chlorides Using a Sterically Relieved Ferrocenyl-Diphosphane. *ACS Catal.* **2012**, *2*, 1033-1041.
- (17) Karlinskii, B. Y.; Kostyukovich, A. Y.; Kucherov, F. A.; Galkin, K. I.; Kozlov, K. S.; Ananikov, V. P. Directing-Group-Free, Carbonyl Group-Promoted Catalytic C–H Arylation of Bio-Based Furans. *ACS Catal.* **2020**, *10*, 11466-11480.
- (18) Yamaguchi, M.; Hagiwara, R.; Gayama, K.; Suzuki, K.; Sato, Y.; Konishi, H.; Manabe, K. Direct C3-Selective Arylation of N-Unsubstituted Indoles with Aryl Chlorides, Triflates, and Nonafates Using a Palladium–Dihydroxyterphenylphosphine Catalyst. *J. Org. Chem.* **2020**, *85*, 10902-10912.
- (19) Zhang, Y.; Lee, J. C. H.; Reese, M. R.; Boscoe, B. P.; Humphrey, J. M.; Helal, C. J. 5-Aryltetrazoles from Direct C–H Arylation with Aryl Bromides. *J. Org. Chem.* **2020**, *85*, 5718-5723.
- (20) Li, Y.; Wang, J.; Huang, M.; Wang, Z.; Wu, Y.; Wu, Y. Direct C–H Arylation of Thiophenes at Low Catalyst Loading of a Phosphine-Free Bis(alkoxo)palladium Complex. *J. Org. Chem.* **2014**, *79*, 2890-2897.
- (21) Bhaskar, R.; Sharma, A. K.; Singh, A. K. Palladium(II) Complexes of N-Heterocyclic Carbene Amidates Derived from Chalcogenated Acetamide-Functionalized 1H-Benzimidazolium Salts: Recyclable Catalyst for Regioselective Arylation of Imidazoles under Aerobic Conditions. *Organometallics* **2018**, *37*, 2669-2681.
- (22) Okazawa, T.; Satoh, T.; Miura, M.; Nomura, M. Palladium-Catalyzed Multiple Arylation of Thiophenes. *J. Am. Chem. Soc.* **2002**, *124*, 5286-5287.
- (23) Matsidik, R.; Martin, J.; Schmidt, S.; Obermayer, J.; Lombeck, F.; Nübling, F.; Komber, H.; Fazzi, D.; Sommer, M. C–H Arylation of Unsubstituted Furan and Thiophene with Acceptor Bromides: Access to Donor–Acceptor–Donor-Type Building Blocks for Organic Electronics. *J. Org. Chem.* **2015**, *80*, 980-987.
- (24) Png, Z. M.; Tam, T. L. D.; Xu, J. Carboxylic Acid Directed C–H Arylation of Azulene. *Org. Lett.* **2020**, *22*, 5009-5013.
- (25) Song, A. X.; Zeng, X.-X.; Ma, B.-B.; Xu, C.; Liu, F.-S. Direct (Hetero)arylation of Heteroarenes Catalyzed by Unsymmetrical Pd-PEPPSI-NHC Complexes under Mild Conditions. *Organometallics* **2020**, *39*, 3524-3534.

- (26) Türker, F.; Bereket, İ.; Barut Celepci, D.; Aktaş, A.; Gök, Y. New Pd-PEPPSI complexes bearing meta-cyanobenzyl-Substituted NHC: Synthesis, characterization, crystal structure and catalytic activity in direct C–H arylation of (Hetero)arenes with aryl bromides. *J. Mol. Struct.* **2020**, *1205*, 127608.
- (27) Hu, L.-Q.; Deng, R.-L.; Li, Y.-F.; Zeng, C.-J.; Shen, D.-S.; Liu, F.-S. Developing Bis(imino)acenaphthene-Supported N-Heterocyclic Carbene Palladium Precatalysts for Direct Arylation of Azoles. *Organometallics* **2018**, *37*, 214-226.
- (28) He, X.-X.; Li, Y.; Ma, B.-B.; Ke, Z.; Liu, F.-S. Sterically Encumbered Tetraarylimidazolium Carbene Pd-PEPPSI Complexes: Highly Efficient Direct Arylation of Imidazoles with Aryl Bromides under Aerobic Conditions. *Organometallics* **2016**, *35*, 2655-2663.
- (29) Canivet, J.; Yamaguchi, J.; Ban, I.; Itami, K. Nickel-Catalyzed Biaryl Coupling of Heteroarenes and Aryl Halides/Triflates. *Org. Lett.* **2009**, *11*, 1733-1736.
- (30) Hachiya, H.; Hirano, K.; Satoh, T.; Miura, M. Nickel-Catalyzed Direct C–H Arylation and Alkenylation of Heteroarenes with Organosilicon Reagents. *Angew. Chem., Int. Ed.* **2010**, *49*, 2202-2205.
- (31) Larson, H.; Schultz, D.; Kalyani, D. Ni-Catalyzed C–H Arylation of Oxazoles and Benzoxazoles Using Pharmaceutically Relevant Aryl Chlorides and Bromides. *J. Org. Chem.* **2019**, *84*, 13092-13103.
- (32) Hachiya, H.; Hirano, K.; Satoh, T.; Miura, M. Nickel-Catalyzed Direct Arylation of Azoles with Aryl Bromides. *Org. Lett.* **2009**, *11*, 1737-1740.
- (33) Zhao, S.; Liu, B.; Zhan, B.-B.; Zhang, W.-D.; Shi, B.-F. Nickel-Catalyzed Ortho-Arylation of Unactivated (Hetero)aryl C–H Bonds with Arylsilanes Using a Removable Auxiliary. *Org. Lett.* **2016**, *18*, 4586-4589.
- (34) Talukder, M. M.; Cue, J. M. O.; Miller, J. T.; Gamage, P. L.; Aslam, A.; McCandless, G. T.; Biewer, M. C.; Stefan, M. C. Ligand Steric Effects of α -Diimine Nickel(II) and Palladium(II) Complexes in the Suzuki–Miyaura Cross-Coupling Reaction. *ACS Omega* **2020**, *5*, 24018-24032.
- (35) Gates, D. P.; Svejda, S. A.; Oñate, E.; Killian, C. M.; Johnson, L. K.; White, P. S.; Brookhart, M. Synthesis of Branched Polyethylene Using (α -Diimine)nickel(II) Catalysts: Influence of Temperature, Ethylene Pressure, and Ligand Structure on Polymer Properties. *Macromolecules* **2000**, *33*, 2320-2334.

- (36) Rhinehart, J. L.; Brown, L. A.; Long, B. K. A Robust Ni(II) α -Diimine Catalyst for High Temperature Ethylene Polymerization. *J. Am. Chem. Soc.* **2013**, *135*, 16316-16319.
- (37) Zhong, L.; Li, G.; Liang, G.; Gao, H.; Wu, Q. Enhancing Thermal Stability and Living Fashion in α -Diimine–Nickel-Catalyzed (Co)polymerization of Ethylene and Polar Monomer by Increasing the Steric Bulk of Ligand Backbone. *Macromolecules* **2017**, *50*, 2675-2682.
- (38) Popeney, C.; Guan, Z. Ligand Electronic Effects on Late Transition Metal Polymerization Catalysts. *Organometallics* **2005**, *24*, 1145-1155.
- (39) Falivene, L.; Credendino, R.; Poater, A.; Petta, A.; Serra, L.; Oliva, R.; Scarano, V.; Cavallo, L. SambVca 2. A Web Tool for Analyzing Catalytic Pockets with Topographic Steric Maps. *Organometallics* **2016**, *35*, 2286-2293.
- (40) Falivene, L.; Cao, Z.; Petta, A.; Serra, L.; Poater, A.; Oliva, R.; Scarano, V.; Cavallo, L. Towards the online computer-aided design of catalytic pockets. *Nat. Chem.* **2019**, *11*, 872-879.
- (41) Marcone, J. E.; Moloy, K. G. Kinetic Study of Reductive Elimination from the Complexes (Diphosphine)Pd(R)(CN). *J. Am. Chem. Soc.* **1998**, *120*, 8527-8528.
- (42) Zhang, L.; Colella, N. S.; Cherniawski, B. P.; Mannsfeld, S. C. B.; Briseno, A. L. Oligothiophene Semiconductors: Synthesis, Characterization, and Applications for Organic Devices. *ACS Appl. Mater. Interfaces* **2014**, *6*, 5327-5343.
- (43) Bugaut, X.; Glorius, F. Palladium-Catalyzed Selective Dehydrogenative Cross-Couplings of Heteroarenes. *Angew. Chem., Int. Ed.* **2011**, *50*, 7479-7481.
- (44) Wakioka, M.; Nakamura, Y.; Hihara, Y.; Ozawa, F.; Sakaki, S. Factors Controlling the Reactivity of Heteroarenes in Direct Arylation with Arylpalladium Acetate Complexes. *Organometallics* **2013**, *32*, 4423-4430.
- (45) Yoshizawa, M.; Catti, L. Bent Anthracene Dimers as Versatile Building Blocks for Supramolecular Capsules. *Acc. Chem. Res.* **2019**, *52*, 2392-2404.
- (46) Sheldrick, G. M. SHELXT-Integrated Space-Group and Crystalstructure Determination. *Acta Crystallogr., Sect. A: Found. Adv.* **2015**, *71*, 3-8.
- (47) Sheldrick, G. M. Crystal Structure Refinement with SHELXL. *Acta Crystallogr., Sect. C: Struct. Chem.* **2015**, *71*, 3-8.

- (48) Dehghanpour, S.; Bouslimani, N.; Welter, R.; Mojahed, F. Synthesis, spectral characterization, properties and structures of copper(I) complexes containing novel bidentate iminopyridine ligands. *Polyhedron* **2007**, *26*, 154-162.
- (49) Bolliger, J. L.; Frech, C. M. The 1,3-Diaminobenzene-Derived Aminophosphine Palladium Pincer Complex {C₆H₃[NHP(piperidiny)]₂2Pd(Cl)} – A Highly Active Suzuki–Miyaura Catalyst with Excellent Functional Group Tolerance. *Adv. Synth. Catal.* **2010**, *352*, 1075-1080.
- (50) Qin, X.; Sun, D.; You, Q.; Cheng, Y.; Lan, J.; You, J. Rh(III)-Catalyzed Decarboxylative ortho-Heteroarylation of Aromatic Carboxylic Acids by Using the Carboxylic Acid as a Traceless Directing Group. *Org. Lett.* **2015**, *17*, 1762-1765.
- (51) Mao, S.; Shi, X.; Soulé, J.-F.; Doucet, H. Exploring Green Solvents Associated to Pd/C as Heterogeneous Catalyst for Direct Arylation of Heteroaromatics with Aryl Bromides. *Adv. Synth. Catal.* **2018**, *360*, 3306-3317.
- (52) Shinde, V. N.; Bhuvanesh, N.; Kumar, A.; Joshi, H. Design and Syntheses of Palladium Complexes of NNN/CNN Pincer Ligands: Catalyst for Cross Dehydrogenative Coupling Reaction of Heteroarenes. *Organometallics* **2020**, *39*, 324-333.
- (53) Cheng, J.; Zhang, F.; Li, K.; Li, J.; Lu, X.; Zheng, J.; Guo, K.; Yang, S.; Dong, Q. A planar dithiafulvene based sensitizer forming J-aggregates on TiO₂ photoanode to enhance the performance of dye-sensitized solar cells. *Dyes Pigm.* **2017**, *136*, 97-103.

BIOGRAPHICAL SKETCH

Md Muktadir Talukder was born and raised in Netrokona, Bangladesh. He obtained his BS in Chemistry in 2013 from The University of Dhaka, Bangladesh. After that, he started his PhD career in Chemistry at The University of Texas at Dallas in Fall 2015. Eventually, he joined the research group of Dr. Miahela C. Stefan and started his research career in catalysis. He has developed novel α -diimine-based group 10 transition metal complexes for cross-coupling reactions. He is passionate about designing clean and sustainable synthetic protocols for synthesizing chemical building blocks with biological, physical, or pharmaceutical properties mainly to design and develop new synthetic tools in cross-coupling chemistry through group 10 metal complexes. After finishing his PhD studies, Md Muktadir plans to work as a postdoctoral researcher for acquiring much more in-depth knowledge and expertise for working in an industry position.

CURRICULUM VITAE

Md Muktadir Talukder

Address: Department of Chemistry and Biochemistry, BE 26

The University of Texas at Dallas

800 W Campbell Rd, Richardson, TX 75080

Email: mxt150630@utdallas.edu

Education:

The University of Texas at Dallas, Richardson, TX

Aug. 2015 – Nov. 2020

Ph.D. candidate in Chemistry

Dissertation: ' α -Diimine Nickel (II) and Palladium (II) Complexes in Cross-Coupling Reactions

Advisor: Prof. Mihaela C. Stefan

The University of Dhaka, Bangladesh

Feb. 2009 – Sep. 2013

B.S. in Chemistry

SUMMARY OF RESEARCH

Highly interested in designing clean and sustainable synthetic protocols for synthesizing chemical building blocks with biological, physical, or pharmaceutical properties. Particularly, to design and develop new synthetic tools in cross-coupling chemistry through group 10 metal complexes. In this possibility, α -diimine 10 metal complexes have fascinated because of the versatile characteristics including tunable sterics and bite angles. In addition, α -diimine complexes have

demonstrated outstanding thermal associated with the air and moisture stabilities. Considering these factors, I'm involved in developing robust α -diimine catalytic systems in cross-coupling reactions through fine-tuning the steric and electronic properties of the ligand frameworks.

RESEARCH PROJECTS

- ❖ **Ligand Steric Effects of α -Diimine Nickel (II) and Palladium (II) Complexes in the Suzuki–Miyaura Cross-Coupling Reaction.** Design and development of low-cost, highly efficient catalyst in C-C cross-coupling for synthesizing valuable biaryl building blocks. Systematic evaluation of ligand sterics in the reaction outcomes through synthesizing both α -diimine nickel (II) and palladium (II) complexes.
- ❖ **Mono- and Dinuclear α -Diimine Nickel (II) and Palladium (II) Complexes in C–S Cross-Coupling.** Design, synthesis, and characterization of novel mononuclear and bridged dinuclear α -diimine nickel (II) and palladium (II) complexes for synthesizing pharmaceutically active thioethers through C-S cross-coupling. Essentially, pharmaceutically active heteroaryl moieties are extensively incorporated from thiol and halide sources.
- ❖ **α -Diimine Nickel (II) and Palladium (II)-Catalyzed C-H Bond Activation of Five-Membered Heteroaromatics.** Synthesizing valuable building blocks for π -conjugated small molecules and polymers through the design and development of α -diimine nickel (II) and palladium (II) catalytic systems.
- ❖ **End group analysis of poly(3-hexylthiophene) from halogenated monomers and their potential application for bis-end-functionalization.** Synthesis, and characterization of bis-end-functionalized poly(3-hexylthiophene) for improved device performance in the organic field-effect transistors.

RESEARCH EXPERIENCE

Ph.D. Student, University of Texas at Dallas, Texas, USA

Aug. 2015 – present

- ❖ Experienced in producing high-quality single crystal and sound knowledge of XRD data interpretation.
- ❖ Established highly efficient novel catalytic systems in C-C and C-S cross-coupling chemistry through examining ligand steric effects in the reaction outcomes.
- ❖ Designed new synthetic procedures in cross-coupling under open air conditions.

- ❖ Proficient in characterization of thermal properties of metal complexes, small molecules, and polymers.
- ❖ Executed multi-step organic synthesis for producing poly(3-hexylthiophene) based block-copolymers and characterization through GPC and MALDI-TOF MS.
- ❖ Basic exposure in surface imaging techniques, photolithography, and device fabrication of organic field-effect transistors.
- ❖ Dedicated leader and mentor with excellent organization skills, having successfully trained undergraduate and graduate students on new instrumentation and techniques.
- ❖ Hands-on experience in designing and building experimental setups, repair, maintain and troubleshoot instruments including GPC, HPLC, GC and GC-MS.

TEACHING EXPERIENCE

Graduate Teaching Assistant, University of Texas at Dallas, Texas, USA

- ❖ Advanced Chemical Synthesis Laboratory Fall 2017
& 2018
 - Guided senior undergraduates for documenting data and lab reports.
 - Instructed students to design innovative experiments.
 - Trained the application of NMR, FT-IR, UV-Vis, and XRD.
- ❖ Organic Chemistry Laboratory II Fall 2015
& 2016
 - Prepared and presented the lecture for **sophomore undergraduates**.
 - Taught the basic synthetic procedures and purification techniques.

CONFERENCE PROCEEDINGS

- ❖ **Talukder, M. M.**; Aslam, A. A.; Biewer, M. C.; Stefan, M. C. Exploring catalytic pockets of α -diimine group 10 complexes. Abstracts of Papers, 259th ACS National Meeting & Exposition, Philadelphia, PA, United States, March 22-26, 2020 (2020), POLY-0711 (**oral**).
- ❖ **Talukder, M. M.**; Biewer, M. C.; Stefan, M. C. End group analysis of poly(3-hexylthiophene) from halogenated monomers and their potential application for bis-end-functionalization. Abstracts of Papers, 258th ACS National Meeting & Exposition, San Diego, CA, United States, August 25-29, 2019 (2019), POLY-0270 (**poster**).

PUBLICATIONS

- ❖ **Talukder, M. M.**; Cue, J. M. O.; Miller, J. T.; Gamage, P. L.; Aslam, A.; McCandless, G. T.; Biewer, M. C.; Stefan, M. C. Ligand Steric Effects of α -Diimine Nickel(II) and Palladium(II) Complexes in the Suzuki–Miyaura Cross-Coupling Reaction. *ACS Omega* **2020**, *5*, 24018-24032.
- ❖ **Talukder, M. M.**; Miller, J. T.; Cue, J. M. O.; Mahesh, U. G.; Bhadran, A.; Biewer, M. C.; Stefan, M. C. Mono- and Dinuclear α -Diimine Nickel (II) and Palladium (II) Complexes in C–S Cross-Coupling. Under review.
- ❖ **Talukder, M. M.**; Miller, J. T.; Cue, J. M. O.; Mahesh, U. G.; Biewer, M. C.; Stefan, M. C. Iminopyridine-Based α -Diimine Nickel (II) and Palladium (II) Complexes in Direct C–H Bond Arylation of Five-Membered Heteroaromatics. In preparation.

AWARDS

- ❖ Ph.D. Research small grant award in 2020 from the University of Texas at Dallas.
- ❖ Ph.D. Research small grant award in 2019 from the University of Texas at Dallas.

TECHNICAL SKILLS & SOFTWARES

- | | |
|---|---------------------------------------|
| ❖ MALDI-TOF Mass Spectrometry | ❖ GC- Mass Spectrometry |
| ❖ Single-crystal X-ray Diffraction | ❖ TGA & DSC |
| ❖ Chromatography (Size-Exclusion, HPLC, GC) | ❖ Scanning electron microscopy |
| ❖ Spin coating | ❖ Photolithography |
| ❖ Probe Station | ❖ FTIR, NMR & UV-Visible spectroscopy |
| ❖ TopSpin for NMR | ❖ Origin Lab & Prism |

PROFESSIONAL AFFILIATIONS

- ❖ Member of American Chemical Society 2017-present